Synthesis of C_{10}-C_{16} linear symmetrical ethers from n-alcohols over heterogeneous acid catalysts

Carlos Casas Fernández

Synthesis of C_{10}-C_{16} linear symmetrical ethers from n-alcohols over heterogeneous acid catalysts

Carlos Casas Fernández

Programa de doctorado de

Ingeniería y Tecnologías Avanzadas

Under the supervision of

Dr. Javier Tejero Salvador

Chemical Engineering Department.
University of Barcelona

Dr. Monsterrat Iborra Urios

Chemical Engineering Department
University of Barcelona

PhD thesis to obtain the degree of doctor in Engineering and Advanced Technologies by the University of Barcelona

Presented by:

Carlos Casas Fernández

Carried out in the research group of "Applied Kinetics and Catalysis" at the

Chemical Engineering Department of the University of Barcelona

Approved by:

Dr. Javier Tejero Salvador

University of Barcelona

Dr. Monsterrat Iborra Urios

University of Barcelona

LIST OF PUBLICATIONS

C.Casas, J. Guilera, E. Ramírez, R. Bringué, M. Iborra, J. Tejero, "Reliability of the synthesis of C10-C16 linear ethers from 1-alkanols over acidic ion exchange resins," ***Biomass Convers. Bioref***., vol. 3, pp. 27-37, 2013.

C. Casas, C. Fité, M. Iborra, J. Tejero, F. Cunill,"Study of the chemical equilibrium of the liquid-phase dehydration of 1-octanol to di-n-octyl ether," ***J. Chem. Eng. Data***, vol. 58, pp. 741-748, 2012.

C. Casas, R. Bringué, E. Ramírez, M. Iborra, J. Tejero,"Liquid phase Dehydration of 1-octanol, 1-hexanol and 1-pentanol to linear symmetrical ethers over ion exchange resins," ***App. Catal. A: Gen***., vol. 396, pp. 129-139, 2011.

C. Casas, R. Bringué, E. Ramírez, M. Iborra, J. Tejero, "Deshidratación de 1-octanol sobre zeolitas y resinas de intercambio iónico," ***Ingeniería Química***, vol. 494, pp. 70-74, 2011.

WORKS IN PROGRESS

C. Casas, R. Bringué, E. Ramírez, M. Iborra, J. Tejero, "Zeolite catalyzed dehydration of linear alcohol to C10-C16 symmetrical ether in the liquid phase". Submitted to ***Microporous & Mesoporous Materials*** on September 2013.

C. Casas, J. Tejero, M. Iborra, C. Fité, R. Bringué, "Kinetics of 1-octanol dehydration to di-n-octyl ether on Amberlyst 70". In preparation.

CONGRESS PARTICIPATIONS

Europacat XI, *Kinetics of the bimolecular dehydration of 1-octanol to di-n-octyl ether over Amberlyst 70.* C. Casas, R. Bringué, M. Iborra, C. Fité, J. Tejero. Lyon (France), 2013. Poster.

XIX International symposium on alcohol fuels (ISAF XIX), *Reliability of the synthesis of C10-C16 linear ethers from 1-alkanols over acidic ion exchange resins.* C. Casas, J. Guilera, E. Ramírez, R. Bringué, M. Iborra, J. Tejero. Verona (Italy), 2011. Poster.

XIII National Congress of Chemical Engineering (CNIQ2010), *Deshidratación de 1-octanol sobre zeolitas y resinas de intercambio iónico.* C. Casas, R. Bringué, E. Ramírez, M. Iborra y J. Tejero. Madrid (Spain), 2010. Poster.

UBiochem, *Synthesis of ethyl octyl ether from diethyl carbonate and 1-octanol over solid catalysts.* J. Guilera, C.Casas, E. Ramírez, R. Bringué, M. Iborra, F. Cunill and J. Tejero. Córdoba (Spain), 2010. Poster.

EuropaCat IX, *Effect of the textural properties of ion-exchange resins on the liquid-phase dehydration of alcohols to linear ethers.* C. Casas, R. Bringué, J. Tejero, M. Iborra, C. Fité, J.F. Izquierdo and F. Cunill. Salamanca (Spain), 2009. Poster.

11th Mediterranean Congress of Chemical Engineering, *Dehydration to linear ether of 1-octanol, 1-hexanol and 1-pentanol in liquid phase over ion exchange resins*. C.Casas, J.Tejero, M. Iborra, R. Bringué, F. Cunill, J.F Izquierdo, C. Fité. Barcelona (Spain), 2008. Poster.

CONTENTS

CHAPTER 1

INTRODUCTION

1.1 The diesel

The diesel or gasoil is a mixture of different refinery streams as well as the required additives to accomplish the legal specifications set for diesel fuels. Main refinery streams used for diesel blending are refinery cuts with boiling point ranging 150-390 ºC, including atmospheric gasoil (AGO) and vacuum gasoil (VGO) from direct crude distillation and cuts from other units such as FCC, visbreaking, coking and desulfuration [1] (see Figure 1.1). Although its composition can vary according to the type of crude (paraffinic, naphthenic, aromatic or asphaltic), generally it is possible to place the diesel cuts in the part of distillation curve corresponding to distillate crude from 25 to 65% of its mass. Within this range of distillation curve, hydrocarbons composing diesel fuel range from 10-12 to 20-22 carbon atoms approximately. An example of composition of a diesel can be found in APPENDIX I.

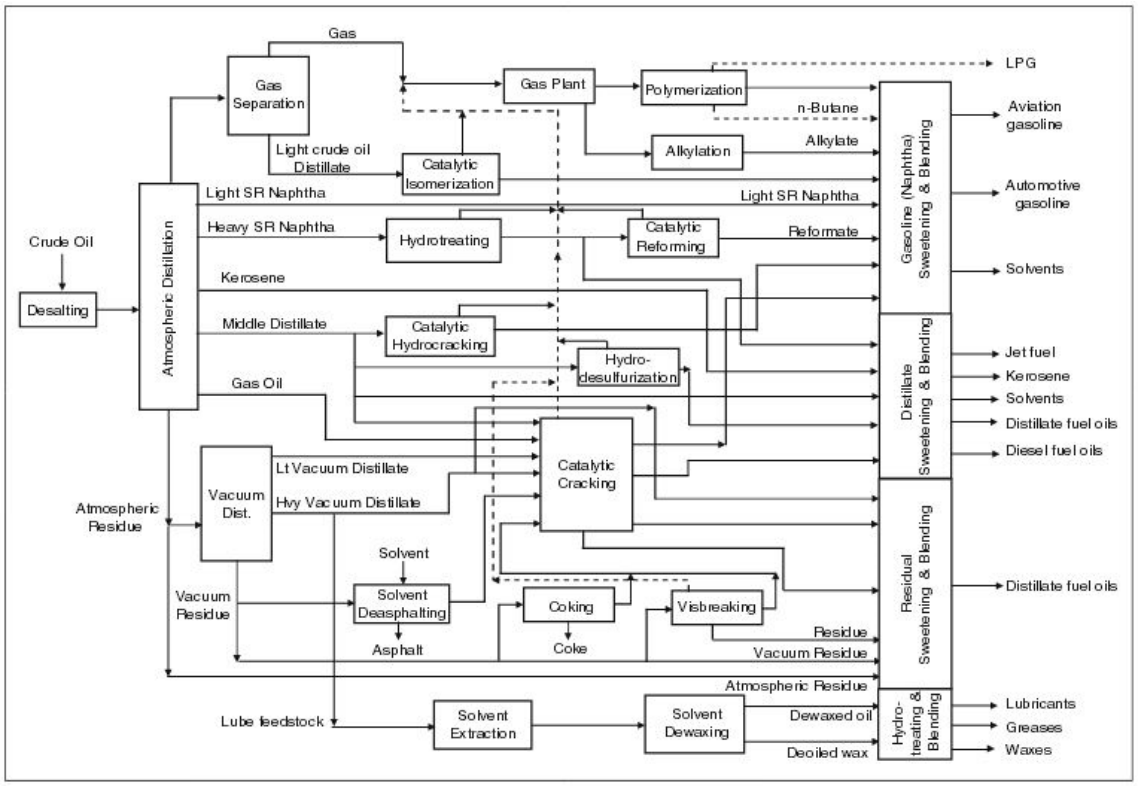

Figure 1.1 Modern refinery [2]

1.2 Problematic of diesel engines emissions

1.2.1 The combustion process of diesel in the diesel engine

Diesel engine is based on the thermodynamic cycle named Diesel, as the inventor of diesel engine, Rudolf Christian Karl Diesel. Diesel thermodynamic cycle consists in an adiabatic compression of the air in the cylinder (compression stroke in Figure 1.2). This compression raises the temperature to the ignition temperature of the fuel mixture which is formed by injecting fuel once the air is compressed (ignition of fuel in Figure 1.2). The adiabatic compression is followed by a constant pressure combustion process, then adiabatic expansion as power stroke and an isovolumetric exhaust (Figure 1.3).

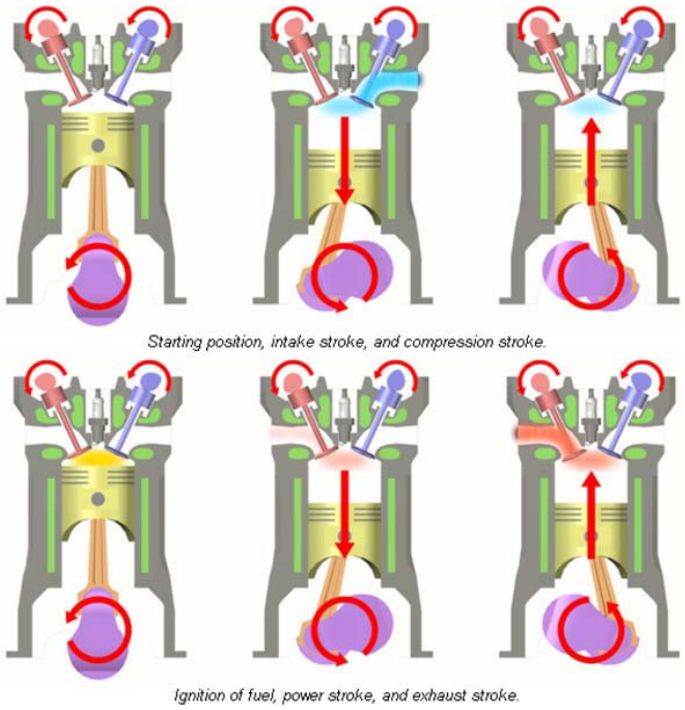

Figure 1.2. Representation of a diesel engine [3]

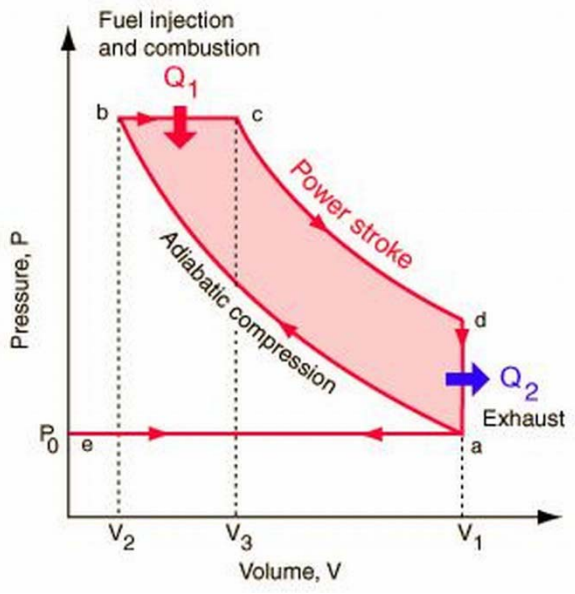

Figure 1.3. Thermodynamic Diesel cycle [4]

In order to get a proper combustion, fuel must vaporize in the injection. Volatility of hydrocarbon compound decreases as molecular weight increases and thus, the combustion process gets more complex. As well, air and fuel must be mixed and must feed ignition and combustion zones.

Ignition of fuel will take place when the fine fuel droplets have enough temperature in the combustion chamber. However, if the molecules of fuel are large and/or there is not enough oxygen and/or low temperature, the combustion of fuel will be partial, and it will be oxidized forming soot particles and other contaminant particles.

When diesel fuel is injected in the cylinder both lean and rich oxygen zones are created in the spray formed (Figure 1.4). In the lean oxygen zones, an excess of fuel promotes the formation of CO, unburned hydrocarbons and soot whereas fuel lean zones give more NO_x due to the excess of oxygen. Unburned hydrocarbons and CO normally are burned before exiting the cylinder with the exhaust gases, but oxidation rate of soot particles is slower and these particles are prone to exit the combustion chamber in the diesel exhausts [5].

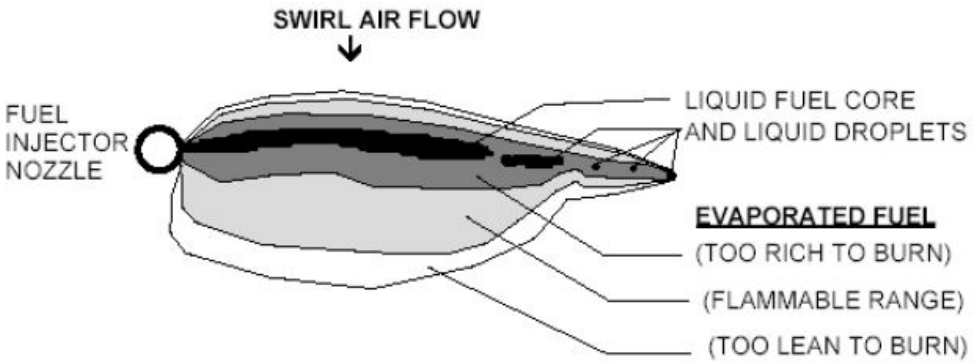

Figure 1.4. Representation of fuel spray zones in diesel injection [5]

Both physical and chemical properties of fuel are important in the fuel combustion. From the moment the fuel is injected until ignition starts (overall compression ignition process), a period of time is observed (delay). This delay is due to the time required for the vaporization of the liquid phase (physical delay) and the time necessary for the gas-phase fuel to react with oxygen and form radicals in the ignition process (chemical delay).

Physical delay depends on:

- Density and temperature of air in the cylinder
- Velocity and turbulence of the air
- Atomization, penetration and shape of the spray
- The properties of fuel, including: density, viscosity, surface tension, specific heat, enthalpy of vaporization, vapor pressure and vapor diffusivity.

For ignition to occur it is necessary that the fuel must be heated to a temperature sufficient for some of the weaker bonds to break and form radicals. The finite rate of these radical forming oxidation reactions is responsible for the chemical delay in compression ignition [5]. Once a sufficient concentration of free radicals is reached, rapid oxidation occurs (ignition). Figure 1.5 summarizes both physical and chemical delays associated to the ignition process.

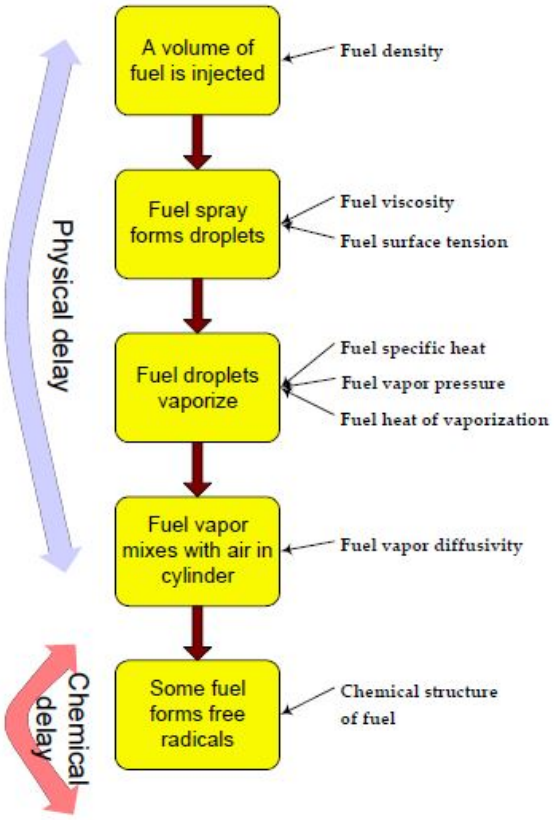

Figure 1.5. Overall compression ignition process [6]

Figure 1.6 shows the variation of the rate of heat release with the crank angle[1], where it is possible to distinguish the different phases of diesel combustion process: start of injection (SOI) and delay period (a-b), premixed combustion phase (b-c), mixing-controlled combustion phase (c-d) and late combustion phase (d-e).

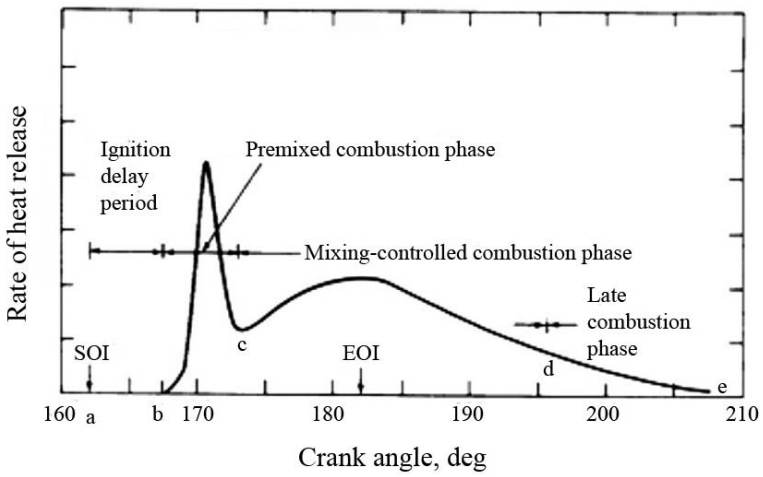

Figure 1.6. Phases in diesel combustion process [7]

As seen in Figure 1.6, after the injection, a premixed fuel-air mixture is burned (premixture combustion phase) rapidly, leading to high heat release rates and rapid cylinder pressure rise. The longer the ignition delay, the more prepared fuel-air mixture with higher initial heat release rates and pressure rise. Thus, in order to avoid excessive heat release rates and to keep rates and pressure rise acceptable, the ignition delay period should be as short as possible [7].

After the premixed fuel-air mixture has been burned, the rate of combustion in mixing-controlled combustion phase is controlled by the rate at which fuel-air mixture becomes available for burning, which is largely dependent on the fuel injection rate and fuel vapor air mixing rates. The heat release in this phase is typically of a lower magnitude and occurs over a much longer duration compared to the rapid combustion phase. This is because the fuel-air mixing time scales are much higher than the chemical reaction time scales. As the injected fuel continues to burn, the piston expands and the heat released decreases. Late combustion is characterized by very low heat release rates due to the combustion of the remaining fuel, CO and soot. This phase is usually terminated by the temperature drop during expansion which slows down the kinetics of the final burning.

[1] Crank angle: angle used to measure piston position.

1.2.2 Diesel exhausts

The exhaust from diesel engines is made of two main parts, gases and soot (particulate). The gas portion of diesel exhaust is mostly CO_2, CO, NO_x (nitric oxide and nitrogen dioxide), sulfur oxides and hydrocarbons, including polycyclic aromatic hydrocarbons (PAHs). The soot portion of diesel exhausts is made of particles such as carbon, organic materials (including PAHs), and traces of metallic compounds.

Carbon dioxide (CO_2)

CO_2 is the main gas in the diesel exhaust; it is not toxic but as a greenhouse gas its excess in the atmosphere contributes to the global warming. However, comparison of diesel and gasoline engines shows that diesel engine thermal efficiency is higher than that of gasoline engine. Actually, diesel engine has the highest thermal efficiency of any standard external or internal combustion engine. From this point of view, diesel engines have the clear advantage of consuming less fuel than gasoline ones, which is reflected in lower *CO_2* emissions per km on road transport than gasoline-powered vehicles.

Carbon monoxide (CO)

Carbon monoxide is a colorless odorless and toxic gas. Its toxicological effects are due to the formation of carboxyhemoglobin in the blood, which inhibits the oxygen intake. At low concentrations, *CO* causes fatigue in healthy people and chest pain in people with heart disease. *CO* can cause as well flu-like symptoms and at very high concentrations causes death [8].

In diesel engine, *CO* formation is promoted when the combustion takes place at low pressure and temperature in the rich fuel zones [5].

Nitrogen oxides (NO_x)

Nitrogen oxides (*NO_x*) comprises, N_2O, NO, N_2O_2, N_2O_3, NO_2, N_2O_4, and N_2O_5, being N_2O_3 and N_2O_5 solids and the rest gases at ambient conditions. *NO_x* emissions from combustion are primarily in the form of *NO* and as well *NO_2* because *NO* is rapidly converted to *NO_2*. *NO_2* is present in the atmosphere and in acid rain in the form of HNO_3.

Both *NO* and NO_2 participate in the ozone formation from the photo reaction of VOC (volatile organic compounds) [9].

At the United States, transportation related sources (on-road, nonroad and aircraft/locomotive/marine) account for approximately 60% of total anthropogenic emissions of NO_x, while stationary sources (electrical utilities and industrial boilers) account for most of the remainder [10].

In diesel engines NO_x comes from the oxidation of N_2 of the air in the intake. Its formation is associated with high combustion pressures and temperatures and also to an excess of air or lack of fuel in the combustion mixture [5].

Sulfur oxides (SO_x)

SO_2 is the component of greatest concern in SO_x and is used as the indicator for the larger group of gaseous sulfur oxides (SO_x). Short-term exposures to SO_2 are related with an array of adverse respiratory effects including bronchoconstriction and increased asthma symptoms. SO_x can react with other compounds in the atmosphere to form small particles, which penetrate deeply into sensitive parts of the lungs and cause or worsen respiratory diseases [8].

In diesel engines SO_x emissions are directly related with the sulfur content of the fuel, which has been lowered continuously by legislation. In Europe, directive 2009/30/EC set in 10 ppm the maxim sulfur content of diesel and in United States, Ultra Low Sulfur Diesel (ULSD) with ≤ 15 ppm was phased in for highway diesel from 2006 to 2010 [8]. Anthropogenic emissions of SO_2 in United States are mainly due to combustion of fossil fuels, being electrical generation and industrial point sources the major contributors (85%) whereas transport-related sources only contribute by 7%.

Although contribution of transport-related sources to anthropogenic emissions of SO_2 is low, lowering sulfur in the fuel is important to avoid catalyst poisoning in the current after-treatment devices and also to prevent sulfate particles formation.

Hydrocarbons (HC)

Heavy-duty vehicles (HDV) emissions contain several substances that are known, probably, or possible human or animal carcinogens, or have serious noncancer health effects. These substances include benzene, formaldehyde, acetaldehyde, 1,3-butadiene, acrolein and dioxin (Table 1.1). Substances in HDV emissions are not limited to those aforementioned but they are the most significant pollutants in HDV emissions [11].

Table 1.1. Most representative toxics of HDV emissions

Substance	Carcinogen	Possibly carcinogen
Benzene	X	
1,3-butadiene	X	
Formaldehyde	X	
Acetaldehyde		X
Acrolein	N.D[a]	
Dioxins	X	

(a) not determined

Although benzene is not a pollutant exclusive from diesel-powered vehicles, at the year 1996 highway mobile sources accounted for 48% of the United States emissions of benzene.

Hydrocarbon emissions in diesel engines have their origin in the oxygen lean zones of the fuel combustion. A lack of oxygen or excess of fuel in the air/fuel mixture leads to the fuel to be partially burned. Also, a poor vaporization of fuel and/or a very low combustion temperature can be the responsible of the presence of some *hydrocarbons* in the diesel exhausts.

Particulate matter (PM)

Although *particulate matter* (*PM*) is a non-chemical pollutant, at elevated concentrations can adversely affect to human health (respiratory diseases, aggravation of respiratory and cardiovascular diseases and increase of susceptibility to respiratory infections), visibility and materials.

PM comprises both coarse fraction (particles with diameters ranging from 2.5 to 10 microns) and fine particle (particles with diameters below 2.5 microns). According to size, *PM* is also classified as PM_{10} (all particles less than 10 microns) and $PM_{2.5}$ (all particles less

than 2.5 microns). According to the moment of formation, *PM* can be divided in primary and secondary particles. Primary particles are those emitted directly to the atmosphere whereas secondary particles are formed by transformations of gaseous emissions of sulfur dioxide, nitrogen oxides and VOCs (volatile organic compounds).

Primary diesel particles mainly consist of carbonaceous material, with a small contribution from sulfuric acid and ash (trace metals). Many of these particles exist in the atmosphere as carbon core with a coating of organic carbon compounds, or as sulfuric acid and ash, sulfuric acid aerosols, or sulfate particles associated with organic carbon. As well, the soluble organic fraction (SOF), which consists in unburned hydrocarbons that have condensed into liquid droplets from diesel exhausts.

While representing a very small portion (less than one percent) of the emissions of metals, and representing a small portion of diesel *particulate matter* (1 to 5%), it should be noted that several trace metals that may have general toxicological significance depending on the specific species are also emitted by diesel engines in small amounts including chromium, manganese, mercury and nickel. In addition, small amounts of dioxins have been measured in diesel exhaust, some of which may partition into the particle phase.

Approximately 80-95% of diesel particle mass is in the size range from 0.05 to 1.0 micrometers with a mean particle diameter of about 0.2 micrometres. These fine particles have a very specific surface area, which make them excellent carriers for adsorbed inorganic and organic compounds that can effectively reach the lowest airways of the lung. Approximately 50-90% of particles in diesel exhaust are in the ultrafine size range from 0.005-0.05 micrometers, averaging about 0.02 micrometers. While accounting for the majority of the number of particles, ultrafine diesel *particulate matter* accounts for 1-20% (w/w) of diesel *particulate matter* [11].

Source of *PM* in diesel engines is attributable to the incomplete combustion of fuel hydrocarbons as well as engine oil and other fuel components such as sulfur [11]. Different studies about the effect of diesel properties and composition on diesel emissions agreed in correlating *PM* with Polycyclic Aromatic Hydrocarbons (PAH) [12].

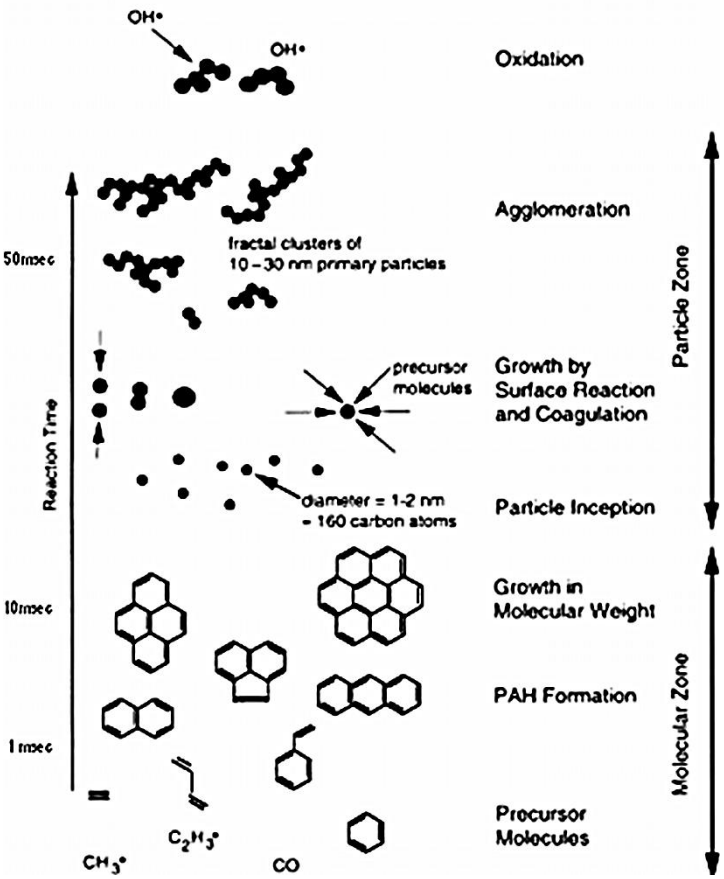

Figure 1.7. Role of PAH in particle formation [13]

In those studies the *PM* emissions observed increased always with the PAH content of diesel fuel. The mechanism sets PAH as the compounds responsible of particle inception (Figure 1.7). This way, precursors of PAH and soot such as ethylene, acetylene and benzene must be removed to avoid PAH growth and soot formation [13].

1.3 Properties of diesel

Composition as well as characteristics of diesel fuel are regulated in Spain by the R.D. 61/2006, January 31st (see APPENDIX II) where diesel is classified according to its use and tax applied. This way, three classes of diesel are set: Class A, used for diesel engines in passenger vehicles, Class B, used for agricultural and maritime use and Class C, for heating purposes.

1.3.1 Ignition quality

As seen, the diesel combustion process is based on auto-ignition of fuel. Between the injection of diesel in the engine and the start of combustion exists a delay period, where

fuel is atomized, evaporated, mixed with air and ignited. Using fuels with low ignition quality increases the ignition delay, the amount of fuel injected during ignition delay period and the share of premixed combustion. All this, results in high pressure gradients, rough engine operation, high noise levels, and even in increased NO_x emissions. Good ignition properties are thus, important. For conventional hydrocarbon fuels, either cetane number determined by a test engine or a calculated cetane index is used to describe ignition quality. Straight-chain paraffinic compounds have the highest ignition quality, which improves as the chain length increases. On the contrary, aromatic compounds have poor ignition quality, as do the alcohols [13].

1.3.2 Density and heating value

All diesel fuel injection systems are based on volumetric metering. To control maximum engine output and emissions, standard EN 590 sets a relatively narrow range for density, 820-845 kg/m^3 at 15 ºC. At a constant heating value, lower density means reduced maximum power output, higher density increased output and increased particle formation. For conventional diesel fuel, heating value is about 36 MJ/L [13].

1.3.3 Flash point

Flash point is the lowest temperature for the formation of an ignitable air-fuel vapor mixture. Storage and handling regulations for fuels are based on the flash point. In Europe, diesel fuel has to have a flash point higher than 55 ºC while in the US, the Class II liquid requirement for flash point is higher than 38ºC.

1.3.4 Water content

The solubility of water into commercial diesel fuel is very limited. Free water even in a very small quantity will cause problems, for example freezing at low temperatures and damaging the injection systems. A high water content will increase as well the risk of phase separation and even the risk of biological instability.

1.3.5 Corrosion, lubricity

The high-pressure injection system is prone to wear and corrosion. Most diesel fuels are treated with multi-functional additive packages to improve lubricity and suppress

corrosion. Wear of injection systems was a big issue when low-sulfur or sulfur-free fuels were introduced.

1.3.6 Viscosity

Viscosity and fuel density are two important parameters when designing fuel systems. As the fuel density, viscosity should also be kept in a rather narrow window. Low viscosity will increase leakage and delay start of injection in fully mechanical injection systems. High viscosity will impose additional loads on the injection system.

1.3.7 Cold performance properties.

Diesel fuels generally develop start-up and operability problems when vehicles and fuel systems are subjected to cold temperatures. As ambient temperatures cool towards their crystallization temperature, high-molecular weight paraffins (*n*-alkanes C_{18}–C_{30}) in diesel nucleate and form wax crystals suspended in a liquid phase composed of shorter-chain *n*-alkanes and aromatics. The solid wax crystals may plug or restrict flow through filters causing start-up and operability problems [14].

Several parameters have been used to monitor cold properties of diesel. Cloud point[2] (CP), pour point[3] (PP), cold filter plugging point[4] (CFPP), and low-temperature flow test (LTFT) are used to characterize the performance of diesel in tanks and fuel systems during cold weathers.

1.3.8 Cetane number and cetane index

Both cetane number and cetane index are used to measure diesel ignition quality. However, their differences must be highlighted since cetane index is used as a estimation of cetane number.

Within characteristics of diesel set in the R.D. 61/2006, **cetane number** is one of the most important parameter for measuring diesel fuel ignition quality. During the 1930s,

[2] Cloud point (CP): temperature where components form crystals and become visible forming a hazy or cloudy suspension.
[3] Pour point (PP): lowest temperature where the fuel flows or can be pumped.
[4] Cold filter plugging point (CFPP): lowest temperature at which a given volume of fuel passes through a standardized filtration device.

Boerlage and Broeze sought a procedure to determine the ignition quality of diesel fuel that was similar to the octane rating method for gasoline using two reference hydrocarbon fuels: 1-hexadecene and α-methyl naphthalene. The first reference fuel, 1-hexadecene, also known as *cetene* or ketene, has a long, straight chain structure and oxidizes relatively easily. This fuel was assigned a *cetene* (ketene) number of 100.

The second reference fuel, α-methyl naphthalene, also known as 1-methylnaphthalene, has two aromatic rings and is highly resistant to oxidation. This fuel was assigned a *cetene* number of 0. The *cetene* number of a fuel was deemed to be the percentage (by mass) of *cetene* in a blend of *cetene* and α-methyl naphthalene that gave the same ignition performance as the fuel under test.

Cetane number appeared later because cetene is difficult to prepare and it is prone to oxidation during storage. This way, *cetane* (n-hexadecane) was used as a reference fuel instead of cetene.

Because of experimental difficulties in working with α-methyl naphthalene, the reference fuel for the lower end of the *cetane* number scale was later changed to 2,2,4,4,6,8,8-heptamethylnonane, with an assigned *cetane* number of 15. In terms of these two reference fuels, the *cetane* number scale is then defined as follows:

$$\text{CN} = \%\ (\text{v/v})\ \text{hexadecane} + 0.15 \cdot (\%\ (\text{v/v})\ \text{heptamethylnonane}) \tag{1.1}$$

As seen, evaluation of cetane number always imply a fuel performance test, for this reason **cetane index** was created as an estimation of cetane number. Environmental Protection Agency (EPA) suggests the method ASTM D976 based in two variables, density and T_{50} (Temperature corresponding to the ASTM D86 50% distilled point) but the newest equation stands up for a four-variable equation described via ASTM D4737:

$$\begin{aligned}\text{CI} = {} & 45.2 + 0.892 \cdot (\text{T}_{10} - 215) + \{0.131 + 0.901 \cdot [\exp(-3.5 \cdot (\text{D} - 0.85) \\ & -1]\} \cdot (\text{T}_{50} - 260) + \{0.0523 - 0.420 \cdot [\exp(-3.5 \cdot (\text{D} - 0.85)) - 1]\} \\ & \cdot (\text{T}_{90} - 310) + 0.00049 \cdot [(\text{T}_{10} - 215)^2 - (\text{T}_{90} - 310)^2] + 107 \\ & \cdot [\exp(-3.5 \cdot (\text{D} - 0.85)) - 1] + 60 \cdot [\exp(-3.5 \cdot (\text{D} - 0.85)) - 1]^2\end{aligned} \tag{1.2}$$

where

CI = *Cetane index.*

T_{10} = Distillation property via ASTM D86: temperature in ^{o}F at which 10 % (v/v) has evaporated.

T_{50} = Distillation property via ASTM D86: temperature in ^{o}F at which 50 % (v/v) has evaporated.

T_{90} = Distillation property via ASTM D86: temperature in ^{o}F at which 90 % (v/v) has evaporated.

D = Density in g/ml at 15 ^{o}C, via ASTM D1298.

The Ethyl corporation showed that *cetane index* does not have a 1:1 correlation with natural cetane number and the following equation appears to provide a much more precise relationship [12]:

$$\text{Natural cetane number} = 1.154 \cdot \textit{cetane index} - 9.231 \qquad (1.3)$$

1.4 How to solve the problem of diesel engine emissions

It has been seen that exhaust management is a complex process, air excess and high combustion temperatures must be avoided to minimize NO_x emissions but at the same time, combustion temperature and oxygen content in the fuel/air mixture must be acceptable enough to avoid unburned hydrocarbons CO and PM. Ideally, the combustion of diesel would proceed with a short ignition delay and a short premixed combustion phase with a moderate rate of heat release so excessive temperature increase and the subsequent formation of NO_x are avoided. An ideal diesel would at the same time shorten the premixed combustion phase and extend the controlled combustion, where fuel/air mixture would have enough oxygen content to ensure complete combustion of CO and hydrocarbons, specially aromatics and polycyclic aromatic hydrocarbons, so soot formation and particle agglomeration are minimized.

The solution to make the combustion of diesel a cleaner process involves a good spray formation, which means that air and fuel are quickly and homogeneously mixed. Both fuel

injection technology and fuel properties are involved to get a quick vaporization of the fuel as well as good contact air-fuel. Short ignition delays require quality fuels with high cetane numbers. Despite the upgrade in injection technologies and good fuel properties, some of the pollutants described might be released in the combustion process. For this reason end-pipe solutions such as diesel particle filters (DPF), in-cylinder control systems and fuel modification can be needed to lower diesel emissions.

1.4.1 In-cylinder control systems

Most effective in-cylinder control systems in reducing exhaust emissions are exhaust gas recirculation (EGR), advanced injection systems (e.g. Common Rail Systems) and electronic controls [15].

EGR system works introducing part of the exhaust gases into the combustion chamber. This way, oxygen content of the intake air is displaced with exhaust gases that have much lower oxygen content. Although EGR system has been applied in light-duty diesel engines and has been effective in reducing tail-pipe NO_x emissions, the reduction of NO_x is at expense of an increase in other emissions from the engine (such as PM), an increase in engine wear and fuel consumption [15]. EGR systems are usually accompanied of sophisticated and controlled injection systems such as common rail, which allows high pressure injection and multiple injection events along with air handling systems such as EGR.

1.4.2 End-pipe solutions

End-pipe devices to control NO_x emissions were developed in the 1970s. They are called **three-way catalysts** because these devices contain zeolites and precious metals (platinum) to reduce emissions of NO_x, unburned hydrocarbons (HC) and CO at the same time. Zeolites act as adsorber of HC from the exhaust stream. Once adsorbed on the zeolite, hydrocarbons will oxidize and create a locally oxygen poor region that is more conducive to reducing NO_x to N_2. The catalyst can incorporate platinum or other precious metals to promote HC oxidation at lower temperatures. However, the presence of the precious metals can lead to production of sulfate PM. As well, modern diesel engines do

not emit enough unburned hydrocarbons in the exhaust to greatly reduce NO_x since diesel engines operate under oxygen rich conditions.

Nowadays, three-way catalysts are used in combination with **NO_x adsorbers**, which store NO_x in oxygen rich conditions such as those of diesel engines. Unfortunately, the storage capacity of the NO_x adsorber is limited, requiring that the stored NO_X be periodically purged from the storage component. If the stored NO_x is released when the net exhaust chemistry is at stoichiometric or net fuel rich conditions, then the three-way catalyst portion of the catalyst can reduce the NO_x oxidizing HC and CO to water and CO_2.

The NO_x storage process can be further broken down into two steps:

- First the NO in the exhaust is oxidized to NO_2 across an oxidation promoting catalyst, typically platinum [11].
- Then the NO_2 is further oxidized and stored on the surface of the catalyst as a metallic nitrate (MNO_3).

The storage components are typically alkali or alkaline earth metals that can form stable metallic nitrates. The most common storage component is barium carbonate ($BaCO_3$) which can store NO_2 as barium nitrate ($Ba(NO_3)_2$) while releasing CO_2 [11]. In order to the NO_x storage function to work, the NO_x must be oxidized to NO_2 prior to storage and a storage site must be available (the device cannot be “full”). During this oxygen rich portion of operation, NO_x is stored while HC and CO emissions are oxidized across the three-way catalyst components by oxygen in the exhaust. This can result in near zero emissions of NO_x, HC, and CO under the net oxygen rich operating conditions typical of diesel engines.

In order to regenerate the NO_x adsorber, fuel rich operating conditions are needed. The metallic nitrate becomes unstable under net fuel rich operating conditions, decomposing and releasing the stored NO_x. Then the NO_x is reduced to N_2 by reducing agents in the exhaust (CO and HC) across a three-way catalyst system.

Diesel **Selective Catalytic Reduction (SCR)** is an adaptation of stationary technology that has been in use for some time. Ammonia (NH_3) is injected into the exhaust upstream of a vanadium/titanium (V_2O_5/TiO_2) catalyst to reduce NO_x. The following reactions occur:

$$4NH_3 + 4\ NO + O_2 \rightarrow 4N_2 + 6H_2O$$

$$2NH_3 + NO + NO_2 \rightarrow 2N_2 + 3H_2O$$

$$4NH_3 + 3NO_2 \rightarrow 7N_2 + 6H_2O$$

The ammonia is typically stored onboard the vehicle as a urea solution ($(NH_2)_2CO$) since ammonia is hazardous in its raw form. The urea solution is then injected upstream of the catalyst which breaks down the urea into ammonia and carbon dioxide.

Finally, it is to be noted that several exhaust emission control devices have been developed to control diesel PM constituents: the **diesel oxidation catalyst (DOC)** (to reduce the SOF portion of the total PM), several **PM filters** and **catalyzed diesel particle filters (CDPF)**.

PM filters are used in modern vehicles, they are placed at the end of exhaust pipe to trap the particles formed in the combustion. PM filters can reduce PM emissions by 85 to 90% or more, but have the problem of regeneration when they become plugged. Un-catalyzed filters require active regeneration which makes the system more expensive (i.e. increasing fuel consumption). On the contrary, CDPF filters are claimed to be more efficient in trapping PM and employ precious metals to reduce the temperature at which regeneration occurs.

1.4.3 Fuel modification: additives for diesel

Despite the modern technologies employed to reduce diesel emissions, fulfilling stringent regulations seems to be a hard task. This fact has encouraged automotive researchers to look for other options to help control diesel emissions. One such option is control diesel emissions through diesel reformulation because it would affect all type of diesel engines regardless the technology used to reduce emissions.

Fuel modification not only can successfully help to reduce diesel emissions in a simple way. Legislation is becoming progressively stringent with mandatory diesel specifications, forcing oil industry to modify its composition in order to accomplish the new standards. European Parliament enforced measures to improve air quality of diesel engines with Directive 2009/30/EC, which sets some mandatory properties for diesel fuels (Table 1.2).

Table 1.2. Mandatory diesel properties from directive 2009/30/EC [16]

Parameter	Value
Cetane index	≥ 51.0
Density at 15 ºC (kg/m^3)	≥ 845.0
$T_{95\%\ v/v}$ (ºC)[a]	< 360.0
PAH content (% m/m)	≤ 8.0
Sulfur content (mg/kg)	≤ 10.0
FAME[b] content (% v/v)	< 7.0

(a) Maximum distillation temperature to evaporate the 95% of the volume. (b) Fatty acid methyl esters ruled by EN 14214 standard

One way of improving the properties of diesel is by the use of *oxygenates* as additives. In the case of gasoline, fuel *oxygenates* have been used as additives for many years. Ethanol is used most often followed by longer alcohols and ethers alternatively. Unlike gasoline, the question of *oxygenates* for diesel fuels is different because is not regulated by legislation (except vegetable diesel esters (FAME)). Introducing *oxygenates* in diesel shows different advantages and drawbacks depending on the compound.

Within the advantages, it is possible to say that generally, oxygenated blends show a great reduction in the PM emissions further higher than their amount of addition. For instance, introducing 5% (w/w) of diethyl carbonate in diesel fuel reduces from 30% to 50% of particulate matter emissions [17]. It is worth mentioning that reduction in PM emission does not cause a significant increase in the NO_x emissions, which in some cases are even reduced [18]. Some *oxygenates* such as long-chain linear ethers reduce hydrocarbon emissions, CO, PM and soot without increasing NO_x emissions. Some molecules are excellent additives for diesel since, depending on the chain length of the oxygenate, cold-start performance, lubricity and blending cetane number can be improved at the same time [13]. Moreover, the addition of a synthetic oxygenate to

diesel will always imply a reduction of undesirable compounds (such as sulfur and PAH) due to the dilution effect.

The fuel properties of *oxygenates* vary significantly with, e.g., length and type of alkyl chains and some drawbacks can be found depending on the oxygenate. Not all *oxygenates* are cetane number improvers and suitable to be mixed straightforwardly with diesel. Some of them present miscibility problems as it will be discussed in the following lines. Other oxygenates may present undesirable properties such as high pour points and cold filter plugging points (CFPP) that can cause a bad cold-start performance of diesel engines.

Oxygenates are generally polar compounds, whereas hydrocarbon fuels are non-polar. This may result in miscibility problems depending on the chemical structure and oxygen content of the oxygenate. The miscibility problems are aggravated if physical properties, e.g., density, also are very different from the properties of diesel. Thus, only some *oxygenates* are easily miscible with diesel fuel and form stable solutions, e.g., di-n-pentyl ether, whereas to blend ethanol with diesel fuel (emulsified) additives are needed.

Oxygenate candidates with higher molecular weight often have higher density, higher boiling point, higher viscosity, better lubricity, lower volatility, and lower flammability than oxygenates with lower molecular weight. Therefore, they are better suited to be used as diesel fuel components.

Generally, the following considerations regarding *oxygenates* can be taken for cetane number and fluid properties (CP and CFPP) [13]:

Table 1.3. Effect of structure and oxygen content on cetane number and cold properties. Desired effect (tick), undesired effect (X)

Variable	Cetane number	CP, CFPP
Branching in alkyl chain	X	X
Oxygen atoms	✓ [a]	X

(a) Up to 3 ether groups in the structure

Summarizing, the oxygenates capable of being introduced into diesel blends are mainly alcohols, esters, ethers and carbonates. Thus, the following lines will be focused on these possible components.

1.4.3.1 Alcohols

The most studied oxygenated compound is *ethanol*. First research was carried out in South Africa in the 1970s and continued in Germany and the United States during the 1980s. Nowadays, *ethanol* is a form of renewable energy that can be produced from agricultural feedstocks. It can be obtained from very common crops such as sugar cane, potato, manioc and maize (corn). The production of bio-ethanol has been doubled in 5 years. The main producers are Brazil and United States, however, China has sharply increased its production in the last years. On the other hand, *ethanol* also is obtained from petroleum products. It is mainly obtained by means of the catalytic hydration of ethylene. Two million tons of petroleum-derived *ethanol* are produced annually [19].

Several properties must be considered to make compatible the technology of a diesel engine with the properties of *ethanol*-diesel blends. When *ethanol* content was 20-40%, high concentrations of additives are needed to stabilize the mixture or attain the required cetane number. In summary, *ethanol* addition reduces the cetane number, fuel viscosity and the mixture stability [20-22].

1.4.3.2 Esters

Nowadays, *ester* fuels are produced from renewable resources. *Bio-diesel* is the name for a variety of *ester* based oxygenated fuel from biological materials such as vegetable oils, recycled cooking oils, animal fats and plant or forest waste products. The use of *bio-diesel* has presented a promising alternative in the world.

Using a mixture of *esters* provides a reduction of many harmful exhaust emissions. A nearly complete absence of sulfur emissions, reduction in PAH emissions and PM is observed with *ester* mixtures. Nevertheless, *bio-diesel* has high pour point temperatures that could present cold flow problems due to fuel gelling [23-28].

As petroleum supplies are becoming constrained, *bio-diesel* is a growing source of fuel for engines. However, vegetable *esters* are not cetane number enhancers. Methyl *esters* in diesel blends will not achieve the mandatory cetane number of the Directive 2009/30/EC (>51) since they have low cetane numbers. Longer chain length *esters* than methyl esters should be used since longer *esters* such as propyl esters have better fuel properties: higher cetane number, calorific value, melting point and viscosity [29]. In order to synthesize longer *esters*, longer alcohols are needed.

1.4.3.3 Carbonates

The main advantage of the *carbonates* is the high oxygen content in their structure. This fact implies less CO and PM emissions, without an increase in NO_x emissions. For instance, a 5% (w/w) mixture in diethyl carbonate increases from 30 to 50 of reduction in particulate matter [17] Moreover dimethyl and diethyl carbonates are readily prepared from methanol or ethanol [17], so they can be produced from renewable resources.

As it occurs with esters, short carbon chain of these mentioned *carbonates* makes difficult to introduce them directly because of their low cetane number and high latent heat of vaporization [30]. Consequently, in order to use cetane improvers, longer *carbonates* are needed. For example, dioctyl carbonate has a cetane number of 63.9 and dioleyl carbonate a cetane number of 107.2 [31]. However, it has to be mentioned that for the same number of carbon atoms, cetane number is higher in esters than in *carbonates*.

1.4.3.4 Ethers

When *ethers* are added to a diesel fuel in a quantity ranging from 5 to 20 % (vol/vol) all diesel properties are substantially improved [32]. Extensive engine tests have shown that overall exhaust emissions are reduced [33-34]. Due to similar properties of *ethers* to commercial diesel, these *ethers* can be used themselves as a fuel.

Between *ethers*, an interesting group is the glycol-ethers one, since they can be obtained from glycols which are an undesired byproduct of the bio-diesel production [35].

Moreover at the same fuel oxygen content, glycol-ethers show a lower sooting tendency than in an ether blend [36]. However, more research studies to synthesize glycol ethers are required.

Finally, as the other groups, to maintain the commercial diesel properties, long chain *ethers* are the most suitable. Unfortunately, due to the higher price of the reactants, long *ethers* are the most expensive ones. The most important property of *ethers* is that they have much higher cetane numbers than diesel fuel, while alcohols have very low cetane number. Moreover, comparing compounds with the same number of carbon atoms in their structure, *ethers* also have much higher cetane numbers than alcohols [37]. For instance, butanol has a cetane number of 25 [38] and diethyl ether a value around 90.

Within the group of long chain ethers, it was shown that **linear symmetrical and asymmetrical mono-ethers** with **more than 9 carbon atoms** are the most suitable to be added to diesel pool since they seem to give the best compromise between cetane characteristics and the behavior at low temperature [39]. Starting with 10 carbon atoms, asymmetrical and symmetrical *linear* ethers such as di-n-pentyl ether (DNPE) and ethyl-octyl ether (EOE) are interesting because both are cetane number enhancers and lower the pour and cloud points of diesel blend [40]. Since European directives 2009/28/EC and 2009/30/EC impose the introduction of bio-compounds in the automobile fuels there is a raising interest in introducing bio-ethanol to diesel market. This way, *linear* ethyl-alkyl ethers produced from bimolecular dehydration of ethanol and n-alcohols could be a way to incorporate bio-ethanol to diesel pool avoiding the problems of direct blending to diesel fuels [22].

Some properties of linear symmetrical (ROR) and asymmetrical (R_1OR_2) ethers as diesel additives are summarized in Table 1.4. In Table 1.4 linear symmetrical ethers DNPE, DNHE and DNOE as well as linear asymmetrical ether EOE are compared to commercial diesel.

Table 1.4. Properties of some linear ethers

Property	EOE	DNPE	DNHE	DNOE	Commercial diesel
CN	97	109	118	119[a]	51
T_b (ºC)	187	157	219	286	170-380
ρ (kg/m^3)	771	787	793	807	848
CP (ºC)		-20	-5	N/A	-2
PP (ºC)		-25	-7	N/A	-9
CFPP (ºC)		-22	N/A	N/A	-15
μ (cSt)		1.6	N/A	N/A	3.6

(a) blending cetane number

DNHE is a linear *symmetrical* ether suitable for diesel. It has a boiling point in the range of diesel and its addition to gasoil increases the fuel cetane number. For instance, the addition of 5% (v/v) of DNHE to diesel increases its cetane number by 3.5 points [40]. DNOE is even better as cetane number enhancer since the addition of 5% (v/v) of DNOE to diesel increases its cetane number by more than 6 points [40].

Both symmetrical and asymmetrical ethers have good properties as diesel additives. However, synthesizing linear *symmetrical* ethers from n-alcohols has a clear advantage: only the *symmetrical* ether is produced in the bimolecular dehydration of the n-alcohol. On the contrary, asymmetrical ethers produced by bimolecular dehydration of alcohols require a mixture of different n-alcohols, which can end up in a mixture of *symmetrical* and asymmetrical ethers as in the case of EOE synthesis from ethanol and 1-octanol [41].

1.5 Syntheses of C_{10}-C_{10+2n} linear symmetrical ethers

C_{10}-C_{10+2n} linear symmetrical ethers from bimolecular dehydration of n-alcohols can be synthesized over acid catalysts. Tejero *et al.* [42, 43], Bringué *et al.*[44-47] and Medina *et al.*[48] studied the biomolecular dehydration of 1-pentanol to DNPE and 1-hexanol to DNHE over acidic ion exchange resins and zeolites. Analogously, DNOE can be produced through the bimolecular dehydration of 1-octanol over acid catalysts. Unfortunately, in addition to bimolecular dehydration to linear ether (ROR), side reactions can occur.

Intramolecular dehydration of alcohol (ROH) to 1-alkene ($R^{=}$), 1-alkene isomerization to olefins and alcohol-olefin reaction to branched ethers (ROR') can take place as well in the three syntheses. Figure 1.8 shows the general reaction scheme for the dehydration of n-alcohols over acid catalysts.

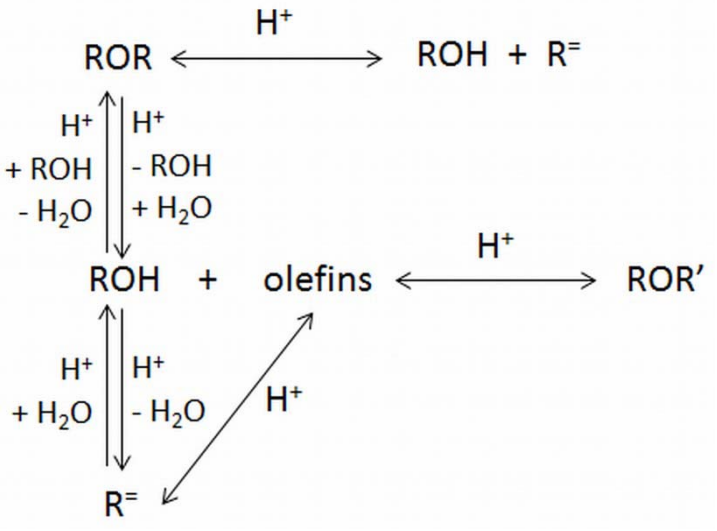

Figure 1.8. General reaction scheme for alcohol dehydration over acid catalysts

In addition, their syntheses might be an option to upgrade refinery streams since 1-octanol, 1-hexanol and 1-pentanol can be produced industrially by the hydroformilation of linear olefins from fluid catalytic cracking or else catalytic polymerization of unsaturated cracker-gas [49, 50]. On the other hand, 1-octanol and 1-hexanol are byproducts of ethanol oligomerization on hydroxyapatite [51]. As a consequence, DNHE and DNOE might be alternatively considered as biodiesel for blend with commercial gasoil.

Literature on the synthesis of DNOE from bimolecular dehydration of 1-octanol on solid acid catalysts is quite scarce [52-54], being absent on ion exchange resins. Hoek *et al.* [52] studied the kinetics of the dehydration of 1-octanol to DNOE with water removal over the zeolite H-BEA. In the study of Hoek a kinetic equation based on LHHW (Langmuir-Hinselwood-Hougen-Watson) mechanism is proposed and further study on water deactivation is suggested. Nel *et al.* [53] studied the dehydration of C_5-C_{12} linear 1-alcohols in gas phase over η-alumina in the range of 250- 350 ºC obtaining high conversions of alcohol but very low selectivity to linear ether, especially at high temperatures.

1.5.1 Catalysts

As seen, bimolecular dehydration of primary alcohols to linear ethers requires acid catalysis. Traditionally, industrial processes for obtaining linear ethers make use of sulfuric acid as catalyst [55]. However, solid acid catalysts have the advantage of easier separation from the reaction mixture [56], and also to yield a reaction product free of blacken compounds. Zeolites and aluminas can be used as catalysts in these dehydration reactions [52-54]; but both types of catalysts require relatively high temperatures to achieve valuable alcohol conversions and are more suitable to intermolecular dehydration because of their high selectivity to olefin formation. Nevertheless, some zeolites have high selectivity to linear ether and present the advantage of high thermal resistance, allowing this way increasing the activity by increasing the working temperature. On the contrary, ion exchange resins have shown good performances in etherification of alcohols. They require lower temperatures and their selectivity to symmetrical ether is normally higher than those of zeolites.

1.5.2 Ion exchange resins

Ion exchange resins are polymeric materials functionalized so they are able to exchange ions with the environment. They offer the advantage of being insoluble, thermally and mechanically resistant. The polymeric matrix is formed by hydrocarbon chains, and a crosslinking agent that can be present in the polymeric matrix in different extent, resulting in a three-dimensional hydrophobic structure. Polymeric matrix is functionalized with the so-called functional groups, which are attached to the matrix and give the resins acid, basic or both characteristics according to the nature of functional groups. Thermal and mechanical resistance of ion exchangers depends on both degree of crosslinking and nature of functional groups.

Within ion exchangers, different types of polystyrene-divinylbenzene (PS-DVB) resins are commonly used in catalysis as well as a perfluoroalkane sulfonic resin called Nafion®. The following lines briefly describe composition and characteristics of these two type of acidic ion exchange resins.

1.5.2.1 Polystyrene-divinylbenzene (PS-DVB) resins

PS-DVB ion exchange resins are based on a polystyrene matrix and a crosslinking agent consisting of divinylbenzene (DVB). The resulting copolymer can be functionalized by means of:

- Acid: As a result, the resin is a cation exchanger. Acids employed can be strong such as sulfuric acid resulting in sulfonic groups (Figure 1.9) or weak carboxylic acids giving carboxylic exchange sites.
- Base: The resulting resins exchange anions and functional groups can be either quaternary ammonia-based groups or polyamines.

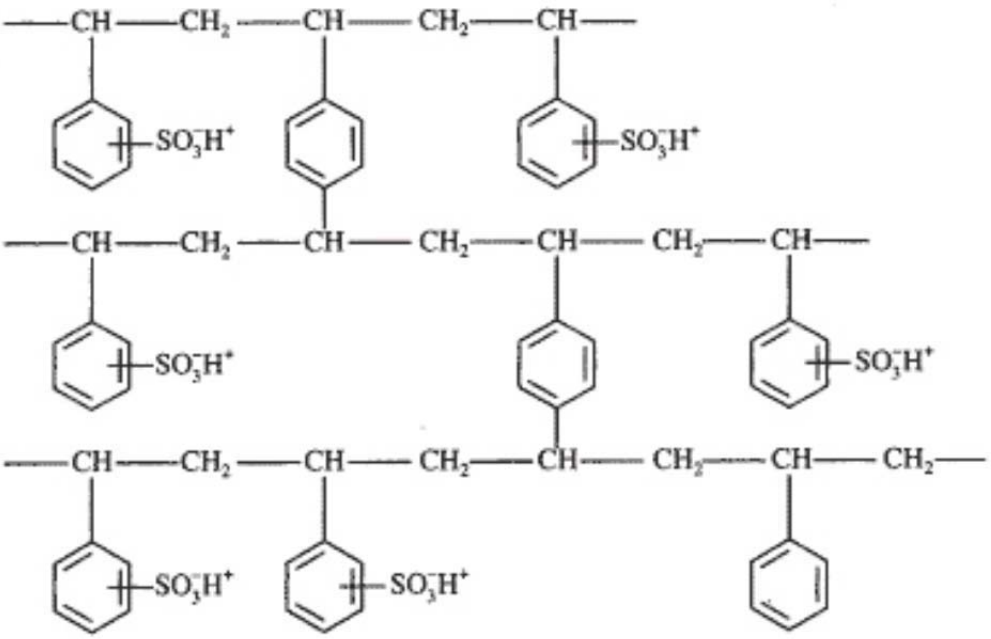

Figure 1.9. Structure of a sulfonated PS-DVB ion exchange resin

PS-DVB ion exchange resins are industrially produced by copolymerization of styrene and DVB in water solution in a stirred reactor. In the process, all the liquids are mixed and styrene-DVB forms big drops in suspension which become smaller as mixing speed rises. When the size of drops is about 1 mm, benzoic peroxide is added and the polymerization starts, generating small plastic spheres as those shown in Figure 1.10. Attending to physical structure of the polymer matrix after being produced, PS-DVB resins can be divided in macroreticular and gel-tpye resins.

Figure 1.10. Small beads of a PS-DVB resin

Gel-type resins contain a 2-8% of DVB, they are synthesized by copolymerization in absence of any porogen agent and thus, they only show porosity when they are swollen in polar media. Its structure is very elastic and they have high swelling capacity in polar solvents.

Macroreticular resins are synthesized with a porogen agent in the copolymerization process (such as heptane or C_4-C_{10} alcohols) that dissolves the monomer but not the polymer. As a result, a permanent porous structure is showed in dry state or in absence of any polar solvent. Macroreticular resins have higher DVB content (8-20% or even more) and its permanent porous structure gives these resins additional physical resistance. However, the higher crossliking degree confers stiffness to the polymeric matrix, making these resins less capable of swelling (Figure 1.11).

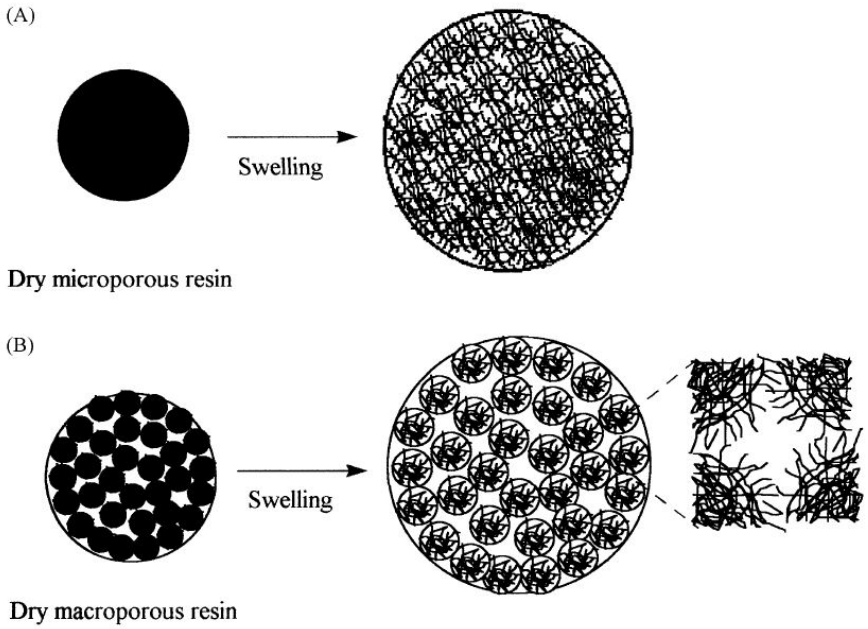

Figure 1.11. Schematic representation of changes in the morphology of gel type bead (A) and macroreticular bead (B) during swelling. The scheme only depicts the basic principles only (not drawn to scale) [57]

Macroreticular resins consist of agglomerates of gel phase microspheres. Between the agglomerates of microspheres a family of macropores (30-80 nm) is found. Macropores are permanent and are responsible of large specific pore volumes of these resins. Mesopores (8-20 nm) are found between gel phase microspheres. They are placed between the nodules of gel phase (Figure 1.12). Macropores can be detected by conventional pore characterization techniques such as nitrogen adsorption or mercury porosimetry. However, mesopores and micropores only appear when the resin is swollen in polar media and they require other techniques to be detected.

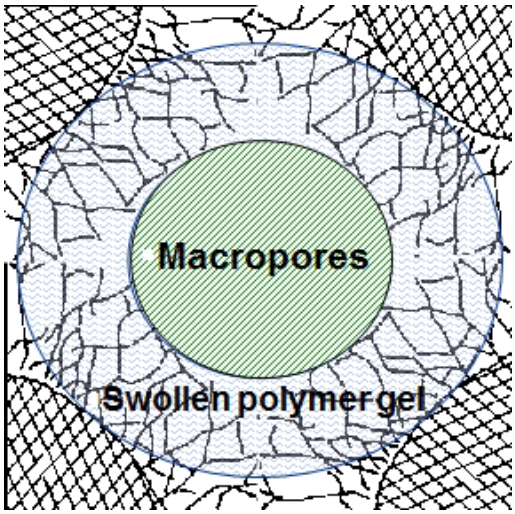

Figure 1.12. Representation of swollen state morphology. Courtesy of K. Jerabek

Until now, only ISEC (Inverse Steric Exclusion Chromatography) technique has been able to characterize the swollen structure of PS-DVB resins. The technique consists on measuring the elution volumes of different solutes of known molecular size, by using a chromatographic column filled with the investigated swollen polymer [58]. This technique permits obtaining polymer density distributions and it will be described in chapter 3.

1.5.2.2 Perfluoroalkane sulfonic resins (Nafion)

Nafion is the commercial name of an ion exchange resin based on the copolymer made of tetrafluoroethylene (Teflon®) and perfluorinated monomers functionalized with sulfonic groups. Teflon® chain acts as a main skeleton and is crossed by the other monomer periodically. Its structure is not completely known but Nafion can be assimilated as hydrophilic regions where ions gather around sulfonic groups. Nafion presents the advantage of having high thermal resistance (up to 210 ºC). Also, the presence of $-CF_2-$ groups in hollow position to sulfonic groups increases the acid strength of such acid groups. Its high price, low porosity, low surface and poor exchange capacity are clear disadvantages.

1.5.3 Zeolites

Zeolites are aluminosilicates of metals of group I and II of the periodic table. They are built with tetrahedrons TO_4, where T is Si^{4+}, Al^{3+} and they are organized in such a way that uniform-size micropores are generated (pore diameter < 2 nm). They can be natural or synthetic and it is possible to control their composition, porous diameter and topology. This way, they offer an endless number of frameworks (Figures 1.13 and 1.14) that can be used in many fields, such as adsorption and gas separation, catalysis, medical applications and any field that requires host-guest interactions.

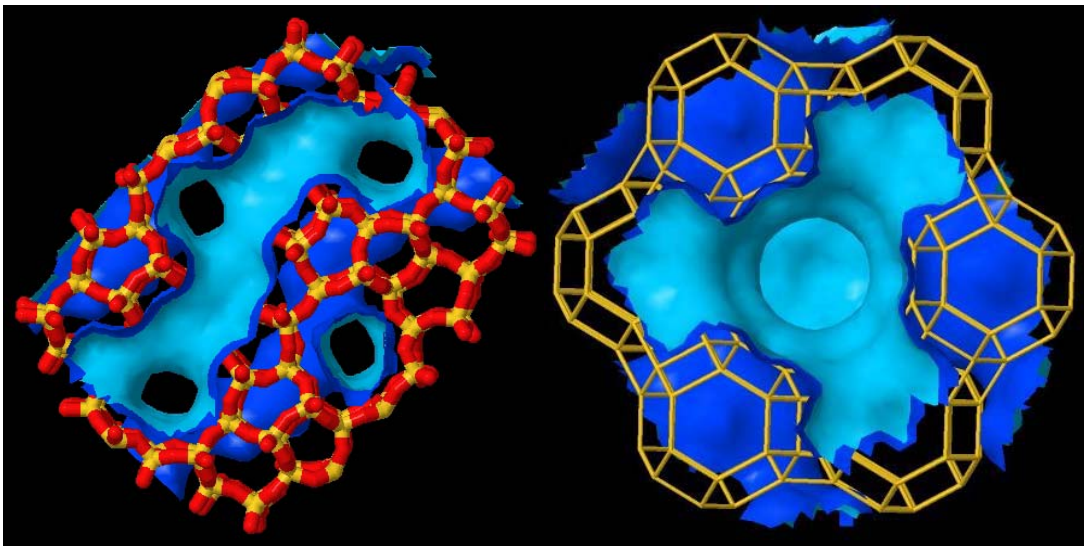

Figure 1.13. Structure and channel systems of MFI (left) and FAU (right) [59]

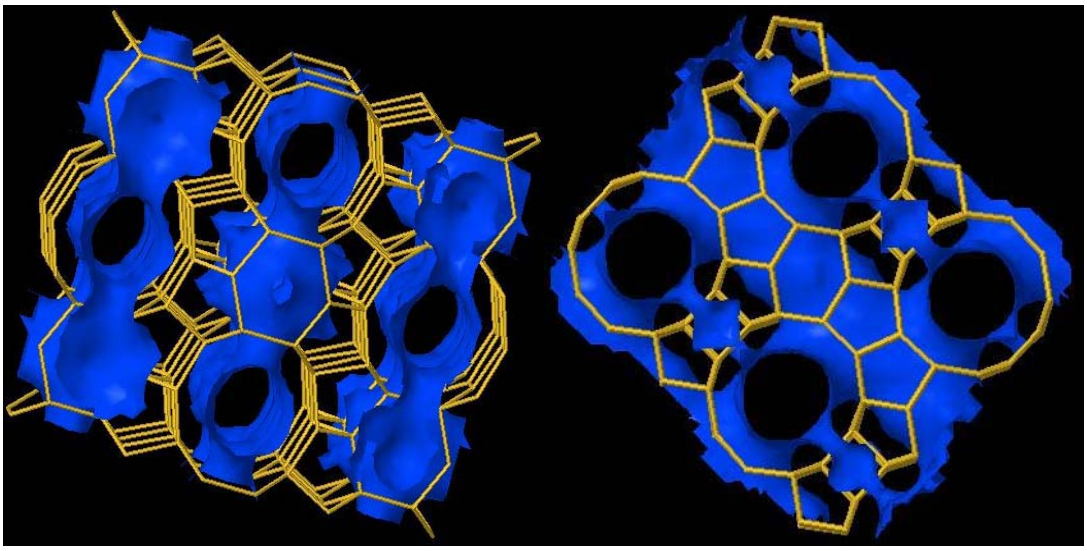

Figure 1.14. Structure and channel systems of FER (left) and BEA (right) [59]

They can be synthesized hydrothermally. Typically, crystallization techniques use water, a source of Si (colloidal silica, silica alcoxydes, etc); a mineralizing agent (OH^-, F^-) and a structure-director agent. The latter fills the pores stabilizing the structure and can be removed after the synthesis by calcination leaving the microporous system.

Generation of active sites on the structure of zeolites is carried out by isomorphic substitution. A zeolite structure composed only by SiO_4^{4-} tetrahedrons is neutral, however, when a AlO_4^{5-} replaces a silica tetrahedron it appears a negative charge. This negative charge can be compensated with an alkaline cation or an organic cation which

acts as a structure director agent. Acidic zeolites can be synthesized with ammonium salts as structure director agent, releasing ammonia when calcined and leaving a H^+ attached to the zeolite structure.

1.6 Kinetics in heterogeneous catalysis

As seen, dehydration reactions of alcohols to linear symmetrical can take place in solid catalysts. Since it is a heterogeneous process and thus, a surface phenomenon is involved, reactants must reach the acid sites of the catalyst and products must be able to leave them and get the bulk phase for the reaction to take place.

The heterogeneous catalytic process by consist of the following elementary steps (Figure 1.15):

A. Diffusion of reactants from fluid phase (bulk phase) to the external layer surrounding the catalyst (external mass transfer).
B. Diffusion of reactants through the catalyst pores (internal mass transfer).
C. Adsorption of reactants on the active site/s.
D. Chemical reaction at the active site/s, which can imply reaction between adsorbed compounds or adsorbed compounds with unadsorbed compounds.
E. Desorption of products on the active site/s.
F. Diffusion of products through the catalyst pores (internal mass transfer).
G. Diffusion of products from external layer to fluid phase (external mass transfer).

Steps A, B, F and G are physical processes whereas C, D and E are of chemical nature. To determine the rate of chemical reaction (process C-D-E), it is necessary to make sure that external and internal mass transfers occur at higher speed than rate of chemical reaction. Mass transfers depend on catalyst particle size, flow conditions at which the reactants and products are in the reactor which can be easily varied to ensure such catalyst and reactor operating conditions to avoid mass transfer limitations.

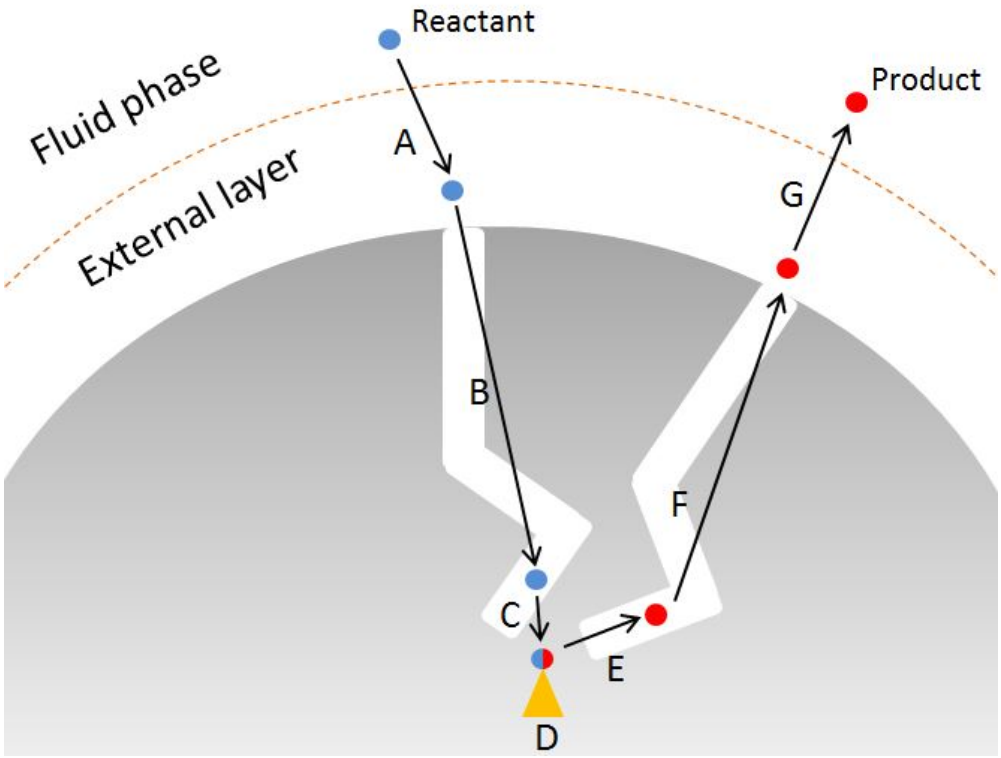

Figure 1.15. Representation of the steps in the heterogeneous catalytic process

To represent the adsorption process of molecules in the active sites, adsorption isotherms are used. Adsorption isotherms are expressions that relate the quantity of adsorbate adsorbed on the catalyst and the concentration of adsorbate in the fluid phase. One of the most used isotherms is Langmuir isotherm, which assumes that the catalyst surface is ideal, which is a surface where molar adsorption enthalpies are constant and independent of the surface coverage.

For a substance A adsorbed in an active site (σ), the adsorption equilibrium:

$$A+\sigma \leftrightarrow A\sigma \tag{1.4}$$

The ideal surface is only covered by a monolayer of molecules, so catalyst surface can be divided in a fraction occupied by the A molecules (θ_A) and the fraction unoccupied (1-θ_A). This way, adsorption rate of A, $r'_{ads,A}$, is proportional to the concentration of A and the fraction unoccupied (1- θ_A) according to de mass action law:

$$r'_{ads,A} = k_{a,A} c_A (1 - \theta_A) \tag{1.5}$$

Correspondingly, desorption rate is then:

$$r'_{des,A} = k_{d,A}\theta_A \tag{1.6}$$

In the equilibrium, adsorption and desorption rates are the same, thus, surface coverage can be written:

$$\theta_A = \frac{K_A c_A}{1 + K_A c_A} \tag{1.7}$$

where, K_A is the adsorption equilibrium constant $k_{a,A}/k_{d,A}$.

Equation 1.7 is the general expression for Langmuir isotherm for single-site adsorption of species A.

To express the chemical reaction rate in the active surface of the catalysts, formalisms based on Langmuir-Hinselwood-Hougen-Watson (LHHW) and Rideal-Eley (RE) mechanisms are used. In those mechanisms three hypothesis are considered:

1. The catalyst surface has a fix number of active sites.
2. All active sites are identical.
3. Reactivity of active sites only depends on the temperature and does not depend on neither the nature nor the quantity of other compounds present in the surface during the reaction.

LHHW mechanisms assume that all the reactants are adsorbed in the catalyst whereas RE mechanisms are a subclass of LHHW mechanisms that consider that some unadsorbed reactants take part in the chemical reaction.

For a simple reaction, A↔P, the general approach is a mechanism with the following elemental steps:

1. Adsorption of A in an active site: A+σ ↔ Aσ
2. Surface chemical reaction: Aσ ↔ Pσ
3. Desorption of P adsorbed in an active site: Pσ ↔ P+σ

Rate of adsorption of A can be written by the law of mass action as:

$$r'_{a,A} = k_{a,A}\left(c_A\hat{c}_v - \frac{\hat{c}_A}{K_A}\right) \tag{1.8}$$

where $\hat{c}_v$ is the concentration of free active sites and $\hat{c}_A$ the concentration of A adsorbed.

Rate of surface chemical reaction:

$$r'_s = \hat{k}\hat{c}_A - \hat{k}'\hat{c}_P = \hat{k}\left(\hat{c}_A - \frac{\hat{c}_P}{\widehat{K}}\right) \tag{1.9}$$

where $\hat{c}_P$ is the concentration of P adsorbed and $\widehat{K}$ the equilibrium constant of surface chemical reaction.

Rate of desorption of P is:

$$r'_{d,P} = k_{a,P}\left(\frac{\hat{c}_P}{K_P} - c_P\hat{c}_v\right) \tag{1.10}$$

These three elemental steps take place in series, but a rate expression accounting the three steps would be too complex. For this reason is common to assume that one of the steps is the rate-limiting one, leading to a more simple equations for reaction rate, all of them with the general scheme:

$$r' = \frac{(Kinetic\ group)(Driving\ force)}{(Adsorption\ term)^n} \tag{1.11}$$

The kinetic group is the product of rate constant of the limiting stage, one or more equilibrium constants and the total number of active sites powered to exponent n, which is the number of active sites involved in the reaction. Total number of active sites is usually unknown and thus, it is generally incorporated to the kinetic group. The driving force is what makes the reaction to take place, being null at the equilibrium. The resistance caused by the adsorption processes in the active sites is represented by the adsorption term and its form depends on the limiting step [60].

CHAPTER 2

SCOPE

In this work, previous studies focused on the synthesis of the linear symmetrical ethers di-n-pentyl ether (DNPE) and di-n-hexyl ether (DNHE) from 1-pentanol and 1-hexanol respectively have been extended. At the same time, to continue with the series of linear symmetrical ethers, di-n-octyl ether (DNOE) synthesis from 1-octanol has been extensively studied, as well as compared with the syntheses of DNPE and DNHE.

For the mentioned purposes, the following objectives have been settled:

1. Check that *1-octanol dehydration to DNOE* can be successfully carried out over acid solid catalysts such as zeolites and PS-DVB ion exchange resins.

2. Carry out a catalyst screening over PS-DVB ion exchange resins for DNPE, DNHE and DNOE syntheses to evaluate the influence of morphological characteristics of PS-DVB *resins* on the synthesis of *DNOE* and compare it with *DNHE* and *DNPE* syntheses.

3. Carry out a catalyst screening to evaluate the influence of *zeolites* textural parameters and different zeolites frameworks on the syntheses of *DNOE*, *DNHE* and *DNPE.*

4. Evaluate the *equilibrium* constant of the dehydration reaction of *1-octanol to DNOE* and main side reactions.

5. Carry out a *kinetic study* and propose a kinetic equation with mechanistical basis for the 1-octanol dehydration to *DNOE* over the thermostable *ion exchange resin* Amberlyst 70 and compare it with DNHE and DNPE syntheses found in the literature.

7 Carry out a *kinetic study* and propose a kinetic equation for the 1-octanol dehydration to *DNOE* and 1-hexanol to *DNHE* over *zeolites* and compare them with the kinetic equation for DNPE synthesis found in the literature.

CHAPTER 3

EXPERIMENTAL

3.1 Chemicals

Purity and source of chemicals used for reactions and as chromatographic patterns in this work are summarized in Table 3.1

Table 3.1. Purity and source of chemicals used in this work

Chemical	Purity	Source
1-octanol	>99% (G.C)	Fluka
DNOE		Fluka
1-octene		Fluka
1-hexanol	99.5% (< 0.3% 2-methyl-1-pentanol, 0.1% water)	Supplied by Fluka and purified by rectification
DNHE	≥ 98%	Obtained in our lab and purified by rectification
1-hexene	≥ 99%	Aldrich
Trans-2-hexene	≥ 98%	Fluka
Cis-2-hexene	≥95%	Fluka
Trans-3-hexene	≥ 97%	Fluka
Cis-3-hexene	≥ 95%	Fluka
2-methyl-1-pentanol	≥ 99%	Fluka
1-pentanol	99% (<1% 2-methyl-1-butanol)	Fluka
DNPE	≥ 99%	
1-pentene	≥ 97%	
Cis-2-pentene	≥ 98%	
Trans-2-pentene	≥ 99%	
2-methyl-1-butanol	≥ 98%	
water		Bidistilled in our lab

3.2 Catalysts

Catalysts employed in this work are ion exchange resins and zeolites. PS-DVB ion exchange resins were used, including high, medium and low-DVB content resins with acid capacities ranging from 0.43 to 5.4 meq H^+/g. The perfluoroalkane sulfonic resin Nafion was employed too. Different structured zeolites (framework types BEA, Faujasite, Mordenite, Ferrierite and MFI) with acid capacities ranging 1-4.6 meq H^+/g were used, as well as MCM material H-MCM-41.

3.2.1 Acidic ion exchange resins

Ion exchange resin catalysts were supplied by Rohm and Haas (Amberlyst 15, Amberlyst 16, Amberlyst 31, Amberlyst 35, Amberlyst 36, Amberlyst 39, Amberlyst 46,

Amberlyst 70 and Amberlyst 121), Purolite (CT 175, CT 224, CT 252, CT 275 and CT 276) and Aldrich (Dowex 50Wx4-50, and Nafion NR50). Main characteristics supplied by the manufacturer and short names are listed in Table 3.2. Physical and textural characterization of ion exchange resins will be discussed in section 3.4.2

Table 3.2. Characteristics of tested ion exchange resins supplied by the manufacturer

Catalyst	Short name	Structure[a]	Sulfonation Type[b]	DVB%
Amberlyst 15	A-15	Macro	C	20
Amberlyst 35	A-35	Macro	O	20
CT 175	CT-175	Macro	C	High
CT 275	CT-275	Macro	O	High
CT 276	CT-276	Macro	O	High
CT 252	CT-252	Macro	O	Medium
Amberlyst 16	A-16	Macro	C	12 [61]
Amberlyst 36	A-36	Macro	O	12 [62]
Amberlyst 39	A-39	Macro	C	8 [63]
Amberlyst 70	A-70	Macro	C	8
CT 224	CT-224	Gel	O	4
Amberlyst 31	A-31	Gel	C	4 [62]
Amberlyst 121	A-121	Gel	C	2 [63]
Dowex 50Wx4-50	DOW5050	Gel	C	4
Amberlyst 46	A-46	Gel	S	High
Nafion NR50	NR50	Gel	-	-

(a) Macroreticular structure (Macro) or gel-type structure (Gel). (b) Conventionally sulfonated (C), oversulfonated (O) and sulfonated only at polymer surface (S)

3.2.2 Acidic zeolites

H-ZSM-5 ($SiO_2/Al_2O_3 \approx 28$) from Degussa Iberica (Barcelona, Spain); H-Beta ($SiO_2/Al_2O_3 \approx 25$) and US-Y ($SiO_2/Al_2O_3 \approx 6$) supplied by Südchemie (Bruckmühl-Heufeld, Germany); CBV 720 faujasite ($SiO_2/Al_2O_3 \approx 30$), CBV 21A mordenite ($SiO_2/Al_2O_3 \approx 20$) and CP 914C ferrierite ($SiO_2/Al_2O_3 \approx 20$) from Zeolyst Int. (Valley Forge, PA, USA), and MCM-41 ($SiO_2/Al_2O_3 \approx 79$) from Aldrich (USA) were used as catalysts. Henceforth, they will be called called H-MFI-28, H-BEA-25, H-FAU-6, H-FAU-30, H-MOR-20, H-FER-20 and H-MCM-79, respectively. In section 3.5 their physical and textural properties will be discussed.

3.3 Set up, analysis and experimental procedure

3.3.1 Set up

Syntheses of DNPE, DNHE and DNOE were carried out in a 100 cm^3 nominal stainless steel autoclave operated in batch mode at the temperature range of 413-473 K. The temperature was controlled to within ± 0.1 K by an electrical furnace. The pressure was set at 2.5 MPa by means of N_2 to maintain the liquid phase. The reactor outlet was connected directly to a sampling valve, which injected 0.2 mm^3 of liquid into a GLC apparatus. The catalyst was injected by means of a catalyst injector consisting of a pressurized vessel connected to the reactor. The reaction was controlled by a PC with a designed LabView software program. Details of the experimental setup are showed in figure 3.1.

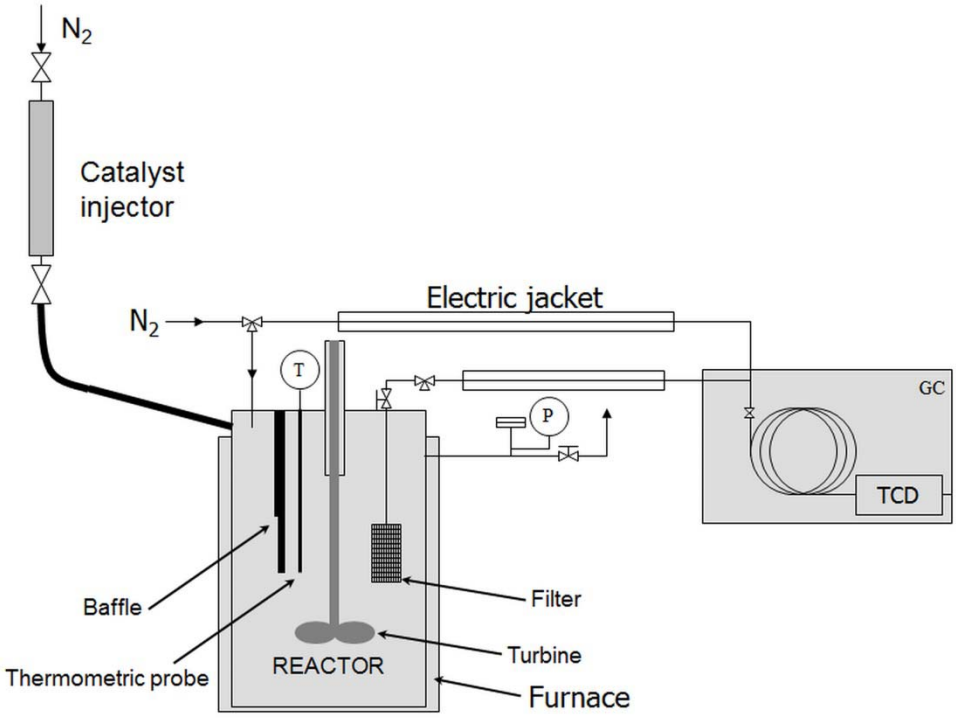

Figure 3.1. Scheme of the experimental set up employed

3.3.2 Analysis

Analyses were carried out by means of a Hewlett-Packard HP6890A GLC equipped with a TCD. A HP-Pona Methyl Siloxane (HP 190915-001) capillary column (50 m length×200 µm I.D.×0.5 µm width of stationary phase) was used to determine the substances present

in the reaction medium. The capillary column was temperature programmed by means of an oven, which maintained the temperature of the column and increased it to separate the different substances. Temperature conditions of capillary column as well as chemicals identified for DNOE, DNHE and DNPE systems are shown in Table 3.3.

Table 3.3 Temperature conditions of capillary column and chemicals identified

Reaction system	Chemicals determined	Column conditions		Reference
		Initial and final temperature (T_0, T_f)	Time (min)	
DNOE	water, 1-octene, 2- octene (cis/trans), 3-octene (cis/trans), 4-octene, 1-octanol, DNOE and C_{16} branched ethers	T_0 = 323 K	0	This work
		Ramp = 10 K·min^{-1}	20	
		T_f = 523 K	6	
DNHE	water, 1-hexene, 2-hexene, 3-hexene, 1-hexanol, DNHE and C_{12} branched ethers (2,2-oxybis hexane and 1,2-oxybis hexane)	T_0 = 318 K	6	[48]
		Ramp = 30 K·min^{-1}	4.5	
		T_f = 453 K	10	
DNPE	water, 1-pentene, 2-pentene 1-pentanol, DNPE and branched ethers (1-(1-methylbutoxy)-pentane, 1-(2-methylbutoxy)-pentane, 2-(1-methylbutoxy)-pentane, and 2-(2-methylbutoxy)-pentane)	T_0 = 318 K	6	[44]
		Ramp = 30 K·min^{-1}	4.5	
		T_f = 453 K	5	

In all systems Helium (30 mL·min^{-1}) was the carrier gas and all the species were identified with a GLC equipped with MS (Agilent GC/MS 5973) and chemical database software.

Chromatographic areas of each compound were correlated with the mass percentage by means of calibration equations obtained from standard mixtures of known composition. Calibration equations and an example of a chromatograph for 1-octanol dehydration to DNOE are shown in APPENDIX III.

3.3.3 Experimental procedure

The catalysts used were pretreated as follows:

Ion exchange resins were dried at 383 K firstly at 1 bar for at least 1 h and secondly in a vacuum oven for 15 h at 10 mbar and 373 K.

Zeolites were activated at the optimal temperature in a muffle furnace. Optimal activation temperature was found to be 773 K for all the zeolites tested but H-MFI-28, which was 673 K [65]. DSC and TG analysis showed that at such temperatures all the zeolites have a nearly constant weight after losing water and ammonia. After activation, catalysts were maintained in a vacuum oven for 15 h at 10 mbar and 373 K.

The procedure with the batch reactor varied according to the type of experiment:

For the catalytic screening with ion exchange resins and zeolites the reactor was loaded with 70 cm^3 of liquid. The liquid mixture was then pressurized at 2.5 MPa, warmed up to the working temperature (423-473 K) and stirred at 500 rpm. Once the working temperature was reached, 1 gram of dried catalyst was placed in the catalyst injector, pressurized and quickly injected into the reactor by means of the pressure difference between the catalyst injector and the reactor. The moment the catalyst was injected was considered as the zero time of the experiment. Samples were taken hourly until the end of experiment (6 h).

In such operating conditions, dehydration of 1-pentanol to DNPE and 1-hexanol to DNHE take place free of the influence of mass transfer limitations [44,48]. Liquid samples were taken out hourly and analyzed online to follow the reaction until the end of the experiment for 6 h. In each experiment, the alcohol conversion (X_{ROH}), selectivity to linear symmetrical ether (S_{ROH}^{ROR}), olefins ($S_{ROH}^{C=}$), and branched ethers ($S_{ROH}^{ROR'}$), as well as yield of linear symmetrical ether (Y_{ROH}^{ROR}) relative to alcohol, were estimated by the expressions 3.1-3.5. Estimated values of conversion, selectivity and yield did not vary further than 2% within replicated experiments.

$$X_{ROH}(t) = \frac{\text{mole of alcohol reacted}}{\text{mole of alcohol initially}} = \frac{n_{ROH}^0 - n_{ROH}(t)}{n_{ROH}^0} \times 100 = \quad (3.1)$$

$$= \frac{2 \cdot n_{ROH}(t) + n_{C=}(t) + 2 \cdot n_{ROR}(t)}{n_{ROH}(t) + 2 \cdot n_{ROR}(t) + n_{c=}(t) + 2 \cdot n_{ROR'}(t)} \times 100 \left[\% \frac{mol}{mol}\right]$$

$$S_{ROH}^{ROR}(t) = \frac{\text{Mole of alcohol reacted to form linear ether}}{\text{Mole of alcohol reacted}} \times 100 = \\ = \frac{2 \cdot n_{ROR}(t)}{2 \cdot n_{ROR}(t) + n_{C=}(t) + 2 \cdot n_{ROR'}(t)} \times 100 \left[\% \frac{mol}{mol}\right] \quad (3.2)$$

$$S_{ROH}^{C=}(t) = \frac{n_{C=}(t)}{2 \cdot n_{ROR}(t) + n_{C=}(t) + 2 \cdot n_{ROR'}(t)} \times 100 \left[\% \frac{mol}{mol}\right] \quad (3.3)$$

$$S_{ROH}^{ROR'}(t) = \frac{2 \cdot n_{ROR'}(t)}{2 \cdot n_{ROR}(t) + n_{C=}(t) + 2 \cdot n_{ROR'}(t)} \times 100 \left[\% \frac{mol}{mol}\right] \quad (3.4)$$

$$Y_{ROH}^{ROR}(t) = \frac{\text{Mole of alochol reacted to form linear ether}}{n_{ROH}^{0}} \times 100 = \\ = \frac{S_{ROH}^{ROR}(t) \cdot X_{ROH}(t)}{100} \left[\% \frac{mol}{mol}\right] \quad (3.5)$$

Initial reaction rates of symmetrical ether (ROR) formation and alcohol (ROH) consumption were computed from the functions of variation of n_{ROR} (mole of ROR) and n_{ROH} (mol of alcohol), respectively, vs. time:

$$r_{ROR}^{0} = \frac{1}{W}\left(\frac{dn_{ROR}}{dt}\right)_{t=0} \left[\frac{mol}{h \cdot kgcat}\right] \quad (3.6)$$

$$-r_{ROH}^{0} = \frac{1}{W}\left(\frac{dn_{ROH}}{dt}\right)_{t=0} \left[\frac{mol}{h \cdot kgcat}\right] \quad (3.7)$$

Initial turnover frequency, TOF, for both ROR formation and ROH consumption were estimating by dividing r_{ROR}^{0} and r_{ROH}^{0} by the acid capacity, respectively:

$$TOF_{ROR}^{0} = \frac{r_{ROR}^{0}}{\text{acid capacity}} \left[\frac{mol}{h \cdot \text{eq } H^{+}}\right] \quad (3.8)$$

$$TOF_{ROH}^{0} = \frac{r_{ROH}^{0}}{\text{acid capacity}} \left[\frac{mol}{h \cdot \text{eq } H^{+}}\right] \quad (3.9)$$

From equations 3.6 to 3.9 it follows that linear ether formation and alcohol consumption rates, and turnover numbers, are related by:

$$r_{ROR} = S_{ROH}^{ROR} \frac{-r_{ROH}}{2} \quad (3.10)$$

$$TOF_{ROR} = S_{ROH}^{ROR} \frac{-TOF_{ROH}}{2} \quad (3.11)$$

For equilibrium determination experiments, reactor was loaded with 70 cm^3 of liquid and 4 grams of dried Amberlyst 70. Amberlyst 70 was selected for equilibrium experiments because of its thermal stability and high selectivity to linear ether formation. Pressure was set at 2.5 MPa, working temperature ranged 413-453 K and stirred speed was set at 300 rpm to avoid catalyst attrition. Samples were taken daily until reaching a constant composition with time (50-75 h).

For the kinetic-type experiments over Amberlyst 70, reactor was loaded with 70 cm^3 of liquid, pressurized at 2.5 MPa, warmed up at the working temperature (413-453 K) and stirred in the range 100-800 rpm. Once the working temperature was reached, 0.5-4 g of Amberlyst 70 (d_p = 0.12-0.9 mm) were injected into the reactor. Liquid samples were taken hourly to follow the reaction until the end of experiment for 6-7 h.

Kinetic experiments over zeolites were analogue to those over Amberlyst 70. Working temperature was 423-473 K, 1 gram of zeolite was used and stirring speed was set at 500 rpm.

3.4 Physical and textural characterization of ion exchange resins

Macroreticular resins used include polymers of low (Amberlyst 39 and 70), medium (Amberlyst 16 and 36, and CT 252) and high crosslinking degree (Amberlyst 15 and 35, and CT 175, CT 275 and CT 276); gel type ones include resins containing from 2 to 8 DVB%. As for sulfonation degree, selected resins include conventionally sulfonated (a –SO_3H group per styrene ring) and oversulfonated (a –SO_3H group per benzene ring). Amberlyst 35 and 36 (*acid capacity* > 5 meq H^+/g) are oversulfonated versions of Amberlyst 15 and 35 (*acid capacity* ≤ 5 meq H^+/g), respectively, and CT 275 and CT 276 of CT 175 (see Table 3.4). Special properties of Amberlyst 70 (with hydrogen atoms of polymer chain substituted by chlorine), Amberlyst 46 (sulfonated *only at the* polymer surface) and NR50 (a gel-type copolymer of Teflon® and perfluoro-alkanesulfonic monomers) have to be emphasized. Fluorine atoms of polymer chains upgrade thermal stability of NR50 and give a higher *acid strength* than PS-DVB resins.

Acid strength was represented by the molar *adsorption enthalpy of ammonia* (ΔH_{ads}), obtained by calorimetric measurements using a combination of differential scanning calorimeter and a downstream mass spectrometer detector. The experimental set up employed for adsorption enthalpy calculations is described by Felix *et al*. [66], but using a mass spectrometer detector instead of a TCD (for calorimeter set up used in the present work and procedure see APPENDIX IV). The value of ΔH_{ads} was obtained calculating the average value of the differential molar enthalpy of adsorption of the irreversibly adsorbed pulses of ammonia up to a given surface coverage (see Table 3.4).

Table 3.4. Physical properties of tested ion exchange resins

	Catalyst	Sulfonation type	Acid capacity[a] (meq H^+/g)	ΔH_{ads}[b] (kJ/mol)	d_b (mm)
High DVB% Macro	A-15	C	4.81	-112	0.74[c]
	A-35	O	5.32	-125	0.51[c]
	CT-175	C	4.98	-120	0.94[f]
	CT-275	O	5.2	-123	0.72[c]
	CT-276	O	5.2		0.76[d]
Medium and low DVB% Macro	CT-252	O	5.4	-138	0.78[d]
	A-16	C	4.8		0.6-0.8[d]
	A-36	O	5.4	-128	0.63[d]
	A-39	C	5.0		0.71[d]
	A-70	C	3.01		0.57[c]
Gel	CT-224	O	5.34		0.32[d]
	A-31	C	4.8	-135	0.62[c]
	A-121	C	4.8	-136	0.77[d]
	DOW5050	C	4.95		0.57[d]
Gel	A-46	S	0.43	-113	
	NR50	-	0.885		2.4[d]

(a) Titration against standard base [67]. (b) Values obtained by calorimetric pulsed NH_3 adsorption measurements. (c) By sieving at atmospheric humidity or from SEM microphotographs. (d) Manufaturer data

Ion exchange resin catalysts are nearly *spherical beads* of sulfonated PS-DVB copolymers. As aforementioned, *macroreticular* resins consist of large agglomerates of gel microspheres, and each micro-sphere shows smaller nodules that are more or less fused together [67]. In between the nodules there is a family of very small pores (micropores), and in between the micro-spheres a second family of intermediate pores with diameter 8–20 nm (mesopores) is observed. A third family of large pores with diameter 30–80 nm is located between the agglomerates (macropores). Macropores are permanent and can be detected by standard techniques of pore analysis, i.e. adsorption–desorption of N_2 at 77 K. Meso- and micropores are non-permanent, and appear when

resin swells by the interaction with the reaction medium. SEM photo-micrographs (Hitachi H-2300) of Amberlyst 15 and CT 224 are shown in Figs. 3.2 and 3.3, respectively, under magnification of 50 and 6000. Commercial beads are nearly spherical (Figs. 3.2 A and 3.3 A).

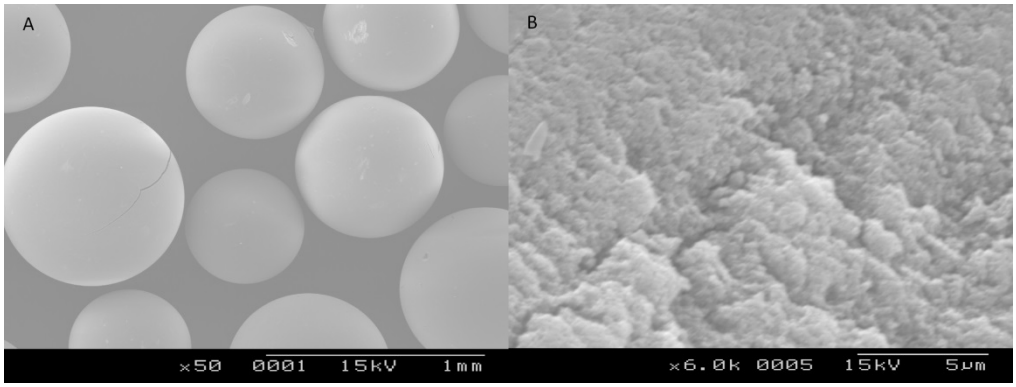

Figure 3.2 SEM micrographs of Amberlyst 15. (A) General view of beads (magnification 50). (B) Surface detail of a bead (magnification 6000)

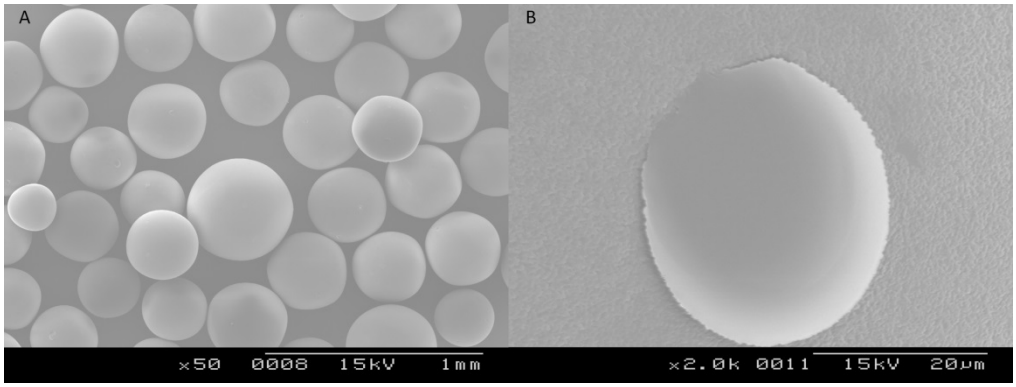

Figure 3.3. SEM photomicrographs of CT 224 (A). General view of beads (magnification 50). (B) Surface detail of a bead (magnification 6000)

A surface view of Amberlyst 15 shows aggregates of microspheres of about 0.5 µm each (Fig. 3.2 B) in agreement with literature [69]. On the contrary, CT 224 surface is smooth and aggregates are not seen. Amberlyst 15 morphology is illustrative of dry *macroreticular* resins of high and medium crosslinking degree, and CT 224 of *gel-type* ones.

Table 3.5 shows skeletal density and textural parameters estimated from N_2-adsorption data at 77 K (Tristar 3000). N_2 adsorption isotherms of macroreticular resins are of type II, typical of macroporous solids [70], as Fig. 3.4 shows for Amberlyst 15 and CT 276 (high croslinking degree).

Table 3.5. Textural parameters of tested resins in dry state and swollen in water

Catalyst	ρ^{a}_{s} (g/cm^3)	Dry state: Adsortion-desorption of N_2 at 77K[b]				Swollen in water (ISEC method)				
						"True pores"			Gel polymer	
		S_{BET} (m^2/g)[c]	V_{pore} (cm^3/g)[d]	d_{pore}[e] (nm)	θ (%)	S_{area} (m^2/g)	V_{pore} (cm^3/g)	d_{pore}[e] (nm)	V_{sp} (cm^3/g)	θ (%)
A-15	1.41	42.0	0.33	31.8	31.7	157	0.63	16.1	0.82	51.5
A-35	1.54	28.9	0.21	23.6	24.5	194	0.63	13.0	0.74	52.3
CT-175	1.50	28.0	0.30	42.9	31.0	157	0.82	20.9	1.00	63.5
CT-275	1.51	21.8	0.18	32.9	21.0	183	0.91	19.9	0.81	61.3
CT-276	1.49	23.5	0.21	40.8	23.7	176	0.66	15.1	0.77	53.0
CT-252	1.49	22.4	0.221	44.4	24.8	132	0.49	14.9	0.98	54.5
A-16	1.40	1.69	0.01	29.7	1.8	149	0.38	10.3	1.25	56.2
A-36	1.57	21.0	0.14	27.0	18.3	147	0.33	9.10	1.00	52.1
A-39	1.42	0.09	$2.9\cdot10^{-4}$	17.6	0.00	181	0.36	7.90	1.45	61.0
A-70	1.52	0.02			0.00	176	0.36	8.10	1.40	62.5
CT-224	1.42	0.95	0.01	3.00	0.08				1.81	61.2
A-31	1.43	0.10	$3.3\cdot10^{-4}$	15.3	0				1.93	63.7
A-121	1.43	0.02	$3.5\cdot10^{-4}$	32.9	0.00				3.26	78.5
DOW5050	1.43	0.01			0.00				1.92	63.5
A-46	1.14	57.4	0.26	19.2	23.0	186	0.48	10.30	0.16	0.00
NR50	2.04	0.35	$2.0\cdot10^{-4}$	3.20	0.04					

(a) Skeletal density. Measured by helium displacement (Accupic 1330). (b) samples dried at vacuum (10^{-4} mmHg. 110 ºC). (c) BET method. (d) Volume of N_2 adsorbed relative pressure (P/P_0) = 0,99. (e) $d_{pore} = 4\ V_{pore}/S_{BET}$ or $d_{pore} = 4\ V_{pore}/S_{area}$, respectively

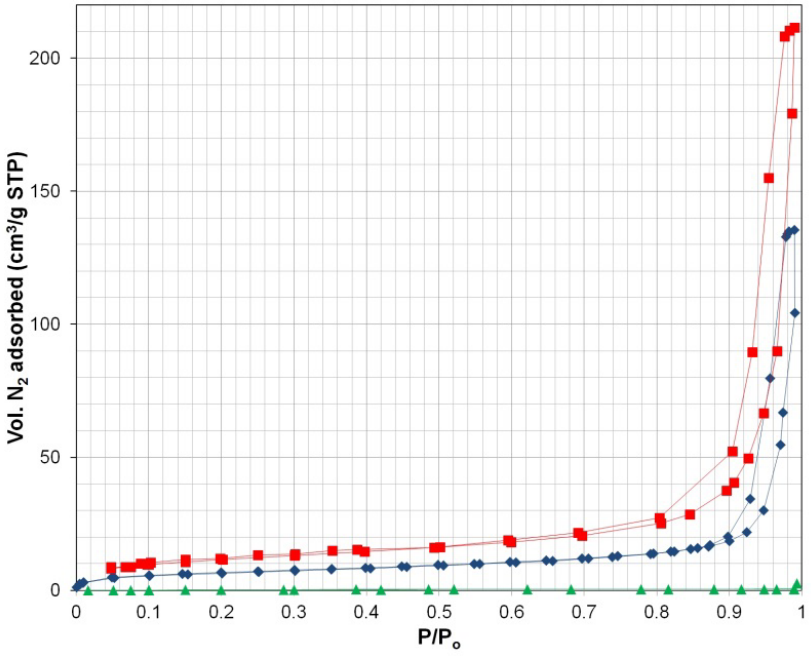

Figure 3.4. Nitrogen adsorption isotherm at 77 K of CT 276 (rhombus), A-15 (square) and CT 224 (triangle)

Despite N_2 adsorption data on ion-exchange resins are scarce, those of Amberlyst 15 agree well with literature (Table 3.6). Adsorption–desorption curves show H1 hysteresis,

typical of solids made by aggregates of spherical particles. Pores have quite uniform size and shape.

Table 3.6. Volume of N_2 adsorbed at 77 K for Amberlyst 15

P/P_0	N_2 adsorbed (cm^3 STP/g)	
	This work	Kunin *et al*. [71]
0.82	27	25
0.552	16.5	16.7
0.5	10	10.8

Barret-Joyner-Halenda (BJH) pore size analysis from desorption curve shows a unimodal distribution in the macroporous region with a maximum around 330 Å(Fig. 3.5).

For Amberlyst 15 this value agree with those reported by Umar *et al*. [72] and Sundmacher and Hoffmann [73]. On the contrary, gel-type resins, for example CT 224, show type I isotherm but as seen, the whole pore volume is very small.

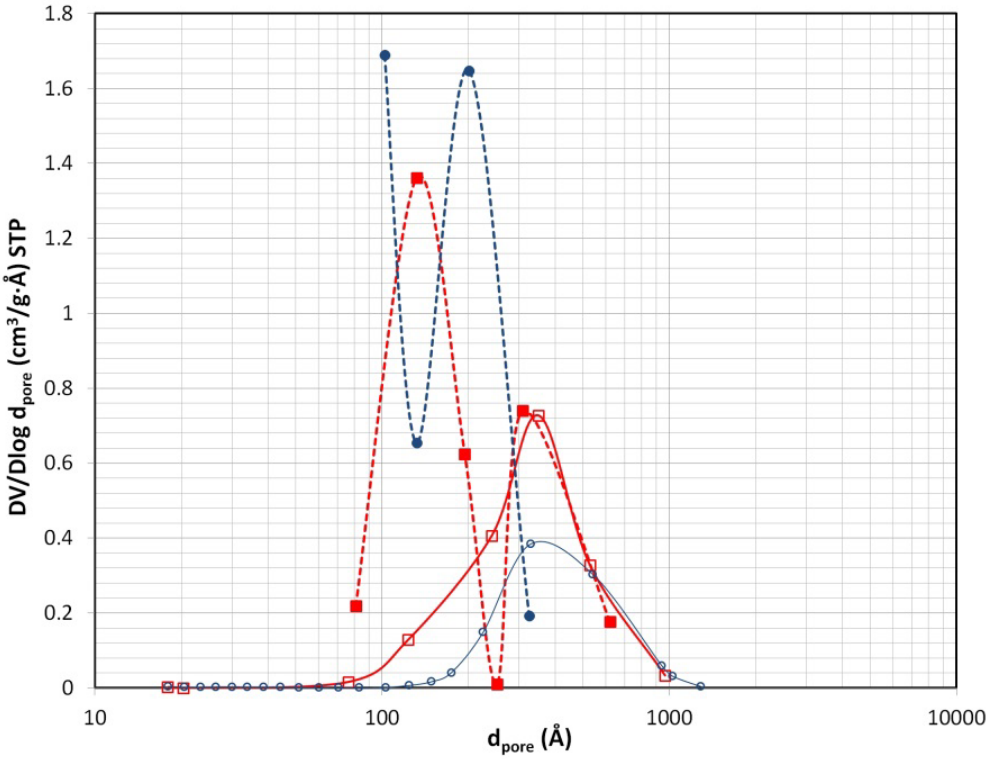

Figure 3.5. Pore size distribution from desorption N_2 curve of A-15 (full square) and CT 276 (full circle), and from ISEC data, A-15 (empty square) and CT 276 (empty circle)

It is well known that ion-exchange resins swell in polar media. As a result, morphology changes and non-permanent pores appear. A useful description of nature and characteristics of these pores can be obtained by Inverse *Steric Exclusion Chromatography* (ISEC) [58]. In macroreticular structures a part of new open spaces (mesopores, between aggregates) can be characterized by the cylindrical pore model. However, this model is not applicable to describe spaces between polymer chains formed by aggregates and nodules swelling. A good view of the three-dimensional network of swollen polymer is given by the geometrical model developed by Ogston [74], in which micropores are described by spaces between randomly oriented rigid rods.

The characteristic parameter of this model is the *specific volume of the swollen polymer* (volume of the free space plus that occupied by the skeleton), V_{sp}. The Ogston model also allows distinguishing zones of swollen gel phase of different density or polymer chain concentration (total rod length per volume unit of swollen polymer, in nm/nm^3 or nm^{-2}). According to this model, density of swollen gel phase is described as the total rod length per unit of volume.

As shown in Table 3.5, macroreticular resins with high and medium crosslinking degree have permanent macropores in dry state. It is to be noted that Amberlyst 16, 39 and 70 resins with DVB% close to 8 show a very low BET surface area. However, comparing with ISEC data, it is clear that those new pores are open in aqueous media: surface area ranges between 132 and 194 m^2/g, and pore volume between 0.36 and 0.91 cm^3/g. Both parameters are far higher than dry state ones showing that new intermediate pores (mesopores) are accessible. Correspondingly pore diameter in aqueous medium is lower than in dry state. Fig. 3.5 shows the pore distribution originated by swelling in CT 276 and Amberlyst 15. In gel-type resins no mesopores originate from the swelling by water or alcohol.

Fig. 3.6 shows the pore distribution in the swollen gel phase, quite representative of the morphology of swollen acidic resins in aqueous alcohol solution. V_{sp} decreases as

DVB% increases both in gel-type and low DVB% macroretucular resins (Fig. 3.6 A) and medium and high DVB% macroreticular resins (Fig. 3.6 B).

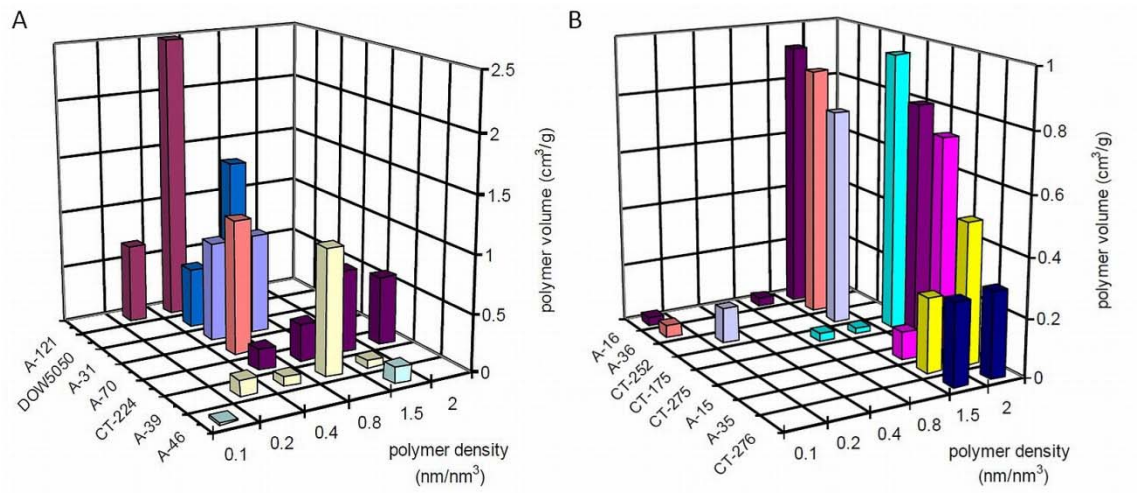

Figure 3.6. ISEC pattern displayed by resins in water. (A) Polymer density distribution of gel-type and low DVB% macroreticular resins. (B) Id. for medium and high DVB% macroreticular resins

It is seen that swollen gel phase of gel-type and low-crosslinked macroreticular resins show chains concentrations of 0.4–0.8 nm^{-2}, typical of a little dense polymer mass; whereas medium and high crosslinked macroreticular resins show densities of 1.5 and 2 nm^{-2}, respectively, typical of high dense polymer mass. In polymer zones with chain density of 0.4 nm^{-2} spaces in the swollen gel phase are equivalent to pores of 2.9 nm; 1.5 nm in density zones of 0.8 nm^{-2}, and ≤1 nm for chain densities higher than 1.5 nm^{-2} [75].

It is to be noted that spaces in swollen gel phase of macroreticular resins of medium and high DVB% are comparable to those of a large pore zeolite. In Table 3.7, resins particle size in air, water, 1-pentanol, 1-hexanol and 1-octanol measured by a laser technique (Beckman Coulter LS Particle size Analyzer) are shown. Particle sizes in air are similar to those measured experimentally (Table 3.4). Size in water and alcohol are higher than in air as a consequence of swelling. It is noteworthy that swelling in alcohol and water are comparable. Swelling by water is due to interaction with sulfonic groups, but in the case of higher alcohols an additional interaction of aliphatic part of the alcohol molecule with polymer chains is possible. Breakage of some resins in the swelling process from dry particles was observed hindering to obtain reliable measurements.

Table 3.7. Particle diameter of some resins swollen in different liquid media

Resin	d_p (mm)				
	Air	water	1-pentanol	1-hexanol	1-octanol
A-15	0.65	0.741[a]	0.820	0.703	0.759
A-35			0.794	0.750[a]	0.733
CT-275	0.61	0.625[a]			0.633
CT-276	0.729	0.652[a]			
CT-252	0.60	0.684[a]			0.678
A-16	0.563	0.690	0.678	0.733[a]	0.532
A-36	0.571	0.729	0.634[a]	0.585[a]	0.544
A-39	0.54	0.768	0.756	0.655	0.758
A-70	0.551	0.783	0.565	0.573	0.586
CT-224	0.342	0.515	0.503	0.477	0.495
A-121	0.441	0.824	0.738	0.745	0.774
DOW5050	0.599	0.830	0.743	0.607	
A-46	0.776	0.814		0.802	0.808

(a) Particle breakage is observed

3.5 Physical and textural characterization of zeolites

Zeolites were used as a powder consisting of aggregates of crystals ranging from 0.4 to 40 μm (mean size between 1 and 9 μm). Aggregates size distribution was measured in air and water by a laser technique with a Microtrack SRA analyzer. SEM micrographs (Hitachi S-2300) showed that crystals composing zeolite powders were smaller than 1 μm. As seen in Table 3.8, crystal size of tested zeolites is, in increasing order, H-BEA-25 < H-MFI-28 < H-FAU-6. Actual SiO_2/Al_2O_3 molar ratios were obtained by X-ray fluorescence (PW1400, Philips; detector: LiF crystal; excitation source Rh). Finally, skeletal density, ρ_s, was measured by He displacement with an Accupyc 1330 from Micromeritics.

Zeolites were characterized texturally from N_2 adsorption-desorption isotherms recorded at 77 K. According to IUPAC classification [70], H-FAU-6/30, H-MFI-28, H-MOR-20 and H-FER-20 isotherms depicted in Figure 3.7 are of type I, as expected for microporous solids. H-BEA-25 shows a type II isotherm that corresponds to a macroporous solid. Finally, H-MCM-79 shows a type IV isotherm, typical of a mesoporous solid.

Table 3.8. Physical and structural properties of zeolites and MCM materials tested

	H-BEA-25	H-FAU-6	H-FAU-30	H-MFI-28	H-MOR-20	H-FER-20	H-MCM-79
SiO_2/Al_2O_3	25.4	5.6	29.3	27.9	19.5	21.1	79
Brönsted acid site conc., mmol/g	1.23	4.59	1.07	1.12	1.40	1.46	0.587
ΔH_{ads} kJ/mol[a]	-108	-95	-106		-128	-109	
Mean particle size, µm	8.5	3.6	2.44	2.9	1.1		
Mean crystal size, µm[b]	0.1	0.7		0.4			
Skeletal density (ρ_s) g/cm^3	2.237	2.026		2.083	2.189	2.181	
BET surface area (S_{BET}) m^2/g	484 ± 17	458 ± 22	693 ± 29	297 ± 13	388 ± 18	255 ± 11	936 ± 3
Pore volume (V_g) cm^3/g	0.663	0.315	0.517	0.206	0.26	0.296	0.945
External surface (S_{ext}) m^2/g[c]	218	59	122	26.5	29.9	30.5	930
Mesopore surface(S_{BJH}) m^2/g[d]	219	82.2	181	64,9	37,5	37.6	838
Mesopore volume (V_{BJH}) cm^3/g[d]	0.527	0.098	0.253	0.084	0.062	0.183	0.741
External volume (V_{ext}) cm^3/g[c]							0.205
Micropore volume, V_μ, cm^3/g[c]	0.123	0.202	0,280	0.140	0.179	0.112	
Micropore diameter, Å[e]	6.5 × 5.6 7.5 × 5.7	7.4	7.4	5.3 × 5.6 5.1 × 5.5	6.5 × 7.0 2.6 × 5.7	4.2 × 5.4 3.5 × 4.8	
Cage diameter Å[e]		11.5	11.5				
Channel system	3D	3D	3D	3D	1D	2D	
Maximum diameter of a sphere that can diffuse along three axes, Å[f]	5.95x5.95x5.95	7.35x7.35x7.35	7.35x7.35x7.35	4.70x4.46x4.46	1.57x2.95x6.45	1.56x3.40x4.69	
Maximum diameter of a sphere that can be included, Å[f]	6.68	11.24	11.24	6.36	6.7	6.31	

(a) Values obtained by calorimetric pulsed NH_3 adsorption measurements. (b) From SEM micrographs. (c) Calculated by the t-method of Lippens-de Boer [76, 77] (d) Calculated by the Barret-Joyner-Halenda method [78]. (e) Values obtained from molecular models [79]. (f) Values from IZA Database of Zeolite Structures [59]

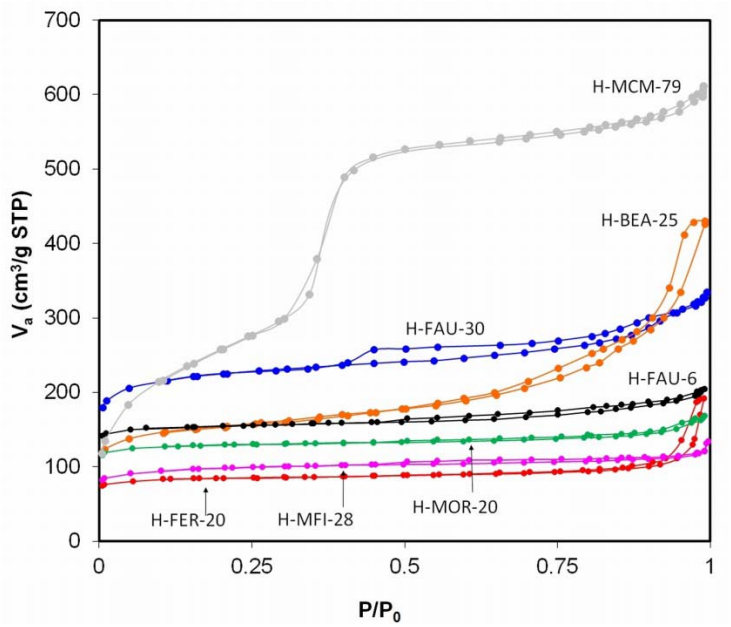

Figure 3.7. N_2 adsorption isotherms of H-BEA-25,H-FAU-6, H-FAU-30, H-MFI-28, H-MOR-20, H-FER-20, and H-MCM-79

As for the hysteresis loop type, H-MCM-79 shows an H1 loop, characteristic of solids consisting of particles crossed by nearly cylindrical pores of uniform size and shape [70]. On the contrary, H-FAU-6/30, H-BEA-25, H-MFI-28, H-MOR-20 and H-FER-20 show H3 loops, characteristic of materials consisting of aggregates or agglomerates of particles forming slit shaped pores of non-uniform size and/or shape, which are usually found in zeolites. BET surface areas (S_{BET}) were measured by using recorded data at $0.05 \leq P/P_0 \leq 0.25$ and total pore volume (V_g) was estimated from the volume of N_2 adsorbed at $P/P_0 \approx 0.99$. In the case of zeolites, external surface area, S_{ext}, and micropore volume, V_μ, was found by using the t-method of Lippens-de Boer [76,77]. Pore size distributions in the mesopore range ($2 \leq d_{pore} \leq 50$ nm) were calculated by the Barret-Joyner-Halenda (BJH) method based on Kelvin equation [78].

As Table 3.8 shows, zeolites have a very distinct surface area and pore volume in this range. It is to be noted that S_{ext} and S_{BJH} estimates agree quite well in the case of H-BEA-25 and H-FAU-6. S_{BJH} estimates of H-FAU-30, H-MFI-28, H-MOR-20 and H-FER-20 are clearly higher than S_{ext} showing that, in this case, pores are far from cylindrical form, as BJH method assumes. As Fig. 3.8 A shows, distinct pore distribution curves are

observed: H-BEA-25, H-FAU-30 and H-FAU-6 have pores in the range 2-50 nm, whereas H-MFI-28, H-MOR-20 and H-FER-20 are almost exempt of mesopores.

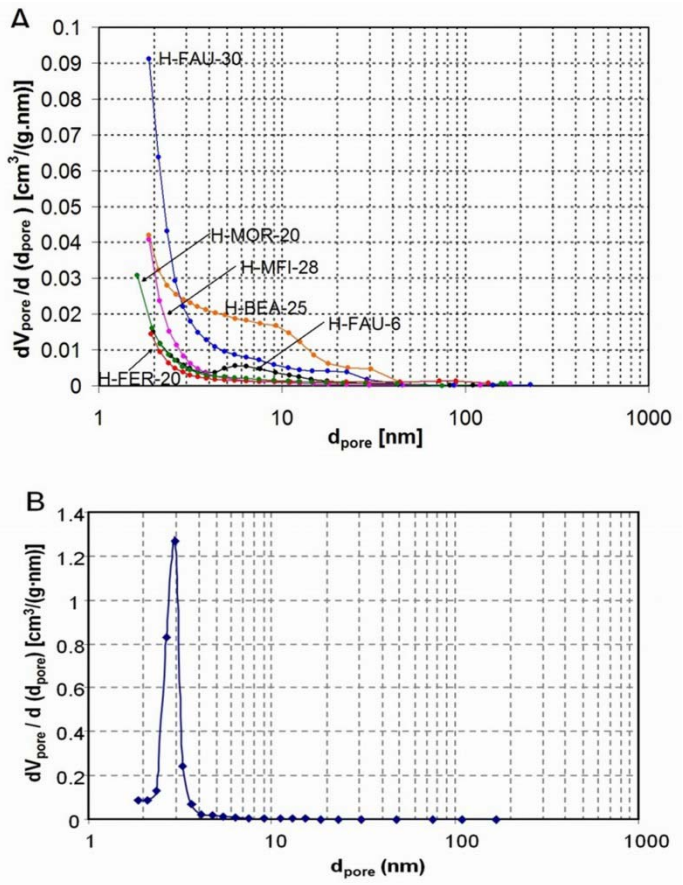

Figure 3.8. Pore distribution in the mesopore range of H-BEA-25, H-FAU-6, H-FAU-30, H-MFI-28 and H-FER-20 (A), and H-MCM-79 (B)

Structural analysis of H-MCM-79 was performed using the high resolution α_s-plot method [80]. In the calculations, a macroporous silica gel SiO_2-A from Davison (Spain) (S_{BET} = 516 m^2/g) was used as a reference adsorbent. The total surface area S_t, primary mesopore volume V_P (uniform cylindrical pores), and external surface area S_{ext} (surface area of macropores and secondary mesopores) were estimated directly from the α_s-plot. Surface area of primary mesopores was obtained as the difference between the total surface area S_t and the external surface area S_{ext}. V_{ext} was estimated accordingly. As seen in Table 3.8, S_t (930 m^2/g) highly agrees with S_{BET}; moreover it was found that the micropores presence was negligible (V_μ = 0.0025 cm^3/g). BJH pore analysis shows a

narrow pore distribution about 3 nm, which proves the pore uniformity of such materials (Figure 3.8 B).

Nature of acid sites in zeolites can be both Brönsted and Lewis type. H-BEA-25 has been associated with a significant number of SiOH groups at the surface [81], but the bridging hydroxyl groups (Si(OH)Al) and Lewis acid sites can be involved as well in alcohol dehydration reactions [82]. Acid site densities were estimated by assuming one Brönsted acid site per lattice Al free of residual cations such as Na^+ [83]. As in ion exchange resins, acid strength was represented by the molar adsorption enthalpy of ammonia (ΔH_{ads}) calculated in the present work with the set up showed in APPENDIX IV.

CHAPTER 4

Influence of properties and textural parameters of PS-DVB resins on the synthesis of DNOE. A comparison with DNHE and DNPE syntheses

4.1 Abstract

Dehydration of 1-octanol, 1-hexanol and 1-pentanol to di-n-octyl ether (DNOE), di-n hexyl ether (DNHE) and di-n-pentyl ether (DNPE), respectively, has been studied in the liquid phase at 423 K in a batch reactor on ion exchange resins as catalysts. Tested catalysts were the macroreticular resins Amberlyst 15, Amberlyst 35, CT 175, CT 275 and CT 276 (high crosslinking degree); Amberlyst 16, Amberlyst 36 and CT 252 (medium crosslinking degree); Amberlyst 39 and Amberlyst 70 (low crosslinking degree), and the gel type ones CT 224, Amberlyst 31, Amberlyst 121 and Dowex 50Wx4-50. Amberlyst 46, an ion-exchange resin sulfonated only at the polymer surface and Nafion NR50 were also tested for comparison purposes. Influence of resin structure and characteristics on the conversion of alcohol, selectivity and yield of linear ether is detailed. Finally, by comparing initial reaction rates of ether formation with those obtained on Amberlyst 46 an estimation of the fraction of sulfonic groups that take part in the reaction is given.

4.2 Results and discussion

Operation conditions described in section 3.3.3 allowed avoid mass transfer limitations. Thus, experimental data represent the chemical steps of the catalytic process, which allowed obtaining information about the reaction scheme and the influence of catalytic properties on the conversion, selectivity, yield and rates.

4.2.1 Reaction scheme of catalytic dehydration of 1-octanol to DNOE

The evolution of reaction medium was similar over all tested resins. Fig. 4.1 shows a typical plot of DNOE and byproducts mole evolution on Amberlyst 39. Reaction proceeds smoothly from the beginning, DNOE being the main product. Byproducts appeared as soon as the reaction begins, and their amount increased continuously through the experiment. Detected byproducts were C_8 olefins (1-octene, cis/trans-2-octene, cis/trans-3-octene, and 4-octene), and C_{16} branched ethers (1,2-oxybis octane, 1,3-oxybis octane and 1,4 oxybis octane); octenes being by far the main byproducts, particularly trans-2-octene and trans-3-octene.

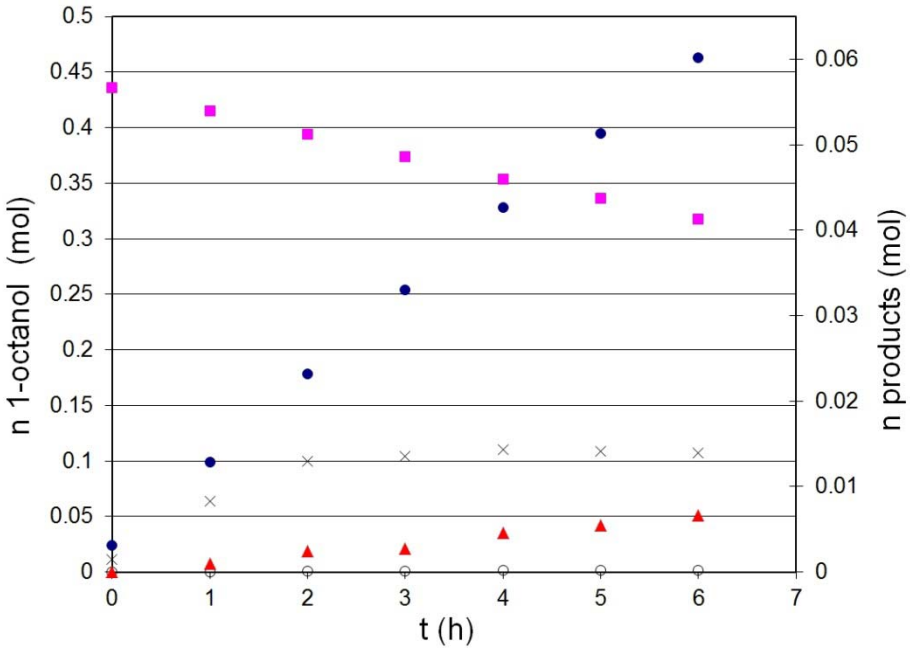

Figure 4.1. Variation of reaction medium composition with time, 1-octanol dehydration to DNOE over 1 g of dry A-39 at 423 K, P= 2.5 MPa, 70 cm^3 1-octanol. 1-octanol (square). Products: C_{16} branched ethers (open circle), DNOE (filled circle), C_8 olefins (triangle), water (x)

It is to be noted that the amount of water in the liquid phase was lower than the stoichiometric one formed from dehydration to DNOE and olefins. Thus, it is inferred that a part of the water remains in the resin and contributes to swell the catalyst according to data of Table 3.7. 1-octanol conversion increased constantly with time, as expected, whereas selectivity to DNOE decreased slightly from the beginning and then stabilized (Fig. 4.2); selectivity to C_8 olefins and C_{16} branched ethers (i.e. 1,2-oxybis octane) shows the opposite behavior.

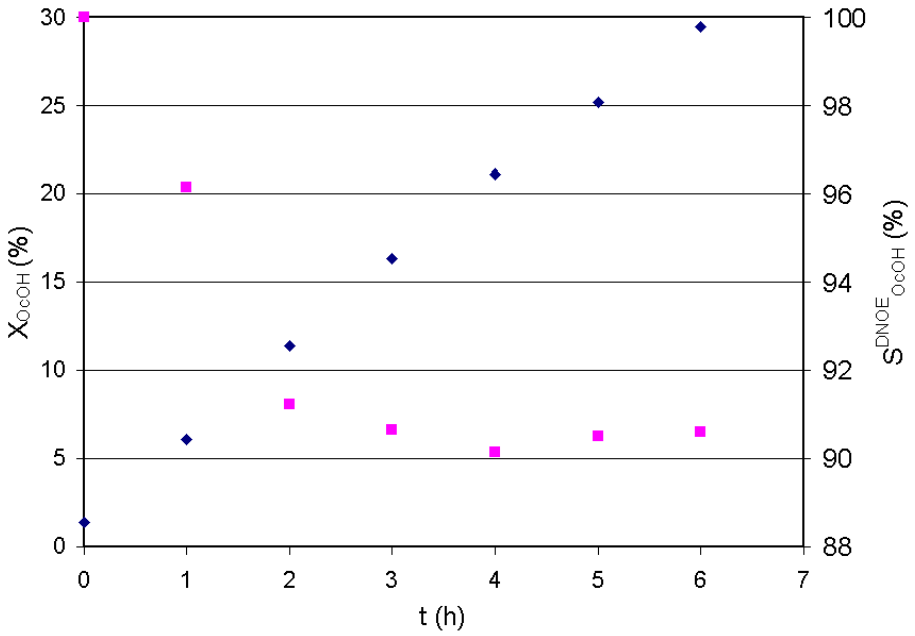

Figure 4.2 Variation of 1-octanol conversion and selectivity to DNOE with time on A-39 (W= 1 g, T= 423 K, P= 2.5 MPa, 70 cm^3 1-octanol). Octanol conversion (rhombus) and selectivity to DNOE with respect to 1-octanol (square)

Since C_8 alcohols other than 1-octanol were not detected, it is assumed that branched ethers come from C_8 olefins and 1-octanol. The scheme reaction proposed is shown in Fig. 4.3.

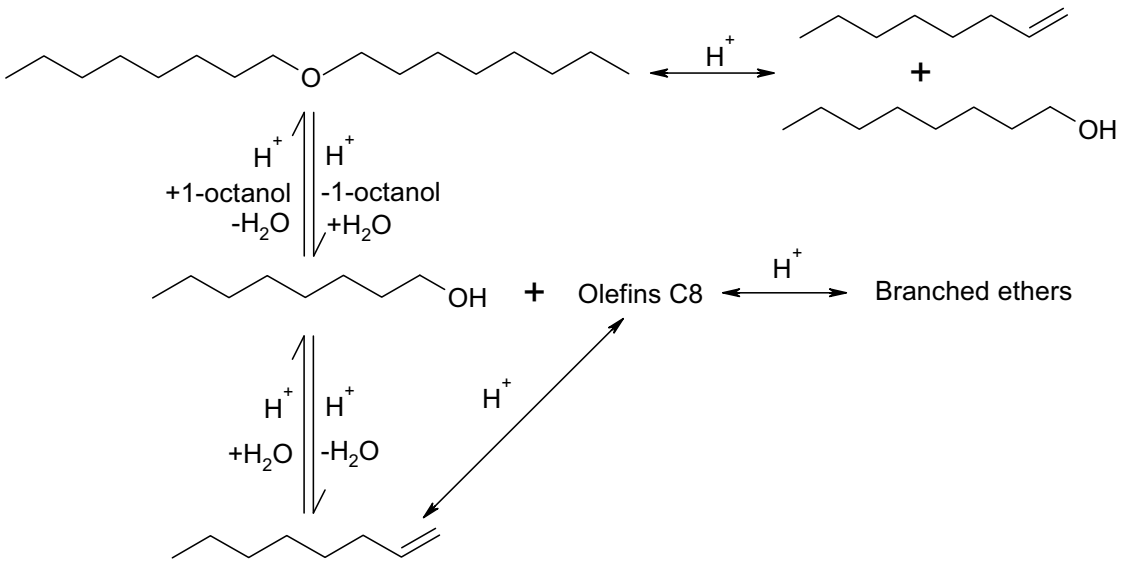

Figure 4.3. Reaction scheme for dehydration of 1-octanol to DNOE

4.2.2 Conversion of 1-octanol, selectivity to DNOE and initial reaction rates at 423 K

1-octanol conversion, (X_{OcOH}), selectivity to DNOE (S_{OcOH}^{DNOE}), C_8 olefins ($S_{OcOH}^{C_8^=}$) and C_{16} branched ethers ($S_{OcOH}^{OcOOc'}$), and yield of DNOE (Y_{OcOH}^{DNOE}) at t = 6 h are shown in Table 4.3.

In general, **1-octanol conversion**, X_{OcOH} increases with *acid capacity* of resins as it is seen by comparing Amberlyst 46 and Nafion NR50 (<1 meqH^+/g), Amberlyst 70 (≈3 meqH^+/g) and the others (4.8–5.4 meqH^+/g). By comparing resins of similar structure but different *acid capacity*, e.g. Amberlyst 15 and 35 or CT 175 and 276 (macroreticular, high *DVB %*), and Amberlyst 16 and 36 (macroreticular, medium *DVB %*), it is seen that X_{OcOH} on *oversulfonated* resins are higher than on the conventionally sulfonated homologues (see Table 4.1).

Table 4.1. Alcohol conversion and acid capacity for selected resins

Type and DVB%	Resin	Acid capacity meq H^+/g	X_{OcOH}
Macro High DVB%	A-15	4.81	19.1
	A-35	5.32	22.5
	CT-175	4.98	22.2
	CT-276	5.2	23.0
Macro Medium DVB%	A-16	4.8	25.0
	A-36	5.4	25.8

Reaction conditions: W = 1 g, T = 423 K, P = 2.5 MPa, 70 cm^3 alcohol

However, polymer structure plays an important role as well. By comparing resins with similar *acid capacity* but different *DVB%* e.g. Amberlyst 15, 16 and 39 (high, medium and low *DVB%*, respectively); Amberlyst 35 and 36, or CT 275 and CT 276 (high *DVB %*), it is seen that X_{OcOH} is higher on resins with less *crosslinking degree*. As seen in Table 4.3, the highest X_{OcOH} was achieved on the Amberlyst 39 (macroreticular, low *DVB %*); high X_{OcOH} values were also found on gel-type resins Amberlyst 31 and 121, and Dowex 50Wx4-50. However, conversion on CT 275 is lower than on CT 276, probably because swollen CT 275, unlike CT 276, does not have spaces in the density zone of 1.5 nm^{-2} (Fig. 3.6 B).

X_{OcOH} on Amberlyst 15 is about four times that of Amberlyst 46. Amberlyst 15 has only about a 5% of $–SO_3H$ groups at the polymer surface (≈0.25 meq H^+/g) [84, 85]. Since this quantity is a half of the *acid capacity* of Amberlyst 46 (sulfonated only at the polymer surface) it can be inferred that in macroreticular resins other than Amberlyst 46 the reaction takes place essentially in the gel phase.

So, in gel-type resins (which have a very small fraction of $–SO_3H$ groups at the resin surface) reaction proceeds almost exclusively in the *swollen polymer*. Therefore, *swelling* is a key factor to explain the catalytic activity of resins.

As a rule, **selectivity** to DNOE, S_{OcOH}^{DNOE} increases with the volume of *swollen gel phase* (V_{sp}).

NR50 shows the highest selectivity to DNOE, followed by Amberlyst 70 (macroreticular, low *DVB %*) and gel-type resins Amberlyst 121 and Dowex 50Wx4-50. Macroreticular resins clearly show that S_{OcOH}^{DNOE} decreases on increasing the *DVB%* (and therefore the resin stiffness) as seen by comparing *conventionally sulfonated* resins Amberlyst 15, 16 and 39 (high, medium and low *DVB%*, respectively), and over-sulfonated resins Amberlyst 35 and 36 (high and medium *DVB %*) (see Table 4.2).

Table 4.2. Selectivity to DNOE and crosslinking degree for selected resins

DVB%	Resin	S_{OcOH}^{DNOE}
High	A-15	58.3
Medium	A-16	76.6
Low	A-39	90.6
High	A-35	57.0
Medium	A-36	71.8

Reaction conditions: W = 1 g, T = 423 K, P = 2.5 MPa, 70 cm^3 alcohol

Table 4.3. Alcohol conversion (%), selectivity to ether (%), olefin (%) and branched ethers (%) with respect of alcohol, and yield of symmetrical ether (%) for 1-octanol, 1-hexanol and 1-pentanol dehydration to ether at 6 h of reaction

	Resin	Sulfonation	X_{OcOH}	X_{HeOH}	X_{PeOH}	S_{OcOH}^{DNOE}	S_{HeOH}^{DNHE}	S_{PeOH}^{DNPE}	$S_{OcOH}^{C_8^=}$	$S_{HeOH}^{C_6^=}$	$S_{PeOH}^{C_5^=}$	$S_{OcOH}^{OcOOc'}$	$S_{HeOH}^{HeOHe'}$	$S_{PeOH}^{PeOPe'}$	Y_{OcOH}^{DNOE}	Y_{HeOH}^{DNHE}	Y_{PeOH}^{DNPE}
Macro High DVB%	A-15	C	19.1	15.7	17.1	58.3	69.8	81.2	28.3	17.9	11.7	13.4	8.6	7.1	11.2	10.9	12.7
	A-35	O	22.5	20.2	20.8	57.0	64.7	73.3	29.1	24.0	16.6	14.0	11.3	10.0	12.8	13.1	13.9
	CT-175	C	22.2			61.9			25.4			12.7			13.7		
	CT-275	O	20.8			59.0			27.7			13.3			12.2		
	CT-276	O	23.0			61.1			25.8			13.1			14.1		
Macro Medium DVB%	CT-252	O	23.0			69.6			19.0			11.4			16.0		
	A-16	C	25.0	21.4	20.4	76.6	85.5	91.5	13.5	9.6	5.2	9.9	4.9	3.3	19.1	18.3	17.0
	A-36	O	25.8	25.5	25.1	71.8	79.0	85.5	17.0	13.5	7.6	11.2	7.5	6.8	18.5	20.1	19.9
Macro Low DVB%	A-39	C	29.5	21.8	20.0	90.6	94.0	96.8	5.0	3.9	1.9	4.4	2.1	1.3	26.7	20.5	17.7
	A-70	C	16.1	16.5	13.7	98.1	97.7	97.8	1.91	0.17	0.94	0	0.77	1.3	15.8	16.1	12.0
Gel	CT-224	O	26.6	23.9	20.9	85.7	96.5	97.3	7.6	1.9	1.2	6.7	1.7	1.6	22.8	23.1	18.5
	A-31	C	28.2	22.5	20.6	93.8	97.0	98.0	2.7	1.7	1.3	3.5	1.3	0.67	26.5	21.8	18.4
	A-121	C	27.7	22.1	19.9	97.3	98.0	99.2	0.89	0.67	0.68	1.8	0.89	0.07	27.0	21.7	18.1
	DOW5050	C	27.8	21.6	19.4	96.1	96.6	97.3	1.8	2.0	1.2	2.1	1.2	1.5	26.7	20.9	17.1
	A-46	S	5.6	4.3	4.0	95.4	94.8	98.4	4.6	5.2	1.6	0	0	0	5.3	4.1	3.6
	NR50	-	12.1	10.3	9.7	100.0	97.9	99.0	0	1.5	0	0	0.64	1.0	12.1	10.0	8.7

Reaction conditions: W = g, T= 423 K, P= 2.5 MPa, 70 cm^3 alcohol

Since the reaction mainly occurs in the gel phase, S_{OcOH}^{DNOE} is closely related to the *gel phase density* of swollen resins.

Amberlyst 121, Dowex 50Wx4-50 and Amberlyst 70, with gel phase density of 0.4 nm^{-2} show selectivities to ether from 98 to 96 % (Table 4.3). In Amberlyst 31 and 39, with polymer density of 0.8 nm^{-2}, S_{OcOH}^{DNOE} is between 94 and 90.6 %. Amberlyst 16 and 36, and CT 252 (macroreticular, medium DVB %) have polymer density of 1.5 nm^{-2} and show selectivities to DNOE ranging from 60 to 77. Finally, Amberlyst 15 and 35, CT 175, CT 275 and CT 276 (macroreticular, high DVB %), with a density of 2.0 nm^{-2}, show selectivities to DNOE lower than 61%.

The low selectivity of CT 224 (86%) compared to the other *gel-type* resins shown in Table 4.3, can be explained by the significant fraction of *polymer densities* in the range of 1.5–2.0 nm^{-2} (see Figure 3.6 A), which are high values compared to the significant fraction of polymer densities of the other *gel-type* resins (0.2-0.8 nm^{-2}).

Less dense swollen resins, with wide spaces between polymer chains, allow permeation of 1-octanol, outwards diffusion of DNOE, and formation of reaction intermediate is not restricted. Therefore, dehydration to DNOE is favored on *gel-type* and macroreticular resins with *low DVB %,* whereas in the less swollen macroreticular resins CT 276, CT 275, CT 175, Amberlyst 15 or 35, selectivity to olefin and branched ethers increases significantly.

Finally, by comparing Amberlyst 15 and 35; Amberlyst 16 and 36; or CT 175 with CT 275 and CT 276 it is seen that oversulfonation does not upgrade S_{OcOH}^{DNOE}. It seems that supplementary -SO_3H groups in oversulfonated resins contribute to hold closer the polymer chains by the presence of additional hydrogen bonds, which would explain selectivities to DNOE lower than those of *conventionally sulfonated* homologues.

As a consecuence selectivity was correlated well to $[H^+]/V_{sp}$ (Fig. 4.4). Acid sites per volume unit of swollen gel phase would be an excellent parameter to explain DNOE formation. Selective resins to DNOE have low $[H^+]/V_{sp}$ values, whereas less selective ones (CT 276, CT 275, CT 175, Amberlyst 15 and 35) show high $[H^+]/V_{sp}$ values. Accordingly, selectivity to olefins and branched ethers is high, what suggest that DNOE

diffusion is hindered, and ether might decompose to 1-octanol and octenes. In this way, they show low X_{OcOH} and S_{OcOH}^{DNOE} values.

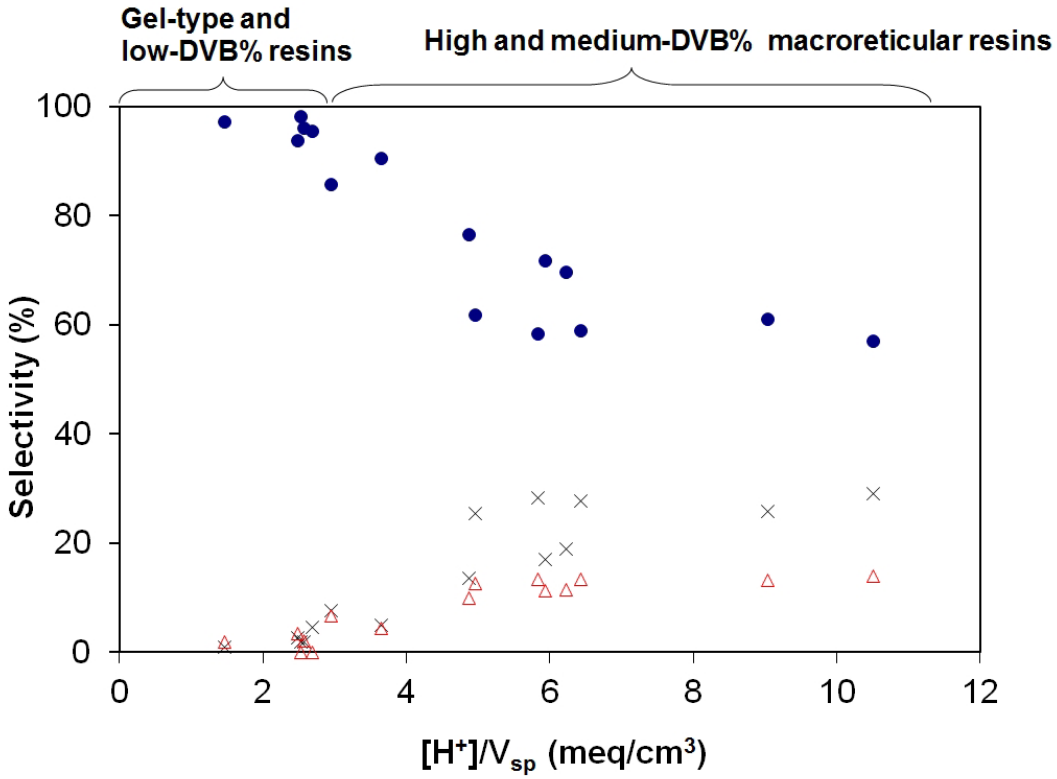

Figure 4.4. Selectivity to DNOE (circle), C_8 olefins (x) and C_{16} branched ethers (triangle) with respect 1-octanol vs. H^+/V_{sp} ratio at t= 6 h (W= 1 g, T= 423 K, P= 2.5 MPa, 70 cm^3 1-octanol

Higher **DNOE yields** were obtained on *gel-type* resins Amberlyst 121, Dowex 50Wx4-50 and Amberlyst 31, and *low-crosslinked* macroreticular resin Amberlyst 39. It is seen in Table 4.3 that on these resins X_{OcOH} is high and S_{OcOH}^{DNOE} ranges between 90 and 98 %. A look to morphology of swollen gel polymer might elucidate the relationship between resin structure and catalytic activity. Tested resins have *gel phase densities* between 0.4 and 2.0 nm^{-2} (Fig. 3.6 A and B), and spaces among polymer chains range from 2.6 to less than 1 nm [75]. Polymer zones of density 0.4 nm^{-2} are accessible to 1-octanol and the bulky DNOE, and there are no restrictions for the reaction intermediate. On the contrary, alcohol permeation, the exit of DNOE or the formation of the reaction intermediate are hindered in polymer zones of density 2.0 nm^{-2}.

Resins have to swell by 1-octanol and water released for the reaction takes place with high DNOE yield. In this way, gel-type resins showing at the same time high V_{sp} values and *swollen polymer densities* of 0.4–0.8 nm^{-2} (spaces of 2.9–1.5 nm) give the best DNOE yields. Gel-type resins greatly swell in 1-octanol-water mixtures so that a high portion of $–SO_3H$ groups are able to take part in the reaction. As a result, X_{OcOH} values are high. As for selectivity, the wide spaces between polymer chains favor the formation and diffusion of DNOE.

As seen in Table 4.3, initial DNOE formation (r^0_{DNOE}) and 1-octanol consumption ($-r^0_{OcOH}$) **rates** fit quite well Eq. 3.10, which is a proof of data reliability. r^0_{DNOE} values are higher on gel-type resins Dowex 50Wx4-50, Amberlyst 31, and Amberlyst 121, in line with the high yield of DNOE observed. As for 1-octanol consumption, Amberlyst 36 and 39 show higher $-r^0_{OcOH}$ values mainly due to significant formation of C_8 olefins and C_{16} branched ethers.

As for **TOF** (turn over frequency), NR50 shows the highest initial value. It is explained by the higher acid strength of $–SO_3H$ groups, due to the presence of fluorine in Nafion chains, as compared to those of PS-DVB resins [44]. Ammonia adsorption enthalpies tabulated in Table 3.4 varied slightly between oversulfonated and conventionally sulfonated resins (e.g. Amberlyst 15 and 35) but generally, acid sites in PS-DVB resins have rather similar acid strength [86] and it is inferred that TOF_{DNOE} values depend on the total number of acid sites. Amberlyst 46, sulfonated only at the polymer surface, should be outlined. Its initial TOF_{DNOE} is clearly higher than those of the other PS-DVB resins. This fact disclose that in swollen PS-DVB resins there is a fraction of $–SO_3H$ groups, located in very dense polymer zones, unavailable for reaction.

So, assuming that all sulfonic groups of Amberlyst 46 take part in the reaction, the *fraction of active sites* taking part in the reaction in the rest of resins can be estimated comparing TOF_{DNOE} values with that of Amberlyst 46. This way, in the more active and selective to DNOE Dowex 50Wx4-50, Amberlyst 31, 121 and 70 between 64 and 61% of sulfonic groups take part in the reaction, but in the less active and selective Amberlyst 15 and 35, CT 175, CT 275 and CT 276 only a fraction of 32–27% participates.

Table 4.4. Initial rates (mol·h^{-1}·kgcat^{-1}) and TOF (mol·h^{-1}·(eqH^{+})$^{-1}$) values for 1-pentanol, 1-hexanol and 1-octanol consumption and DNPE, DNHE and DNOE formation

RESIN	$-r^0_{OcOH}$	$-r^0_{HeOH}$	$-r^0_{PeOH}$	r^0_{DNOE}	r^0_{DNHE}	r^0_{DNPE}	$-TOF^0_{OcOH}$	$-TOF^0_{HeOH}$	$-TOF^0_{PeOH}$	TOF^0_{DNOE}	TOF^0_{DNHE}	TOF^0_{DNPE}
A-15	20.0 ± 1.6	21.7 ± 2.0	32.7 ± 2.1	4.7± 0.1	8.4± 0.4	12.4 ± 0.8	4.2 ± 0.3	4.5 ± 0.4	6.8 ± 0.4	1.0 ± 0.0	1.7 ± 0.1	2.6 ± 0.2
A-35	20.0 ± 3.2	26.8 ± 6.7	49.7 ± 1.1	5.1 ± 0.3	7.9± 1.9	17.0 ± 0.9	3.8 ± 0.6	5.0 ± 1.3	9.4 ± 0.2	1.0 ± 0.1	1.5 ± 0.4	3.2 ± 0.2
CT-175				5.2 ± 0.6						1.1 ± 0.1		
CT-275	16.2 ± 0.8			4.7 ± 0.4			3.1 ± 0.2			0.9 ± 0.1		
CT-276				5.6 ± 0.5						1.1 ± 0.1		
CT-252	20.7 ± 0.6			6.1 ± 0.4			3.8 ± 0.1			1.1 ± 0.1		
A-16	18.5 ± 0.7	27.3 ± 3.2	36.1 ± 2.2	7.5 ± 1.0	12.7± 0.3	15.8± 0.6	3.9 ± 0.1	5.7 ± 0.7	7.5 ± 0.5	1.6 ± 0.2	2.7 ± 0.1	3.3 ± 0.1
A-36	25.8 ± 2.0	40.1 ± 5.9	45.3 ± 6.4	9.4 ± 0.7	17.8± 1.6	19.5 ± 3.8	4.8 ± 0.4	7.4 ± 1.1	8.4 ± 1.2	1.7 ± 0.1	3.3 ± 0.3	3.6 ± 0.7
A-39	25.5 ± 2.2	22.7 ± 0.4	31.2 ± 0.5	8.9 ± 1.1	10.8 ± 1.0	14.2 ± 0.2	5.1 ± 0.4	4.5 ± 0.1	6.2 ± 0.1	1.8 ± 0.2	2.2 ± 0.2	2.9 ± 0.0
A-70	12.9 ± 0.4	19.6 ± 1.4	21.1 ± 1.7	6.3 ± 0.4	10.9 ± 1.4	7.8 ± 0.6	4.3 ± 0.1	6.5 ± 0.5	7.0± 0.6	2.1 ± 0.1	3.6 ± 0.5	2.6 ± 0.2
CT-224	19.5 ± 0.5	46.5 ± 0.8	32.2 ± 2.3	8.5 ± 0.4	12.1 ± 1.6	14.2 ± 0.9	3.7 ± 0.1	8.7 ± 0.1	6.0 ± 0.4	1.6 ± 0.1	2.3 ± 0.3	2.7 ± 0.2
A-31	21.3 ± 0.6	22.3 ± 3.0	29.6 ± 2.6	10.3 ± 1.2	11.3± 1.0	13.6 ± 0.7	4.4 ± 0.1	4.7 ± 0.6	6.2 ± 0.5	2.2 ± 0.3	2.4 ± 0.2	2.8 ± 0.2
A-121	19.9 ± 1.9	24.0 ± 1.0	26.3 ± 1.2	9.9 ± 0.3	11.2 ± 0.7	11.9 ± 1.0	4.2 ± 0.4	5.0 ± 0.2	5.4 ± 0.3	2.1 ± 0.1	2.3 ± 0.1	2.5 ± 0.2
DOW5050	19.7± 2.5	22.7 ± 0.9	26.6± 2.8	10.1 ± 1.1	10.8 ± 1.2	12.7 ± 1.4	4.0 ± 0.5	4.6 ± 0.2	5.4 ± 0.6	2.0 ± 0.2	2.2 ± 0.2	2.6 ± 0.3
A-46	3.0 ± 0.4	4.2 ± 0.3	4.2 ± 0.2	1.5 ± 0.2	1.7 ± 0.1	2.0 ± 0.1	7.0 ± 0.9	9.7 ± 0.7	9.9 ± 0.5	3.4 ± 0.4	4.0 ± 0.2	4.6 ± 0.2
NR50	7.9 ± 0.7	9.7 ± 1.0	11.0 ± 0.5	4.2 ± 0.2	4.7 ± 0.4	5.3 ± 0.8	8.9 ± 0.7	10.9 ± 1.1	12.4 ± 0.6	4.7 ± 0.3	5.3 ± 0.4	6.0 ± 1.0

Reaction conditions: W = g, T= 423 K, P= 2.5 MPa, 70 cm^3 alcohol

As for initial $-TOF_{OcOH}$, Nafion NR50 shows the highest value, a little higher than that of Amberlyst 46, in agreement with their different acid strength. PS-DVB resins show smaller values because a fraction of active sites is inaccessible to 1-octanol. By comparing with Amberlyst 46 TOF it is seen that accessible sites to alcohol range from 73% (Amberlyst 39) to 54% (Amberlyst 35).

$-\mathrm{TOF}^{0}_{\mathrm{OcOH}}$ values are greater than twice $-\mathrm{TOF}^{0}_{\mathrm{DNOE}}$ ones, suggesting again that in resins with very dense swollen gel phase, it is partially accessible to 1-octanol but the formation and diffusion of DNOE is actually hindered. Unlike fluorine atoms in NR50, chlorine atoms in Amberlyst 70 chains do not upgrade acid strength. Chlorine atoms give Amberlyst 70 additional thermal stability allowing at the same time the swelling phenomenon in aqueous media. As a result, selectivity to DNOE is slightly higher than that of Amberlyst 39 (similar crosslinking degree but conventionally sulfonated). Due to its thermal stability, Amberlyst 70 could be a suitable catalyst for industrial use.

4.3 Comparison of DNHE, DNPE and DNOE synthesis data

Synthesis of DNPE and DNHE from 1-pentanol and 1-hexanol, respectively, was studied on resins of Table 3.2, but CT 175, CT 275, CT 276 and CT 252. Despite DNOE yield was low on macroreticular resins with high or medium DVB%, Amberlyst 15, 35, 16 and 36 were used for comparison purposes (see APPENDIX V for detailed information about the resins tested in this work). Data of DNPE synthesis on Dowex50Wx4-50, CT 224, Amberlyst 70 and 36, and NR50 are in agreement with reported previously [44]. Byproducts of DNPE and DNHE syntheses were C_5 and C_6 olefins, respectively; however, unlike 1-octanol dehydration to DNOE, traces of secondary, tertiary and branched alcohols were detected in 1-pentanol and 1-hexanol dehydrations. 1-pentanol and 1-hexanol dehydrations show a similar pattern to that of 1-octanol, and the variation of 1-pentanol ($\mathrm{X_{PeOH}}$) and 1-hexanol ($\mathrm{X_{HeOH}}$) conversion, and selectivity to DNPE ($\mathrm{S^{DNPE}_{PeOH}}$) and DNHE ($\mathrm{S^{DNHE}_{HeOH}}$) with time is analogue to that found in DNOE synthesis.

4.3.1 Conversion

In this way, X_{PeOH} and X_{HeOH} were higher on increasing resins *acid capacity* (Table 4.2), and alcohol conversions were higher on *oversulfonated* resins than on conventionally sulfonated homologues in both DNPE and DNHE synthesis (see Amberlyst 15 and 35; or Amberlyst 16 and 36). Resin morphology is also an important factor to achieve high conversions. The same as in DNOE synthesis, the highest X_{PeOH} and X_{HeOH} values were found on *gel-type*, macroreticular resins of *low crosslinking degree* as well as Amberlyst-36. In general, it is seen that $X_{OcOH} \geq X_{HeOH} \geq X_{PeOH}$ for each resin.

However, this fact could be misleading as for comparing the resin activity in the three reaction systems. All experiments were performed by using the same alcohol volume and catalysts mass. Since the three alcohols have different molecular weight and density, the initial ratio alcohol moles (n^0_{ROH}) to catalyst mass (W) greatly changes from 1-pentanol to 1-octanol. So, to compare catalysts activity suitably, the factor $X_{ROH} \cdot n^0_{ROH}/W$ is used.

As seen in Fig. 4.5 this factor decreases as alcohol is longer on macroreticular Amberlyst 15, Amberlyst 35, Amberlyst 16 and Amberlyst 36 (high and medium DVB %). On the contrary, on gel-type Amberlyst 31, 121, CT 224 and Dowex 50Wx4-50 and on low-DVB% macroreticular Amberlyst 39 and 70 conversions are similar for the three alcohols. In swollen state the first group of macroreticular resins has spaces in gel phase less than 1 nm, where 1-octanol motion could be more restricted than that of 1-pentanol and 1-hexanol.

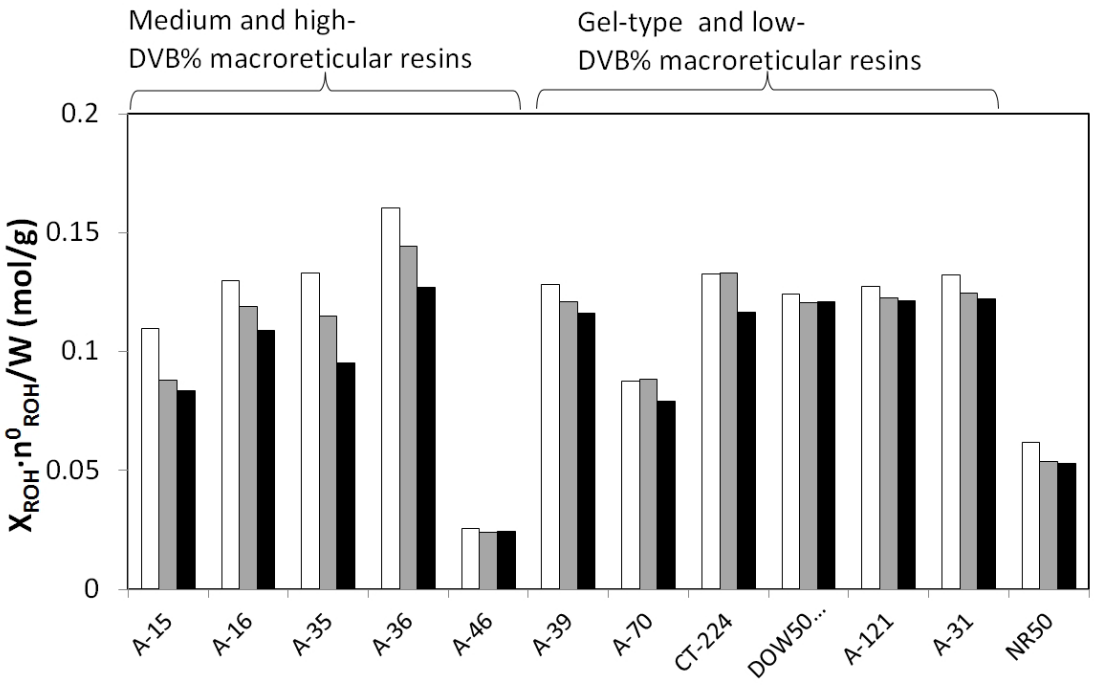

Figure 4.5. Comparison of 1-pentanol (white bar), 1-hexanol (grey bar) and 1-octanol (black bar) conversions on tested resins at t = 6 h, (W = 1 g, T = 423 K, P = 2.5 MPa, 70 cm^3 alcohol)

The small differences observed in gel-type resins highlight that spaces originated on swelling are wide enough for the three alcohols to access to active sites. Fig. 4.6 compares alcohols conversion on CT 224, Amberlyst 31 and Dowex 50Wx4-50. Despite the three resins have different acid capacity the small differences in conversion factor can be explained by the different morphology rather than by the different acid capacity.

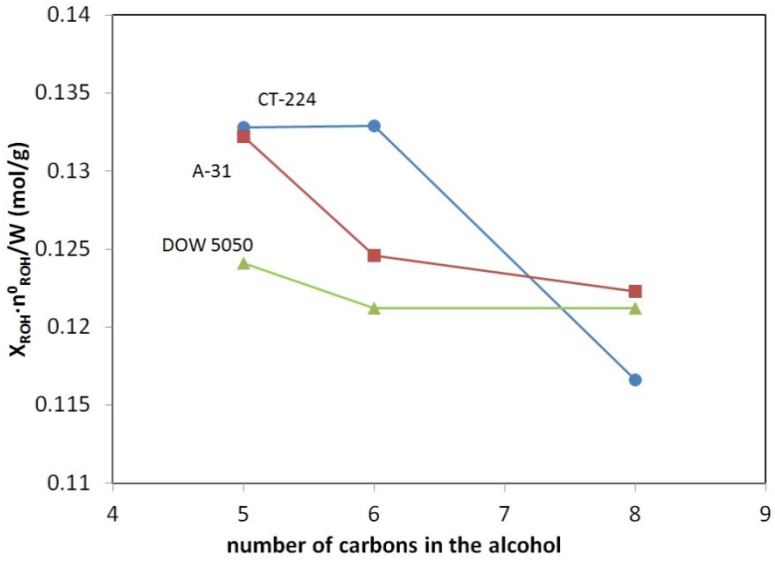

Figure 4.6. Influence of alcohol length and sulfonation type on alcohol conversion at t = 6 h. (W = 1 g, T = 423 K, P = 2.5 MPa, 70 cm^3 alcohol). 5.34 meqH^+/g (circle), 4.95 meqH^+/g (triangle), 4.8 meqH^+/g (square)

Amberlyst 31 and Dowex 50Wx4-50 have gel phase densities of 0.4 and 0.8 nm^{-2}. but in CT 224 where gel phase zones of density 1.5 nm^{-2} predominates, X_{OcOH} drops suggesting that 1-octanol have more restricted motion in this resin than 1-pentanol, 1-hexanol, and DNOE than DNPE and DNHE. In oversulfonated resin CT 224 additional acid centers (with regard to Amberlyst 31 and Dowex 50Wx4-50) mainly contributes to form new hydrogen bonds between chains; as a result accessibility to gel phase of 1-pentanol or 1-hexanol is higher than that of 1-octanol.

4.3.2 Selectivity

As for selectivity to linear ether, Fig. 4.7 shows that *gel-type* resins have high selectivity ranging from 95 to 99%. In general, it is found that $S_{PeOH}^{DNPE} > S_{HeOH}^{DNHE} > S_{OcOH}^{DNOE}$ on each resin.

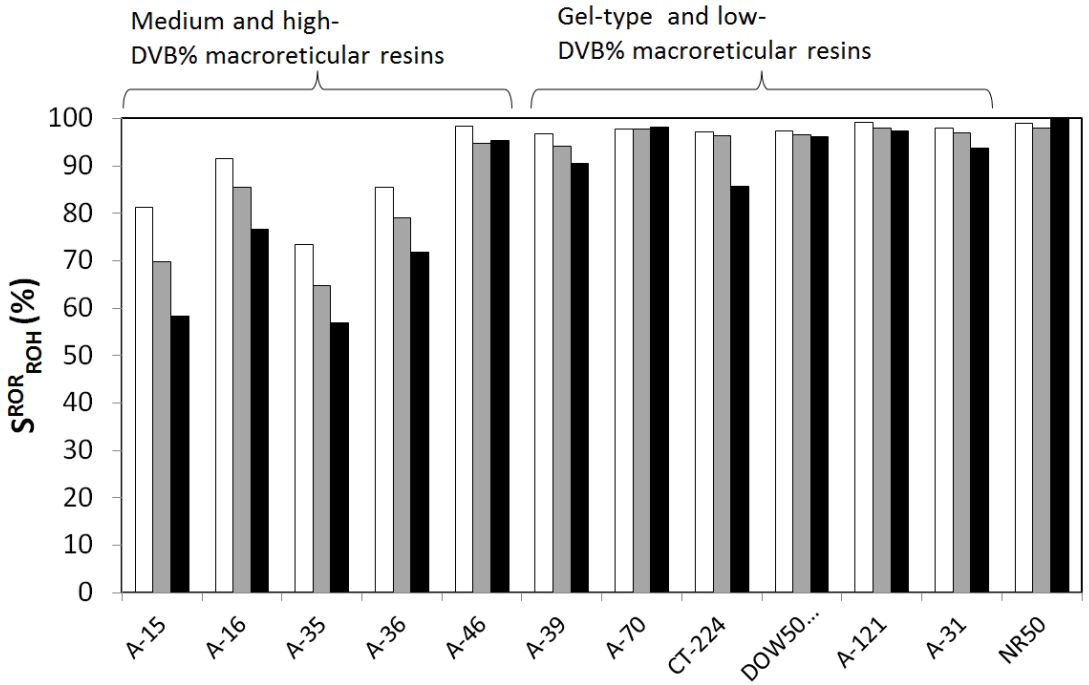

Figure 4.7. Selectivity to DNPE (white bar), DNHE (grey bar) and DNOE (black bar) on tested resins at t = 6 h (W = 1 g, T = 423 K, P = 2.5 MPa, 70 cm^3 alcohol)

Conversely, selectivity to olefins and branched ethers increase from DNPE synthesis to that of DNOE (Table 4.3). This fact suggests that *diffusion of alcohol* and *linear ether*, as well as the formation of reaction intermediate are more *hindered* as *alcohol is larger*, and as a result when produced *ether is bulkier*. Diffusion of long-chain ethers in swollen resins with zones of density ranging from 1.5 to 2 nm^{-2} (Fig. 3.6 B) is hindered, and its decomposition to olefin and alcohol favored.

As Fig. 4.7 shows, differences in S_{PeOH}^{DNPE}, $S_{HeOH}^{DNHE}$and S_{OcOH}^{DNOE} are small in *gel-type* resins. The drop in S_{OcOH}^{DNOE} for CT 224 is noticeable, and similarly to X_{OcOH} drop, it is explained because CT 224 has zones of higher chain density than the other *gel-type* resins. *Swelling* depends on DVB% of resins so that *crosslinking degree* is indicative of their ability for linear ether formation.

As seen, selectivity to linear ether is strongly related to the available space in the *swollen gel phase*. The *specific volume of the swollen polymer* (V_{sp}) was found to clearly influence the selectivity to long-chain ethers. High and medium DVB% macroreticular resins have lower V_{sp} values whereas gel-type ones gather V_{sp} values close to 2 cm^3/g and even higher than 3 cm^3/g in the case of Amberlyst 121. In Fig.4.8 it is showed the influence of V_{sp} value on selectivity to linear ether, where it can be inferred as well the influence of *ether length* on the selectivity in the case of macroreticular resins with medium and high DVB%.

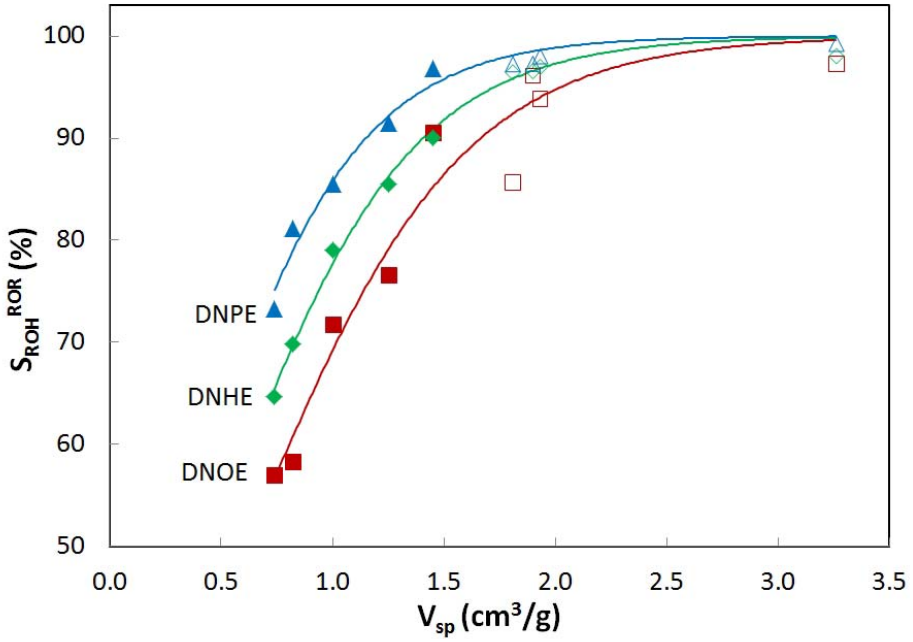

Figure 4.8. Influence of V_{sp} of selectivity to linear ether. S_{OcOH}^{DNOE} of gel-type (open square) and macroreticular (filled square) resins. S_{HeOH}^{DNHE} of gel-type (open rhombus) and macroreticular (filled rhombus) resins. S_{PeOH}^{DNPE} of gel-type (open triangle) and macroreticular (filled triangle) resins. (t = 6 h, W = 1 g, T = 423 K, P = 2.5 MPa, 70 cm^3 alcohol)

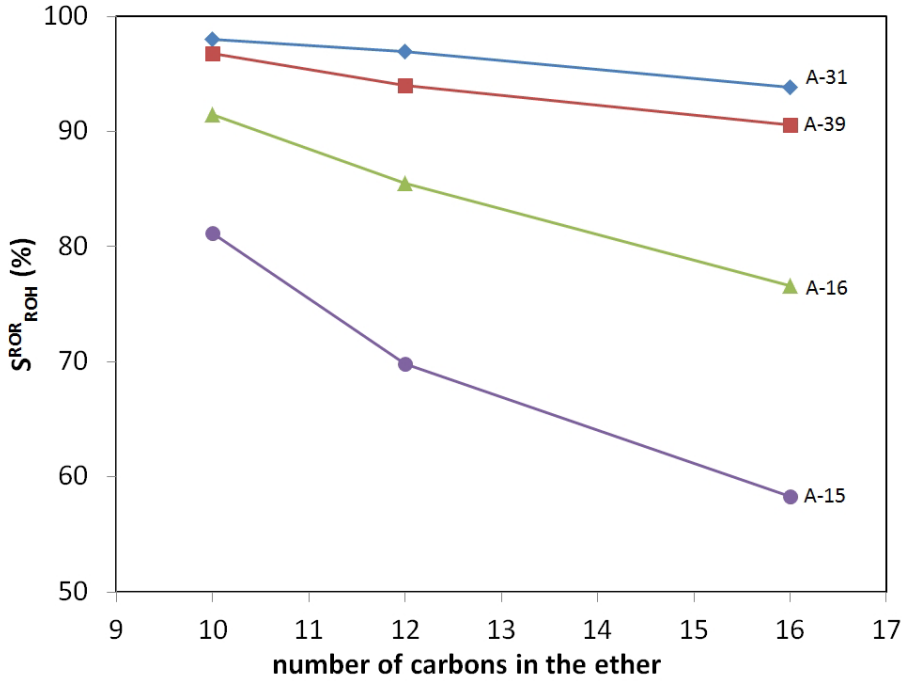

Figure 4.9. Influence of crosslinking degree on the selectivity to DNPE, DNHE and DNOE 20% DVB (circle), 12% DVB (triangle), 8% DVB (square), 4% DVB (rhombus). (W = 1 g, T = 423 K, P = 2.5 MPa, 70 cm^3 alcohol)

Fig. 4.9 compares selectivity to linear ether of four resins. It is observed that selectivity to ether decreases on increasing *crosslinking degree*. Moreover, in stiffer resins the difference between S^{DNPE}_{PeOH} and S^{DNOE}_{OcOH} is higher.

4.3.3 Initial reaction rates

Analogously to DNOE synthesis, initial 1-pentanol ($-r^0_{PeOH}$) and 1-hexanol ($-r^0_{HeOH}$) consumption rates and DNPE (r^0_{DNPE}) and DNHE (r^0_{DNHE}) formation rates fit well Eq. 3.10.

As seen in Table 4.4 the higher r^0_{DNPE} values are found on Amberlyst 39 (macroreticular; low DVB %), Amberlyst 16 and 36 (medium DVB %), and Amberlyst 35 (high crosslinking degree). In the case of DNHE, higher r^0_{DNHE} values are shown by gel-type resin CT 224 and macroreticular Amberlyst 16 and 36 (medium DVB %).

For each resin, it is clearly seen that $r^0_{DNPE} > r^0_{DNHE} > r^0_{DNOE}$ on macroreticular resins with *high and medium crosslinking degree* (Amberlyst 15, Amberlyst 35, Amberlyst 16 and Amberlyst 36). On *gel-type* resins (Amberlyst 31, Amberlyst 121, Dowex 50Wx4-50, CT 224) and macroreticular of *low crosslinking degree* (Amberlyst 39, Amberlyst 70) differences are smaller.

Bulkier ethers production is more hindered by the less swollen macroreticular resins in agreement with initial rate data. The less dense gel phase of swollen gel-type resins even the rates of DNPE, DNHE and DNOE syntheses, as they are able to accommodate better bulky molecules. Once more, the slightly denser structure of CT 224 is highlighted due to higher r^0_{ROR} differences than the other gel-type resins.

As observed in DNOE synthesis, NR50 shows the highest TOF^0_{ROR} values, and Amberlyst 46 achieves the highest values on PS-DVB resins. Taking as a reference initial TOF of DNPE and DNHE formation on Amberlyst 46, it can be drawn that in macroreticular resins Amberlyst 15, Amberlyst 35, Amberlyst 16 and Amberlyst 36 the *fraction of active centers* taking part in DNPE synthesis ranges from 56 to 79%; it is between 44 and 67% in DNHE synthesis and between 29 and 52% in the DNOE synthesis.

It is also seen that the *fraction of active sites* taking part in the reaction decreases in the order DNPE>DNHE>DNOE syntheses (i.e. a 56% of Amberlyst 15 active sites take part in DNPE synthesis, a 44% in DNHE one and a 29% in that of DNOE).

In relation to high-selective resins (Amberlyst 70, Amberlyst 39, Amberlyst 121, Amberlyst 31, and Dowex50x4) the *fraction of active sites* involved in ether synthesis is nearly the same in the three reaction systems (54–61%), i.e. 54% of acid sites of Amberlyst 121 are accessible for DNPE formation, 58% for DNHE formation and 61% for that of DNOE. In the case of CT 224, it is seen again that the fraction of sites taking part in DNOE synthesis is lower (47%) than in DNPE and DNHE ones (58%). Similar trends are found in alcohol consumption.

4.4 Conclusions

The dehydration of 1-octanol to DNOE at 423 K and 2.5 MPa takes place successfully over ion exchange resins as well as 1-hexanol and 1-pentanol dehydrations. High Y^{ROR}_{ROH} values are found on resins with **high acid capacity and V_{sp} values**. Best resins for DNOE synthesis are gel-type resins with 2–4 DVB%. In general oversulfonated resins do not upgrade the behavior of their conventionally sulfonated homologues. By comparing the synthesis of DNPE, DNHE and DNOE it is found as a rule for each resin that

$X_{PeOH} \cdot n^0_{PeOH}/W > X_{HeOH} \cdot n^0_{HeOH}/W > X_{OcOH} \cdot n^0_{OcOH}/W$, but differences are small in gel-type resins. It is also observed that $\mathbf{S^{DNPE}_{PeOH} > S^{DNHE}_{HeOH} > S^{DNOE}_{OcOH}}$ on macroreticular resins but differences in selectivity lessens on decreasing the **crosslinking degree**. High selectivity to symmetrical linear ether was found on **gel-type** resins for the three ethers. **Swelling** is a key factor to achieve high selectivity to linear ether, and a clear relationship between volume of swollen polymer (V_{sp}) and the ratio $\mathbf{H^+/V_{sp}}$ and selectivity is observed. NR50 showed the highest TOF^0 values due to its higher acid strength. TOF^0 values of Amberlyst 46, a special resin with all sulfonic groups at the polymer surface, and so wholly accessible to alcohol, were the highest between PS-DVB resins. Lower TOF^0 values shown by the other PS-DVB resins reveal that only a fraction of active centers is available for reaction, so that ether formation is hindered in less swollen polymers. Linear ether formation is influenced by resin swelling and it is generally observed that $r^0_{DNPE} > r^0_{DNHE} > r^0_{DNOE}$.

CHAPTER 5

Influence of textural properties of zeolites on the catalyzed dehydration of linear alcohols to C_{10}-C_{16} symmetrical ethers

5.1 Abstract

The liquid-phase dehydration of 1-octanol, 1-hexanol and 1-pentanol to di-n-octyl ether (DNOE), di-n-hexyl ether (DNHE) and di-n-pentyl ether (DNPE), respectively, has been studied over H-MFI-28, H-BEA-25, H-FAU-6, H-FAU-30, H-FER-20, H-MOR-20 and H-MCM-79 at 423-473 K and 2.5 MPa in a batch reactor (see APPENDIX V for detailed information about the zeolites tested in this work). Dependence of textural parameters of large and medium pore zeolites on the activity and selectivity at different temperatures is shown.

5.2 Results and discussion

Catalytic activity of zeolites depends on their structure, and also on concentration, nature and acid strength of acid sites. It has been observed that acid-catalyzed reactions undergone by aliphatic alcohols on zeolites yield symmetrical ethers (by intermolecular dehydration) and also the corresponding alkenes (by intramolecular dehydration), though the catalytic requirements for these two competitive reactions are quite different [87-93].

Mechanistic studies on 2-butanol dehydration [93], and the formation of methyl tert-butyl ether from methanol and tert-butanol [92] revealed that etherification of alcohols over acid zeolites follows a reaction pathway compatible with a typical S_N2 mechanism with a total inversion of configuration and retention of the heavier alcohol oxygen. Accordingly, it can be assumed that the dehydration reaction of alcohol to ether involves the in situ formation of an oxonium ion at the catalyst surface [94]. Linear ether is formed by the nucleophilic attack of a second alcohol molecule on the oxonium ion in a S_N2 type bimolecular reaction, and the alcohol molecule acting as an electrophile undergoes inversion of its configuration [93-95]. On the other hand, the oxonium ion can also give place to 1-olefin via an E_1 elimination reaction. In such case, water exiting leads to a carbocation and double bond is consequently created.

In order that alcohol dehydration reaction takes place fast and selectively, reactants have to reach all active sites and reaction intermediates fit pores suitably. Literature suggests that pore diameter must be larger than 2.5 times the random coil diameter of

the largest molecule involved in the chemical system so that pore dimensions do not become kinetically restrictive [95]. Random coil diameter, Φ_d, is related to the molecular weight of a molecule, M_W, by eq. 5.1 [96]. It does not take into account molecular shape, which may end up in unreliable values as spherical-type molecules in the case of small linear molecules.

$$\Phi_d = 0.2457(M_w)^{0.5882} \tag{5.1}$$

On the contrary, Balaban index (eq. 5.2) represents extended connectivity and it is a good descriptor for the shape of molecules [97], which is represented by the ovality, O, defined as the molecular area (A) divided by the area of a sphere of the same volume (V) as the molecule (eq. 5.3). Balaban index is computed by means of the number of bonds (m), atoms (n) and rings (γ) as well as the sum of the rows/columns (D_i/D_j) of the topological distance matrix of the molecule [98].

$$J = \frac{m}{\gamma + 1}\sum_{i=1}^{n}\sum_{j=1}^{n}(D_i D_j)^{-1/2} \tag{5.2}$$

$$O = \frac{A}{4\pi\left(\frac{3V}{4\pi}\right)^{2/3}} \tag{5.3}$$

Balaban index does not increase substantially with molecular weight, but it does with molecules length. As seen in Fig. 5.1 A, ovality of the molecules showed the same trend with random coil diameter but in parallel series, one for linear molecules and another one for branched molecules.

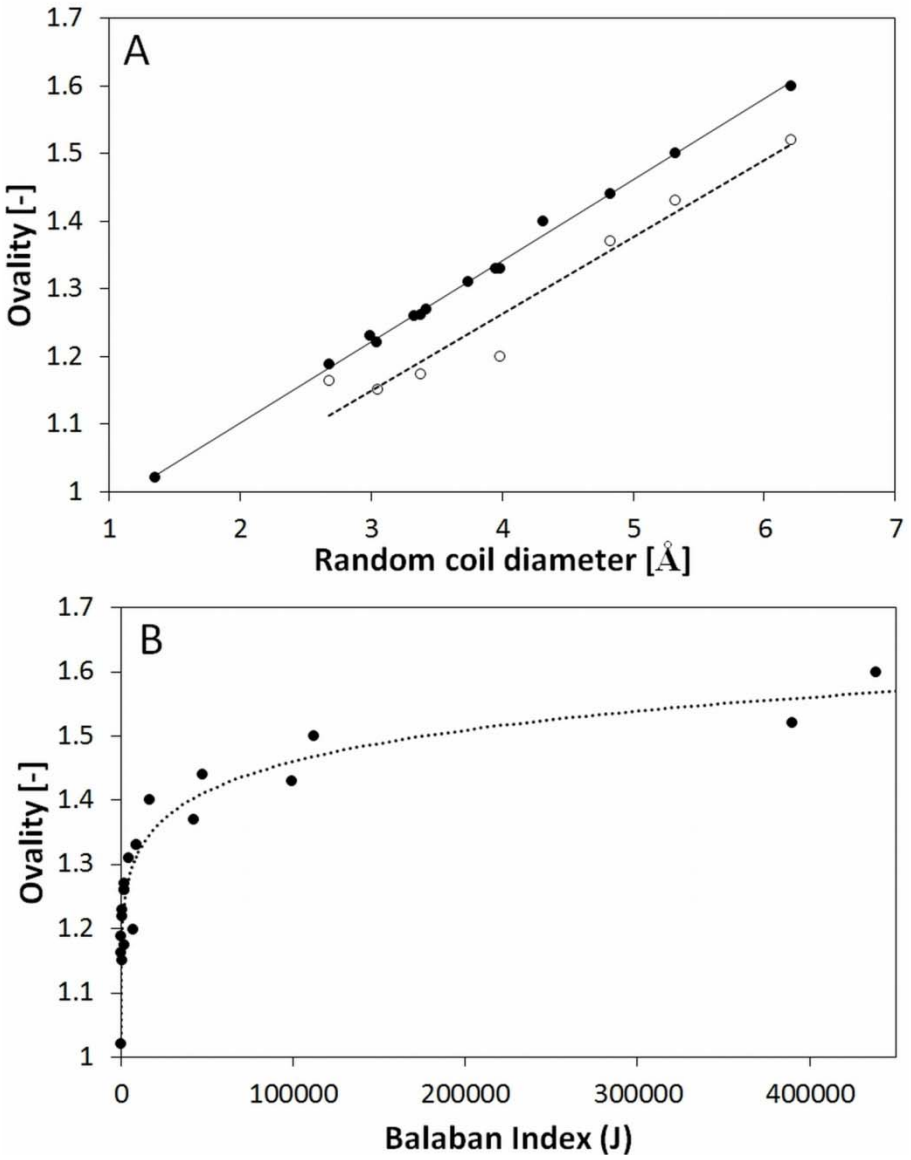

Figure 5.1 (A) Variation of ovality with Random coil diameter of molecules of Table 5.1. Linear molecules (filled circle), branched molecules (open circle). (B) Variation of ovality with Balaban index of molecules of Table 5.1

Branched molecules had equal random coil diameters but lower ovalities (rounder shapes) than their linear homologues. Fig 5.1 B shows the relationship between the Balaban index and molecular shape. Branched molecules have lower Balaban indexes than their linear homologues (Table 5.1), unifying in this way the description of the ovality for all type of molecules. As can be seen, only water diffusion is not restricted in the zeolites micropore system (see micropore diameters in Table 3.8). Olefins, alcohols and especially ethers may have diffusion problems. However, small alcohols such as 1-pentanol and branched ethers have lower Balaban indexes (see Table 5.1) which might imply an extra advantage to be placed and react in the pores/cages of zeolites and

diffuse along the zeolites micropores system, especially in the micropores of medium pore zeolites.

Table 5.1. Molecular weights, random coil diameters, molecule lengths, ovalities and Balaban indexes of different alcohol, ether and hydrocarbon molecules

Molecule	M_W (g/mol)	Φ_d (Å)	$2.5 \cdot \Phi_d$ (Å)	Molecule length (Å)[a]	Balaban Index, J[a]	Ovality[a]
1-Octanol	130.23	4.31	10.77	11.8	17079	1.40
1-Hexanol	102.18	3.74	9.34	9.2	4650	1.31
1-Pentanol	88.15	3.42	8.56	8.0	2076	1.27
1-Octene	112.24	3.95	9.87	10.6	9299	1.33
1-Hexene	84.16	3.33	8.33	8.1	2076	1.26
1-Pentene	70.14	2.99	7.48	6.8	791	1.23
DNOE	242.45	6.21	15.52	20.8	438650	1.60
DNHE	186.34	5.32	13.30	15.8	112231	1.50
DNPE	158.29	4.83	12.08	13.3	47833	1.44
Water	18.02	1.35	3.36	1.5	0	1.02
Butane	58.12	2.68			237	1.19
Pentane	72.15	3.04			791	1.22
Hexane	86.18	3.38			2076	1.26
Octane	114.23	3.99			9299	1.33
1-methylpropane	58.12	2.68			213	1.16
2,2-dimethylpropane	72.15	3.04			633	1.15
3-methylpentane	86.18	3.38			1838	1.17
3,4-dimethylhexane	114.23	3.99			7528	1.20
1,3-pentybispentane	158.29	4.83			42619	1.37
1,3-hexybishexane	186.34	5.32			99263	1.43
1,3-oxybisoctane	242.45	6.21			390017	1.52

(a) Calculated with Chembiodraw software

Selectivity to ether or olefin depends firstly on pore structure of catalyst so that in the very constricted pore space S_N2 dehydration reaction might be highly limited by steric hindrance, E_1 elimination reaction being conversely favored. In line with these ideas, it can be seen in Table 5.2 that regarding zeolites with SiO_2/Al_2O_3 ratios between 20 and 30, S_{HeOH}^{DNHE} decreases (and $S_{HeOH}^{C_6^=}$ increases) in the order H-FAU-30, H-BEA-25, H-MOR-20, H-FER-20 and H-MFI-28. As expected, large pore zeolites are more selective to linear ether. Furthermore, as ethers formation might be kinetically hindered by diffusion, it is assumed that contribution to ether synthesis of sterically non-restricted zones of the catalyst (such as mesopore or external surfaces) could become significant. Therefore, in order to see the variation of catalytic activity with temperature, some zeolites were tested in the range 423-473 K. Alcohol conversion, selectivity and yield data obtained on tested zeolite catalysts are shown in Table 5.2.

5.2.1 Alcohol conversion

Alcohol conversion increased with temperature regardless the alcohol length. As a whole, conversion levels of the three alcohols are similar at each temperature and no clear trend is depicted. Only a slight trend is observed at 453 K on H-FAU-6, being $X_{PeOH} < X_{HeOH} < X_{OcOH}$. By comparing H-BEA-25, H-FAU-6 and H-FAU-30 it is seen that conversions on H-FAU-6 are a bit higher at the lower temperatures of the range, but at the higher temperatures H-BEA-25 and H-FAU-30 gave higher conversions.

However, in all the cases selectivity to linear ether is lower on H-FAU-6, and conversely selectivity to alkenes is higher. To explain this behavior it is suitable to consider both acid sites number and zeolites morphology. H-FAU-6 (4.59 mmol/g) has much higher acid site concentration than H-BEA-25 (1.23 mmol/g) and H-FAU-30 (1.07 mmol/g), but mesoporous surface is clearly smaller (82 m^2/g in front of 219 and 181, respectively). So, it is likely that the relatively bulky alcohols react preferably in the sterically non-restricted mesoporous surface. In the case of H-FAU-6, the noticeable selectivity to olefins and branched ethers suggests that the microporous system could take part in a significant extent favoring the least sterically demanding E1 dehydration to olefin.

Table 5.2. Conversion of alcohol (X_{ROH}), selectivity to linear ether (S_{ROH}^{ROR}), olefins ($S_{ROH}^{C^=}$) and branched ethers ($S_{ROH}^{ROR'}$) and yield of linear ether (Y_{ROH}^{ROR}) at 6 h of reaction

Zeolite	T (K)	X_{ROH} (%)			S_{ROH}^{ROR} (%)			$S_{ROH}^{C^=}$ (%)			$S_{ROH}^{ROR'}$ (%)			Y_{ROH}^{ROR} (%)		
		X_{PeOH}	X_{HeOH}	X_{OcOH}	S_{PeOH}^{DNPE}	S_{HeOH}^{DNHE}	S_{OcOH}^{DNOE}	$S_{PeOH}^{C_5^=}$	$S_{HeOH}^{C_6^=}$	$S_{OcOH}^{C_8^=}$	$S_{PeOH}^{PeOPe'}$	$S_{HeOH}^{HeOHe'}$	$S_{OcOH}^{OcOOc'}$	Y_{PeOH}^{DNPE}	Y_{HeOH}^{DNHE}	Y_{OcOH}^{DNOE}
H-BEA-25	423	4.3		5.45	89.6		77.1	3.07		6.64	7.30		16.3	3.84		4.20
	433	8.9	6.65		91.8	92.2		2.66	2.84		5.58	4.99		8.14	6.13	
	443	16.9	15.9		92.2	89.5		2.65	4.56		5.15	5.95		15.5	14.3	
	453	32.0	33.7	29.5	92.2	87.8	79.6	3.01	6.51	9.69	4.83	5.73	10.8	29.5	29.6	23.4
	463	50.3	56.2		94.9	87.9		2.19	7.69		2.96	4.43		47.8	49.3	
	473		75.4			93.2			6.15			0.64			70.3	
H-FAU-6	423			7.52			52.7			22.1			25.2			3.96
	433		8.79			81.2			9.91			8.88			7.14	
	443		15.2			81.1			8.63			10.3			12.4	
	453	22.7	27.9	33.5	86.6	77.2	58.3	6.92	12.3	23.2	6.49	10.5	18.6	19.6	21.6	19.5
	463		40.5			76.9			13.6			9.52			31.2	
	473		50.3			78.0			14.3			7.34			39.2	
H-FAU-30	423			2.28			100			0			0			2.28
	433		5.99	3.62		94.6	100		3.45	0		1.95	0		5.67	3.62
	443		11.6	13.0		95.3	90.2		2.65	5.04		2.07	4.74		11.1	11.7
	453	22.8	23.9	22.1	96.4	94.6	89.6	1.85	2.74	4.06	1.74	2.63	6.32	22.0	22.6	19.8
	463		42.2	41.9		94.3	87.1		2.27	6.27		2.78	6.67		39.8	36.0
	473		61.9	53.8		92.7	86.0		4.92	8.76		2.35	5.21		57.4	46.3
H-MFI-28	443		7.50			27.7			62.3			9.96			2.08	
	453	34.3	15.7		36.6	23.6		43.3	62.7		20.1	14.2		12.6	3.70	
	463		24.6			25.4			54.9			19.7			3.25	
H-MOR-20	423			0.881			70.1			30.0			0			0.617
	453	5.64	5.09	4.64	59.6	59.8	45.7	30.7	31.6	34.9	9.70	8.60	19.4	3.36	3.04	2.12
H-FER-20	453	2.15	1.79	2.74	59.2	43.2	61.4	39.2	52.7	38.6	1.63	4.18	0	1.27	0.77	1.68
H-MCM-79	453		1.94			76.7			18.7			4.58			1.49	
	463		3.80			79.0			16.0			5.01			3.00	

Reaction conditions: W= 1 g, P = 2.5 MPa, 70 cm^3 alcohol

H-MFI-28 has 4.5-4.7 Å micropores (see Table 3.8), very close to 1-octanol and 1-hexanol random coil diameters. As seen in Table 5.2, conversion greatly decreases from 1-pentanol to 1-hexanol; being 1-pentanol conversion twice that of 1-hexanol. This fact might be in line with the smaller random coil diameter of 1-pentanol and also by its molecular shape, closer to a sphere than 1-hexanol. H-FER-20 and H-MOR-20 showed poor conversions. Their low mesoporous surface and narrow micropores represented a clear hindrance for the alcohols to react.

H-MCM-79 showed very low conversions. The very low acid site concentration (0.6 mmol/g) effect cannot be compensated by its very high mesoporous surface.

5.2.1.1 Response surfaces

Data at 453 K for H-BEA-25, H-FAU-30, H-FAU-6, H-MOR-20 and H-FER-20 allowed comparing the influence of zeolite morphology and number of acid sites on conversion for the three reacting systems. In order to figure out the influence of textural properties on alcohol conversion, response surfaces based on mesoporous surface (S_{BJH}), external surface (S_{ext}), BET surface (S_{BET}), microporous surface ($S_{micro} = S_{BET}$-S_{BJH}), acid site concentration ($[H^+]$) and acid strength (in terms of ammonia adsorption enthalpy, ΔH_{ads}) were fitted to conversion data. The response surfaces tested are displayed in Table 5.3 as well as their residual sum of squares. It is seen that the above mentioned morphological properties affect conversion in a different way as a function of the alcohol length. Since 1-pentanol, 1-hexanol and 1-octanol have different density and molecular weight, initial mass of alcohol and thus, the initial number of moles (n^0_{ROH}) were slightly different. Therefore, the number of alcohol moles consumed, defined by eq. 5.4, was used to compare the conversion of the three alcohols.

$$N_{ROH} = X_{ROH} \cdot n^0_{ROH} \tag{5.4}$$

Since reaction can occur in both mesoporous and microporous surface, different combinations of these surfaces areas were fitted to conversion data. Most surface response equations are functions of acid site concentration and the ratio of mesoporous and microporous areas to BET surface area. Equations where mesoporous and microporous surface areas are in separated terms gave better fits. This fact suggests that conversion is related to surface areas closer than to surface areas ratios.

As Table 5.3 shows, the lowest residual sum of squares for the three alcohols as a whole corresponds to model RS9.

Table 5.3. Response surface equations and their residual sum of squares

Model	$N = X_{ROH} \cdot n^0_{ROH}$	$\sum_{i=1}^{n}(N_{calc} - N_{exp})_i^2$		
		OcOH	HeOH	PeOH
RS1	$a \cdot \left(\frac{S_{BJH}}{S_{BET}}\right) + b \cdot \left(\frac{S_{micro}}{S_{BET}}\right)$	93.1	99.4	79.3
RS2	$a \cdot \left(\frac{S_{BJH}}{S_{BET}}\right) \cdot [H^+] + b \cdot \left(\frac{S_{micro}}{S_{BET}}\right)$	33.7	113	161
RS3	$a \cdot \left(\frac{S_{BJH}}{S_{BET}}\right) + b \cdot \left(\frac{S_{micro}}{S_{BET}}\right) \cdot [H^+]$	43.1	66.9	61
RS4	$a \cdot \left(\frac{S_{BJH}}{S_{BET}}\right) \cdot [H^+] + b \cdot \left(\frac{S_{micro}}{S_{BET}}\right) \cdot [H^+]$	33.7	113	163
RS5	$a \cdot (S_{BJH}) + b \cdot (S_{micro}) \cdot [H^+]$	16.9	25.6	19.8
RS6	$a \cdot (S_{BJH}) \cdot [H^+] + b \cdot (S_{micro}) \cdot [H^+]$	7.63	55.4	94.4
RS7	$a \cdot \left(\frac{S^2_{BJH}}{S_{BET}}\right) \cdot [H^+] + b \cdot \left(\frac{S^2_{micro}}{S_{BET}}\right) \cdot [H^+]$	7.53	18.5	28.7
RS8	$a \cdot (S_{BJH}) \cdot [H^+] + b \cdot \left(\frac{S^2_{micro}}{S_{BET}}\right) \cdot [H^+]$	7.63	55.4	94.4
RS9	$a \cdot (S^2_{BJH}) \cdot [H^+] + b \cdot (S^2_{micro}) \cdot [H^+]$	1.12	0.471	3.91
RS10	$a \cdot (S^2_{BJH}) \cdot [H^+] \cdot \Delta H_{ads} + b \cdot (S^2_{micro}) \cdot [H^+] \cdot \Delta H_{ads}$	4.32	0.706	0.790
RS11	$a \cdot (S^2_{BJH}) \cdot [H^+] + b \cdot (S^2_{micro}) \cdot [H^+] \cdot \Delta H_{ads}$	3.01	0.225	2.26
RS12	$a \cdot (S_{BJH}) \cdot [H^+] + b \cdot (S_{micro}) \cdot [H^+]$	7.63	55.4	94.4
RS13	$a \cdot \frac{[H^+]}{S_{ext}} + b \cdot \frac{[H^+]}{S_{micro}}$	162	355	431
RS14	$a \cdot \frac{[H^+]^2}{S_{ext}} + b \cdot \frac{[H^+]^2}{S_{micro}}$	216	478	591
RS15	$a \cdot \frac{[H^+]}{S^2_{ext}} + b \cdot \frac{[H^+]}{S^2_{micro}}$	273	539	621
RS16	$a \cdot \left(\frac{S_{ext}}{S_{BET}}\right)[H^+] + b \cdot \left(\frac{S_{micro}}{S_{BET}}\right)[H^+]$	36.1	89.8	124

The introduction of acid strength (ΔH_{ads}) upgraded the fit for 1-pentanol in model RS10, and for 1-hexanol in model RS11, but the two equations fit 1-octanol conversion data worse than model RS9. Therefore, the N_{ROH} relationship as a function of acid capacity and mesoporous and microporous surface areas is best represented by model RS9:

$$N_{ROH} = a \cdot \left(S_{BJH}{}^2 \cdot [H^+]\right) + b \cdot \left(S_{micro}{}^2 \cdot [H^+]\right) \quad (5.5)$$

The first term accounts for the contribution of mesoporous surface to conversion, whereas the second one accounts for that of micropores. Figure 5.2 shows the goodness of equation 5.5 by comparing estimated conversion values (N_{calc}) to conversion data (N_{exp}).

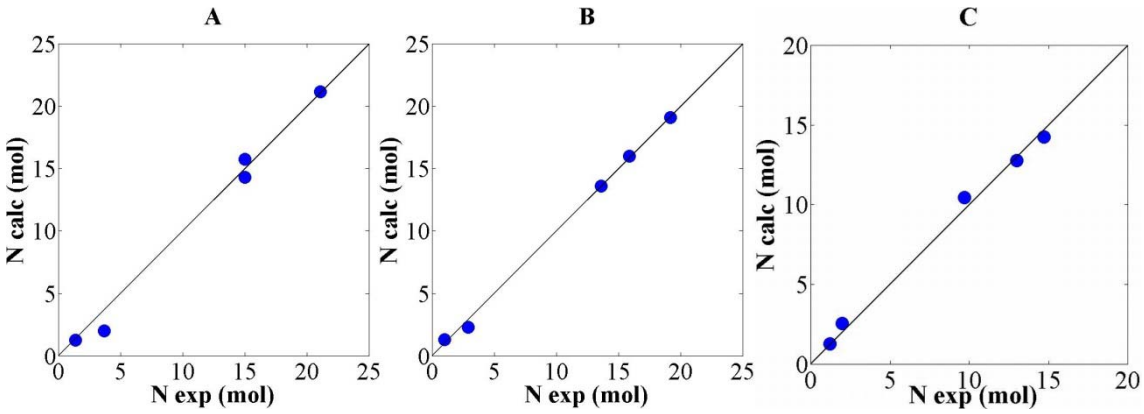

Figure 5.2. Experimental (N exp) and predicted (N calc) conversion values for 1-pentanol (A), 1-hexanol (B) and 1-octanol (C)

Values of parameters a and b for the three alcohols are shown in Table 5.4. It is seen that a values decrease with the alcohol length whereas b increases. It is to be noted that the weight of the microporous term for 1-octanol (6%) is higher than for the other alcohols.

Table 5.4. Values of parameters of equation 5.5 (a,b) and contribution of mesoporous and microporous surface to conversion

Alcohol	$a \cdot 10^4$ ($mol \cdot g^3/(m^4 \cdot mmol\ H^+)$)	$b \cdot 10^4$ ($mol \cdot g^3/(m^4 \cdot mmol\ H^+)$)	Contribution of mesopores (%)	Contribution of micropores (%)
1-pentanol	3.4757	0.0766	97.8	2.2
1-hexanol	3.0975	0.0989	96.9	3.1
1-octanol	1.9809	0.1251	94.1	5.9

This fact can be attributed to the different molecular size of compounds involved: 1-pentanol and 1-hexanol conversion takes place in a great extent in the mesopores and the symmetrical ether is the product preferably formed since there is low steric hindrance. In a minor extent, conversion of 1-pentanol and 1-hexanol takes place in micropores, but inside micropores DNPE and DNHE formation competes with that of olefins and branched ethers. The presence of DNPE and DNHE in the zeolite

micropores might slow down olefins and branched ethers formation. In the case of 1-octanol, the micropores have negative effect on DNOE formation, and the dehydration of 1-octanol to 1-octene and C_{16} branched ethers formation would be favored.

5.2.2 Selectivity

Selectivity to linear ether did not change significantly with the extent of reaction in the alcohol conversion range explored. For example, as can be seen in Figure 5.3 selectivity to DNOE of H-FAU-30 at 453 K hardly changes after 1h of reaction within the limits of the experimental error. For this reason, selectivity at the end of the experiment (6 h of reaction time) was representative enough to compare the catalysts behavior.

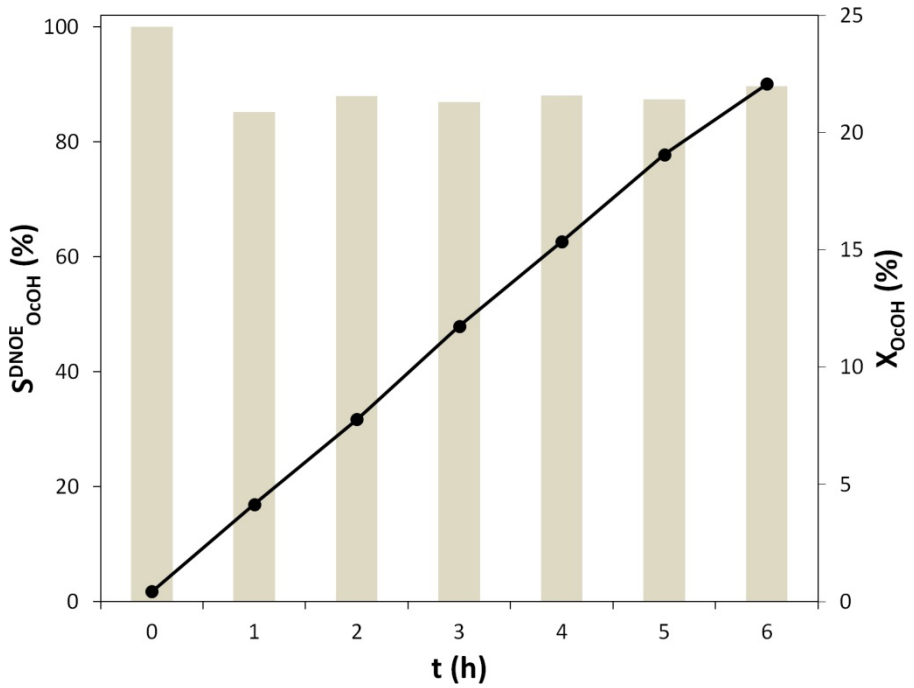

Figure 5.3. Variation of selectivity to DNOE (grey bars) and conversion of 1-octanol (circles) with time. H-FAU-30, W = 1 g, T = 453 K, P = 2.5 MPa

Selectivity data of zeolites with $20 \leq SiO_2/Al_2O_3 \leq 30$ show that large pore H-BEA-25 and H-FAU-30 are much more selective to linear ether than medium pore zeolites (Table 5.2), which indicates that having large external surface areas is essential for the formation of symmetrical ethers.

H-MOR-20 and H-FER-20

It is interesting to compare the medium pore zeolites H-MOR-20 and H-FER-20. They have similar acid site number and *mesoporous surface* but different pore structure. The 1D pore system of H-MOR-20 has 6.45 Å channels and 6.7 Å cages whereas H-FER-20 has a 2D channel system with narrow pores (4.69 Å) and 6.31 Å cages [59] (Table 3.8). In the case of 1-octanol, it is not likely a significant formation of DNOE in the narrow pores of H-FER-20. As a result, DNOE synthesis takes place at the *mesoporous surface* whereas olefin formation is promoted in H-FER-20 micropores.

However, selectivity to *branched ethers* showed a noticeable trend. As seen, random coil diameter set the same molecular size for branched and linear ethers (Table 5.1), not taking into account that *branched ethers* are rounder molecules than linear ethers. On the contrary Balaban indexes of *branched ethers* are lower than their respective linear homologues. This way, taking a look to Balaban indexes it is possible to infer that *branched ethers* are less space-demanding molecules to be created in narrow structures than linear ethers. Since *branched ethers* are smaller molecules than their linear homologues, they could fit the micropores to some extent. This is generally seen comparing $S_{OcOH}^{OcOOc'}$, $S_{HeOH}^{HeOHe'}$ and $S_{PeOH}^{PeOPe'}$ of H-MOR-20. Its selectivity to olefins is similar for the three reaction systems but $S_{OcOH}^{OcOOc'}$ is clearly the highest; showing that in this case C_{16} branched ethers formation competes with DNOE formation.

The absence of C_{16} *branched ethers* on H-FER-20 (Table 5.2), suggests that olefin-alcohol reaction does not take place at *mesoporous surface* of H-FER-20, and its narrow micropores are not able to accommodate them. On the contrary, C_{10} and C_{12} *branched ethers* are likely to fit in the micropores someway. From $S_{OcOH}^{OcOOc'}$ values at 453 K (Table 5.2) it is seen that H-MOR-20 was able to accommodate C_{16} *branched ethers* better than H-FER-20. As a result, it can be deduced that the micropore critical size to give place to C_{16} *branched ethers* lies between that of H-MOR-20 and H-FER-20 micropores.

Large pore zeolites

The 3D pore systems of H-BEA-25, H-FAU-6 and H-FAU-30 have large pore and wide cages. A clear trend on selectivity to linear ether is seen on these zeolites: $S_{PeOH}^{DNPE} > S_{HeOH}^{DNHE} > S_{OcOH}^{DNOE}$ is generally observed at all temperatures. Selectivity values reveal that large molecules are sterically hindered in a large extent in the micropores.

H-FAU-6 and H-FAU-30 have the same micropore structure but highly different acid site concentrations and *mesopore surfaces*. Selectivity to linear ether is higher on H-FAU-30 with lower acid site concentration but higher external (and *mesoporous*) *surface* than H-FAU-6. Small *mesoporous surface* of H-FAU-6 could force the alcohol to react within micropores in a higher extent than on H-FAU-30, and thus, selectivity of H-FAU-6 to bulky linear ethers is less than over H-FAU-30 as seen in Table 5.2. Conversely selectivity to olefins is much higher on H-FAU-6.

H-MFI-28 and H-MCM-79

The lowest selectivity to linear ether was found on H-MFI-28 (Table 5.2). Despite it has higher *mesoporous* surface than H-MOR-20 and H-FER-20, its micropores are almost cylindrical and wide enough to allow alcohols react toward olefins and branched ethers, but too narrow to work for linear ether formation.

As for H-MCM-79, its high BET surface fully corresponded to the *mesoporous* part, with almost uniform mesopores around 3-nm width. Comparing pore distributions in Fig. 3.8 (see section 3.5) it is seen that H-BEA-25 or H-FAU-30 mesopores are wider than those of H-MCM-79, which is reflected in the higher selectivity to linear ether of the former zeolites.

It is seen that dependence of selectivity to ether, olefin or branched ether on morphology of zeolites is quite complex. Shape selectivity was observed since some zeolites promoted olefin or branched ethers formation instead of that of linear ether. It is to be noted that reactant, product as well as transition state shape selectivity can play an important role in the products distribution of many reactions carried out over different zeolites [99]. In this case we have not enough data to quantify the observed

selectivity and thus, response surfaces were not used to study the relationship between selectivity and textural parameters.

5.2.3 Yield

Catalytic activity of the most active zeolite in the hexanol-DNHE-water system was compared with dehydration reaction of 1-pentanol to DNPE and 1-octanol to DNOE data. As shown in Table 5.2, H-BEA-25 gave the best linear ether yield. The combination of high conversion and selectivity to linear ethers makes this zeolite the most suitable one to produce linear ethers. It has the highest mesoporous surface as well as the highest ratio of mesoporous to BET area. These facts suggest that for zeolites to have high microporous volume with large pores (for example H-FAU structures) is not as important as having large surface area in the range of mesopores. H-MCM-79 did not show good linear ether yields despite macro and mesopores contribute vastly to the whole surface area of this material. This can be explained by the low acid site number, which is a drawback to achieve valuable conversions. Figure 5.4 shows a graphical summary of the relation of yield to linear ether and mesoporous surface of zeolites.

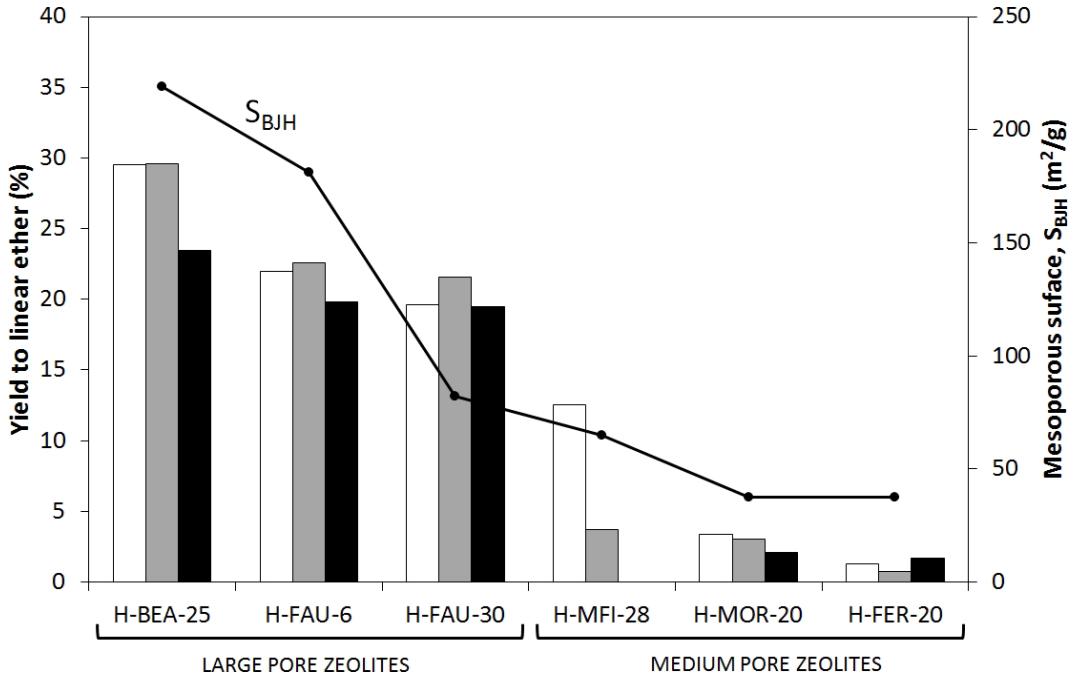

Figure. 5.4. Graphic summary of yield to linear ether, Y_{PeOH}^{DNPE} (white bars), Y_{HeOH}^{DNHE} (grey bars), Y_{OcOH}^{DNOE} (black bars) and mesoporous surface (dots). (W = 1 g, T = 453 K, P = 2.5 MPa, 70 cm^3 alcohol, t = 6 h)

5.2.4 Initial reaction rates

Initial reaction rates of alcohol consumption and ether formation can be useful to highlight the extent of secondary reactions. In the absence of olefin and branched ethers formation, initial reaction rate of linear ether formation should be about a half of that of alcohol consumption. However, only the highly selective H-BEA-25 or H-FAU-30 show initial rates of ether formation close to a half of the alcohol consumption ones, particularly at the lower temperatures of the explored range (Tables 5.5 and 5.6).

Reaction rate of olefins formation rises faster with temperature than that of linear ether synthesis which is reflected by the fact that, at the higher temperatures of the explored range, initial reaction rates of alcohol consumption are more than twice those of linear ether synthesis. On the other hand, as seen in Tables 5.5 and 5.6, reaction rates are highly sensitive to temperature since, as a rule, both initial reaction rates of alcohol consumption and ether formation are more than doubled when temperature rises 10 K.

Tabe 5.5. Initial reaction rates of alcohol consumption

$-r^0_{ROH}$ (mol·h^{-1}·kg^{-1})		T(K)					
Zeolite		423	433	443	453	463	473
H-BEA-25	PeOH	3.98±0.22	9.21±0.31	19.3 ± 0.7	41.4 ± 2.5	116 ±2	
	HeOH		5.50±0.26	14.2 ± 0.3	30.2 ± 1.1	63.7 ±2.7	111.8±6.4
	OcOH	3.06±0.21			24.0 ±0.7		
H-FAU-6	PeOH				46.2 ± 2.0		
	HeOH		10.20±0.85	17.6 ± 1.2	26.1 ± 2.1	82.0 ± 9.1	126 ± 21
	OcOH	6.42±0.74			65.2 ± 8.0		
H-FAU-30	PeOH				29.1 ± 1.2		
	HeOH		4.97±0.13	10.6 ± 0.4	26.0 ± 0.5	42.5 ± 0.3	79.3±4.0
	OcOH	1.14±0.17	2.20±0.19	9.16±0.02	17.12±0.03	41.5 ± 0.4	62.2±5.3
H-MFI-28	PeOH				67 ± 13		
	HeOH			10.3±0.9	20.0±0.7	41±1	
H-MOR-20	PeOH				8.7 ± 1.8		
	HeOH				3.83±0.63		
	OcOH	0.46±0.31			3.64±0.29		
H-FER-20	PeOH				2.06±0.24		
	HeOH				3.04±0.81		
	OcOH				2.64±0.33		
H-MCM-79	PeOH				3.65± 0.56		
	HeOH				1.7± 0.6	2.5± 0.2	

Conditions: W = 1 g, T = 453 K, P = 2.5 MPa, 70 cm^3 alcohol

Table 5.6. Initial reaction rates of linear ether formation

r^0_{ROR} (mol·h^{-1}·kg^{-1})		T(K)					
Zeolite		423	433	443	453	463	473
H-BEA-25	DNPE	1.69±0.05	3.85±0.09	8.52±0.26	18.3±1.1	32.0±0.6	
	DNHE		2.49±0.14	6.04±0.16	12.5±0.8	28.0±1.5	56.0±11.7
	DNOE	1.31±0.10			8.68±0.20		
H-FAU-6	DNPE				19.1±0.6		
	DNHE		3.77±0.09	6.63±0.22	10.7±0.8	29.0±4.6	49.4±4.0
	DNOE	1.32±0.08			7.2 ± 0.9		
H-FAU-30	DNPE				13.8 ± 0.6		
	DNHE		2.27±0.05	4.67±0.11	8.9 ± 0.3	19.9±0.5	38.1±2.4
	DNOE	0.54±0.09	1.20±0.18	4.05±0.31	7.29 ± 0.12	17.3±0.5	28.3±2.3
H-MFI-28	DNPE				25 ± 5		
	DNHE			0.98	2.20	3.5	
H-MOR-20	DNPE				2.3 ±0.4		
	DNHE				0.98 ± 0.05		
	DNOE	0.23±0.16			0.61 ± 0.01		
H-FER-20	DNPE				0.65 ± 0.04		
	DNHE				0.28 ± 0.02		
	DNOE				0.46 ± 0.07		
H-MCM-79	DNPE				1.2± 0.3		
	DNHE				0.84± 0.04	1.6± 0.1	

Conditions: W = 1 g, T = 453 K, P = 2.5 MPa, 70 cm^3 alcohol

5.3 Conclusions

The dehydration reactions of 1-pentanol, 1-hexanol and 1-octanol to DNPE, DNHE and DNOE respectively were performed over H-BEA-25, H-FAU-6, H-FAU-30, H-MFI-28, H-MOR-20, H-FER-20 and H-MCM-49. The selectivity, conversion, yield and initial reaction rates of DNPE, DNHE and DNOE synthesis have been compared and related to the structural properties of zeolites. **Conversion** was found to be strongly related to the zeolites **mesoporous surface** and the **acid sites number**. As for **selectivity** to linear ether, $\mathbf{S^{DNPE}_{PeOH} > S^{DNHE}_{HeOH} > S^{DNOE}_{OcOH}}$ it was generally observed, which reveals a great steric hindrance for bulky molecules. A decrease of selectivity to ether on increasing temperature was also observed over all zeolites tested. Zeolites with high acid capacity and low external surfaces such as H-FAU-6 forced the alcohol to react in micropores promoting this way the elimination to olefins instead of large linear ether. Initial reaction rates of alcohol consumption doubled their values each 10 K increase whereas

initial reaction rates of ether formation did not because of the rise of olefin formation with temperature. **H-BEA-25** gave the best **yield of linear ether**, as a consequence of showing high alcohol conversion and selectivity to linear ether.

CHAPTER 6

Chemical equilibrium of the liquid-phase dehydration of 1-octanol to DNOE

6.1 Abstract

The equilibrium constants for the liquid-phase dehydration of 1-octanol to di-n-octyl ether (DNOE) and water have been determined in the temperature range 413-453 K over Amberlyst 70. The equilibrium constants for the main side reactions, intramolecular dehydration of 1-octanol to 1-octene and 1-octene isomerization to 2-octene, have been determined as well. Etherification of 1-octanol was shown to be exothermic, whereas intramolecular dehydration of 1-octanol has been found to be endothermic and isomerization of 1-octene to 2-octene exothermic. An experimental value for the standard molar entropy in the liquid phase for DNOE has been proposed.

6.2 Results and discussion

Exploratory experiments carried out in the batch reactor in the temperature range 413-453 K over Amberlyst 70, starting from pure 1-octanol, show that alcohol equilibrium conversion was higher than 96 %. Amberlyst 70 was selected for equilibrium experiments because of its high selectivity and activity and thermal resistance, which permitted to work in a wider range of temperatures than the other PS-DVB resins.

It was considered that chemical equilibrium was reached when the composition of the reaction medium remained constant, and in addition, thermodynamic equilibrium constants reached a constant value over time within the limits of the experimental error. Experiments carried out at 413 and 453 K were repeated to evaluate the reliability of data.

Since water is partially miscible in 1-octanol, and DNOE is practically immiscible in water, at such alcohol conversions some problems arose by the split of reaction medium into two immiscible phases by the presence of water in large amounts. First, taking online reliable liquid samples of each phase without stopping the reaction is difficult. In addition, analysis of data is complex with simultaneous chemical and phase equilibria. Therefore, mixtures of composition close to equilibrium were used as raw material instead of pure alcohol.

Delion *et al*.[100] used 1,4-dioxane and a number of solvents in the determination of the equilibrium constant of the 2-methyl-1- propene hydration to 2-methyl-2-propanol on ion-exchange resins. It was found that the values of the chemical equilibrium constant determined from the composition at equilibrium were similar regardless the solvent used within the limits of the experimental error.

It is to be noted that the resin catalyst does not undergo morphological changes by interaction with 1,4-dioxane since it has been reported that this cyclical ether does not swell the Amberlyst 70 beads [45]. Finally, it was checked in blank experiments that 1,4-dioxane did not undergo any chemical reaction in the assayed temperature range [45]. As a consequence,1,4-dioxane was used as solvent to avoid the liquid splitting into aqueous and organic phases, as it was found suitable in previous works [45, 101].

6.2.1 Experimental equilibrium constants, enthalpy and entropy changes

To evaluate the chemical equilibrium constant of the dehydration of 1-octanol to DNOE, the composition of the reaction medium has to be determined, which involves the chemical species participating in the main reaction (water, 1-octanol, and DNOE), and byproducts formed by secondary reactions.

1-octene, (2Z)-2-octene, (2E)-2-octene, (3Z)-3-octene, (3E)-3-octene, (4E)-4-octene, and (4Z)-4-octene were detected as well as very small amounts of C_{16} branched ethers. Olefins other than 1-octene were produced by isomerization reactions, while 1-octene was formed by the intramolecular dehydration of 1-octanol. Branched ethers were produced via etherification of olefins with 1-octanol since no secondary alcohols were detected in the temperature range 413-453 K. Figure 6.1 shows the reactions studied in this chapter. They are the intermolecular dehydration of 1-octanol to DNOE (I), intramolecular dehydration of 1-octanol to 1-octene (II), and the isomerization of 1-octene to 2-octene (III).

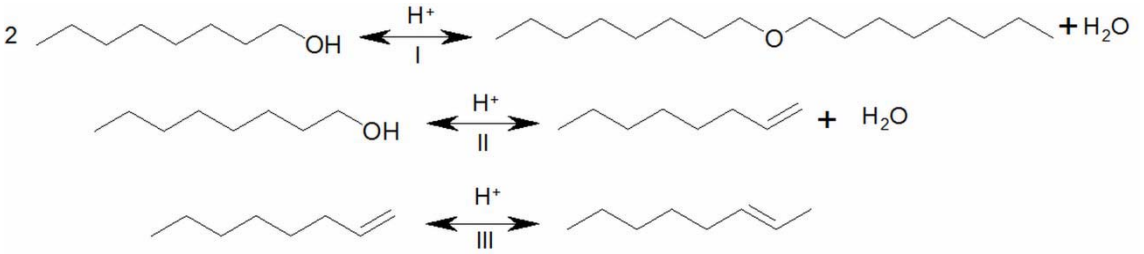

Figure 6.1. Equilibria reaction studied. (I) Intermolecular dehydration of 1-octanol to DNOE, (II) intramolecular dehydration of 1-octanol to 1-octene, (III) isomerization of 1-octene to 2-octene

Different molecular shapes (cyclic 1,4-dioxane, water, C_8 linear alcohol, C_8 linear olefins, C_{16} linear ether) and intermolecular force strengths (hydrogen bonds, van der Waals forces) present in the liquid caused the mixture diverge from the concept of ideal solution [102]. For this reason, the use of activities was necessary in the calculation of the chemical equilibrium constants. Figure 6.2 shows the evolution of compounds activity with time through an experiment.

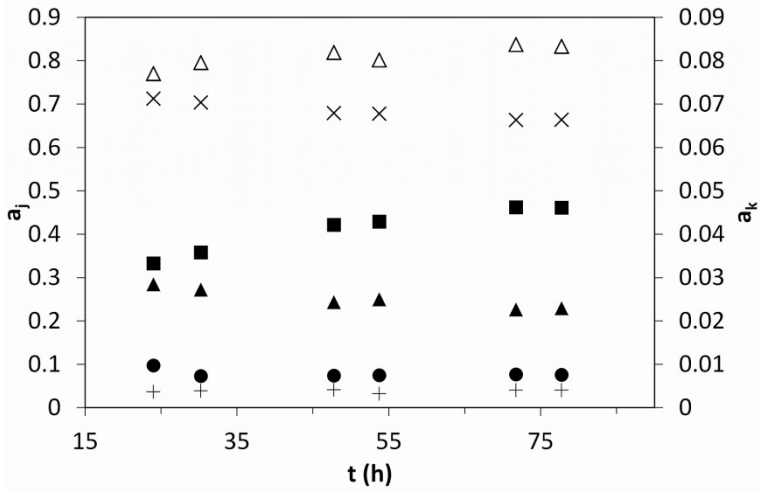

Figure 6.2. Evolution of activities during an experiment at 453 K. j: 1,4-dioxane (x symbol), water (square). k: 2-octene (open triangle), DNOE (filled triangle), 1-octanol (circle), 1-octene (+ symbol)

The experiment was carried out at the highest temperature of the working range, which favored the intramolecular dehydration of 1-octanol to form 1-octene, with the subsequent isomerization to 2-octene. As a consequence, in relation to the initial mixture composition, when chemical equilibria were reached, DNOE and 1-octanol activities have decreased slightly, activities of water and 2-octene have risen slowly, and that of 1-octene remained almost constant. It was considered that the reaction system was at chemical equilibrium at 80 h provided that equilibrium constants hardly changed within the limits of the experimental error. The activity of a compound, a_j, is

defined as the product of its molar fraction in the liquid, x_j, and its activity coefficient, $\gamma_{x,j}$.

Activity coefficients were estimated by using the UNIFACDORTMUND predictive method [103], and the thermodynamic equilibrium constant for each reaction, K, was calculated from the molar fractions and activity coefficients of species at equilibrium as follows:

$$K = \prod_{j=1}^{S} (a_j)_e^{\nu_j} = \prod_{j=1}^{S} (\gamma_{x,j} \cdot x_j)_e^{\nu_j} = \prod_{j=1}^{S} (\gamma_{x,j})_e^{\nu_j} \prod_{j=1}^{S} (x_j)_e^{\nu_j} = K_\gamma \cdot K_x \quad (6.1)$$

$$K^I = K_\gamma^I \cdot K_x^I = \frac{\gamma_{x,DNOE} \cdot \gamma_{x,water}}{\gamma_{x,1-octanol}^2} \cdot \frac{x_{DNOE} \cdot x_{water}}{x_{1-octanol}^2} \quad (6.2)$$

$$K^{II} = K_\gamma^{II} \cdot K_x^{II} = \frac{\gamma_{x,1-octene} \cdot \gamma_{x,water}}{\gamma_{x,1-octanol}} \cdot \frac{x_{1-octene} \cdot x_{water}}{x_{1-octanol}} \quad (6.3)$$

$$K^{III} = K_\gamma^{III} \cdot K_x^{III} = \frac{\gamma_{x,2-octene}}{\gamma_{x,1-octene}} \cdot \frac{x_{2-octene}}{x_{1-octene}} \quad (6.4)$$

Superscripts I, II, and III refer to 1-octanol dehydration to DNOE, intramolecular dehydration of 1-octanol to 1-octene, and 1-octene isomerization to 2-octene, respectively. K_γ is the product of activity coefficients, and K_x is the equilibrium constant as a function of molar fractions. As can be seen in Figure 6.2, water and 1,4-dioxane had the highest activities. Activity coefficients at equilibrium were estimated to be: 3.391 (water), 1.372 (2-octene), 1.315 (1-octene), 1.079 (1-octanol), 1.038 (DNOE), and 1.031 (1,4- dioxane). Accordingly, the high activity of water was due to its very nonideal behavior. On the contrary, the high activity of 1,4-dioxane was due to its high concentration since the activity coefficient is close to unity. Activities of DNOE, 1-octanol, and 2-octene were low since their activity coefficients were only a bit higher than 1. The activity of 1-octene was the lowest in all experiments due to its very low molar fraction in the liquid. The 1-octene concentration in the liquid was close to the threshold of chromatographic detection which caused that standard errors of equilibrium constants of reaction II were higher than those of reactions I and III. The reliability of the universal functional coefficient (UNIFAC)-DORTMUND predictive method for activity coefficient estimation has been shown in particular cases, such as infinite dilution activity coefficients for binary mixtures [104].

In nonideal systems, as in the case of ethanol−water mixtures the average deviation of the UNIFAC estimation can be evaluated with the factor UF, defined as UF = $\gamma_{\text{experimental}}/\gamma_{\text{UNIFAC}}$ [105] In the case of ethanol−water mixtures UF mean values range between 1.015 for ethanol and 1.061 for water, with standard deviations of 0.033 and 0.041, respectively [105].

Equilibrium constants for the reactions are shown in Table 6.1. As can be observed, the high activity coefficients of water resulted in K_{γ}^{I} and K_{γ}^{II} values quite different from unity, which show the need of taking into account the nonideality of mixtures in the calculation of chemical equilibrium constants. Concerning equilibrium constants it is seen that $K^{I} > K^{III} > K^{II}$. As a result, high equilibrium conversions of 1-octanol can be expected in an industrial process for DNOE synthesis from 1-octanol, and the quantities of olefin formed would be very little; 2-octene being the olefin in a higher amount.

From the temperature dependence of K it is seen that the dehydration of 1-octanol to DNOE and the 1-octene isomerization to 2-octene were exothermic reactions because their equilibrium constants decreased with temperature. On the contrary, the dehydration of 1-octanol to 1-octene was endothermic since its equilibrium constant increased with temperature. These facts are in agreement with the general patterns found in literature about formation of ether by alcohol dehydration, olefin isomerization, and dehydration of alcohol to olefin [45, 101].

As the reactor pressure (2.5 MPa) greatly differed from standard pressure (0.1 MPa), the effect of pressure on equilibrium constants was evaluated by the Poynting correction factor K_{Γ} [106]:

$$K_{\Gamma}^{i} = \exp\left[\frac{P - P^{0}}{RT}\sum_{j=1}^{S}\nu_{i,j}\cdot V_{j}\right] \tag{6.5}$$

where P is the working pressure, P^{0} the standard pressure, V_j the molar volume of compound j and $\nu_{i,j}$ the stequiometric coefficient of the compound j in the reaction i. V_j was estimated by the Hankinson−Brobst−Thomson method [107] and K_{Γ}values for

all reactions were found to be very close to unity (0.995 for reactions I and III, and 1.040 for reaction II).

Table 6.1. Mean experimental values and standard uncertainties of the equilibrium constant of the different reactions at the range of 413 to 453 K and 2.5 MPa

	I			II			III		
T (K)	K_x	K_γ	K	$K_x \cdot 10^1$	K_γ	$K \cdot 10^1$	K_x	K_γ	K
413.2	94.2 ± 2.9	3.026 ± 0.002	285 ± 9	1.25 ± 0.23	2.950 ± 0.077	3.7 ± 0.7	28.4 ± 2.2	1.0513 ± 0.0002	29.8 ± 2.3
423.2	84.9 ± 1.6	2.835 ± 0.002	244 ± 5	1.13 ± 0.16	2.746 ± 0.011	3.1 ± 0.4	27.4 ± 2.5	1.0512 ± 0.0002	28.8 ± 2.6
433.2	84.9 ± 0.3	2.656 ± 0.004	225 ± 1	1.24 ± 0.11	2.473 ± 0.013	3.0 ± 0.3	24.7 ± 1.7	1.047 ± 0.001	25.9 ± 1.7
443.2	90.8 ± 1.8	2.411 ± 0.002	219 ± 4	3.38 ± 0.37	2.103 ± 0.006	7.1 ± 0.8	23.3 ± 3.5	1.0294 ± 0.004	24.0 ± 3.6
453.2	85.9 ±5.3	2.27 ± 0.01	195 ± 12	4.04 ± 0.73	1.912 ± 0.023	7.7 ± 1.4	20.6 ± 1.6	1.023 ± 0.001	21.1 ± 1.6

(I) Intermolecular Dehydration of 1-octanol to DNOE, (II) intramolecular dehydration of 1-octanol to 1-octene, (III) isomerization of 1-octene to 2-octene. Molar fraction contribution to equilibrium constant (K_x), activity contribution to equilibrium constant (K_γ), and equilibrium constant (K)

Table 6.2. Standard Gibbs energy (Δ_rG^0), enthalpy (Δ_rH^0) and entropy (Δ_rS^0) changes of (I) 1-octanol dehydration to DNOE, (II) Intramolecular dehydration of 1-octanol, (III) 1-octene isomerization to 2-octene at 298.15 K

	I			II			III		
	Δ_rH^0(I)	Δ_rS^0(I)	Δ_rG^0(I)	Δ_rH^0(I)	Δ_rS^0(I)	Δ_rG^0(I)	Δ_rH^0(I)	Δ_rS^0(I)	Δ_rG^0(I)
	kJ·mol^{-1}	J·mol^{-1}·K^{-1}	kJ·mol^{-1}	kJ·mol^{-1}	J·mol^{-1}·K^{-1}	kJ·mol^{-1}	kJ·mol^{-1}	J·mol^{-1}·K^{-1}	kJ·mol^{-1}
Δ_rH^0 (I)ct	-13.5 ± 1.7	14.0 ± 4.0	-17.7 ± 2.1	35.4 ± 15.8	75.3 ± 36.6	13.0 ± 19.2	-13.5 ± 1.5	-4.2 ± 3.6	-12.3 ± 1.9
Δ_rH^0 (I)f(T)	-13.6 ± 1.7	13.9 ± 4.0	-17.7 ± 2.1	35.6 ± 15.4	75.8 ± 35.7	13.1 ± 18.7	-13.5 ± 1.6	-4.2 ± 3.7	-12.2 ± 1.9
Theoretical[a]	-15.9	-15.5	-11.3	16.7	72.8	-5.0	-11.2	-5.3	-9.6

(a) Computed from eq. 6.6 and standard molar entropies and formation enthalpy changes (Table 6.3)

As the effect on the K values ($K = K_x \cdot K_\gamma \cdot K_\Gamma$) was lower than the experimental uncertainty, it can be assumed that the effect of pressure on the equilibrium constants was negligible. Therefore, it was not taken into account in further calculations. The thermodynamic equilibrium constant of a chemical reaction can be written in terms of enthalpy and entropy changes ($\Delta_r H^0$ (l) and $\Delta_r S^0$ (l)) as follows:

$$\ln K = \left(\frac{-\Delta_r G^0 \text{ (l)}}{RT}\right) = \left(\frac{-\Delta_r H^0 \text{ (l)}}{RT} + \frac{\Delta_r S^0 \text{ (l)}}{R}\right) \quad (6.6)$$

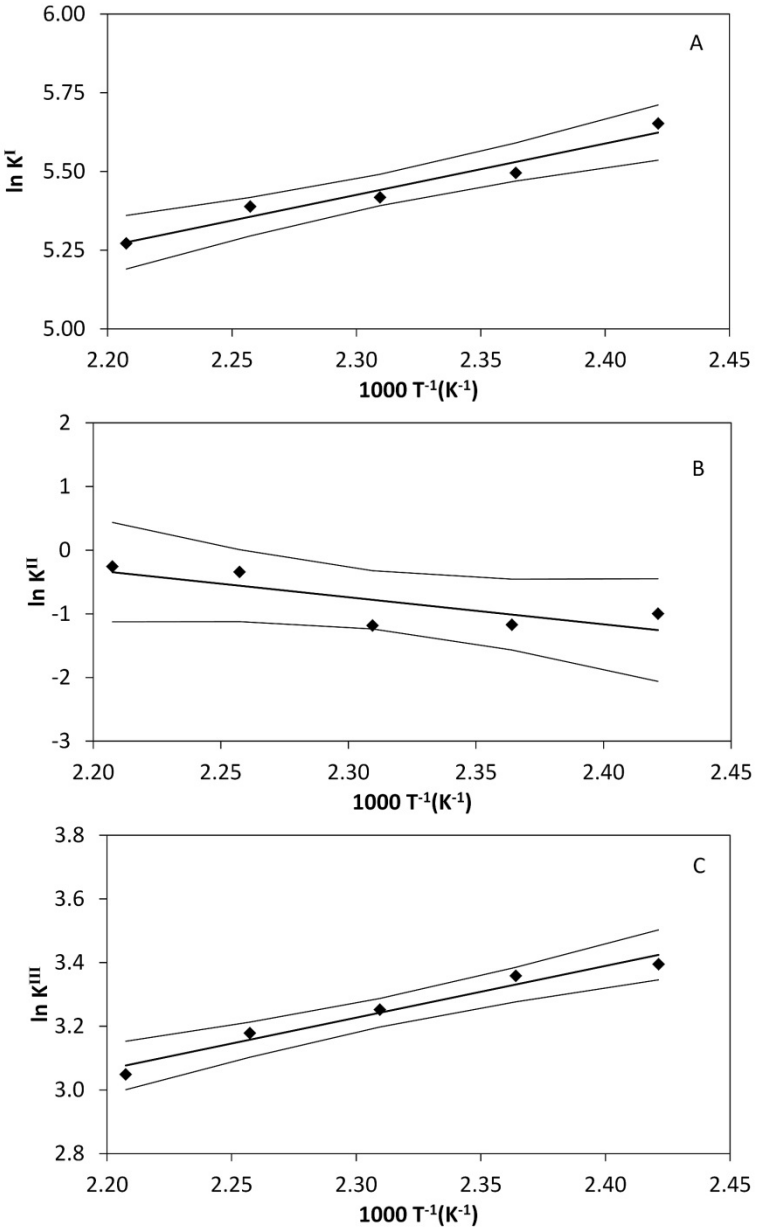

Figure 6.3. Mean experimental values of ln K (rhombus) versus 1/T. Predictive linear model (central solid line) and 0.95-level-of-confidence loci for predicted values (external solid lines). (A) 1-octanol dehydration to DNOE, (B) intramolecular dehydration of 1-octanol, (C) 1-octene isomerization to 2-octene

Assuming that the enthalpy change of reaction does not vary over the temperature range ($\Delta_r H^0$ (l)ct), $\Delta_r H^0$ (l) and $\Delta_r S^0$ (l) were obtained by fitting equation 6.6 to K values of Table 6.1 as Figure 6.3 shows. The intervals at level of confidence 0.95 for predicted values of $\ln K$ are shown too. The temperature dependence of equilibrium constants is given by equations 6.7 to 6.9. The $\Delta_r H^0$ (l) and $\Delta_r S^0$ (l) values for each reaction were computed from the slope and the y-intercept, respectively.

$$\ln K^I = \frac{(1629 \pm 207)}{T} + (1.7 \pm 0.5) \tag{6.7}$$

$$\ln K^{II} = \frac{(-4259 \pm 1902)}{T} + (9.1 \pm 4.4) \tag{6.8}$$

$$\ln K^{III} = \frac{(1625 \pm 186)}{T} - (0.5 \pm 0.4) \tag{6.9}$$

6.2.2 Confidence regions of parameters

It is seen in equations 6.7 to 6.9 that the value of intercept had a relative error higher than the slope. This fact is also shown in Table 6.2, since the uncertainty of $\Delta_r S^0$ (l) is higher than those of $\Delta_r H^0$ (l) and $\Delta_r G^0$ (l) for the three reactions. To evaluate whether the linear model $\ln K = \beta_0 + \beta_1 \frac{1}{T}$ (being $\beta_0 = \frac{\Delta_r S^0 \text{ (l)}}{R}$ and $\beta_1 = \frac{-\Delta_r H^0 \text{ (l)}}{R}$ represented the variation of ln K with $1/T$ satisfactorily from an statistical standpoint, an F-test for each reaction data was performed. By computing the variance due to regression line (s_r^2) and the dispersion due to experimental error (s_e^2) it was possible to compare the variance ratio s_r^2/s_e^2 with the critical value of the F distribution to ascertain if both variances were statistically different. For all reactions, the ratio s_r^2/s_e^2 was lower than the critical value of F-distribution for a probability of 0.95 [108]. Thus, the model $\ln K = \beta_0 + \beta_1 \frac{1}{T}$ represented adequately reactions equilibrium data and the enthalpy and entropy changes of reaction found are significant.

The uncertainties of the slope and intercept have been shown separately in equations 6.7-6.9. However, a simultaneous analysis of the parameters error is more representative for the actual uncertainties of the parameters. In this case, a joint

confidence region for the slope and the intercept is required. To this purpose, the linear model $\ln K = \beta_0' + \beta_1(\frac{1}{T} - \frac{1}{\bar{T}})$ is considered instead of $\ln K = \beta_0 + \beta_1 \frac{1}{T}$, because β_0' and β_1 are stochastically independent, whereas β_0 and β_1 are not. Nevertheless, the confidence region for $\beta_0 = \frac{\Delta_r S^0\ (l)}{R}$ and $\beta_1 = \frac{-\Delta_r H^0\ (l)}{R}$ can be easily obtained from the relationship $\beta_0 = \beta_0' - \beta_1 \frac{1}{\bar{T}}$.

The contour for joint confidence region is obtained by forming the following variance ratio, which has an F-distribution [108]:

$$\frac{\frac{1}{2}[(b_0' - \beta_0')^2 \sum_{i=1}^{n} p_i + (b_1 - \beta_1)^2 \sum_{i=1}^{n} p_i (x_i - \bar{x})^2]}{s_{\bar{Y}_i}^2} = F \qquad (6.10)$$

Being $Y = \ln K$, x the inverse of temperature and p_i.the number of i-experiments. b_0' and b_1 are the estimates of the intercept and the slope, respectively. Given a 0.05 level of significance, equation 6.10 turns into:

$$(b_0' - \beta_0')^2 \sum_{i=1}^{n} p_i + (b_1 - \beta_1)^2 \sum_{i=1}^{n} p_i (x_i - \bar{x})^2 = 2 s_{\bar{Y}_i}^2 F_{0.95} \qquad (6.11)$$

Equation 6.11 represents an ellipse centered in (β_1, β_0') = (b_1, b_0') whose contour delineates the locus of the boundary of an area that includes the values of the parameters β_0' and β_1 with a 0.95 level of confidence. Figure 6.4 represents 0.95-level-of-confidence regions for all the parameters obtained by fitting the pair lnK-T^{-1} experimental values to $y = \beta_0' + \beta_1(x - \bar{x})$ linear models. It is inferred from joint confidence regions that for 1-octanol dehydration to DNOE and 1-octene isomerization β_1 values are located within the positive region of the axis. Since $\Delta_r H^0$ is calculated from β_1 ($\beta_1 = \frac{-\Delta_r H^0\ (l)}{R}$), it is concluded that both DNOE formation and 1-octene isomerization are exothermic reactions. For intramolecular dehydration of 1-octanol the range of joint confidence interval of parameter β_1 includes positive and negative values, which cast light about the uncertainty associated to the K values of this reaction. It must be taken into account that the calculation of β_1 and β_0' confident

regions are made by means of $F_{0.95}$-distribution critical values, which can end up in too conservative intervals compared to those given in Table 6.1 (standard error).

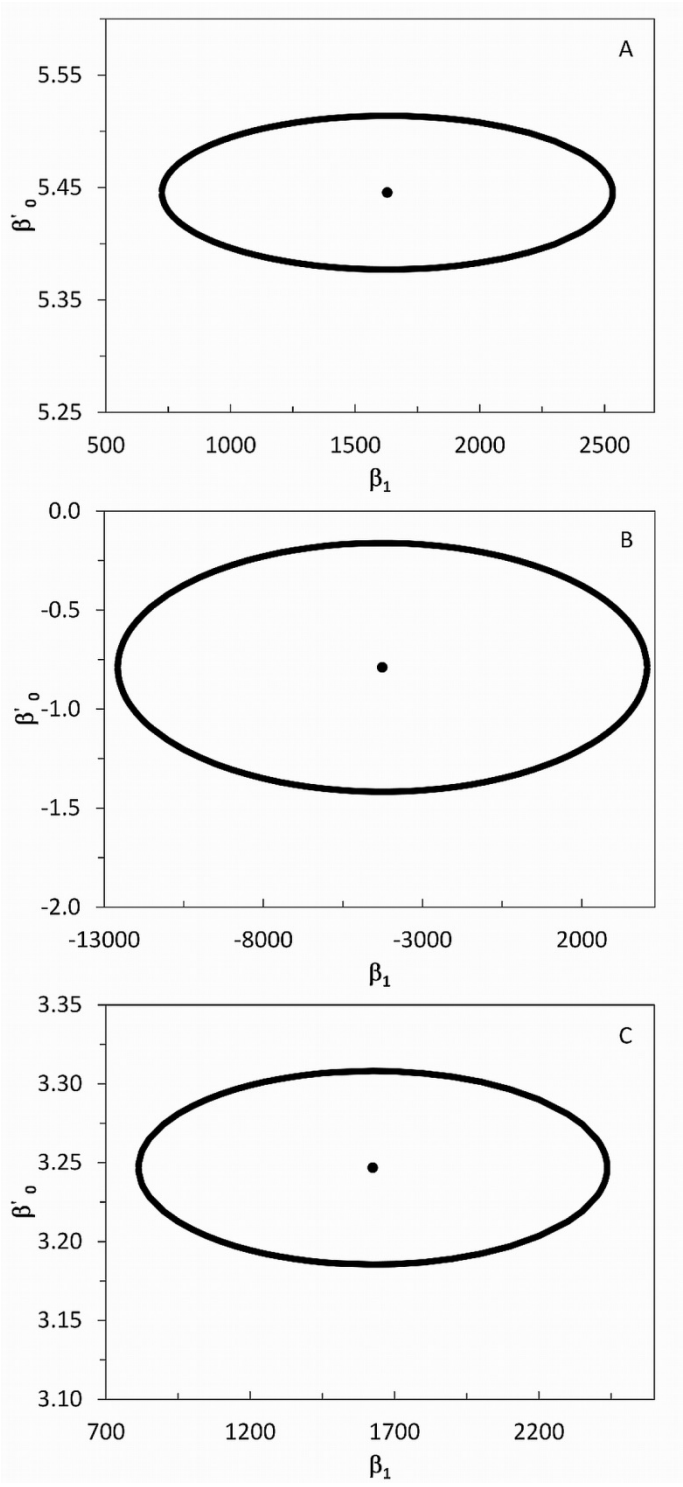

Figure 6.4 Joint 0.95-level-of-confidence region for β_1 and β_0'. Contour of confidence region (solid line) and (b_1, b_0') (solid point). (A) 1-octanol dehydration to DNOE, (B) intramolecular dehydration of 1-octanol to 1-octene, (C) 1-octene isomerization to 2-octene

In particular, for intramolecular dehydration of 1-octanol b_1 is negative, what indicates that this reaction is more likely to be endothermic. In any confidence region a sign change in the value of β_0' is contemplated, however it is necessary to evaluate β_0 to really understand the variability of $\Delta_r S^0$ since it depends directly on β_0 according to $\Delta_r S^o\,(l) = \beta_0/R$. Dependence of β_0 on β_1 makes increase the uncertainty of β_0' as it can be observed for 1-octanol dehydration to DNOE in Figure 6.5.

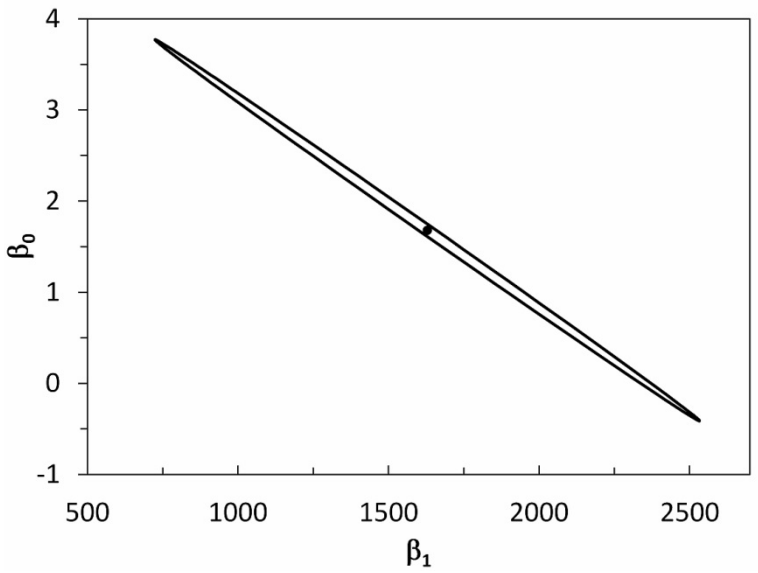

Figure 6.5. Joint 0.95-level-of-confidence region for β_1 and β_0 in 1-octanol dehydration to DNOE. Contour of confidence region (solid line) and (b_1, b_0) (solid point)

In the case of Figure 6.5, relative uncertainty of β_0 is high because is related to β_1 value. Thus, entropy values are bound to a major variation within confidence limits.

Summarizing, 1-octanol dehydration to DNOE and isomerization of 1-octene to 2-octene are exothermic reactions. In this case, there is no doubt about the exothermic nature of these reactions since uncertainty of β_1 leave $\Delta_r H^0\,(l)$ of these two reactions within a negative range of values. On the contrary, it was concluded that 1-octanol dehydration to 1-octene and water is more likely to be endothermic since the range of possible values for $\Delta_r H^0\,(l)$ is mostly positive.

6.2.3 Enthalpy and entropy changes accounting enthalpy variation with temperature

In equations 6.7 to 6.9 the enthalpy change of reactions was considered to be constant over the whole temperature range. However, as a matter of fact, the enthalpy change of reaction is a function of temperature ($\Delta_r H^0$ (l)f(T)). If such variation is taken into account, the relationship between the enthalpy change of reaction and temperature is given by Kirchhoff equation (equation 6.12), and the relationship between the equilibrium constant and temperature is given by van't Hoff equation (equation 6.13).

$$\frac{d\Delta_r H^0}{dT} = \sum_j \nu_j \cdot C^0_{p,m,j} \tag{6.12}$$

$$\frac{d\,\ln K}{dT} = \frac{\Delta_r H^0}{RT^2} \tag{6.13}$$

$C^0_{p,m,j}$ is the molar heat capacity of the compound j involved in the reaction. If $C^0_{p,m,j}$ polynomial dependence on temperature is considered into Kirchhoff and van't Hoff equations, the enthalpy, entropy, and Gibbs energy changes and $\ln K$ as a function of temperature are given for each reaction by equations 6.14 to 6.17 obtained by combining equation 6.6 and integrated expressions of equations 6.12 and 6.13.

$$\Delta_r H^0_{(l)} = I_K + aT + \frac{b}{2}T^2 + \frac{c}{3}T^3 + \frac{d}{4}T^4 \tag{6.14}$$

$$\Delta_r S^0_{(l)} = R \cdot I_H + a\,(\ln T + 1) + bT + \frac{c}{2}T^2 + \frac{d}{3}T^3 \tag{6.15}$$

$$\Delta_r G^0_{(l)} = I_K - R \cdot I_H T - aT\ln T - \frac{b}{2}T^2 - \frac{c}{6}T^3 - \frac{d}{12}T^4 \tag{6.16}$$

$$\ln K = I_H - \frac{I_K}{RT} + \frac{a}{R}\ln T + \frac{b}{2R}T + \frac{c}{6R}T^2 + \frac{d}{12R}T^3 \tag{6.17}$$

where
$a = \sum_j \nu_j \cdot a_j$; $b = \sum_j \nu_j \cdot b_j$; $c = \sum_j \nu_j \cdot c_j$; $d = \sum_j \nu_j \cdot d_j$

and a_j, b_j, c_j and d_j are the coefficients of $C^0_{p,m,j}$ polynomial equations (Table 6.3).

Gathering the terms containing a, b, c, and d as f(T) and $\ln K$ (equation 6.17), I_K and I_H are then obtained from the slope and the intercept of the linear dependence of $\ln K$ + f(T) on 1/T (Figure 6.6), respectively. The following expressions were obtained by linear regression:

$$\ln K^{I} + f(T) = \frac{(1594 \pm 207)}{T} + (4.0 \pm 0.5) \quad 6.18$$

$$\ln K^{II} + f(T) = \frac{(-4284 \pm 1856)}{T} + (9.1 \pm 4.3) \quad 6.19$$

$$\ln K^{III} + f(T) = \frac{(1621 \pm 191)}{T} - (0.5 \pm 0.4) \quad 6.20$$

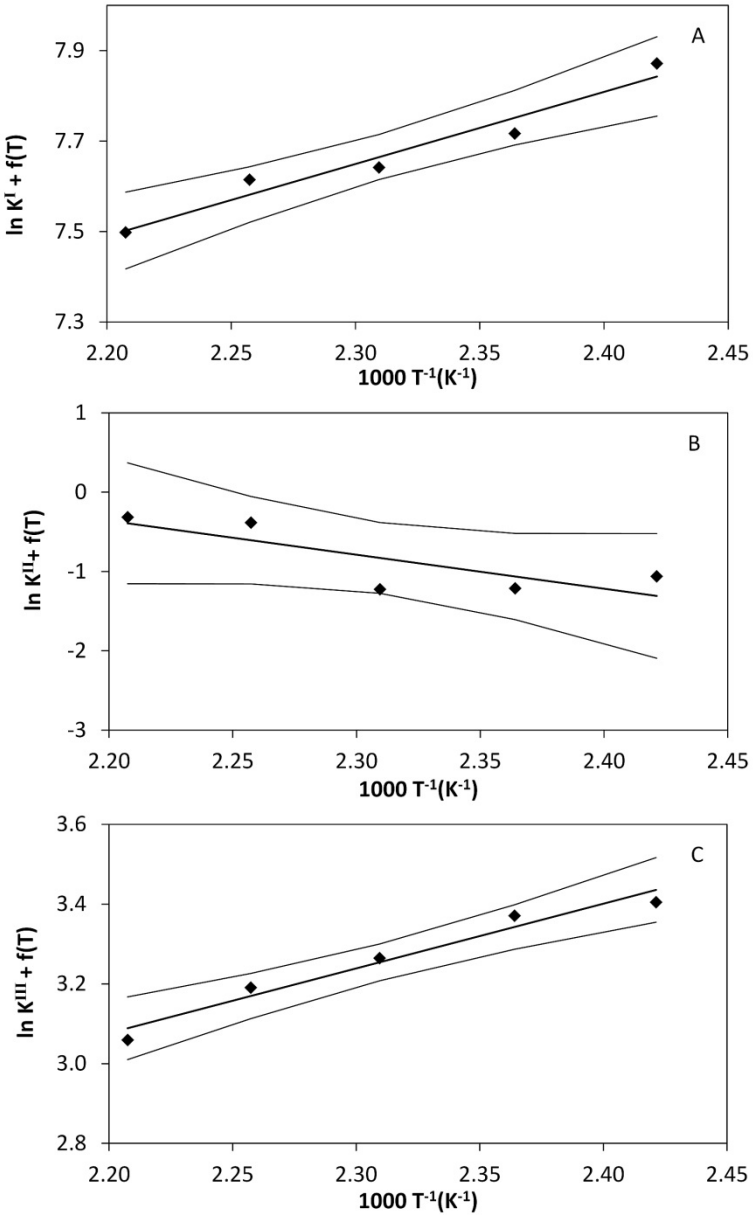

Figure 6.6. Mean experimental values of ln K + f(T) (rhombus) versus 1/T. Predictive linear model (central solid line) and 0.95-level-of-confidence loci for predicted values (external solid lines). (A) 1-octanol dehydration to DNOE, (B) intramolecular dehydration of 1-octanol, (C) 1-octene isomerization to 2-octene

Comparing equations 6.18 to 6.20 with 6.7 to 6.9, it is observed that the slope and intercept values did not change significantly. As Table 6.2 shows, standard enthalpy, entropy, and Gibbs energy changes at 298.15 K computed by considering the dependence of $\Delta_r H^0$ (l) on temperature ($\Delta_r H^0$ (l)f(T)) were very similar to those obtained by considering $\Delta_r H^0$ (l) constant in the whole temperature range ($\Delta_r H^0$ (l) ct). This is not usual since generally the enthalpy change of reaction changes with temperature, and it could be due to the fact that heat capacity of the medium hardly varied with temperature. On the other hand, on comparing $\Delta_r S^0$ (l), $\Delta_r H^0$ (l), and $\Delta_r G^0$ (l) with values found from formation enthalpy changes and molar entropies of compounds at 298.15 K, it is seen that $\Delta_r H^0$ (l) for reactions I and III and $\Delta_r S^0$ (l) for reactions II and III agree well with theoretical values. The difference between $\Delta_r H^0$ (l) computed in present work and theoretical value for reaction II can be ascribed to uncertainty in chemical analysis (1-octanol and 1-octene were minor components at equilibrium), whereas the difference between values of $\Delta_r S^0$ (l) for the dehydration to DNOE could be due to a poor estimate of DNOE molar entropy.

6.2.4 Estimation of thermodynamic state functions

Relevant thermochemical data of the compounds involved in these reactions are shown in Table 6.3. Some thermochemical properties were estimated since to the best of our knowledge values found experimentally were not available in the open literature. Liquid molar entropy of DNOE and (2E)-2-octene were calculated by equations 6.21 to 6.24 proposed by Stull *et al*. [109] and standard enthalpy of formation for 2-octene (E) was calculated by equation 6.25:

$$S^0(l) = S^0(g) - \Delta_v S^0 - \Delta_c S^0 - \Delta_{ig} S^0 \tag{6.21}$$

where

$$\Delta_v S^0 = \frac{\Delta_{vap} H}{T} \tag{6.22}$$

$$\Delta_c S^0 = -R \ln\left(\frac{P^0}{P^s}\right) \tag{6.23}$$

$$\Delta_{ig} S^0 = \frac{27}{32} \frac{R T_c^3}{P_c T^3} P^0 \tag{6.24}$$

$$\Delta_f H^0(l) = \Delta_f H^0(g) - \Delta_{vap} H \tag{6.25}$$

Equation 6.21 takes into account the entropy variations due to phase change at 298.15 K ($\Delta_v S^0$), vapor compression from saturation pressure at 298.15 K to 101.325 kPa ($\Delta_c S^0$), and the deviation of ideality of the vapor at 298.15 K and 101.325 kPa ($\Delta_{ig} S^0$). Saturation pressures (P^s) of DNOE and 2-octene at 298.15 K were estimated by the Gomez−Thodos vapor pressure equation [107].The critical temperature and pressure of DNOE were estimated by the Jobak method [107] while 2-octene values were obtained experimentally and found in the open literature [107].The entropy increment due to effect of pressure depends on the saturation pressure of the substance, and for substances with low saturation pressure this increment became very significant in the calculation of $S^0(l)$. The need for the correction due to the effect of pressure was already showed in previous works [101]. For example, in the calculation of S^0(DNOE, l, 298.15) the vapor compression increment ($\Delta_c S^0$) represented 18 % of the $S^0(g) - \Delta_v S^0$ value. In the case of 2-octene, with a higher saturation pressure, this value dropped to 10 %.

6.2.5 Comparison of DNOE, DNHE and DNPE thermochemical data

By comparing the values obtained for DNOE synthesis in this work with other n-alkyl ether synthesis such as those of DNPE [45] and DNHE [101], it is observed that the standard enthalpy and Gibbs energy changes of reaction become more negative as the length of the ether increases (Table 6.4).

It is also seen that the assumption of $\Delta_r H^0$ (l) to be constant over the whole temperature range is not fulfilled in the DNPE synthesis, but $\Delta_r H^0$ (l) is almost independent of temperature for DNHE and DNOE formation.

On the other hand, the standard entropy change of reaction does not have a clear trend. Nevertheless, values of standard entropy change found from equilibrium data are positive and have the same magnitude order. As can be seen in Table 6.4, the standard entropy change found from equilibrium data did not match the estimated one from *standard molar entropies* in liquid phase (Theoretical values in Table 6.4) in the case of DNPE and DNOE systems. For DNPE, the *standard molar entropy* was not calculated taking into account the contributions of equations 6.23 and 6.24. This fact could have been the cause of the discrepancy between experimental and estimated

from molar entropy values shown in the work of Bringué *et al*.[45]. In the present work, S^0(DNOE, l, 298.15) was calculated from the *standard molar entropies* of water and 1-octanol (Table 6.3) and the standard entropy of reaction, $\Delta_r S^0$ (l, 298.15). From $\Delta_r S^0$ (l, 298.15) values found by considering first $\Delta_r H^0$ (l) constant, and after $\Delta_r H^0$ (l) = f(T), S^0(DNOE, l, 298.15) was computed to be (658 ± 4) J·mol^{-1}·K^{-1}.

Table 6.3. Thermochemical data of 1-octanol, DNOE, water, 1-octene and (2E)-2-octene

Property	units	1-octanol	DNOE	water	1-octene	(2E)-2-octene
$C_{p,m,j}$ = =a+bT+cT^2+dT^3	kJ/(mol·K)					
a_j	kJ/(mol·K)	0.2771[a]	-3.383[d]	0.10661[h]	0.2329[j]	0.2109[j]
b_j	kJ/(mol·K^2)	-3.26·10^{-4} [a]	0.0322[d]	-2.06·10^{-4} [h]	-3.75·10^{-4} [j]	-1.44·10^{-4} [j]
c_j	kJ/(mol·K^3)	8.68·10^{-7} [a]	-9.06·10^{-5} [d]	3.78·10^{-7} [h]	-1.61·10^{-6} [j]	1.03·10^{-6} [j]
d_j	kJ/(mol·K^4)	0	8.62·10^{-8} [d]	-1.23·10^{-10} [h]	-8.45·10^{-10} [j]	-4.55·10^{-10} [j]
S_m^0(l, 298.15 K)	J/(mol·K)	357.1[b]	628.8[e]	69.9[i]	360[e]	374.1[e]
$\Delta_f H^0$(l, 298.15 K)	kJ/mol	-426.5[c]	-583.1[f]	-285.8[c]	-124[k]	-135.2[l]
S_m^0(g, 298.15 K)	J/(mol·K)		822.29[g]		464.36[g]	460.87[i]
$\Delta_f H^0$(g, 298.15 K)	kJ/mol					-94.58[m]
$\Delta_{vap} H^0$ (298.15 K)	kJ/mol		85.37[f]		34.07[j]	34.83[j]

Molar heat capacity at constant pressure ($C_{p,m,j}$), standard molar entropy (S_m^0), standard formation enthalpy ($\Delta_f H^0$) and standard vapporization enthalpy ($\Delta_{vap} H^0$). (a). Yaws *et al*. [110], (b). Miltenburg *et al*. [111], (c). Handbook of Chemistry and Physics. D.R. Lide [112], (d). Obtained by calorimetry and fitted to a third-order equation. (e). Estimated by means of eq. 6.24. (f). Estimated by a modified Benson method [113], (g). Calculated from Shomate equation and fitted to a third-order equation [114], (h). I.N. Levine [115], (i). Liessmann *et al*. [116] (j). Shacham *et al*. [117], (k). Estimated by means of eq.6.25, (l). Property Data Bank. R.C. Reid *et al* [107]

Table 6.4. Standard Gibbs energy ($\Delta_r H^0$ (l)), enthalpy ($\Delta_r S^0$ (l)) and entropy ($\Delta_r G^0$ (l)) changes of DNPE, DNHE and DNOE synthesis reaction in the liquid phase at 298.15 K

	DNPE [45]			DNHE [101]			DNOE		
	$\Delta_r H^0$ (l)	$\Delta_r S^0$ (l)	$\Delta_r G^0$ (l)	$\Delta_r H^0$ (l)	$\Delta_r S^0$ (l)	$\Delta_r G^0$ (l)	$\Delta_r H^0$ (l)	$\Delta_r S^0$ (l)	$\Delta_r G^0$ (l)
	kJ·mol^{-1}	J·mol^{-1}·K^{-1}	kJ·mol^{-1}	kJ·mol^{-1}	J·mol^{-1}·K^{-1}	kJ·mol^{-1}	kJ·mol^{-1}	J·mol^{-1}·K^{-1}	kJ·mol^{-1}
$\Delta_r H^0$ (l)	-6.5 ± 0.6	18.1 ± 1.4	-11.9 ± 1.1	-8.5 ± 0.2	15.2 ± 0.5	-13.0 ± 0.4	-13.5 ± 1.7	14.0 ± 4.0	-17.7 ± 2.1
$\Delta_r H^0$ (l)	-3.8 ± 0.6	25.7 ± 3.1	-11.5 ± 0.3	-9.5 ± 0.2	12.5 ± 1.1	-13.2 ± 0.1	-13.6 ± 1.7	13.9 ± 4.0	-17.7 ± 2.1
Theoretical[a]	-17.8	-48.4	-3.4	-11.9	13.0	-15.8	-15.9[a]	-15.5[a]	-11.3[a]

(a) Computed from equation 6.6 and standard molar entropies and formation enthalpy changes of compounds at 298.15 K

On the other hand, from equations 6.21 to 6.24, S^0(DNOE, l, 298.15) was estimated to be 628.8 J·mol^{-1}·K^{-1}. As seen, the last value is lower by 5 % than the one obtained from equilibrium data. Consequently, the value S^0(DNOE, l, 298.15) = (658 ± 4) J·mol^{-1}·K^{-1} has been proposed since it explains satisfactorily equilibrium reaction data.

As for the *standard formation enthalpy change* of DNOE, $\Delta_f H^0$ (DNOE, l, 298.15) was computed from standard enthalpy change of reaction and *standard formation enthalpy* of water and 1-octanol. $\Delta_f H^0$(DNOE, l, 298.15) was computed to be (−581 ± 2) kJ·mol^{-1}, which greatly coincides with the one estimated from a Benson modified method by Verevkin [113] (−583.1 kJ·mol^{-1}) shown in Table 6.3. Both values differ by 0.4 %. Thus, it can be concluded that values of contributing groups proposed in Verevkin work [113] resulted in a proper estimation of $\Delta_f H^0$(DNOE, l, 298.15).

6.3 Conclusions

1-octanol dehydration to DNOE and water proved to be **exothermic**, with an enthalpy change of reaction of (−13.6 ± 1.7) kJ·mol^{-1} at 298.15 K. The standard formation enthalpy of DNOE computed from the standard enthalpy change of reaction was found to be (−581 ± 2) kJ·mol^{-1} which was in good agreement with the one estimate by a modified Benson method. Although the correction factor concerning the pressure change improved the estimation of S^0(DNOE, l, 298.15), some differences between the values of $\Delta_r S^0$ (l, 298.15) estimated from standard molar entropies and computed from equilibrium data were observed. Based on this fact, the value **S^0(DNOE, l, 298.15) = (658 ± 4) J·mol^{-1}·K^{-1} was proposed**. As for secondary reactions, **1-octene isomerization to 2-octene** was proved to be **exothermic**, whereas intramolecular dehydration of **1-octanol to 1-octene** and water was **endothermic**.

The comparison of the experimental values for dehydrations to DNPE, DNHE, and DNOE indicates that, as the ether chain gets longer, the reaction enthalpy change tends to be lower (more exothermic). However, the reaction entropy change did not show a clear trend since its determination was associated to a higher uncertainty.

CHAPTER 7

KINETIC STUDY

7.1 Abstract

The kinetics of alcohol dehydration to linear ether was investigated on zeolites and the PS-DVB resin Amberlyst 70.

Over Amberlyst 70, the kinetics of the dehydration of 1-octanol to DNOE and the influence of products and solvent (1,4-dioxane) on the reaction rate was investigated. The kinetic analysis was performed by fitting reaction rate models based on Langmuir-Hinshelwood-Hougen-Watson and Eley-Rideal mechanisms to rate data. From 1-octanol experiments, kinetic models where all active sites are occupied and water and 1-octanol are the compounds preferentially adsorbed on the catalyst were selected. Influence of DNOE, water and solvent (1,4-dioxane) on the reaction rate was evaluated too. Water effect on reaction rate was quantified by correction factors based on the estimation of the fraction of active sites not blocked by water.

On zeolites, the kinetics of 1-octanol and 1-hexanol dehydration to DNOE and DNHE respectively were evaluated. Moreover, kinetic models found in this work for DNOE and DNHE synthesis were compared to those of DNPE synthesis over H-BEA-25 in the literature. Rate models that better represent rate data on zeolites assume that surface reaction is the rate-limiting step and the fraction of free active sites is negligible.

7.2 Results and discussion

Kinetic analysis

Because it deals with non-ideal mixtures, the rate equations are given in terms of alcohol (ROH) linear ether (ROR) and water activities. Activities were calculated by means of UNIFAC-DORTMUND predictive method [103]. Kinetic models proposed in this work are based on the well-known Langmuir-Hinselwood-Hougen-Watson (LHHW) mechanism and its derived form, Eley-Rideal (ER). Considering the chemical reaction as the rate limiting step, the following mechanisms were considered:

Mechanism 1: Two alcohol molecules, each one adsorbed on an active site react to yield the ether (LHHW type):

$$ROH + \sigma \leftrightarrow ROH{\cdot}\sigma$$

$$2\ ROH{\cdot}\sigma \leftrightarrow ROR\ \sigma + H_2O\ \sigma$$

$$ROR\ \sigma \leftrightarrow ROR + \sigma$$

$$H_2O\ \sigma \leftrightarrow H_2O + \sigma$$

In this case, the formalism lead to the following equation with two active sites participating in the reaction (exponent of the adsorption term = 2):

$$r'_{ROR} = \frac{\widehat{k'} \cdot K_{a,ROH}^2 \cdot \left[a_{ROH}^2 - \frac{a_{ROR} \cdot a_{H2O}}{K}\right]}{\left(1 + K_{a,ROH} \cdot a_{ROH} + K_{a,ROR} \cdot a_{ROR} + K_{a,H2O} \cdot a_{H2O}\right)^2} \qquad (7.1)$$

Where $\widehat{k'}$ is the rate constant of the direct chemical reaction at the surface, $K_{a,j}$ the adsorption equilibrium constant for the species j and K the equilibrium constant of the reaction.

Mechanism 2: One molecule of alcohol adsorbed on a single site reacts with another alcohol molecule from solution giving rise to an ether molecule adsorbed on the zeolite surface (Rideal-Eley (RE) type):

$$ROH + \sigma \leftrightarrow ROH{\cdot}\sigma$$

$$ROH{\cdot}\sigma + ROH \leftrightarrow ROR\ \sigma + H_2O$$

$$ROR\ \sigma \leftrightarrow ROR + \sigma$$

In this case, the RE formalism leads to equation 7.2, where 1 active site (n = 1) participates in the reaction:

$$r'_{ROR} = \frac{\widehat{k'} \cdot K_{a,ROH} \cdot \left[a_{ROH}^2 - \frac{a_{ROR} \cdot a_{H2O}}{K}\right]}{\left(1 + K_{a,ROH} \cdot a_{ROH} + K_{a,ROR} \cdot a_{ROR}\right)} \qquad (7.2)$$

Mechanism 3: One absorbed molecule of alcohol on a single site reacts with another alcohol molecule from solution releasing an ether molecule into solution:

$$ROH + \sigma \leftrightarrow ROH{\cdot}\sigma$$

$$ROH{\cdot}\sigma + ROH \leftrightarrow ROR + H_2O{\cdot}\,\sigma$$

$$H_2O{\cdot}\,\sigma \leftrightarrow H_2O + \sigma$$

Mechanism 3 leads to equation 7.3, where 1 active site (n= 1) participates in the reaction:

$$r'_{ROR} = \frac{\widehat{k'} \cdot K_{a,ROH} \cdot \left[a_{ROH}^2 - \frac{a_{ROR} \cdot a_{H2O}}{K}\right]}{\left(1 + K_{a,ROH} \cdot a_{ROH} + K_{a,H2O} \cdot a_{H2O}\right)} \tag{7.3}$$

Two general expressions combining these two type of mechanisms (LHHW and RE) and widening the range of active sites or clusters up to three (n) has been used for fitting purposes (equations 7.4 and 7.5). The unit term in the adsorption term (denominator) is missing for the expression that considers negligible the number of free active sites (equation 7.5), which is feasible for liquid-phase catalyzed reactions.

$$r'_{ROR} = \frac{A \cdot \left[a_{ROH}^2 - \frac{a_{ROR} - a_{H2O}}{K}\right]}{(1 + B \cdot a_{ROH} + C \cdot a_{ROR} + D \cdot a_{H2O})^n} \tag{7.4}$$

$$r'_{ROR} = \frac{A \cdot \left[a_{ROH}^2 - \frac{a_{ROR} - a_{H2O}}{K}\right]}{(a_{ROH} + B \cdot a_{ROR} + C \cdot a_{H2O})^n} \tag{7.5}$$

From expressions 7.4 and 7.5 the kinetic models are obtained by assuming negligible the adsorption of terms of DNOE and/or water and/or 1-octanol with respect to the others. This way, expressions 7.4 and 7.5 generate the 42 different models showed in Table 7.1 (14 types of models with n = 1, 2 or 3 each), which constants A, B, C and D vary with temperature according to equation 7.6:

$$A, B, C, D = \exp(a_1, b_1, c_1, d_1) \cdot \exp\left[-(a_2, b_2, c_2, d_2) \cdot \left(\frac{1}{T} - \frac{1}{\overline{T}}\right)\right] \quad (7.6)$$

In equation 7.4 constant $A = \widehat{k'} \cdot K_{a,ROH}^2$ (for LHHW mechanism), $A = \widehat{k'} \cdot K_{a,ROH}$ (for RE mechanism) and B, C and D are $K_{a,j}$. In equation 7.5, $A = \widehat{k'} \cdot K_{a,ROH}^{n-2}$ (for LHHW mechanism), $A = \widehat{k'} \cdot K_{a,ROH}^{n-1}$ (for RE mechanism) and $B, C = K_{a,j}/K_{ROH}$. Thus, constant A gives information about the frequency factor (A) or preexponential term and apparent/true activation energy (E_a) whereas constants B, C and D about adsorption enthalpy, $\Delta H_{a,j}$ and adsorption entropy, $\Delta S_{a,j}$(in the case of equation 7.4) and $\Delta H_{a,j} - \Delta H_{a,ROH}$ and $\Delta S_{a,j} - \Delta S_{a,ROH}$ (in the case of equation 7.5).

Dependence of equilibrium constants with temperature for the 1-pentanol and 1-hexanol dehydration to DNPE and DNHE respectively are described by equations 7.7 and 7.8 respectively and can be found in the literature [45, 101]. Equilibrium constant for 1-octanol dehydration to DNOE and its variation with temperature in the range of 413-453 K was found in chapter 6 (equation 7.9):

$$K = \exp(2.9) \cdot \exp(779/T) \quad (7.7)$$

$$K = \exp(1.8) \cdot \exp(1020/T) \quad (7.8)$$

$$K = \exp(1.7) \cdot \exp(1629/T) \quad (7.9)$$

Table 7.1. Kinetic models tested. n = number of active sites participating in the reaction, being 1, 2 or 3 in this work

Model Type	Equation
1	$r' = \frac{A \cdot \left[a_{ROH}^2 - \frac{a_{ROR} \cdot a_{H2O}}{K}\right]}{(a_{ROH})^n}$
2	$r' = \frac{A \cdot \left[a_{ROH}^2 - \frac{a_{ROR} \cdot a_{H2O}}{K}\right]}{(1 + B \cdot a_{ROH})^n}$
3	$r' = \frac{A \cdot \left[a_{ROH}^2 - \frac{a_{ROR} \cdot a_{H2O}}{K}\right]}{(a_{ROR})^n}$
4	$r' = \frac{A \cdot \left[a_{ROH}^2 - \frac{a_{ROR} \cdot a_{H2O}}{K}\right]}{(1 + B \cdot a_{ROR})^n}$
5	$r' = \frac{A \cdot \left[a_{ROH}^2 - \frac{a_{ROR} \cdot a_{H2O}}{K}\right]}{(a_{H2O})^n}$
6	$r' = \frac{A \cdot \left[a_{ROH}^2 - \frac{a_{ROR} \cdot a_{H2O}}{K}\right]}{(1 + B \cdot a_{H2O})^n}$
7	$r' = \frac{A \cdot \left[a_{ROH}^2 - \frac{a_{ROR} \cdot a_{H2O}}{K}\right]}{(a_{ROH} + B \cdot a_{ROR})^n}$
8	$r' = \frac{A \cdot \left[a_{ROH}^2 - \frac{a_{ROR} \cdot a_{H2O}}{K}\right]}{(1 + B \cdot a_{ROH} + C \cdot a_{ROR})^n}$
9	$r' = \frac{A \cdot \left[a_{ROH}^2 - \frac{a_{ROR} \cdot a_{H2O}}{K}\right]}{(a_{ROH} + B \cdot a_{H2O})^n}$
10	$r' = \frac{A \cdot \left[a_{ROH}^2 - \frac{a_{ROR} \cdot a_{H2O}}{K}\right]}{(1 + B \cdot a_{ROH} + C \cdot a_{H2O})^n}$
11	$r' = \frac{A \cdot \left[a_{ROH}^2 - \frac{a_{ROR} \cdot a_{H2O}}{K}\right]}{(a_{ROR} + B \cdot a_{H2O})^n}$
12	$r' = \frac{A \cdot \left[a_{ROH}^2 - \frac{a_{ROR} \cdot a_{H2O}}{K}\right]}{(1 + B \cdot a_{ROR} + C \cdot a_{H2O})^n}$
13	$r' = \frac{A \cdot \left[a_{ROH}^2 - \frac{a_{ROR} \cdot a_{H2O}}{K}\right]}{(a_{ROH} + B \cdot a_{ROR} + C \cdot a_{H2O})^n}$
14	$r' = \frac{A \cdot \left[a_{ROH}^2 - \frac{a_{ROR} \cdot a_{H2O}}{K}\right]}{(1 + B \cdot a_{ROH} + C \cdot a_{ROR} + D \cdot a_{H2O})^n}$

The notation used describes the kinetic models with two numbers separated by a dot. For instance model 9.1 is a type 9 model (Table 7.1) with n = 1, model 10.2, is a type 10 model with n = 2, etc. Model types named with even numbers consider that the number of free active sites is significant whereas model types with odd number do not. Only type 13 and 14 models have all the contributions in the adsorption term. The other models have been obtained from type 13 and 14 models assuming that the

adsorption of one or more species is negligible with respect to that of the other species.

7.2.1 Kinetic analysis of DNOE rate data on Amberlyst 70

As seen in chapter 4, gel type and macroreticular resin with low DVB% were the most selective to linear symmetrical ether. However, only Amberlyst 70 and Nafion are stable at high temperatures. Amberlyst 70 is highly selective to DNOE formation, stable up to 463 K and more active than Nafion. Thus, Amberlyst 70 was selected to perform the kinetic analysis.

7.2.1.1 Preliminary experiments

In order to figure out the operation conditions to avoid mass transfer limitations when measuring the reaction rate, a set of preliminary experiments were conducted. Influence of the mass of catalyst (W), the stirring speed (N) and the bead size of Amberlyst 70 on the reaction rate was evaluated.

Influence of the **mass of catalyst** on reaction rate was conducted starting with pure 1-octanol over Amberlyst 31 at 423 K. High selectivity and activity at 423 K of Amberlyst 31 allowed working with pure 1-octanol and a wide range of catalyst masses without yielding high quantities of water, avoiding phase splitting. External mass transfer depends on the liquid (viscosity and density), on the diffusivity of the reactants and products in the mixture and as well as on the particle diameter and mixing conditions. Thus, maintaining the same liquid (1-octanol) and mixing speed, type of catalyst will not affect when evaluating the effect of mass (W) on the reaction rate since bead sizes of tested resins are similar.

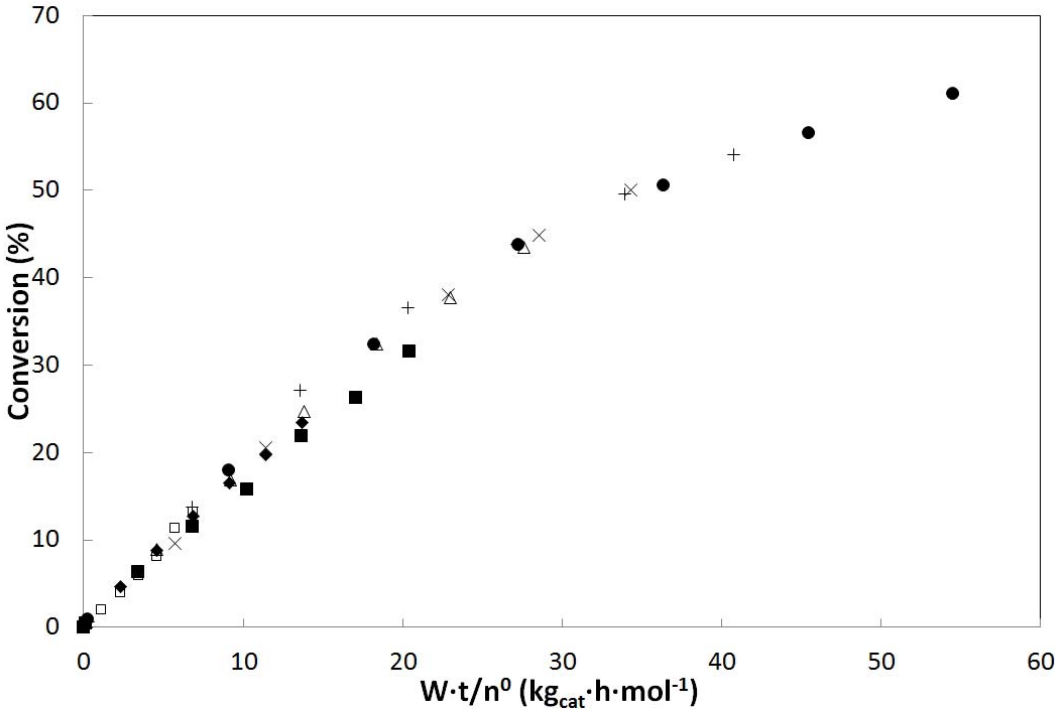

Figure 7.1. Influence of catalyst mass on conversion of 1-octanol. (open square) 0.501 g, (rhombus) 1.004 g, (filled square) 1.497 g, (open triangle) 2.004 g, (x) 2.501 g, (+) 3.002 g, (filled circle) 4.005 g. Commercial Amberlyst 31, T = 423 K, N = 500 rpm

The effect of changing the catalyst mass on the conversion vs. $t \cdot W/n^0$ is studied (Figure 7.1). The time has been corrected by W and initial number of moles of 1-octanol (n^0), as for a given value of $t \cdot W/n^0$ conversion should be constant if there are no mass transfer limitations. It can be seen from Figure 7.1 that all the mass series highly coincide, which indicates that conversion values are independent from catalyst mass in the range studied. In previous works it was reported that no mass transfer limitations occurred in the dehydration of 1-pentanol to di-n-pentyl ether (DNPE) and 1-hexanol to di-n-h-exyl ether (DNHE) below 3 and 4 grams of catalyst respectively [44, 47].

Working within these range of mass catalysts, influence of the **bead size** and stirring speed on reaction rate were evaluated over Amberlyst 70. Commercial Amberlyst 70 was sieved to obtain different bead sizes of 0.12, 0.21, 0.32, 0.52, 0.72, and 0.9 mm. Working temperature was set to 453 K in order to speed up chemical reaction and thus assure no mass transfer effects in the range of 413-453 K. From Figure 7.2 it can be inferred that there is no significant effect of bead size on the rate of DNOE (r^0_{DNOE}) formation since the variation of r^0_{DNOE} with bead size lies between the 95%-confidence

intervals of the r^0_{DNOE} calculations. As a result, commercial size of Amberlyst 70 was used for the kinetic experiments.

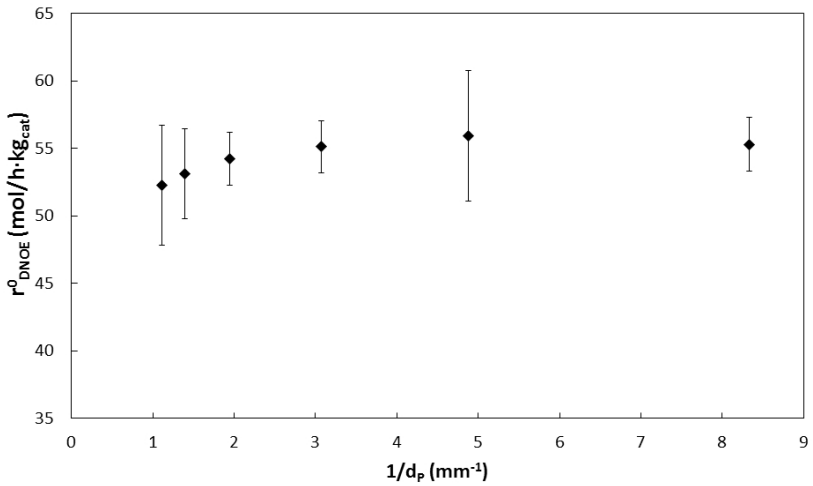

Figure 7.2. Influence of bead size on the rate of DNOE formation. W = 1 g, Amberlyst 70, T = 453 K, N = 500 rpm

Finally, the influence of external mass transfer on the reaction rate was evaluated at 453 K over commercial Amberlyst 70 in a set of experiments with **stirring speeds** of 100-800 rpm. As shown in Figure 7.3, the reaction rate did not vary with the stirring speed further than the 95%-confidence intervals for the calculation of the reaction rates. Thus, stirring speed was set at 500 rpm for the kinetic experiments.

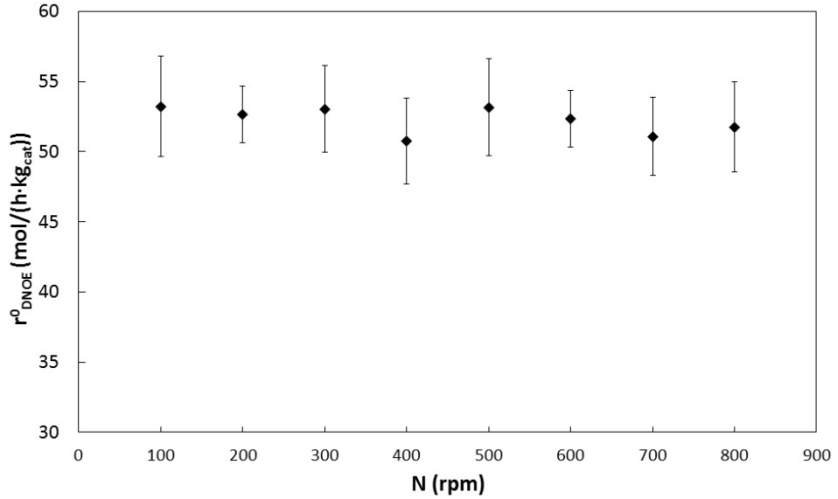

Figure. 7.3. Influence of stirring speed (N) on rate of DNOE formation. W = 1 g, commercial Amberlyst 70, T = 453K

7.2.1.2 Kinetic models

The preliminary experiments show that no mass transfer limitations occur when measuring the chemical reaction rates below 453 K. Kinetic experiments were carried out at different temperatures and initial concentrations. In Table 7.2 the kinetic experiments done in this work are summarized.

Table 7.2 Temperature, catalyst mass and initial concentrations (w/w) of kinetic experiments

T (K)	% 1-octanol	% DNOE	% water	% 1,4-dioxane	W (g)
413	100				1
413	100				2
423	100				1
423	100				2
433	100				1
433	100				2
443	100				1
443	100				2
453	100				1
433	98	2			1
433	92	4			1
433	84	16			1
433	68	32			1
433	55	45			1
453	90	10			1
453	80	20			1
433	44		1	55	1
433	43		2	55	1
433	41		4	55	1
453	44.5		0.5	55	1
453	42		3	55	1
453	39		6	55	1
423	45			55	1
423	55			45	1
423	65			35	1

Commercial Amberlyst 70. N = 500 rpm

Table 7.2 shows the different series of experiments performed: the experiments in pure 1-octanol as reactant, mixtures of 1-octanol/DNOE, mixtures of 1-octanol/water/1,4-dioxane and mixtures of 1-octanol/1,4-dioxane. 1,4-dioxane was added to the mixtures of 1-octanol/water to avoid phase splitting [45, 101] and

experiments with 1,4-dioxane and 1-octanol were carried out to check the influence 1,4-dioxane might cause on the reaction rate.

Kinetic analysis of pure 1-octanol experiments

All 42 kinetic models derived from expressions in Table 7.1 were fitted to the first set of experiments carried out only with 1-octanol as reactant. As seen in Figure 7.4 reaction rate is high at high 1-octanol concentrations (activity close to 1) and quickly rises with temperature increase.

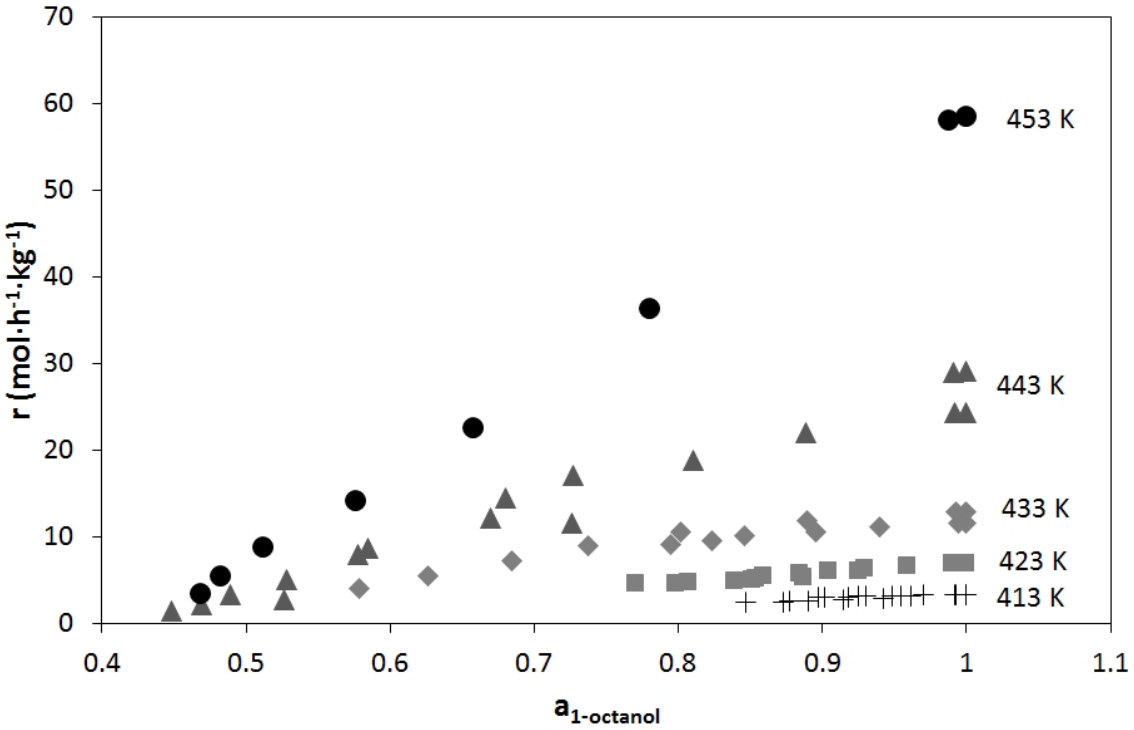

Figure 7.4. Experimental reaction rates vs. 1-octanol activity at different temperatures. Commercial Amberlyst 70. N =500 rpm. 70 $cm^3$of 1-octanol. W = 1-2 g. 413 K (+), 423 K (square), 433 K (rhombus), 443 K (triangle), 453 K (circle)

Best group of models from a statistical standpoint (lowest sum of residual squares (RSSQ), random residuals and low parameter uncertainty, the last computed as root of sum of the square relative errors (RSSQRE) of parameters) with physicochemical meaning (positive E_a) were type 9 and 7 models (see APPENDIX VI):

$$r' = \frac{A \cdot \left[a_{OcOH}^2 - \frac{a_{DNOE} \cdot a_{H2O}}{K}\right]}{(a_{OcOH} + B \cdot a_{H2O})^n} \qquad (7.10)$$

$$r' = \frac{A \cdot \left[a_{OcOH}^2 - \frac{a_{DNOE} \cdot a_{H2O}}{K}\right]}{(a_{OcOH} + B \cdot a_{DNOE})^n} \quad (7.11)$$

Constant A gathers the kinetic rate constant and the adsorption equilibrium constant for 1-octanol $K_{a,OcOH}$, for LHHW and RE mechanisms respectively:

$$A = \hat{k}'/K_{a,OcOH}^{n-2} \quad (7.12)$$

$$A = \hat{k}'/K_{a,OcOH}^{n-1} \quad (7.13)$$

Constant B depends on the type of model. For type 7 models:

$$B = \frac{K_{a,DNOE}}{K_{a,OcOH}} \quad (7.14)$$

For type 9 models:

$$B = \frac{K_{a,H2O}}{K_{a,OcOH}} \quad (7.15)$$

RSSQ and RSSQRE of each model were calculated according to:

$$RSSQ = \sum_{i=1}^{n} \left(r_{exp_i} - r_{calc_i}\right)^2 \quad (7.16)$$

$$RSSQRE = \left[\sum_{i=1}^{p} \left(\frac{\varepsilon_{p_i}}{p_i}\right)^2\right]^{1/2} \quad (7.17)$$

being r_{exp} and r_{calc} the observed and estimated rates and $\varepsilon_{p_i}$the uncertainty of parameter p_i for a 95% of confidence, calculated by means of linear least squares method.

Both types of models were similar in terms of residual sum of squares but parameters of type 9 models had lower uncertainty (lower RSSQRE) than those of type 7 models. (Table 7.3) The plots of estimated vs. experimental reaction rates (r_{calc} vs r_{exp}) (Figures 7.5 and 7.6) do not show great differences when changing the number of

active sites involved in the reaction (n) but it can be seen a reduction of the dispersion for type 9 models with respect to the type 7 models, especially for n = 2 and 3.

Table 7.3. Parameters, residual sum of squares (RSSQ), root of sum of the square relative errors of parameters for type 7 and 9 models

Model	RSSQ	RSSQRE	a_1	a_2	b_1	b_2
7.1	261	151	2.38±0.08	$(10.0\pm0.6)\cdot10^{5}$	$-4\cdot10^{-3}$	$6\cdot10^{5}$
7.2	278	11.3	2.37±0.09	$(1.00\pm0.06)\cdot10^{6}$	$3\cdot10^{-2}$	$5\cdot10^{5}$
7.3	300	4.17	2.37±0.09	$(1.00\pm0.06)\cdot10^{6}$	$6\cdot10^{-2}$	$4\cdot10^{5}$
9.1	250	2.58	2.39±0.08	$(10.0\pm0.6)\cdot10^{5}$	$-2\cdot10^{-1}$	$5\cdot10^{5}$
9.2	257	1.62	2.39±0.09	$(1.00\pm0.06)\cdot10^{6}$	$-2\cdot10^{-1}$	$3\cdot10^{5}$
9.3	269	0.929	2.4±0.4	$(1.0\pm0.2)\cdot10^{6}$	-0.2	$2.3\cdot10^{5}$

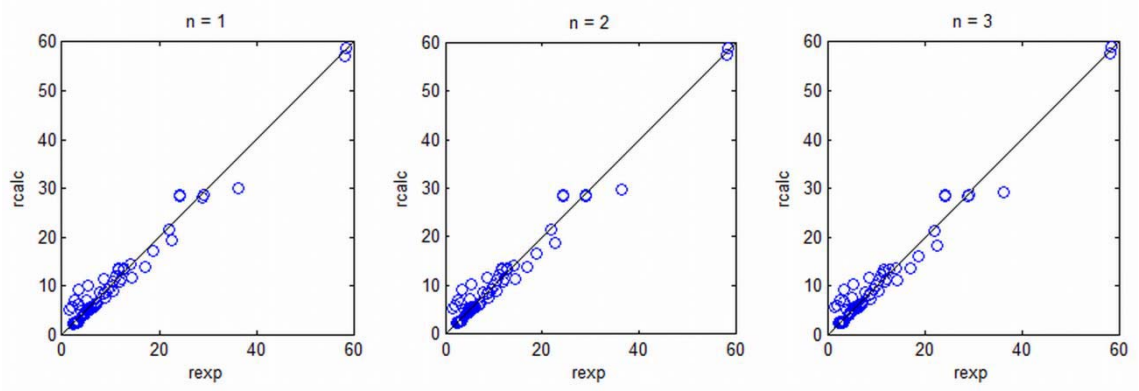

Figure 7.5. r_{calc} vs. r_{exp} for type 7 models

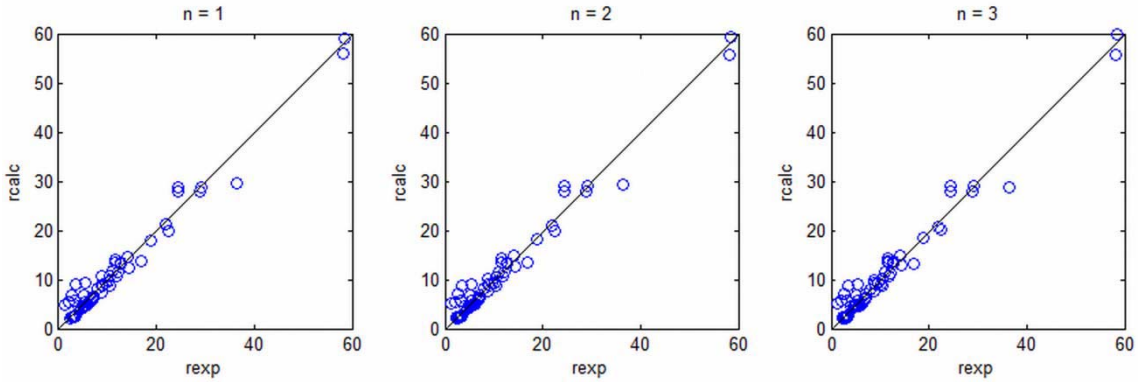

Figure 7.6. rcalc vs. rexp for type 9 models

From parameters a_1 and a_2 defined in equation 7.6 it can be obtained the frequency factor (A) and the activation energy (E_a) respectively (in the case of constant A). Parameters b_1 and b_2 (in the case of constant B) give information about both adsorption entropy and enthalpy differences respectively between DNOE/water and 1-octanol for type 9/7 models according to equations 7.14 and 7.15.

As can be seen in Table 7.4 both type of models had similar preexponential terms (4-5·10^{15} mol·h^{-1}·kg_{cat}^{-1}) and apparent/true activation energies (120 kJ/mol). As seen in equations 7.12 and 7.13, adsorption equilibrium constant of 1-octanol could take part as well in constant A depending on the type of mechanism (LHHW or ER) and number of active sites involved in the reaction (n).

Table 7.4. Thermodynamic data for type 7 and 9 models

Model	A (mol·h^{-1}·kg_{cat}^{-1})	E_a (kJ·mol^{-1})	$\Delta S_{H2O} - \Delta S_{OcOH}$ (J·mol^{-1}·K^{-1})	$\Delta H_{H2O} - \Delta H_{OcOH}$ (kJ·mol^{-1})	$\Delta S_{DNOE} - \Delta S_{OcOH}$ (J·mol^{-1}·K^{-1})	$\Delta H_{DNOE} - \Delta H_{OcOH}$ (kJ·mol^{-1})
7.1	4·10^{15}	120±7			182±119	78±49
7.2	5·10^{15}	120±7			134±66	57±27
7.3	5·10^{15}	121±8			113±47	48±19
9.1	4·10^{15}	120±7	130±118	57±49		
9.2	4·10^{15}	120±7	82±64	36±26		
9.3	5·10^{14}	120±27	62±27	27±11		

According to equations 7.12 and 7.13, to point out if the value of E_a would correspond to true or apparent activation energy is not possible unless the type of mechanism and number of active sites involved in the reaction are determined. As seen in Table 7.3, model 9.1 was the one which better fitted the kinetic data in terms of residual sum of squares, but the uncertainty associated to parameters of model 9.3 (RSSQRE column) was lower than model 9.1. As for molar adsorption enthalpy and entropy differences (Table 7.4), it is possible to see that adsorption of 1-octanol is stronger (more exothermic) than that of water (type 9 models) and adsorption of DNOE is weaker than that of 1-octanol (type 7 models). High uncertainty associated to parameters b_1 and b_2 resulted in poor estimates of adsorption entropy and enthalpy differences which suggest little sensitivity to these parameters in the fit.

Type 9 models were the ones which had the lowest RSSQ and parameter error as a whole. However, choosing a model within the three possibilities (n=1, 2 or 3) is not a clear decision. For this reason, the kinetic study has been extended, incorporating new experiments with 1,4-dioxane as solvent and different amounts of DNOE and water as reactants (Table 7.2). These additional experiments allowed to enlarge the range of activities scanned in the optimization of the models and quantifying at the same time the effect of solvent, DNOE and water on the reaction rate.

Effect of DNOE, water and 1,4-dioxane on the reaction rate

Water and DNOE effect on the reaction rate has been evaluated, as well as the effect of the solvent (1,4-dioxane) employed. Water showed a strong inhibition effect in other reactions carried out over ion exchange resins as reported in the literature [118-122]. Du Toit *et al.* [118, 119] observed that water had a strong inhibition effect over the formation of mesityl oxide and water from acetone over Amberlyst 16, and proposed a kinetic equation to represent such effect. Limbeck [120] described and quantified the water inhibiting effect on the reaction of cyclic etherification of 1,4-butanediol to tetrahydrofuran over an acidic polystyrene DVB resin. Yang [121, 122] studied the synthesis of tert-amyl methyl ether (TAME) from methanol and tert-amyl alcohol and the synthesis of tert-butyl ether from ethanol and tert-butyl alcohol over Amberlyst 15 and observed and quantified the water inhibiting effect on both syntheses.

Water inhibition effect on reaction rate was reported for DNPE synthesis from 1-pentanol [46]. In this work the influence of water on the synthesis of DNOE was found to be negative as well, its initial presence lowered drastically the initial reaction rate as can be seen in Figure 7.7. The rate's drop was more noticeable at the highest temperature as can be inferred comparing both temperature series. As water content increased (4-6%), rate depletion at 453 K tended to approach to that observed at 433 K, lowering the initial rate values down to 1 $mol \cdot h^{-1} \cdot kg_{cat}^{-1}$. However, neither DNOE nor 1,4-dioxane showed the inhibiting effect observed in the presence of water (Figures 7.8 and 7.9). This fact sets 1,4-dioxane suitable as a solvent for kinetic experiments.

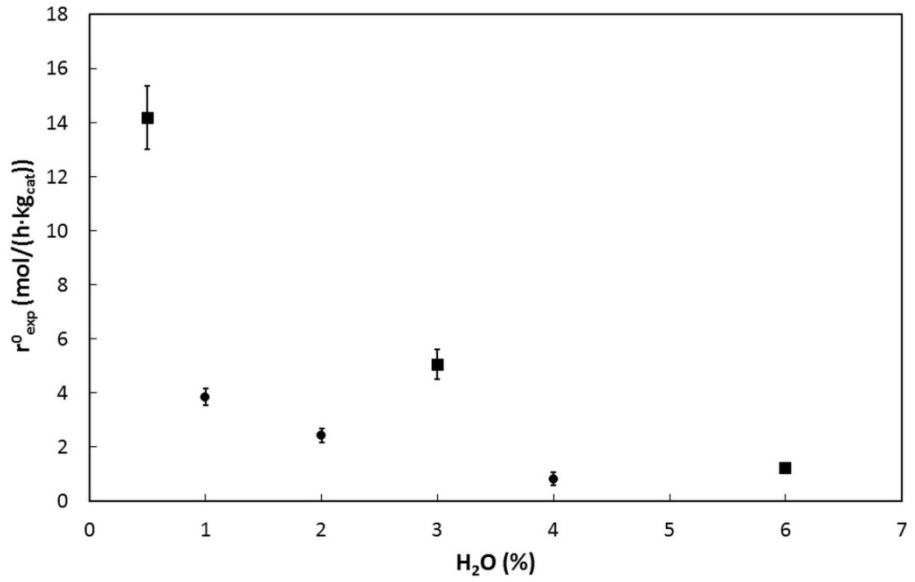

Figure 7.7. Influence of water concentration (w/w) on initial reaction rate of DNOE formation. (square) 453 K, (circle) 433 K

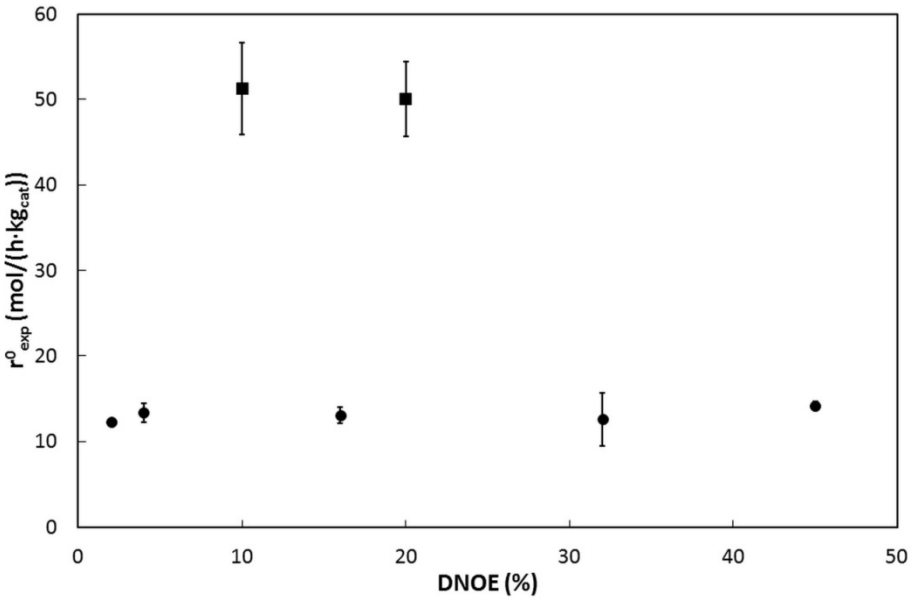

Figure 7.8. Influence of DNOE concentration(w/w) on initial reaction rate of DNOE formation. (square) 453 K, (circle) 433 K

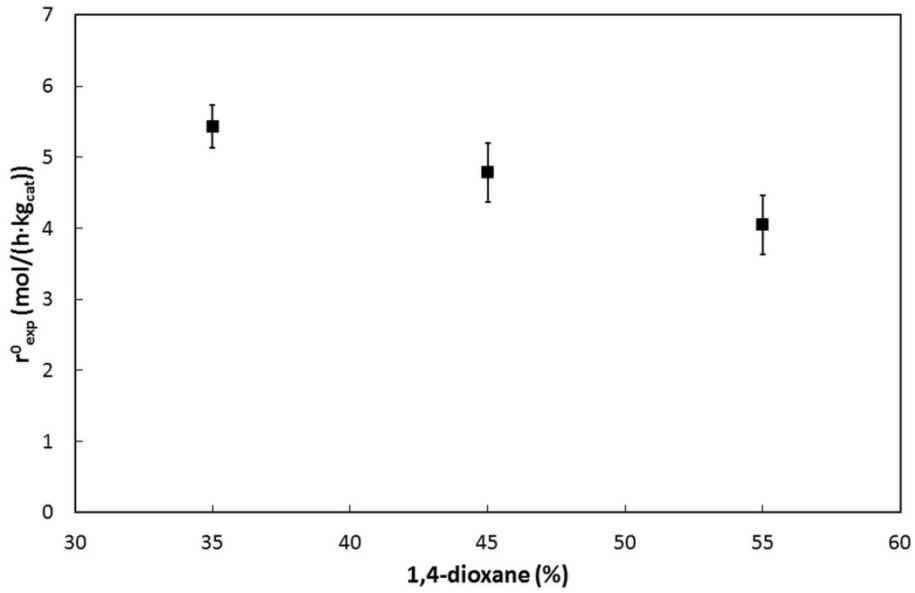

Figure 7.9. Influence of 1,4-dioxane concentration (w/w) on initial reaction rate of DNOE formation at 423 K

As a result of incorporating the experiments with water, DNOE and 1,4-dioxane, the range of activities was enlarged. Thus, optimisation of the parameters of the kinetic models described in Table 7.2 was done again. Within thermodynamically consistent models, model 9.1 was clearly the one which better explained the rate data among the whole range of activities. The residual sum of squares (RSSQ) of model 9.1 was 1301, clearly lower than model 9.2 (3393) and 9.3 (17226) (see APPENDIX VI).

Water deactivation models

To quantify the inhibitor effect of water on the kinetics of the dehydration of 1-octanol to DNOE, the models of Table 7.1 were modified with water-related terms. All of the water-deactivating terms found in the literature are based in modifying the rate constant so only available active sites are taken into account. Bringué *et al.* [46] used the parameter ψ, related to the resin backbone swelling and the accessibility to resin sulfonic groups, developed by Fité *et al*. as an attempt of accounting for the reaction medium-resin interaction. However, this parameter did not successfully explained water inhibition since the resin does not swell gradually over the reaction but it swells completely with the small amounts of water released initially [46]. Thus, this parameter was not present among the correction factors presented in this work.

As du Toit *et al*. [118, 119] reported, the fraction of acid sites blocked by water molecules can be quantified with adsorption isotherms, thus, the rate constant can be modified with a correction factor $f(a_{H2O})$ so:

$$\widehat{k'} = k_0 \cdot f(a_{H2O}) = k_0 \cdot (1 - \theta_{H2O}) \tag{7.18}$$

being θ_{H2O} the fraction of acid sites blocked by water molecules, expressed by an adsorption isotherm. Common adsorption isotherms used are that of Langmuir and expressions derived from them, as well as Freundlich isotherm, which stems from applying to Langmuir isotherm a logarithmic depletion of adsorption enthalpy with the catalyst coverage [60]. In Table 7.5 isotherms and their derived correction factors used in this work are summarized.

Table 7.5 Isotherms and correction factors to represent water inhibiting effect on reaction rate used in this work

Equation	Isotherm (θ_{H2O})	Correction factor	Reference
CF1	$\frac{K_{H2O}\sqrt{a_{H2O}}}{1+K_{H2O}\sqrt{a_{H2O}}}$	$\frac{1}{1+K_{H2O}\sqrt{a_{H2O}}}$	[120]
CF2	$\frac{K_{H2O}a_{H2O}}{1+K_{H2O}a_{H2O}}$	$\frac{1}{1+K_{H2O}a_{H2O}}$	[121]
CF3	$\frac{K_{H2O}a_{H2O}^2}{1+K_{H2O}a_{H2O}^2}$	$\frac{1}{1+K_{H2O}a_{H2O}^2}$	[122]
CF4	$\frac{K_{H2O}a_{H2O}^t}{1+K_{H2O}a_{H2O}^t}$	$\frac{1}{1+K_{H2O}a_{H2O}^t}$	This work
CF5	$K_{H2O}a_{H2O}^{1/\propto}$	$1-K_{H2O}a_{H2O}^{1/\propto}$	[119]

K_{H2O} was defined analogously to constants A, B, C and D in equation 7.6:

$$K_{H2O} = \exp\left(K_{H2O}(1)\right) \cdot \exp\left[-K_{H2O}(2) \cdot \left(\frac{1}{T} - \frac{1}{\overline{T}}\right)\right] \tag{7.19}$$

and α in equation CF5 was defined:

$$\propto = \frac{K_{\propto}}{T} \tag{7.20}$$

Correction factors were applied to those models in Table 7.1 not containing water in the adsorption term, thus, only type 1, 2, 3, 4, 7 and 8 models were modified with correction factors showed in Table 7.5. Type 3, 4 and 8 models and models 1.2 and 1.3 modified by correction factors described in Table 7.5 resulted in either negative activation energies and/or positive adsorption enthalpies/entropies, which invalidated

the models in terms of physicochemical meaning. Model 2.1 corrected by equations CF3, CF4 and CF5 of Table 7.5 resulted as well in negative activation energies and/or positive adsorption enthalpies/entropies.

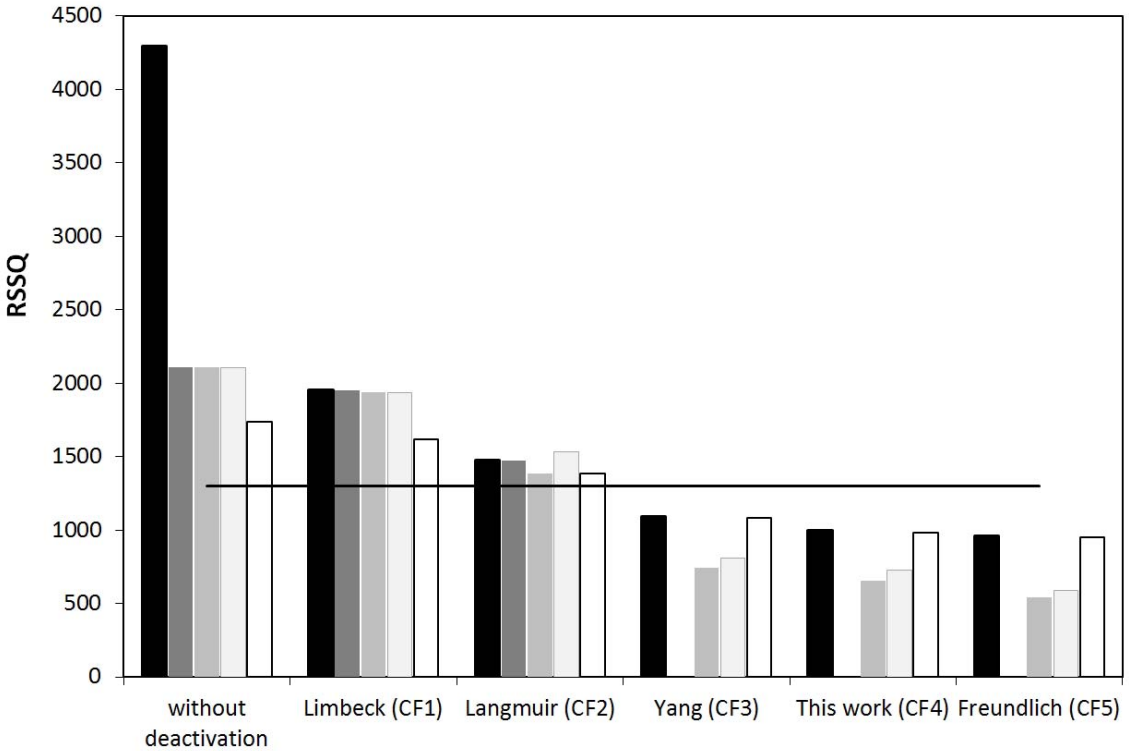

Figure 7.10. RSSQ for model 9.1 and models 1.1, 2.1, 2.2, 2.3 and 7.1 with deactivation correction factors. Model 1.1 ■Model 2.1 ■Model 2.2 ■Model 2.3 ■Model 7.1 □ Model 9.1 (line)

As can be seen in Figure 7.10, only equation CF3, described by Yang [122], equation CF4 (this work) and equation CF5 (Freundlich isotherm) lowered the residual sum of squares with respect model 9.1 (without deactivation term). The use of Langmuir isotherm separately for water as a correction factor did not improve the fit in any model compared to model 9.1. Neither did equation CF1 proposed by Limbeck *et al.* [120], suggesting a kind of Langmuir isotherm where two active sites adsorbing one molecule of water at the same time.

Although models 2.2 and 2.3 modified by equations CF3, CF4 and CF5 had the lowest residual sum of squares, low activation energies were determined with these models (20-70 kJ/mol), which contrasted with those found in literature for other dehydrations and that determined in the kinetic analysis of pure 1-octanol experiments (120 kJ/mol). Modified models from model 7.1 did not represent an improvement in RSSQ with respect modified models from model 1.1 and thus,

modified models from model 1.1 were preferred for having 2 parameters less than those stemmed from model 7.1.

Table 7.6. Parameters, frequency factors (A), activation energies (E_a) and enthalpies and entropies differences for model 9.1 and model 1.1 corrected by equations CF3, CF4 and CF5

		Models derived from model 1.1 corrected by eqs. CF3-CF5		
	Model 9.1	Equation CF3	Equation CF4	Equation CF5
a_1	2.79±0.07	2.78±0.1	2.76±0.05	2.79±0.05
a_2	$(9.5\pm0.6)\cdot10^5$	$(9.4\pm0.9)\cdot10^5$	$(9.4\pm0.5)\cdot10^5$	$(9.2\pm0.4)\cdot10^5$
b_1	-0.5±0.6	-	-	-
b_2	$(7\pm5)\cdot10^5$	-	-	-
$K_{H2O(1)}$	-	1.18±0.6	2.4±0.8	0.5±0.4
$K_{H2O(2)}$	-	$(7\pm5)\cdot10^5$	$(5.2\pm4.7)\cdot10^5$	$(2.4\pm2.1)\cdot10^5$
K_α	-	-	-	272±49
z	-	-	3.2±0.6	-
A (mol·h^{-1}·kg_{cat}^{-1})	$7\cdot10^{14}$	$6\cdot10^{15}$	$5\cdot10^{14}$	$3\cdot10^{14}$
E_a (kJ·mol^{-1})	114±7	113±10	113±5	110±5
$\Delta S_{H2O} - \Delta S_{OcOH}$ (J·mol^{-1}·K^{-1})	194±127	-	-	-
$\Delta H_{H2O} - \Delta H_{OcOH}$ (kJ·mol^{-1})	86±83	-	-	-
RSSQ	1301	1095	997	962
RSSQ var.	-	74.5	76.8	77.6
RSSQRE	1.41	0.977	0.991	1.15

As can be seen in Table 7.6, correction factors described by Yang (equation CF3), this work (equation CF4) and Freundlich isotherm (equation CF5) lower the RSSQ and the parameter error (RSSQRE) with respect model 9.1. Also, this three models upgrade model 1.1 (without correction factor) in a similar extent (RSSQ variation 75-78%).

Equation CF3 can be seen as a Langmuir isotherm where two molecules of water are adsorbed in an active site. Extending the number of molecules of water adsorbed in a single active site as a parameter to optimize (z) (equation CF4), the kinetic model proposed in this work sets 3.2 molecules adsorbed each active site. It is clear that this parameter z is strictly empiric but model 1.1 corrected with equation CF4 may suggest a scenario where more than a molecule of water is adsorbed or surrounds an active site. However, the use of Freundlich isotherm lowered the sum of squares (962) in the largest extent by using the same number of parameters as model 1.1 corrected with equation CF4. For this reason, model 1.1 modified with a Freundlich isotherm

(equation CF5) for water deactivation was selected to explain rate data stemmed from experiments seen in Table 7.2.

$$r' = \frac{A \cdot \left[a_{OcOH}^2 - \frac{a_{DNOE} \cdot a_{H2O}}{K}\right]}{(a_{OcOH})} \cdot \left[1 - K_{H2O} a_{H2O}^{T/K_\alpha}\right] \tag{7.21}$$

The final form of equation 7.21 according to equation 7.6 and values in Table 7.6 is:

$$r' = \frac{\exp(2.79) \cdot \exp\left[-9.2 \cdot 10^5 \cdot \left(\frac{1}{T} - \frac{1}{\overline{T}}\right)\right] \cdot \left[a_{OcOH}^2 - \frac{a_{DNOE} \cdot a_{H2O}}{K}\right]}{a_{OcOH}} \cdot \\ \cdot \left[1 - \exp(0.5) \cdot \exp\left[-2.4 \cdot 10^5 \cdot \left(\frac{1}{T} - \frac{1}{\overline{T}}\right)\right] \cdot a_{H2O}^{T/272}\right] \tag{7.22}$$

being $\overline{T} = 434.8\ K$

As literature reports [46, 118], Freundlich isotherm has successfully explained water deactivation of 1-pentanol dehydration to di-n-pentyl ether (DNPE) over Amberlyst 70 [46] and acetone dehydration to mesityl oxide over Amberlyst 16 [118, 119]. Analogously to 1-pentanol dehydration [46], 1-octanol dehydration to DNOE follows an Eley-Rideal mechanism where an adsorbed molecule of 1-octanol reacts with a molecule of 1-octanol from the liquid phase. Water presence was found to be determinant in the kinetic model since it deactivated the catalyst by covering the active sites following a Freundlich-type isotherm.

7.2.2 Kinetic analysis on zeolites

It has been reported in previous works that reaction rates are no mass transfer limited working with the same setup at 500 rpm on ion exchange resins with beads ranging from 0.3-0.8 mm [44, 47]. Zeolite particles are considerably smaller (1-8.5 µm). Therefore, diffusion effects on reaction rate are expected to be negligible over H-BEA-25 crystals smaller than 100 µm [44]. As a result, measured reaction rates are considered to be free of mass transfer effects.

DNHE and DNOE rate data

Models of Table 7.1 were fitted to reaction rate data of DNOE synthesis over H-FAU-30 and rate data of DNHE synthesis over H-BEA-25, H-FAU-6, H-FAU-30 and H-MFI-28.

Regarding DNOE synthesis, rate models were fitted to DNOE reaction rates measured on H-FAU-30 at each temperature. As a result of the fit, type 4, 6, 8, 10, 12 and 14 models are not thermodynamically consistent because their parameters ended up in either positive enthalpies or entropies of adsorption. Between type 1, 2, 3, 5, 7, 9 and 11 models, type 9 ones were selected since they had the lowest sum of residual squares (RSSQ) as well as low parametrical error (see APPENDIX VII).

Type 13 models were rejected because the factor C ($K_{a,H2O}/K_{a,ROH}$) did not upgrade the fit as compared to type 9 models (see APPENDIX VII).

Regarding DNHE synthesis, reaction rate models have been fitted to DNHE reaction rates over tested zeolites and selected following the same screening criteria. Type 7 and 9 models represent better rate data (see APPENDIX VII). The two types of models differ in the adsorption term: water adsorption term is neglected in type 7 models (equation 7.23), whereas ether adsorption is neglected in type 9 models (equation 7.24).

$$r' = \frac{A \cdot \left[a_{ROH}^2 - \frac{a_{ROR} \cdot a_{H2O}}{K}\right]}{\left(a_{ROH} + \frac{K_{a,ROR}}{K_{a,ROH}} \cdot a_{ROR}\right)^n} \tag{7.23}$$

$$r' = \frac{A \cdot \left[a_{ROH}^2 - \frac{a_{ROR} \cdot a_{H2O}}{K}\right]}{\left(a_{ROH} + \frac{K_{a,H2O}}{K_{a,ROH}} \cdot a_{H2O}\right)^n} \tag{7.24}$$

Analysis of models fit revealed that residuals were random. In this way, no clear trends in the residuals against activities or reaction rates plots were observed for models 7.1, 7.2, 7.3 and 9.1, 9.2, 9.3 (see APPENDIX VIII). That is why differentiation between type 7 and type 9 models was performed on the basis of the minimal sum of squares (Figures. 7.11 and 7.12) together with the lowest root of sum of the squares of relative errors (RSSQRE) of the optimized parameters as Table 7.7 shows.

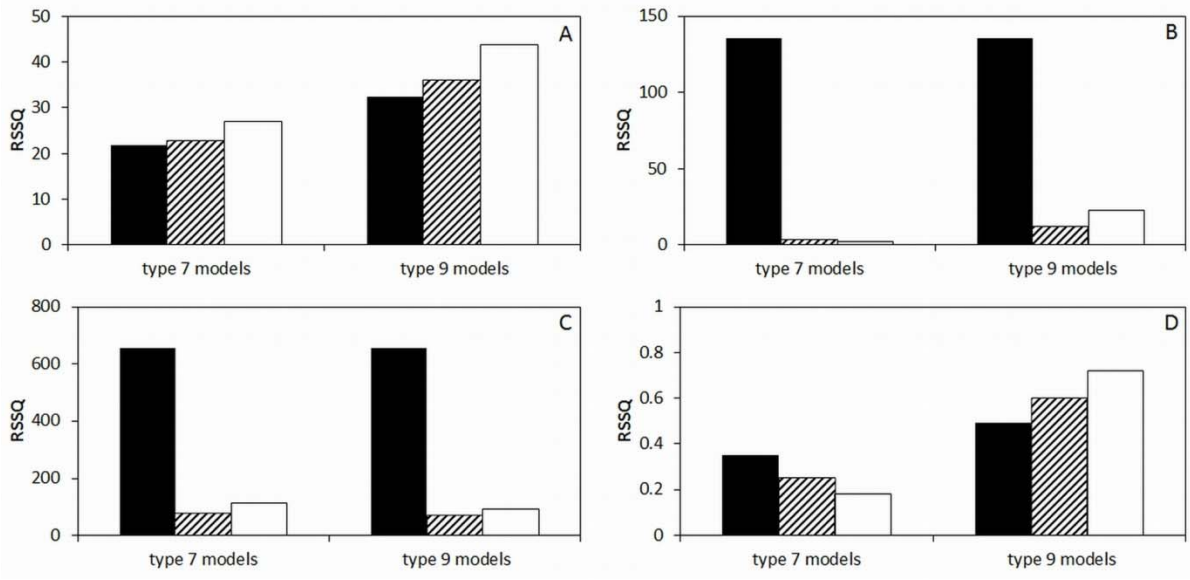

Figure 7.11. Residual sum of squares (RSSQ) of type 7 and 9 models for DNHE synthesis. n = 1 (black), n = 2 (black and white), n = 3 (white). (A). H-FAU-6. (B) H-FAU-30. (C) H-BEA-25. (D) H-MFI-28

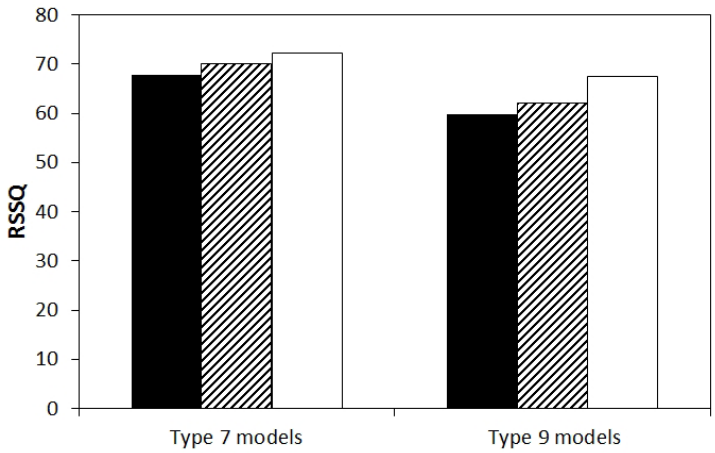

Figure 7.12. Residual sum of squares (RSSQ) of type 7 and 9 models for DNOE synthesis over H-FAU-30. n = 1 (black), n = 2 (black and white), n = 3 (white)

Table 7.7. Fitted parameters of rate equations based on type 7 and 9 models

	Zeolite	Model	a_1	a_2	b_1	b_2	RSSQRE
DNHE	H-FAU-6	7.1	2.68±0.06	(1.10±0.06)·10^6	0.96±0.29	(8±2)·10^5	0.44
		7.2	2.66±0.06	(1.09±0.06)·10^6	0.68±0.19	(6±2)·10^5	0.40
		7.3	2.64±0.07	(1.10±0.06)·10^6	0.58±0.15	(5±1)·10^5	0.38
	H-FAU-30	7.2	2.30±0.03	(10.0±0.2)·10^5	-0.70±0.25	(-5±2)·10^5	0.55
		7.3	2.27±0.02	(10.0±0.2)·10^5	-0.45±0.09	(-6±7)·10^4	1.21
	H-BEA-25	9.2	2.7±0.1	(8.4±0.8)·10^5	-0.61±0.47	(-1.2±0.4)·10^6	0.85
		9.3	2.7±0.4	(8±2)·10^5	-0.36±0.19	(-5.7±0.7)·10^5	0.60
	H-MFI-28	7.1	0.63±0.06	(1±1)·10^5	-8±2·10^4	(0.001±3)·10^{10}	3146
		7.2	0.60±0.06	(1.0±0.1)·10^6	1.03±0.81	(1±1)·10^6	1.23
		7.3	0.58±0.06	(1.00±0.09)·10^6	1.43±0.33	(7±5)·10^5	0.71
DNOE	H-FAU-30	9.1	1.84±0.09	(9.2±0.9)·10^5	-1±1	(1.4±0.7)·10^6	1.12
		9.2	1.8±0.1	(10±1)·10^5	-0.5±0.6	(8±3)·10^5	1.29
		9.3	1.8±0.3	(10±2)·10^5	-0.2±0.1	(5.9±0.5)·10^5	0.56

In the case of H-MFI-28, it is clear that model 7.3 gave the lowest RSSQ and parameter error within type 7 models. Although it is the best from a statistical point, the presence of 3 active sites in the rate-limiting step might be unreliable from a physicochemical standpoint. A third active site can cooperate, for instance, in the adsorption of long linear ether but such fact has not been reported in the dehydration of alcohol to linear ether open literature. It is clear that alcohol adsorption has to be taken into account in the reaction rate expressions over all tested zeolites; the activity of alcohol appears in both adsorption terms of type 7 and 9 models. However, the role of ether/water adsorption is not so clear.

Comparing rate models for DNPE synthesis in the literature it is seen that for H-BEA-25 DNPE adsorption is significant since type 7 models are reported. However, in this work water adsorption was found significant in DNHE synthesis over H-BEA (Table 7.8). This difference could be due to the different solubility of water in 1-pentanol and 1-hexanol. In this case, and according to polarity, 1-hexanol would be less soluble in water, which could force water to adsorb onto the zeolite in a greater extent than in the case of 1-pentanol. In such scenario, 1-pentanol allows a higher level of water in the liquid and DNPE adsorption contributes to the adsorption process.

Table 7.8. Best rate models for DNPE, DNHE and DNOE syntheses over some zeolites

Model	System		
Zeolite	DNPE	DNHE	DNOE
H-FAU-6		7.1-7.2-7.3	
H-FAU-30		7.2	9.1-9.2-9.3
H-BEA-25	7.1-7.2-7.3[a]	9.2	
H-MFI-28		7.2-7.3	

(a) Bringué *et al.*[123]

A similar view can be applied to H-FAU-30 with 1-hexanol and 1-octanol. In this case, high insolubility of water in 1-octanol could be the cause of the significant role of water in the adsorption term. Therefore, type 9 model is the one which best explains reaction rate data for etherification of 1-octanol.

From Table 7.7 parameters it can be obtained the frequency factor, A (from parameter a_1) and the apparent activation energy (from parameter a_2) and adsorption entropy (from parameter b_1) and enthalpy differences (from parameter b_2) between water and alcohol for type 9 models or water and linear ether for type 7 ones. They are

displayed in Table 7.9 for dehydration reaction of 1-octanol to DNOE and in Table 7.10 for that of 1-hexanol to DNHE. As can be seen, apparent activation energies ranging from 100-120 kJ·mol^{-1} were obtained for the two reactions on tested zeolites.

Table 7.9. Frequency factors (A), apparent activation energies (E_a) and adsorption enthalpy and entropy differences between water and 1-octanol

Catalyst	H-FAU-30		
Rate equation	9.1	9.2	9.3
A (mol·h^{-1}·kg^{-1}))	5·10^{13}	1·10^{14}	3·10^{14}
E_a (kJ·mol^{-1})	110±11	114±12	117±22
$\Delta H_{a,\ H2O}$-$\Delta H_{a,\ OcOH}$ (kJ·mol^{-1})	169±83	95±40	71±6
$\Delta S_{a,H2O}$-$\Delta S_{a,\ OcOH}$ (J/mol^{-1}·K^{-1})	366±186	209±91	156±14

Uncertainties estimated at 95% probability level

Table 7.10. Frequency factors (A), activation energy (E_a) and adsorption enthalpy and entropy differences between DNHE and 1-hexanol and water and 1-hexanol

Catalyst	H-BEA-25	H-FAU-30	H-FAU-6			H-MFI-28
Rate equation	9.2	7.2	7.1	7.2	7.3	7.3
A (mol·h^{-1}·kg^{-1})	6·10^{12}	6·10^{14}	3·10^{16}	2·10^{16}	2·10^{16}	1·10^{14}
E_a (kJ·mol^{-1})	101±10	121±3	119±7	121±7	121±7	121±11
$\Delta H_{a,DNHE}$-$\Delta H_{a,HeOH}$ (kJ·mol^{-1})		-56±23	95±29	68±19	57±15	89±58
$\Delta S_{a,DNHE}$-$\Delta S_{a,HeOH}$ (J/(mol·K))		-129±52	217±65	156±42	131±34	207±128
$\Delta H_{a,\ H2O}$-$\Delta H_{a,HeOH}$ (kJ/mol)	-147±47					
$\Delta S_{a,H2O}$-$\Delta S_{a,\ HeOH}$ (J/mol^{-1}·K^{-1})	-330±104					

Activation energy of 121±2 kJ·mol^{-1} was reported over H-BEA-25 for the 1-pentanol dehydration to DNPE [44] and 148±11 for that of 1-hexanol to DNHE [47]. As for the adsorption enthalpy difference between alcohol and water, it is shown in Table 7.9 that 1-octanol adsorption over H-FAU-30 would be more exothermic than the adsorption of water. On the contrary, the adsorption of water in H-BEA-25 seems to be more exothermic than the adsorption of 1-hexanol as can be inferred from Table 7.10. As for DNHE adsorption enthalpy, it is seen that 1-hexanol adsorption over H-FAU-6 and H-MFI-28 would be more exothermic than that of DNHE whereas on H-FAU-30, DNHE adsorption is more exothermic than that of water. Adsorption entropy followed the same trend as enthalpy.

7.3. Conclusions

A kinetic study of the alcohol dehydration to linear ether was performed over zeolites and the thermostable resin Amberlyst 70. Firstly, the kinetics of the liquid phase dehydration of 1-octanol to DNOE was investigated in a stirred tank reactor at 413-453 K over Amberlyst 70. Preliminary experiments showed that neither internal nor external mass transfer limitations occurred by working with masses of 1-2 grams of catalyst with commercial bead size of Amberlyst 70 and 500 rpm of stirring speed.

Kinetic equations based on LHHW-RE mechanisms were fitted to rate data. The reaction at the catalyst surface was assumed to be the limiting step. Kinetic models fitted to rate data of pure 1-octanol as reactant revealed that kinetic models where 1-octanol and water are the adsorbed compounds in the resin and the fraction of free active sites is negligible fit the best.

Apparent activation energies of 120±7 $kJ \cdot mol^{-1}$ were determined through these type of models. Water, DNOE and solvent (1,4-dioxane) influence on the reaction rate was evaluated. DNOE and 1,4-dioxane did not show significant effects on the reaction rate whereas water showed a strong inhibition effect.

Langmuir and Freundlich isotherms, as well as variations of Langmuir isotherm found in literature and proposed in this work were used to quantify the fraction of acid sites in the catalyst blocked by water. LHHW-ER mechanistic models were corrected by the fraction of active sites not blocked by water according to different adsorption isotherms. Freundlich isotherm was found to describe better the water inhibition effect in a scenario where one molecule of 1-octanol adsorbed reacts with another molecule of 1-octanol of the liquid phase in a Eley-Rideal mechanism. Activation energy determined by fitting the model found to the whole range of rate data was 110±5 $kJ \cdot mol^{-1}$.

Secondly, a kinetic study was performed for DNHE and DNOE syntheses over zeolites, and their results compared to literature data of DNPE synthesis. Two reaction rate equations based on LHHW and ER mechanisms were proposed for DNHE and DNOE syntheses. Both equations assume that surface reaction is the rate-limiting step

and the fraction of free active sites is negligible. The first equation assumes that alcohol and ether are adsorbed in the zeolite surface, in agreement with kinetic equation found in literature for DNPE synthesis. The second one assumes that alcohol and water preferably adsorb through the reaction. The latter was found for DNHE and DNOE syntheses only over H-BEA-25 and H-FAU-30, respectively. Apparent activation energy of 100-120 kJ/mol was estimated for the reactions on tested zeolites.

CHAPTER 8

SUMMARY

Summary

It has been seen that diesel combustion in a diesel engine is a complex process where several pollutants are emitted in the engine exhausts. To solve this problem and at the same time accomplish with the increasingly stringent regulations for diesel composition, **diesel reformulation** with oxygenate compounds is proposed.

Linear symmetrical ethers with more than 9 carbon atoms represent a group of oxygenate compounds with excellent properties as diesel additives. Its addition in small quantities to diesel enhances the blending cetane number, improves cold start performance of diesel engine and dilutes sulfur and other non-desired diesel components, such as PAHs. C_{10}-C_{16} linear ethers such as **DNPE, DNHE and DNOE** are three linear symmetrical ethers with excellent properties to be added to commercial diesel.

This work proves that the synthesis of DNOE from 1-octanol dehydration over acid catalysts (acidic zeolites and PS-DVB ion exchange resins) is possible at 413-473 K. At the same time, the present work continues with the series of synthesis of **linear symmetrical ethers from n-alcohols** started with DNPE and DNHE in previous works.

A catalyst screening of acidic **PS-DVB ion exchange resins** showed best performances to yield DNPE, DNHE and DNOE selectively on low-crosslinked macroreticular and gel-type resins with high acid capacity. The ability to swell in the reaction media of **low-crosslinked and gel-type resins** can be proved with their high **volume of swollen polymer** (V_{sp}) values characterized with the ISEC technique. This way, the elastic polymer matrix of these resins allowed the diffusion of alcohols and ethers almost equally regardless the length of the molecules.

On medium and large pore **zeolites** synthesis of linear symmetrical ether was found to be strongly related to the zeolites **mesoporous surface** and the **acid sites number**. Selectivity to linear ether generally followed the trend: $\mathbf{S_{PeOH}^{DNPE} > S_{HeOH}^{DNHE} > S_{OcOH}^{DNOE}}$ which revealed a great steric hindrance for bulky molecules. Reaction rates of alcohol consumption doubled their values each 10 K increase but selectivity to linear ether

declined. The large pore zeolite **H-BEA-25** showed the best yield of linear ether due to the combination of high conversion of alcohol and high selectivity to linear ether.

Thermodynamic equilibrium constants of 1-pentanol and 1-hexanol dehydration reactions to DNPE and DNHE respectively were determined in previous works. In this work, the **thermodynamic equilibrium constant** of 1-octanol dehydration to DNOE was determined, proving that dehydration of 1-octanol to DNOE is an **exothermic reaction** ($\Delta_r H^0$ (298.15 K) = -13.6±1.7 kJ·mol^{-1}). The study, allowed at the same time improving current methods to estimate molar entropy of DNOE, this way the value of 658 ±4 kJ·mol^{-1}·K^{-1} was proposed for **molar entropy of DNOE** at 298.15 K. A review of the literature data for DNPE and DNHE equilibrium constants showed that the reaction enthalpy change tends to be more exothermic as the ether chain gets longer.

A **kinetic study** of the alcohol dehydration to linear ether was performed over zeolites and the thermostable resin Amberlyst 70.

Over **Amberlyst 70** a series of kinetic equations based on LHHW-RE mechanisms were fitted to rate data of **1-octanol dehydration to DNOE**. Pure 1-octanol experiments revealed that kinetic models where 1-octanol and water are the adsorbed compounds in the resin and the **fraction of free active sites is negligible** fit the best. In this case apparent activation energies of 120 ± 7 kJ·mol^{-1} were determined. Influence of products (water and DNOE) and solvent (1,4-dioxane) was evaluated which revealed a strong inhibition effect of water.

Inhibition effect of water was quantified by means of correction factors which described the fraction of active sites not blocked by water according to different adsorption isotherms. **Freundlich isotherm** was found to better describe the water inhibition effect in an scenario where one molecule of 1-octanol adsorbed reacts with another molecule of 1-octanol of the liquid phase in a **Rideal-Eley mechanism**. **Activation energy** determined accounting water deactivation was **110 ± 5 kJ·mol^{-1}**.

Over **zeolites**, a kinetic study was performed for **DNHE and DNOE synthesis** and was compared with that of DNPE in the literature. LHHW-RE kinetic models were fitted to rate data for DNHE and DNOE synthesis showing that the best kinetic models assume

that the **fraction of active sites is negligible**. Within these models, two type of equations were found to best represent rate data, one assumes that **alcohol and linear ether are adsorbed in the zeolite surface**, which agreed with kinetic equation found for DNPE synthesis. The other equation assumes that **alcohol and water are preferably adsorbed** through the reaction. **Apparent activation energy of 100-120 kJ·mol^{-1}** were estimated for the reactions on tested zeolites.

CHAPTER 9

References, nomenclature, list of tables, equations and figures

9.1 References

[1] J.-P. Wauquier. *Crude oil, Petroleum Products, Process Flowsheets*. Paris: Technip, 1995.

[2] M. Fahim, T. Al-Sahhaf, A. Elkilani. *Fundamentals of Petroleum Refining*. Elsevier, 2010.

[3] www.epicphysics.com

[4] www.springerimages.com

[5] I. Ciria. "Estudio de la combustión en motores diésel," *www.wearcheckibérica.es*.

[6] M.J.Murphy, J.D. Taylor and R.L. McCormick, "Compendium of Experimental Cetane Number Data," *National Renewable Energy Laboratory*, 2004.

[7] S.N. Soid, Z.A. Zainal. "Spray and combustion characterization for internal c ombustion engines using optical measuring techniques- a review," *Energy*, vol. 36, pp. 724-741, 2011.

[8] EPA web site: www.epa.org.

[9] EPA technical bulletin: EPA-456/F-99-006R, "Nitrogen Oxides (NO_x), Why and How They are Controlled," 1999.

[10] EPA technical bulletin: EPA-452/R-11-004a, "Policy Assessment for the Review of the Secondary National Ambient Air Quality Standards for Oxides of Nitrogen and Oxides of Sulfur," 2011.

[11] EPA technical bulletin: EPA420-R-00-026, "Regulatory Impact Analysis: Heavy-Duty Engine and Vehicle Standards and Highway Diesel Sulfur Control Requirements," 2000.

[12] EPA technical bulletin: EPA420-P-01-001. "Strategies and Issues in Correlating Diesel Fuel Properties with Emissions,"2001.

[13] N.-O. Nylund, P. Aakko, S. Niemi, T. Paanu, R. Berg, "Alcohols/Ethers as Oxygenates in Diesel Fuel: Properties of Blended Fuels and Evaluation of Practical Experiences," *Annex XXVI of the 27th Meeting of IEA Implementing Agreement on Advanced Motor Fuels. Report TEC 3/2005*, 2005.

[14] R. O. Dunn, “Effects of minor constituents on cold flow properties and performance of biodiesel,” *Prog. Energy Combust. Sci.*, vol. 35, pp. 481-489, 2009.

[15] M. Kozak, J. Merkisz, “Some considerations on the oxygenated fuels for diesel engines,” *TEKA Kom. Mot. Energ. Roln.- OL PAN*, vol. 7, pp. 129-136, 2007.

[16] H.G Pöttering, P. Necas, “Directive 2009/30/EC of the European parliament and of the Council of 23 April 2009 amending Directive 98/70/EC as regards the specification of petrol, diesel and gas-oil introducing a mechanism to monitor and reduce greenhouse gas emissions and amending Council Directive 1999/32/EC as regards the specification of fuel used by inland waterway vessels and repealing Directive 93/12/EC,” *Off. J. Eur. Union*, vol. 140, 88-112, 2009.

[17] B.C. Dunn, C. Guenneau, S. A. Hilton, J. Pahnke, E. M. Eyring, “Production of diethyl carbonate from ethanol and carbon monoxide over a heterogeneous catalyst,” *Energy Fuels*, vol. 16, pp. 177-181, 2002.

[18] Y. Ren, Z. H. Huang, D. M. Jiang, L. X. Liu, K. Zeng, B. Liu, X. B. Wang, “Engine performance and emission characteristics of a compression ignition engine fuelled with diesel/dimethoxymethane blends,”J. of Autom. Engin., vol. 219, pp. 905-914, 2005.

[19] International Energy Agency web: www.iea.org.

[20] P. S. Caro, Z. Mouloungui, G. Vaitilingom, J. C. Berge, “Interest of combining an additive with diesel-ethanol blends for use in diesel engines,” *Fuel*, vol. 80, pp. 565-574, 2001.

[21] X. Shi, Y. Yu, H. He, S. Shuai, J. Wang, R. Li, “Emission characteristics using methyl soyate-ethanol-diesel fuel blends on a diesel engine," *Fuel*, vol. 84, pp. 1543-1549, 2005.

[22] A.C. Hansen, Q. Zhang, P. Lyne, “Ethanol-diesel fuels-A review,” *Bioresour. Technol.* vol. 96, pp. 277-285, 2005.

[23] A.S. Ramadhas, S. Jayaraj, C. Muraleedharan, “Use of vegetable oils as I.C. engine fuels –A review,” *Renewable Energy*, vol. 29, pp. 727-742, 2004.

[24] M. N. Nabi, M. Akhter, M. Z. Shahadat, “Improvement of engine emissions with conventional diesel fuel and diesel-biodiesel blends,” *Bioresour. Technol.*, vol. 97, pp. 372-378, 2006.

[25] D.C. Drown, K. Harper, E. Frame, "Screening vegetable oil alcohol esters as fuel lubricity enhancers," *J. Am. Oil Chem. Soc*., vol. 78, pp. 579-584, 2001.

[26] S. Win Lee, T. Herage, B. Young, "Emission reduction potential from the combustion of soy methyl ester fuel blended with petroleum distillate fuel", *Fuel,* vol. 83, pp. 1607-1613, 2004.

[27] D. Altiparmak, A. Keskin, A. Koca, M. Gürü, "Alternative fuel properties of tall oil fatty acid methyl ester-diesel fuel blends,"*Bioresour. Technol*., vol. 98, pp. 241-246, 2007.

[28] L.A. Johnson, E.G. Hammond, US Patent 5.520.708, 1996.

[29] G. Knothe, "Dependence of biodiesel fuel properties on the structure of structure of fatty acid alkyl esters,"*Fuel Process.Technol*, vol. 86, pp. 1059-1070, 2005.

[30] Z. H. Huang, D.M. Jiang, K. Zeng, B. Liu Z. L. Yang, "Combustion characteristics and heat release analysis of a direct injection compression ignition engine fuelled with diesel—dimethyl carbonate blends," *J. Automob. Eng*., vol. 217, pp. 595-605, 2003.

[31] J. A. Kenar, G. Knothe, R.O. Dunn, T. W. Ryan, A. Matheaus, "Physical properties of oleochemical carbonates," *J. Am. Oil Chem. Soc*., vol. 82, pp. 201-205, 2005.

[32] G.A. Olah, US Patent WO 95/25153, 1995.

[33] Z. Huang, H. Wang, H. Chen, L. Zhou, D. Jiang, "Study of combustion characteristics of a compression ignition engine fuelled with dimethyl ether," *J. Automob. Eng*., vol. 213, pp. 647-652, 1999.

[34] H. Teng, J.C. McCandless, J.B. Schneyer, "Thermochemical Characteristics of Dimethyl Ether – An alternative Fuel for Compression-Ignition Engines," *SAE Technical Paper* 2001-01-0154, 2001, doi: 10.4271/2001-01-0154.

[35] K. Klepácova, D. Mravec, A. Kaszonyi, M. Bajus, "Etherification of glycerol and ethylene glycol by isobutylene," *Appl. Catal. A: Gen.*, vol. 328, pp. 1-13, 2007.

[36] C. Beatrice, C. Bertoli, N.D. Giacomo,"New findings on combustion behavior of oxygenated synthetic diesel fuels," *Combust. Sci. Technol*., vol. 137, pp. 31-50, 1998.

[37] T. Dogu, D. Varisli, Turk, "Alcohols as Alternatives to Petroleum for Environmentally Clean Fuels and Petrochemicals," *J. Chem.*, vol. 31, pp. 551-567, 2007.

[38] D.C. Rakopoulos, C.D. Rakopoulos, E.G. Giakoumis, A.M. Dimaratos, D.C. Kyritsis, "Effects of butanol-diesel blends on the performance and emissions of a high-speed DI diesel engine," *Energy Convers. Manage.*, vol. 51, pp. 1989-1997, 2010.

[39] G.C. Pecci, M.G. Clerici, F. Giavazzi, F. Ancillotti, M. Marchionna, R. Patrini, "Oxygenated Diesel Fuels. Part 1 – Structure and properties correlation," ISAF, 1993.

[40] G. A. Olah, —Cleaner burning and cetane enhancing diesel fuel supplements, U.S. Patent US 5520710, 1996.

[41] J. Guilera, R. Bringué, E. Ramírez, M. Iborra, J. Tejero, "Comparison between ethanol and diethyl carbonate as ethylating agents for ethyl octyl ether synthesis over acidic ion-exchange resins," *Ind. Eng. Chem. Res*., vol. 51, pp. 16525-16530, 2012.

[42] J. Tejero, F. Cunill. M. Iborra, J.F. Izquierdo, C. Fité, "Dehydration of 1-pentanol to di-*n*-pentyl ether over ion-exchange resin catalysts," *J. Mol. Catal. A: Chem.,* vol. 182-183, 541-554, 2002.

[43] J. Tejero, C. Fité, M. Iborra, J.F. Izquierdo, F. Cunill, R. Bringué, "Liquid-phase dehydrocondensation of 1-pentanol to di-n-pentyl ether (DNPE) over medium and large pore acidic zeolites," *Microporous Mesoporous. Mater.,* vol. 117, pp. 650-660, 2009.

[44] R. Bringué, M. Iborra, J. Tejero, J.F. Izquierdo, F. Cunill, V.J. Cruz, "Thermally stable ion-exchange resins as catalysts for the liquid-phase dehydration of 1-pentanol to di-*n*-pentyl ether (DNPE)," *J. Catal.,* vol. 244, pp. 33-42, 2006.

[45] R. Bringué, J. Tejero, M. Iborra, J.F. Izquierdo, C. Fité, F. Cunill, "Experimental Study of the Chemical Equilibria in the Liquid-Phase Dehydration of 1-Pentanol to Di-*n*-pentyl Ether," *Ind. Eng. Chem. Res*., vol. 46, pp. 6865-6872, 2007.

[46] R. Bringué, J. Tejero, M. Iborra, J.F. Izquierdo, C. Fité, F. Cunill, "Water effect on the kinetics of 1-pentanol dehydration to di-n-pentyl ether (DNPE) on amberlyst 70," *Top. Catal.*, vol. 45, pp. 1-4, 2007.

[47] R. Bringué, J. Tejero, M. Iborra, J.F. Izquierdo, C. Fité, F. Cunill, "Supported Nafion catalyst for 1-pentanol dehydration reaction in liquid phase," *Chem. Eng. J*., vol. 145, pp. 135-141, 2008.

[48] E. Medina, R. Bringué, J. Tejero, M. Iborra, C. Fité, "Conversion of 1-hexanol to di-n-hexyl ether on acidic catalysts," *App. Catal. A: Gen.,* vol. 374, pp. 41-47, 2010.

[49] Fischer-Tropsch Archive, www.Fischer-Tropsch.org.

[50] D.P. Krinkin, D.M. Rudkovskii, A.G. Trifel, "Side reactions in the oxo process," *Chem. Technol. Fuels Oils,* vol. 1, pp. 511–514, 1965.

[51] T. Tsichida, S. Sakuma, "Method of synthesizing Higher-Molecular Alcohol," US Patent 20070255079, 2007.

[52] I. Hoek, T.A. Nijhuis, A. I. Stankiewicz, J. A. Moulijn, "Kinetics of solid acid catalysed etherification of symmetrical primary alcohols: zeolite BEA catalysed etherification of 1-octanol," *Appl. Catal. A: Gen*., vol. 266, pp. 109-116, 2004.

[53] R. J. J. Nel, A. de Klerk, "Dehydration of C_5-C_{12} linear 1-alcohols over η-alumina to fuel ethers," *Ind. Eng. Chem. Res.*, vol. 48, pp. 5230-5238, 2009.

[54] N.P. Makgoba, T.M. Sakuneka, J.G. Koortzen, C. Van Schalkwyk, J.M Botha, C.P. Nicolaides, "Silication of γ-alumina catalyst during the dehydration of linear primary alcohols," *Appl. Catal. A: Gen.*, vol. 297, pp. 145-150, 2006.

[55] J.F. Norris, G.W. Rigby, "The reactivity of atoms and groups in organic compounds," *J. Am. Chem. Soc*., vol. 54, pp. 2088-2100, 1932.

[56] A. Corma A, H. García, "Crossing the borders between homogeneous and heterogeneous catalysis: developing recoverable and reusable catalytic systems," *Top. Catal.*, vol. 48, pp. 8-31, 2008.

[57] B. Corain, M. Zecca, K. Jeřábek, "Catalysis and polymer networks-the role of morphology and molecular accessibility," *J. Mol. Catal. A: Chem*., vol. 177, pp. 3-20, 2001.

[58] K. Jerabek, "Cross-evaluation of strategie, size-exclusion chromatography. (Inverse steric exclusion chromatography as a tool for morphology characterization)," ACS Symp., ser. 635, pp. 211-224, 1996.

[59] IZA web: www.iza-structure.org.

[60] J.F. Izquierdo, F. Cunill, J. Tejero, M. Iborra, C. Fité. *Cinética de las Reacciones Químicas*. Edicions Universitat de Barcelona, 2004.

[61] P.K. Kiviranta-Pääkkönen, L.K. Struckmann (née Rihko), J.A. Linnekoski, A.O.I. Krause, "Dehydration of the alcohol in the etherification of isoamylenes with methanol and ethanol," *Ind. Eng. Chem. Res.*, vol. 37, pp. 18-24, 1998.

[62] S.C.M. dos Reis, E.R. Lachter, R.S.V. Nascimento, J.A. Rodrigues Jr., M.G. Reid, "Transesterification of Brazilian vegetable oils with methanol over ion-exchange resins," *J. Am. Oil Chem. Soc.*, vol. 82, pp. 661-665, 2005.

[63] M.L. Honkela, A. Root, M. Lindblad, A. Outi, I. Krause, "Comparison of ion-exchange resin catalysts in the dimerization of isobutene," *Appl. Catal. A*, vol. 295, pp. 216-223, 2005.

[64] Kapila et al., US Patent US2005/0137428A1 (2005).

[65] J. Tejero, A. Zywert, R. Bringué, S. Kowalak, E. Janiszewska, M. Iborra, "Zeolite catalysed dehydration of alcohol to linear ether," *Stud. Surf. Sci. Catal.,* vol. 174 B, pp. 1115-1118, 2008.

[66] S. P. Felix, C, Savill-Jovitt, D.R. Brown, "Base adsorption calorimetry for characterising surface acidity: a comparison between pulse and conventional "static" techniques," *Thermochimica Acta*, vol. 433, pp. 59-65, 2005.

[67] S. Fischer, R. Kunin, "Routine exchange capacity determination of ion exchange resins," *Anal. Chem.*, vol. 27, pp. 1191, 1955.

[68] A. Guyot, D.C. Sherrington, in: P. Hodge (Ed.). *Syntheses and Separations Using Polymers Supports*. Chichester (UK): Wiley, 1988.

[69] M. Iborra, J. Tejero, J.F. Izquierdo, F. Cunill, "Influence of resin structure on the addition of ethanol to isobutene in the vapor phase," *Br. Polym. J*., vol. 23, pp. 117-127, 1990.

[70] G. Leofanti, M. Padovan, G. Tozzola, B. Venturelli, "Surface area and pore texture catalysts," *Catal. Today*, vol. 41, pp. 207-219, 1998.

[71] R. Kunin, E.F. Meitzner, J.A. Oline, S.A. Fischer, N. Frish, "Characterization of Amberlyst 15. Macroreticular sulfonic acid cation exchange resin," *Ind. Eng. Chem. Prod. Res*. *Dev.,* vol. 1, pp. 140-144, 1962.

[72] M. Umar, D. Patel, B. Saha, "Kinetic studies of liquid phase ethyl tert-butyl ether (ETBE) synthesis using macroporous and gelular ion exchange resin catalysts," *Chem. Eng. Sci.*, vol. 64, pp. 4424-4432, 2009.

[73] K. Sundmacher, U. Hoffmann, "Macrokinetic analysis of MTBE-synthesis in chemical potentials", *Chem. Eng. Sci.*, vol. 49, pp. 3077-3089, 1994.

[74] A.G. Ogston, "The spaces in a uniform random suspension of fibres," *Trans. Faraday Soc*., vol. 54, pp. 1754-1757, 1958.

[75] K. Jerabek, L. Holub, 13th International IUPAC Conference on Polymers and Organic Chemistry, Montreal, 2009.

[76] A.J. Lecloux, Texture of Catalysts, in J.R. Anderson, M. Boudart (Eds.). *Catalysis Science and Technology*. *Vol. 2*. Springer-Verlag, 1981.

[77] M.J. Remy, G. Poncelet, "A new approach to the determination of the external surface and micropore volume of zeolites from the nitrogen adsorption isotherm at 77 K," *J. Phys. Chem.*, vol. 99, pp. 773-779, 1995.

[78] E.P. Barrett, L.G. Joyner, P.P. Halenda, "The determination of pore volume and area distributions in porous substances. I. Computations from nitrogen isotherms," *J. Am. Chem. Soc.*, vol. 73, pp. 373-380, 1951.

[79] R. Szostack. *Handbook of Molecular Sieves*. New York : Van Nostrand Reinhold, 1992.

[80] M. Kruk, M. Jaroniec, A. Sayari, "Application of large pore MCM-41 molecular sieves to improve pore size analysis using nitrogen adsorption measurements," *Langmuir*, vol. 13, pp. 6267-6273, 1997.

[81] M. Papajewska, J. Tejero, E. Medina, R. Bringué, S. Kowalak, E. Janiszewska, "Zeolites as catalysts for the dehydration reaction of 1-hexanol to di-n-hexyl ether (DNHE)," Proceedings of XIVth Zeolite Forum, Kocierz, pp. 287-292, 2007.

[82] A. Zywert, E. Janiszewska, R. Bringué, J. F. Izquierdo, K. Tejero, S. Kowalak, "Dehydration of alcohols over zeolite catalysts," Proceedings of XVth Zeolite Forum, Kocierz, pp. 221-226, 2008.

[83] A.A. Nikolopoulos, A. Kogelbauer, J.G. Goodwin Jr., G. Marcelin, "Effect of dealumination on the catalytic activity of acid zeolites for the gas phase synthesis of MTBE," *Appl. Catal., A*, vol. 119, pp. 69-81, 1994.

[84] S. Ihm, M. Chung, K. Park, "Activity difference between the internal and external sulfonic groups of macroreticular ion-exchange resin catalysts in isobutylene hydration Ind," *Eng. Chem. Res*., vol. 27, pp. 41-45, 1988.

[85] R.B. Diemer Jr., K.M. Dooley, B.C. Gates, R.L. Albright,"Sulfonated poly(styrene-divinylbenzene) catalysts: III. The influence of polymer physical properties on the kinetics of methanol dehydration," *J. Catal.*, vol. 74, pp. 373-381, 1982.

[86] S. Koujout, B.M. Kiernan, D.R. Brown, H.G.M. Edwards, J.A. Dale, S. Plant, "The Nature of the Internal Acid Solution in Sulfonated Poly (styrene-co-divinylbenzene) Resins," *Catal. Lett*., vol. 85, pp. 33-40, 2003.

[87] C.P. Bezoukhanova, Y.A. Kalvachev, "Alcohol reactivity on zeolites and molecular sieves," *Catal. Rev.,* vol. 36, pp. 125-143, 1994.

[88] M.A. Makarova, E.A. Paukshtis, J.M. Thomas, C. Williams, K.I. Zamaraev, "Dehydration of *n*-butanol on zeolite H-ZSM-5 and amorphous aluminosilicate: Detailed mechanistic study and the effect of pore confinement," *J. Catal.*, vol. 149, pp. 36-51, 1994.

[89] M.A. Makarova, C. Williams, K.I. Zamaraev, J.M. Thomas, Mechanistic study of sec-butyl alcohol dehydration on zeolite H-ZSM-5 and amorphous aluminosilicate," *J. Chem. Soc.*, *Faraday Trans.*, vol. 90, pp. 2147-2153, 1994.

[90] K.J. Balkus, A.K. Khanmamedova, "Dehydration of methyl α-hydroxybutyrate catalized by zeolites," *J. Catal.*, vol. 151, pp. 10-16, 1995.

[91] T. Barzetti, E. Selli, D. Moscotti, L. J. Forni, "Pyridine and ammonia as probes for FTIR analysis of solid acid catalysts," *J. Chem. Soc., Faraday Trans*., vol. 92, pp. 1401-07, 1996.

[92] K. Klier, Q. Sun, O.C. Feeley, M. Johansson, R.G. Herman, "Coupling of alcohols to ethers: the dominance of the surface S_N2 reaction pathway," *Stud. Surf. Sci. Catal.*, vol. 101, pp. 601-610, 1996.

[93] B. Shi, B.H. Davis, "Alcohol dehydration: mechanism of ether formation using an alumina catalyst," *J. Catal.*, vol. 157, pp. 359-367, 1995.

[94] G.A. Olah, T. Shamma, G.K. Surya Prakash, "Dehydration of alcohols to ethers over Nafion-H, a solid perfluoroalkanesulfonic acid resin catalyst," *Catal. Lett*., vol. 46, pp. 1-4, 1997.

[95] I. Halasz, M. Kornel, "Pore size of solids," *Angew, Chem. Int. Ed. Engl.*, vol. 17, pp. 901-908, 1978.

[96] R.L. Albright, "Porous polymers as an anchor for catalysis," *React. Polym.*, vol. 4, pp. 155-174, 1986.

[97] A. Thakur, M. Thakur, P.V. Khadikar, C.T. Supuran, P. Sudele, "QSAR study on benzenesulphonamide carbonic anhydrase inhibitors: topological approach using Balaban index," *Bioorg. Med. Chem*., vol. 12, pp. 789-793, 2004.

[98] R. Todeschini, V. Consonni. *Handbook of Molecular Descriptors, vol. 11*. Germany: WILEY-VCH, 2000.

[99] S. Kulprathipanja, R. B. James. *Zeolites in Industrial Separation and Catalysis*. Germany: Wiley-VCH, 2010.

[100] A. Delion, B. Torck, M. Hellin, "Equilibrium Constant for the Liquid-Phase Hydration of Isobutylene over Ion-Exchange Resin," *Ind. Eng. Chem. Process Des. Dev*., vol.25, pp. 889-893, 1986.

[101] R. Bringué, J. Tejero, M. Iborra, C. Fité, J.F. Izquierdo, F. Cunill, "Study of the Chemical Equilibrium of the Liquid-Phase Dehydration of 1-Hexanol to Dihexyl Ether," *J. Chem. Eng. Data*, vol. 53, pp. 2854-2860, 2008.

[102] P. Atkins, J. Paula, *Physical Chemistry for the life sciences*. New York: W.H. Freeman and Company, 2006.

[103] R. Witting, J. Lohmann, "Vapor-Liquid Equilibria by UNIFAC Group Contribution. 6. Revision and Extension,"*Ind. Eng. Chem. Res*., vol. 42, pp. 183-188, 2003.

[104] J.W.Kang, V. Diky, R.D. Chirico, J.W. Magee, C.D. Muzny, I. Abdulagatov, A.F. Kazakov, M. Frenkel,"A new method for evaluation of UNIFAC interaction parameters," *Fluid Phase Equilibria,* vol. 309, pp. 68-75, 2011.

[105] Saadet Ulas. Uncertainties in Chemicals Biological and Molecular Systems and Optimal Control. ProQuest: Michigan, 2007.

[106] J.M. Smith, H.C. Van Ness, M.M. Abbot. *Introduction to Chemical Engineering Thermodynamics*. Ohio: McGraw-Hill, 1996.

[107] R.C. Reid, J.M. Prausnitz, B.E. Poling. *The properties of Gases and Liquids*. New York: McGraw-Hill, 1987.

[108] D.M. Himmelblau. *Process Analysis by Statistical Methods*. New York: John Wiley & Sons, 1970.

[109] D.R. Stull, E.F., Jr. Westrum, G.C. Sinke. *The Chemical Thermodynamics of Organic Compounds*. New York: John Wiley, 1969.

[110] C.L. Yaws, X. Pan, "Liquid Heat Capacity for Organics,"*Chem. Eng*., vol. 99, pp. 130-134, 1992.

[111] J. C. van Miltenburg, H. Gabrielova, K. Ruzicka, "Heat capacities and derived thermodynamic functions of 1-hexanol, 1-heptanol, 1-octanol, and 1-decanol between [5 K and 390 K," *J. Chem. Eng. Data*, vol. 48, pp. 1323-1331, 2003.

[112] D.R. Lide. *Handbook of Chemistry and Physics*. Boca Ratón: CRC, 2009.

[113] S.P. Verevkin, "Improved Benson Increments for the Estimation of Standard Enthalpies of Formation and Enthalpies of Vaporization of Alkyl Ethers, Acetals, Ketals, and Ortho Esters," *J. Chem. Eng. Data*, vol. 47, pp. 1071-1097, 2002.

[114] M.W. Jr. Chase, "NIST-JANAF Thermochemical Tables," *J. Phys. and Chem. Ref. Data*, vol. 9, pp. 1-1951, 1998.

[115] I.N. Levine. *FISICOQUIMICA vol. 1*. Madrid: McGraw-Hill, 1996.

[116] G. Liessmann, W. Schmidt, S. Reiffarth, "Recommended Thermophysical Data, "*Data compilation of the Saechische Olefinwerke Boehlen*,"pp. 11, 13, 1995.

[117] M. Shacham, N. Brauner, G. St. Cholakov, R. P. Stateva, "Property Prediction by Correlations Based on Similarity of Molecular Structures", *AIChE J*., vol. 50, pp. 2481-2492, 2004.

[118] E. du Toit, W. Nicol. "The rate inhibiting effect of water as a product on reactions catalysed by cation exchange resins: formation of mesityl oxide from acetone as case study," *App. Catal. A: Gen*., vol. 277, pp. 219-225, 2004.

[119] E. du Toit, R. Schwarzer, W. Nicol. Acetone condensation on a cation exchange resin catalyst: the pseudo equilibrium phenomenon *Chem. Eng. Sci*., vol. 59, pp. 5545-5550, 2004.

[120] U. Limbeck, C. Altwicker, U. Kunz, U. Hoffmann. "Rate expression for THFsynthesis on acidic ion exchange resin," *Chem. Eng. Sci*., vol. 56, pp. 2171-2178, 2001.

[121] B. Yang, M. Maeda, S. Goto. Kinetics of liquid phase synthesis of *tert*-amyl methyl ether from *tert*-amyl alcohol and methanol catalyzed by ion exchange resin," *J. Chem. Kinet.*, vol. 30, pp. 137-143, 1997.

[122] B. Yang, S. Yang, R. Yao. "Synthesis of ethyl *tert*-butyl ether from *tert*-butyl alcohol and ethanol on strong acid cation-exchange resins," *React. Funct. Polym*., vol. 44, pp. 167-175, 2000.

[123] R. Bringué, "*Thermally stable ion-exchange resins as catalysts for the liquid-phase dehydration of 1-pentanol to di-n-pentyl ether*". Phd Thesis. University of Barcelona, 2007.

9.2 Nomenclature

Notation

A	constant A (function of temperature)
A	preexponential term, $mol \cdot h^{-1} \cdot kg^{-1}$
a_1	first parameter of constant A
a_2	second parameter of constant A, K
a_j	activity of compound j
a_j	activity of compound j
B	constant B (function of temperature)
b_1	first parameter of constant B
b_2	second parameter of constant B, K
C	constant C (function of temperature)
c_1	first parameter of constant C
c_2	second parameter of constant C, K
c_j	concentration of compound j ($mol \cdot L^{-1}$)
$\hat{c}_j$	concentration of compound j adsorbed in the surface ($mol \cdot L^{-1}$)
$c_{p,m,j}$	molar heat capacity of compound j ($J \cdot mol^{-1}\ K^{-1}$)
$\hat{c}_v$	concentration of vacant active sites ($mol \cdot L^{-1}$)
D	constant D (function of temperature)
d_1	first parameter of constant D

d_2	second parameter of constant D, K
d_b	bead size (mm)
d_p	particle diameter (mm)
d_{pore}	pore diameter (nm)
E_a	activavion energy ($kJ \cdot mol^{-1}$)
f (a_{H2O})	correction factor
J	Balaban Index
K	chemical equilibrium constant
$\widehat{K}$	equilibrium constant of surface chemical reaction
$\hat{k}'$	apparent rate constant of direct reaction at the surface, $mol \cdot h^{-1} \cdot kg^{-1}$
K_0	true rate constant of direct reaction, $mol \cdot h^{-1} \cdot kg^{-1}$
$K_{a,A}$	adsorption equilibrium constant of A
$K_{a,j}$	adsorption constant of compound j
$k_{d,A}$	rate constant of A desorption ($m^3 \cdot (g \cdot s)^{-1}$)
K_{H2O}	adsorption constant of water
K_{H2O} (1)	first parameter of constant K_{H2O}
K_{H2O} (2)	second parameter of constant K_{H2O}, K
K_x	equilibrium constant as a function of molar fractions
K_Γ^i	Poynting correction factor for reaction i
K_α	Freundlich parameter, K
K_γ	equilibrium constant as a function of activity coefficients
M_w	molecular weight ($g \cdot mol^{-1}$)
n_j^0	initial number of moles of j (mol)
n	number of active centres involved in the chemical reaction
N	stirring speed, rpm
n_j	number of moles of j (mol)

N_j	number of moles consume (mol)
O	ovality
P^0	standard pressure
P^S	saturation pressure
p_i	parameter i
r_j^0	initial reaction rate of j formation (mol·h^{-1}·kg^{-1})
$-r_j^0$	initial reaction rate of j consumption (mol·h^{-1}·kg^{-1})
r'	reaction rate per mass unit of catalyst (mol·(g·s)$^{-1}$
$r'_{ads,A}$	adsorption rate of A (mol·(g·s)$^{-1}$)
r_{calc}	estimated rate (mol·h^{-1}·kg^{-1})
r_{DNOE}	DNOE formation rate (mol·h^{-1}·kg^{-1})
$r'_{des,A}$	desorption rate of A (mol·(g·s)$^{-1}$)
r_{exp}	experimental rate (mol·h^{-1}·kg^{-1})
r'_s	rate of surface chemical reaction (mol·(g·s)$^{-1}$
$S^0_{(g)}$	gas molar entropy (J·mol^{-1}·K^{-1})
$S^0_{(l)}$	liquid molar entropy (J·mol^{-1}·K^{-1})
S^0_m	standard molar entropy (J·mol^{-1}·K^{-1})
S_j^k	selectivity to k relative to j (% mol/mol)
S_{area}	total surface area (m^2·g^{-1})
S_{area}	surface area (m^2·g^{-1})
S_{BET}	BET surface (m^2·g^{-1})
S_{BET}	BET surface (m^2·g^{-1})
S_{BJH}	mesopore surface (m^2·g^{-1})
S_{ext}	external surface area (m^2·g^{-1})
T	temperature (K)
t	time (h)

$\bar{T}$	mean temperature (K)
T_b	boiling temperature, (ºC)
TOF^0_j	initial TOF of j formation (mol·(h·meqH^+)$^{-1}$
$-TOF^0_j$	initial TOF of j consumption (mol·(h·meqH^+)$^{-1}$
V_{BJH}	mesopore volume (cm^3·g^{-1})
V_{ext}	external volume (cm^3·g^{-1})
V_j	molar volume of compound j (L·mol^{-1})
V_{pore}	pore volume (cm^3·g^{-1})
V_{sp}	volume of swollen phase (cm^3·g^{-1})
W	catalyst mass (kg)
X_j	conversion of j
x_j	molar fraction of compound j
Y_j^k	yield of k relative to j (% mol/mol)
$\Delta_c S^0$	entropy increment due to vapor compression
$\Delta_f H^0$	standard formation enthalpy (kJ·mol^{-1})
$\Delta_{ig} S^0$	entropy increment due to deviation of ideality of the vapor
$\Delta_r G^0$(l)	standard liquid Gibbs energy change of reaction (kJ·mol^{-1})
$\Delta_r H^0$(l)	standard liquid enthalpy change of reaction (kJ·mol^{-1})
$\Delta_r S^0$(l)	standard liquid entropy change of reaction (J·mol^{-1}·K^{-1})
$\Delta_v S^0$	entropy increment due to phase change
$\Delta_{vap} H^0$	standard vaporization enthalpy (kJ·mol^{-1})
$\Delta H_{a,j}$	adsorption enthalpy of compound j (kJ·mol^{-1})
ΔH_{ads}	ammonia enthalpy of adsorption (kJ·mol^{-1})
$\Delta S_{a,j}$	adsorption entropy of compound j (J·mol^{-1}·K^{-1})
[H^+]	acid capacity (meq H^+·g^{-1})

Greek symbols

α	Freundlich constant
ε_p	uncertainty of p
θ	porosity (%)
θ_{H2O}	fraction of active sites blocked by water
ρ	density, ($kg \cdot m^{-3}$)
μ	viscosity, (cSt)
σ	active site
ρ_s	skeletal density ($g \cdot cm^{-3}$)
Φ_d	random coil diameter (Å)
$\gamma_{x,j}$	activity coefficient of compound j for molar fractions
$\nu_{i,j}$	stoichiometric coefficient of compound j in the reaction i

Abbreviations

1D	one-dimension
2D	two-dimension
3D	three-dimension
AGO	atmospheric gasoil
BET	Brunauer-Emmet-Teller
BJH	Barret-Joyner-Halenda
$C_5^=$	pentenes: 1-pentene, 2 (E/Z)-pentene
$C_6^=$	hexenes : 1-hexene, (E/Z)-2-hexene, (E/Z)-3-hexene
$C_8^=$	octenes: 1-octene, (E/Z)-2-octene, (E/Z)-3-octene, 4-octene
CDPF	catalytic diesel particle filter
CFPP	cold filter plugging point (ºC)
CI	cetane index

CN	cetane number
CP	cloud point
DNHE	di-n-hexyl-ether
DNOE	di-n-octyl-ether
DNPE	di-n-pentyl-ether
DNPE	di-n-pentyl ether
DOC	diesel oxidation catalyst
DPF	diesel particle filter
DSC	differential scanning calorimetry
DVB	divinylbenzene
E_1	first order elimination reaction
EGR	exhaust gas recirculation
EOE	ethyl octyl ether
EOI	end of injection
EPA	Environmental Protection Agency
FAME	fatty acid methyl ester
FCC	fluid catalytic cracking
GLC	gas-liquid chromatograph
GLC	gas-liquid chromatograph
HC	hydrocarbons
HDV	heavy duty vehicles
HeOH	1-hexanol
ISEC	inverse steric exclusion chromatography
IUPAC	International Union of Pure and Applied Chemistry
IZA	Internatonal Zeolite Association
LHHW-ER	Langmuir Hinselwood Hougen Watson-Eley Rideal

MS	mass spectrometer
OcOH	1-octanol
PAHs	polyaromatic hydrocarbons
PeOH	1-pentanol
PM	particulate matter
PP	pour point (ºC)
PS-DVB	polystyrene-divinylbenzene
RSSQ	residual sum of squares
RSSQRE	root of sum of squares of relative errors
SCR	selective catalytic reduction
SEM	scanning electronic microscopy
S_N2	Second order nucleophilic substitution reaction
SOF	soluble organic fraction
SOI	start of injection
TCD	thermal conductivity detector
TG	thermal gravimetry
TOF	turn over frequency
ULSD	ultra low sulfur diesel
VGO	vacuum gasoil
VOCs	volatile organic compounds

Subscripts and superscripts

$C^{=}$	olefin
$C_5^{=}$	pentenes: 1-pentene, 2 (E/Z)-pentene
$C_6^{=}$	hexenes : 1-hexene, (E/Z)-2-hexene, (E/Z)-3-hexene

$C_8^=$	octenes: 1-octene, (E/Z)-2-octene, (E/Z)-3-octene, 4-octene
DNHE	di-n-hexyl-ether
DNOE	di-n-octyl-ether
DNPE	di-n-pentyl-ether
DNPE	di-n-pentyl ether
H2O	water
HeOH	1-hexanol
HeOHe'	C_{12} branched ethers: 2,2-oxybis hexane, 1,2-oxybis hexane.
OcOH	1-octanol
OcOOc'	C_{16} branched ethers: 1,2-oxybis octane, 1,3-oxybis octane, 1,4-oxybis octane
PeOH	1-pentanol
PeOPe'	C_{10} branched ethers: 1-(1-methylbutoxy)-pentane, 1-(2-methylbutoxy)-pentane, 2-(1-methylbutoxy)-pentane, 2-(2-methylbutoxy)-pentane
ROH	alcohol
ROR	linear symmetrical ether
ROR'	branched ether

9.3 List of Tables

9.4 List of equations

9.5 List of Figures

CHAPTER 10

APPENDICES

APPENDIX I. Example of composition of a diesel fuel

Composition	value
Paraffins (w/w %)	36.5
Naphthenes (w/w %)	24.3
Monoaromatics (w/w %)	14.2
Diaromatics (w/w %)	15.4
Triaromatics (w/w %)	1.8
Thiophenes (w/w %)	7.7
Total aromatics (w/w %)	39.1
Sulfur content (ppm)	11.6
Nitrogen content (ppm)	216

Source: J.-P. Wauquier. *Crude oil, Petroleum Products, Process Flowsheets*. Paris: Technip, 1995

APPENDIX II. Specifications for diesel fuel ruled by RD 61/2006

ANEXO II

ESPECIFICACIONES DEL GASÓLEO DE AUTOMOCIÓN (CLASE A)

Características	Unidad de medida	Límites (1)		Métodos de ensayo		
		Mínimos	Máximos	En EN 590 (2)	Normas ASTM (5)	Normas UNE (5)
Número de cetano		51,0	-	EN ISO 5165	D-613	UNE EN ISO 5165
Índice de cetano		46,0	-	EN ISO 4264	D 4737	UNE EN ISO 4264
Densidad a 15ºC	kg/m3	820	845	EN ISO 3675 EN ISO 12185	D 4052	UNE EN ISO 3675 UNE EN ISO 12185
Hidrocarburos policíclicos aromáticos (3)	%m/m	-	11	EN ISO 12916		UNE EN 12916
Contenido en azufre (4)	mg/kg	-	50	EN ISO 20846 EN ISO 20847 EN ISO 20884		UNE EN ISO 20846 UNE EN ISO 20847 UNE EN ISO 20884
Destilación : · 65% recogido · 85% recogido · 95% recogido	ºC	 250 	 350 360	EN ISO 3405	D 86	UNE EN ISO 3405
Viscosidad cinemática a 40 ºC	mm2/s	2,00	4,50	EN ISO 3104	D 445	UNE EN ISO 3104
Punto de inflamación	ºC	superior a 55		EN ISO 2719	D 93	UNE EN ISO 2719
Punto de obstrucción filtro frío : · Invierno (1 oct.-31 marzo) · Verano (1 abril-30 sept.)	ºC	 - -	 - 10 0	EN 116		UNE EN 116
Residuo carbonoso (sobre 10 % v/v residuo de destilación)	%m/m	-	0,30	EN ISO 10370	D 4530	UNE EN ISO 10370
Lubricidad, diámetro huella corregido (wsd 1.4) a 60 ºC	µm	-	460	EN ISO 12156-1		UNE EN ISO 12156-1
Agua	mg/kg	-	200	EN ISO 12937		UNE EN ISO 12937
Contaminación total (partículas sólidas)	mg/kg	-	24	EN ISO 12662		UNE EN 12662
Contenido de cenizas	%m/m	-	0,01	EN ISO 6245	D 482	UNE EN ISO 6245
Corrosión lámina de cobre (3 h. a 50 ºC)	escala	-	clase 1	EN ISO 2160	D 130	UNE EN ISO 2160
Estabilidad a la oxidación	g/m3	-	25	EN ISO 12205	D 2274	UNE EN ISO 12205
Color			2		D 1500	
Transparencia y brillo		Cumple			D 4176	
Aditivos y agentes trazadores	Regulados por la Orden del Ministerio de la Presidencia PRE/1724/2002, de 5 de julio, modificada por la Orden del Ministerio de la Presidencia PRE/3493/2004, de 22 de octubre.					

NOTAS:

(1) Los valores indicados en la especificación son "valores reales". Para determinar los valores límite, se ha recurrido a los términos del documento EN ISO 4259 "Petroleum products - Determination and application of precision data in relation to methods of test". Para determinar un valor mínimo, se ha tenido en cuenta una diferencia mínima de 2 R por encima de cero (R = reproducibilidad). Los resultados de las mediciones individuales se interpretarán sobre la base de los criterios descritos en la norma EN ISO 4259 (publicada en 1995).

(2) Se han tenido en cuenta los especificados en la norma UNE EN 590 (2004), pudiendo, no obstante, adoptarse otros métodos analíticos, siempre que éstos ofrezcan, al menos, la misma exactitud y el mismo nivel de precisión que los especificados en la norma citada.
Para más información sobre métodos analíticos y su prevalencia en caso de discrepancia, ver la norma UNE EN 590 (2004).
Los métodos de ensayo a aplicar serán los correspondientes a la última versión publicada.

(3) Definido como los hidrocarburos aromáticos totales menos los hidrocarburos monoaromáticos.

(4) El método EN ISO 20847 no será utilizado como método en caso de disputa. Para la determinación hasta 10 ppm de azufre, se utilizarán indistintamente los EN ISO 20846 y EN ISO 20884.

(5) Los métodos de ensayo a aplicar serán los correspondientes a la última versión publicada.

ANEXO III

ESPECIFICACIONES DE LOS GASÓLEOS PARA USOS AGRÍCOLA Y MARÍTIMO (CLASE B) Y DE CALEFACCIÓN (CLASE C)

Características	Unidades de medida	Gasóleo Clase B	Gasóleo Calefacción Clase C	Métodos de ensayo	
				Normas UNE (2)	Normas ASTM (2)
Densidad a 15º (máx/mín)	kg/m^3	880/820	900/--	EN ISO 3675 EN ISO 12185	D-4052
Color		Rojo	Azul		D-1500
Azufre, máx	% m/m	0,20 (1)	0,20 (1)	EN 874 EN 24260	
Índice de cetano , mín.		46		EN ISO 4264	D-4737
Número de cetano, mín.		49		ISO 5165	D-613
Destilación				EN ISO 3405	D-86
65% recogido, mín	ºC	250	250		
80% recogido, máx	ºC		390		
85% recogido, máx	ºC	350			
95% recogido, máx	ºC	370	Anotar		
Viscosidad cinemática a 40 ºC mín/máx	mm^2/s	2,0/4,5	--/7,0	EN ISO 3104	D-445
Punto de inflamación, mín	ºC	60	60	EN 22179	D-93
Punto de obstrucción filtro frío				EN 116	
Invierno (1 octubre-31 marzo), máx	ºC	-10	-6		
Verano (1 abril-30septiembre), máx	ºC	0	-6		
Punto de enturbiamento				EN 23015	D-2500
Invierno(1 octubre-31 marzo), máx	ºC		4		D-5772
Verano (1 abril-30septiembre), máx	ºC		4		
Residuo carbonoso (sobre 10% V/V final destilación), máx	% m/m	0,30	0,35	EN ISO 10370	D-4530
Agua y sedimentos, máx	% V/V		0,1	UNE 51083	D-2709
Agua, máx	mg/kg	200		EN ISO 12937	D-1744
Contaminación total (partículas sólidas), máx	mg/kg	24		EN 12662	
Contenido de cenizas, máx	% m/m	0,01		EN ISO 6245	D-482
Corrosión lámina de cobre (3 horas a 50 ºC), máx.	Escala	Clase 1	Clase 2	EN ISO 2160	D-130
Transparencia y brillo		Cumple			D-4176
Estabilidad a la oxidación, máx	g/m^3	25		EN ISO 12205	D-2274
Aditivos y agentes trazadores	Regulados por la Orden del Ministerio de la Presidencia PRE/1724/2002, de 5 de julio, modificada por la Orden del Ministerio de la Presidencia PRE/3493/2004, de 22 de octubre.				

NOTAS:

(1) Con las excepciones recogidas en el artículo 3 de este real decreto.

El método de referencia adoptado para determinar el contenido de azufre en el gasóleo clase B para uso marítimo será el definido en las normas UNE EN ISO 8754 (1996) y UNE EN ISO 14596 (1999).

Del mismo modo, el método de referencia adoptado para determinar el contenido de azufre en el gasóleo clase C será el definido en las normas UNE EN 24260 (1996), UNE EN ISO 8754 (1996) y UNE EN ISO 14596 (1999).

El método de arbitraje será el UNE EN ISO 14596 (1999). La interpretación estadística de la comprobación del contenido de azufre de los gasóleos utilizados se efectuará conforme a la norma UNE EN ISO 4259 (1997).

(2) Los métodos de ensayo a aplicar serán los correspondientes a la última versión publicada.

APPENDIX III

Calibration equations used to correlate % (w/w) of a compound (y) and its % of chromatographic area (x)

For experiments without 1,4-dioxane:

$$y = 1.0679x + 0.298 \text{ , } R^2 = 0.9992 \text{ (DNOE)}$$

$$y = 1.0673x - 6.6572 \text{ , } R^2 = 0.9996 \text{ (1-octanol)}$$

$$y = 0.8506x - 0.0616 \text{ , } R^2 = 0.9879 \text{ (water)}$$

$$y = 0.9073x + 0.0093 \text{ , } R^2 = 0.9994 \text{ (octenes)}$$

For experiments with 1,4-dioxane:

$$y = 0.0002x^3 - 0.0265x^2 + 2.4042x - 19.444 \text{ ,} R^2 = 0.9994 \text{ (1,4-dioxane)}$$

$$y = 1.0482x, \ R^2 = 0.9995 \text{ (DNOE)}$$

$$y = 0.9771x - 0.3009 \text{ , } R^2 = 0.9994 \text{ (1-octanol)}$$

$$y = 0.7666x - 0.3009 \text{ , } R^2 = 0.9994 \text{ (water)}$$

$$y = 0.837x \text{ , } R^2 = 0.9997 \text{ (octenes)}$$

Example of a chromatogram for the1-octanol dehydration system

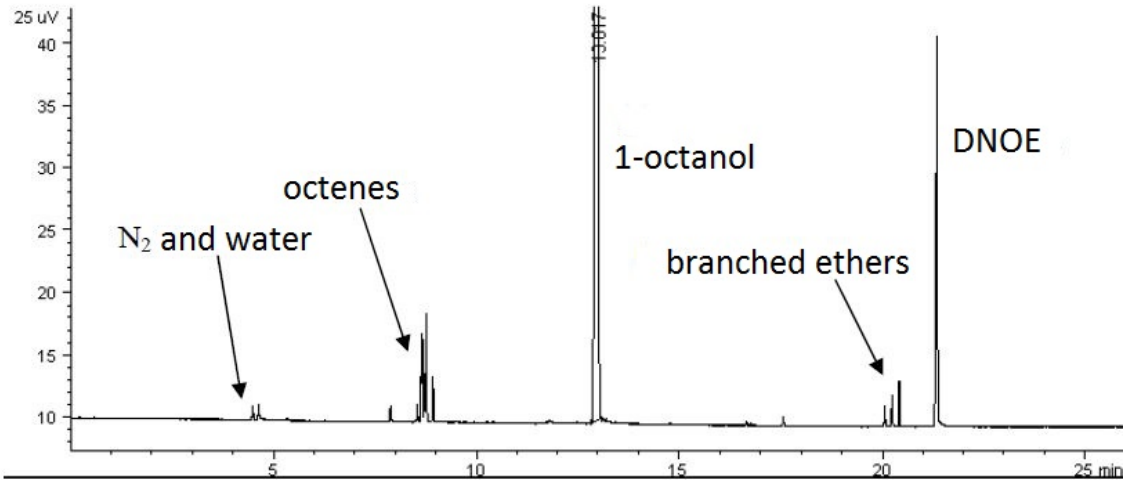

APPENDIX IV. Differential scanning calorimeter. Adsorption enthalpy data

Set up and analysis

Adsorption enthalpy of ammonia over ion exchange resins and zeolites was measured with a calorimeter connected to a mass spectrometer (see figure below).

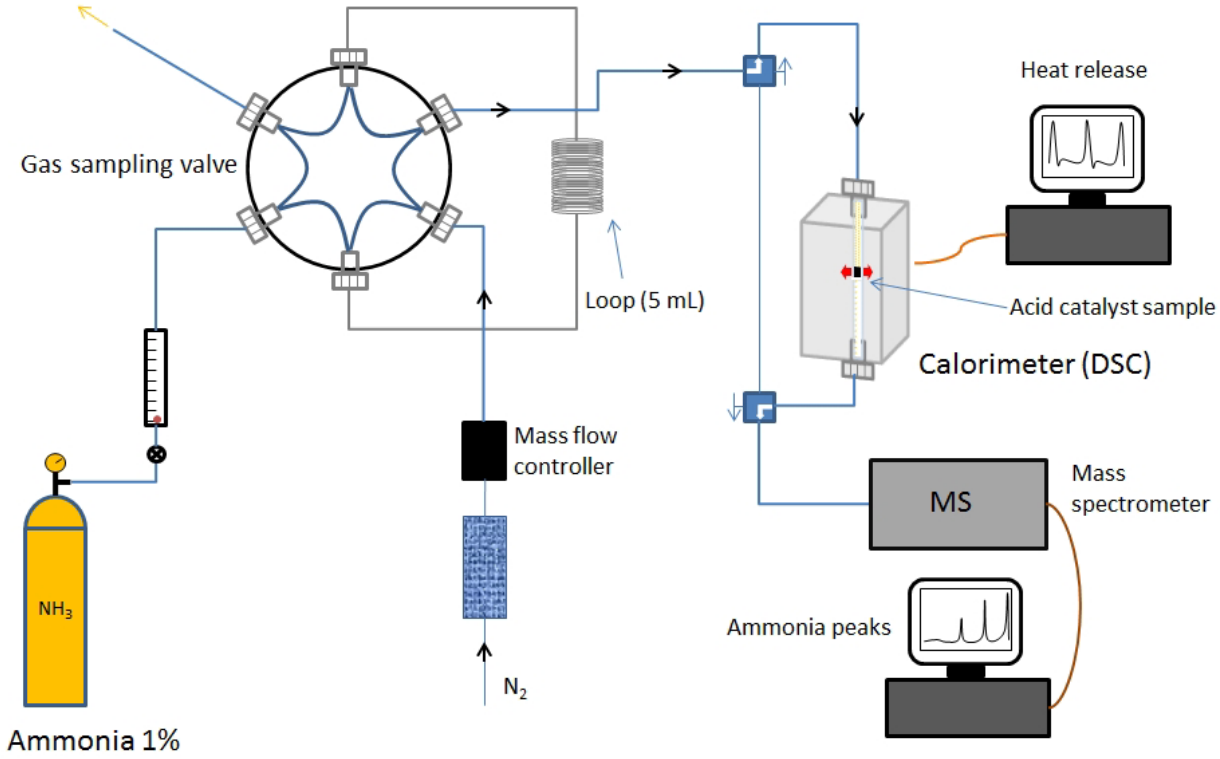

Experimental set up employed for ammonia adsorption enthalpy determination.

Ammonia adsorption calorimetry was performed under flow conditions, using a system based on a flow-through Setaram 111 differential scanning calorimeter (DSC) and an automated gas flow and switching system, with a mass spectrometer detector for the down-stream gas flow (Hiden HPR20).

Experimental procedure

In a typical experiment the sample of acid catalyst (3-20 mg) was placed in the DSC and firstly heated under dried nitrogen (5 ml·min^{-1}) for 2 h at 373 K. Small pulses (5 mL) of ammonia (1%) were then injected at regular intervals into the carrier gas stream from a gas-sampling valve. The concentration of ammonia downstream of the sample was monitored with the mass spectrometer. The interval between pulses was 1 h, which was enough time to ensure that the ammonia concentration in the carrier gas returned to zero and the DSC baseline re-established itself. An important feature of the flow

calorimetric technique is that net heat measurements relate only to ammonia bound irreversibly to the samples. Weakly bound (physisorbed) ammonia desorbs immediately the gas flow reverts to the carrier gas. The net amount of ammonia irreversibly adsorbed from each pulse was determined by comparing the mass spectrometer signal during each pulse with a signal recorded during a control experiment through a blank sample tube. Net heat released for each pulse was calculated from the DSC thermal curve. From this the molar enthalpy of ammonia adsorption (ΔH_{ads}) was obtained for the ammonia adsorbed from each pulse.

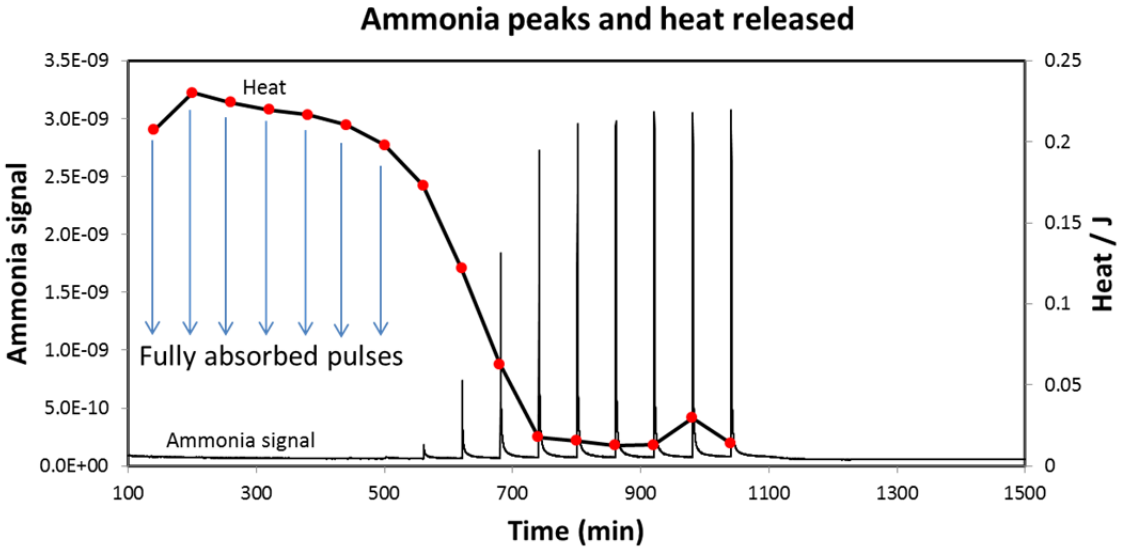

Net heat released in each pulse and ammonia signal observed. A-15, W_{cat} = 4.24 mg, T_{ads} = 373 K

APPENDIX V. Summary of experiments

List of resins tested in this work (●) and in previous works (○) at 423 K

Resin	DNOE	DNHE	DNPE
A-15	●	●	●
A-16	●	●	●
A-35	●	●	●
A-36	●	●	○
A-39	●	●	●
A-46	●	●	●
A-70	●	○	○
CT 175	●		
CT 224	●	●	○
CT 252	●		
CT 275	●		
CT 276	●		
DOW5050	●	●	○
NR50	●	○	○

List of zeolites tested in this work (●) and in previous works (○)

Zeolite	T (K)	System		
		DNOE	DNHE	DNPE
H-BEA-25	423	●		○
	433		○	○
	443		○	○
	453	●	○	○
	463		○	○
	473		○	
H-FAU-6	423	●		
	433		○	
	443		○	
	453	●	○	●
	463		○	
	473		○	
H-FAU-30	423	●		
	433	●	○	
	443	●	○	
	453	●	○	●
	463	●	○	
	473	●	○	
H-MFI-28	443		○	
	453		○	●
	463		○	
H-MOR-20	423	●		
	453	●	●	●
H-FER-20	453	●	●	●
H-MCM-79	453		●	
	463		●	

APPENDIX VI.RSSQ and RSSQRE for kinetic models on Amberlyst 70

RSSQ and RSSQRE for kinetic models fitted to DNOE rates of pure 1-octanol experiments on Amberlyst 70. Models crossed out are thermodynamically inconsistent.

Model	RSSQ	RSSQRE
1.1	1866	0.170
1.2	5179	0.371
1.3	1866	0.884
2.1	385	395
2.2	409	328
2.3	368	3.21E+58
3.1	5115	
3.2	5510	
3.3	5567	
~~4.1~~		
~~4.2~~		
~~4.3~~		
5.1	4744	
5.2	5546	
5.3	5572	
~~6.1~~		
~~6.2~~		
~~6.3~~		
7.1	261	154
7.2	278	11.3
7.3	300	4.167
~~8.1~~		
~~8.2~~		
~~8.3~~		
9.1	**250**	**2.58**
9.2	**257**	**1.62**
9.3	**269**	**0.929**
~~10.1~~		
~~10.2~~		
~~10.3~~		
11.1	4744	
11.2	5819	
11.3	6232	
~~12.1~~		
~~12.2~~		
~~12.3~~		
13.1	250	1.72E+108
13.2	257	215
13.3	269	25.2
~~14.1~~		
~~14.2~~		
~~14.3~~		

RSSQ and RSSQRE for kinetic models fitted to DNOE rates of experiments of Table 7.2 on Amberlyst 70. Models crossed out are thermodynamically inconsistent.

Model	RSSQ	RSSQRE
1.1	4294	0.113
1.2	14609	0.448
1.3	28811	3.347
2.1	2109	12.384
2.2	2109	11.960
2.3	2109	12.026
3.1	17636	64.4
3.2	18890	52.5
3.3	19645	50.6
~~4.1~~		
~~4.2~~		
~~4.3~~		
5.1	13824	0.437
5.2	17697	0.659
5.3	19292	1.01
~~6.1~~		
~~6.2~~		
~~6.3~~		
7.1	1740	1.10
7.2	13559	2.28
7.3	29152	97488
~~8.1~~		
~~8.2~~		
~~8.3~~		
9.1	**1301**	**1.41**
9.2	3393	3.10
9.3	17226	0.436
~~10.1~~		
~~10.2~~		
~~10.3~~		
11.1	12110	7.09
11.2	14618	4.18
11.3	15359	3.10
~~12.1~~		
~~12.2~~		
~~12.3~~		
13.1	1305	221
13.2	3394	96.8
13.3	17169	70326
~~14.1~~		
~~14.2~~		
~~14.3~~		

APPENDIX VII. RSSQ and RSSQRE for kinetic models on zeolites

RSSQ and RSSQRE for kinetic models fitted to DNOE rates measured on H-FAU-30. Models crossed out are thermodynamically inconsistent.

Model	RSSQ	RSSQRE
1.1	131.64	0.126
1.2	267.99	0.218
1.3	473.54	0.398
2.1	72.55	3.951
2.2	72.71	2.132
2.3	72.72	2.011
3.1	1247.47	0.248
3.2	1964.82	1.167
3.3	1996.10	1.201
~~4.1~~		
~~4.2~~		
~~4.3~~		
5.1	1106.28	0.217
5.2	2011.21	1.556
5.3	2026.30	1.645
~~6.1~~		
~~6.2~~		
~~6.3~~		
7.1	67.89	1.154
7.2	70.22	1.060
7.3	72.30	1.068
~~8.1~~		
~~8.2~~		
~~8.3~~		
9.1	**59.83**	**1.117**
9.2	**62.20**	**1.293**
9.3	**67.45**	**0.560**
~~10.1~~		
~~10.2~~		
~~10.3~~		
11.1	1696.83	594.865
11.2	1964.57	20.143
11.3	1995.56	489.096
~~12.1~~		
~~12.2~~		
~~12.3~~		
13.1	57.23	4.297
13.2	56.78	2.325
13.3	56.94	2.086
~~14.1~~		
~~14.2~~		
~~14.3~~		

RSSQ and RSSQRE for kinetic models fitted to DNHE rates measured on H-FAU-30. Models crossed out are thermodynamically inconsistent.

Model	RSSQ	RSSQRE
1.1	135.57	0.09
1.2	142.58	0.11
1.3	1089.00	0.39
~~2.1~~		
~~2.2~~		
~~2.3~~		
3.1	7331.13	0.87
3.2	7982.34	0.62
3.3	8048.62	0.47
4.1	1065.75	1466.98
4.2	1100.69	1428.23
4.3	1064.40	2133.09
5.1	7039.74	1.66
5.2	8020.42	1.32
5.3	8123.46	1.05
6.1	1037.80	2.75E+05
6.2	1017.81	2.24E+07
6.3	959.13	2.33E+123
7.1	135.57	1.04E+11
7.2	**3.40**	**0.55**
7.3	**2.30**	**1.21**
~~8.1~~		
~~8.2~~		
~~8.3~~		
9.1	135.57	1.43E+11
9.2	12.31	1.00
9.3	22.60	0.51
~~10.1~~		1.67E+06
~~10.2~~		154.17
~~10.3~~		10.15
11.1	7039.74	0.00
11.2	8275.34	1512.27
11.3	8736.21	9324.34
12.1	983.17	198.17
12.2	1036.77	14.41
12.3	973.70	95.91
13.1	135.57	1.13E+11
13.2	3.40	1.25
13.3	2.32	5.52
~~14.1~~		
~~14.2~~		
~~14.3~~		

RSSQ and RSSQRE for kinetic models fitted to DNHE rates measured on H-FAU-6. Models crossed out are thermodynamically inconsistent.

Model	RSSQ	RSSQRE
1.1	896.75	0.313
1.2	1659.14	0.561
1.3	2423.26	1.085
2.1	314.06	287.307
2.2	314.77	657.106
2.3	316.52	256.254
3.1	2048.65	0.485
3.2	2908.12	0.313
3.3	3061.39	0.228
~~4.1~~		
~~4.2~~		
~~4.3~~		
5.1	1645.05	0.694
5.2	2697.60	0.391
5.3	2917.57	0.322
~~6.1~~		
~~6.2~~		
~~6.3~~		
7.1	**21.83**	**0.437**
7.2	**22.70**	**0.399**
7.3	**26.88**	**0.383**
~~8.1~~		
~~8.2~~		
~~8.3~~		
9.1	32.43	1.179
9.2	35.85	1.031
9.3	43.80	2.748
~~10.1~~		
~~10.2~~		
~~10.3~~		
11.1	1667.39	0.000
11.2	2816.11	2290.58
11.3	3432.26	1.05E+06
~~12.1~~		
~~12.2~~		
~~12.3~~		
13.1	20.02	1.280
13.2	19.28	1.859
13.3	18.53	2.374
~~14.1~~		
~~14.2~~		
~~14.3~~		

RSSQ and RSSQRE for kinetic models fitted to DNHE rates measured on H-BEA-25. Models crossed out are thermodynamically inconsistent.

Model	RSSQ	RSSQRE
1.1	656.01	0.15
1.2	303.29	0.13
1.3	2608.50	0.16
~~2.1~~		
~~2.2~~		
~~2.3~~		
3.1	10644.00	0.93
3.2	11668.00	0.60
3.3	11806.00	0.43
4.1	2765.86	43.61
4.2	2769.90	7757.84
4.3	2772.60	7185.37
5.1	10172.00	1.55
5.2	11588.00	1.00
5.3	11784.00	0.76
6.1	2765.08	53.66
6.2	2765.18	51.82
6.3	2765.21	52.80
7.1	655.43	46.55
7.2	73.02	1.30
7.3	113.47	1.61
~~8.1~~		
~~8.2~~		
~~8.3~~		
9.1	655.10	52.08
9.2	**67.00**	**0.85**
9.3	**94.15**	**0.60**
~~10.1~~		
~~10.2~~		
~~10.3~~		
11.1	1.02E+04	8298.35
11.2	1.19E+04	240.52
11.3	1.25E+04	12682.76
~~12.1~~		
~~12.2~~		
~~12.3~~		
13.1	655.18	3.97E+08
13.2	62.93	137765.22
13.3	80.12	3.21
~~14.1~~		
~~14.2~~		
~~14.3~~		

RSSQ and RSSQRE for kinetic models fitted to DNHE rates measured on H-MFI-28. Models crossed out are thermodynamically inconsistent.

Model	RSSQ	RSSQRE
1.1	0.82	0.18
1.2	2.57	0.39
1.3	5.58	0.80
2.1	0.46	4.81
2.2	0.45	2.39
2.3	0.45	1.57
3.1	48.15	0.98
3.2	57.46	0.91
3.3	58.55	0.71
~~4.1~~		
~~4.2~~		
~~4.3~~		
5.1	43.89	1.28
5.2	58.14	1.54
5.3	60.60	1.44
~~6.1~~		
~~6.2~~		
~~6.3~~		
7.1	**0.35**	**3145.78**
7.2	**0.25**	**1.23**
7.3	**0.18**	**0.71**
~~8.1~~		
~~8.2~~		
~~8.3~~		
9.1	0.49	11307.79
9.2	0.60	2.20
9.3	0.72	1.60
~~10.1~~		
~~10.2~~		
~~10.3~~		
11.1	43.89	2.17E+09
11.2	60.14	0.00
11.3	65.73	0.00
~~12.1~~		
~~12.2~~		
~~12.3~~		
13.1	0.50	17.35
13.2	0.32	6.38
13.3	0.22	2.81
~~14.1~~		
~~14.2~~		
~~14.3~~		

APPENDIX VIII. Distribution of residuals of type 7 and 9 models for zeolites

Residuals vs r_{calc} of type 9 models fitted to DNOE rate data on H-FAU-30.

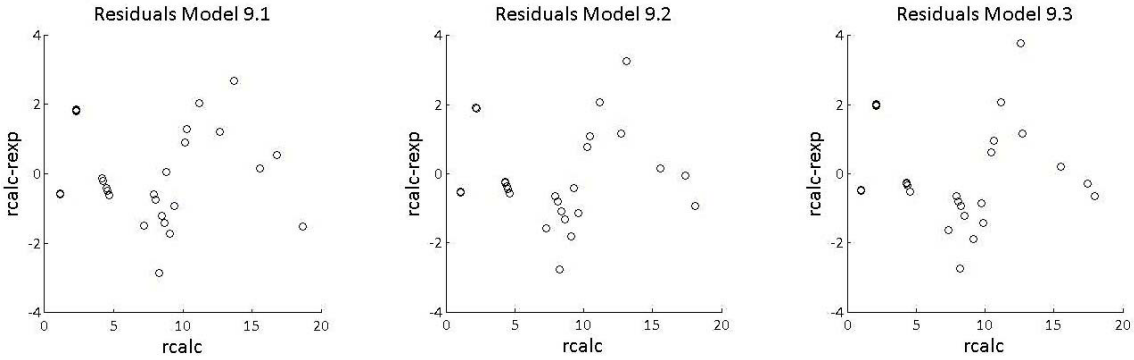

Residuals vs r_{calc} of type 7 models fitted to DNHE rate data on H-FAU-30

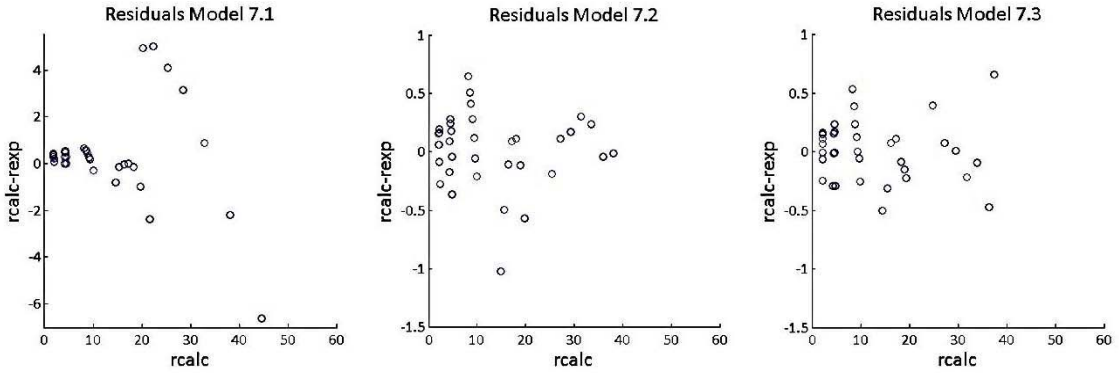

Residuals vs r_{calc} of type 7 models fitted to DNHE rate data on H-FAU-6.

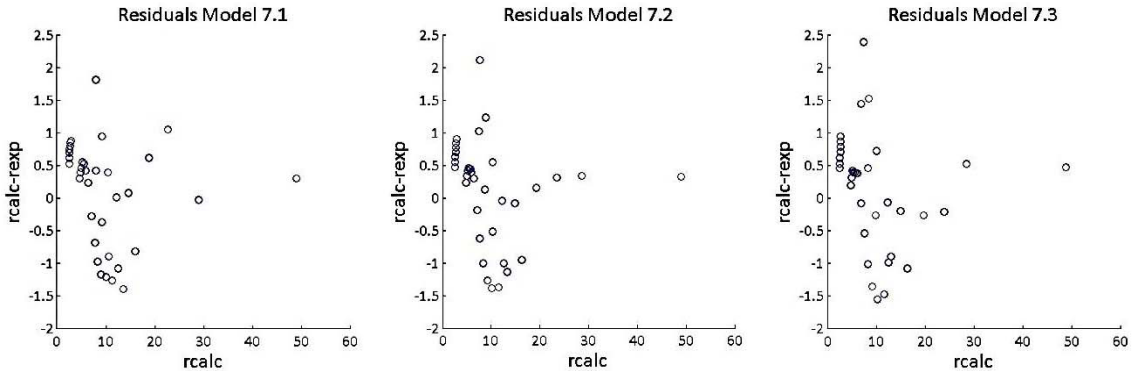

Residuals vs r_{calc} of type 9 models fitted to DNHE rate data on H-BEA-25.

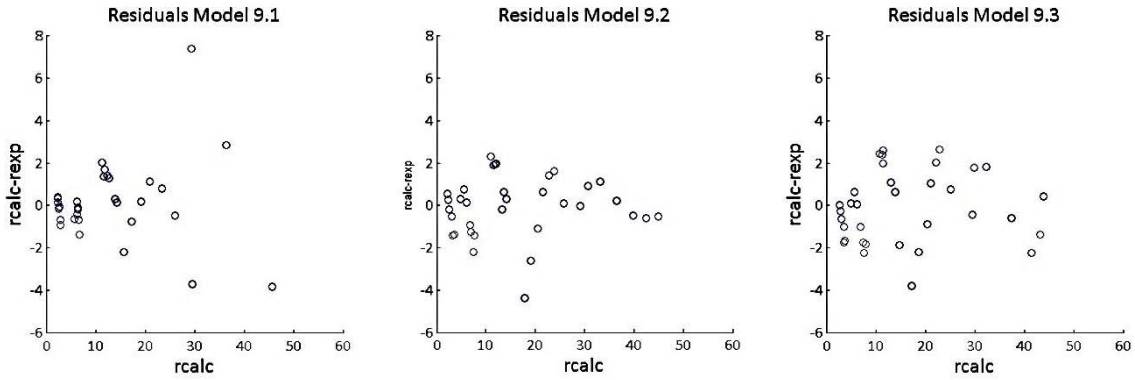

Residuals vs r_{calc} of type 7 models fitted to DNHE rate data on H-MFI-28

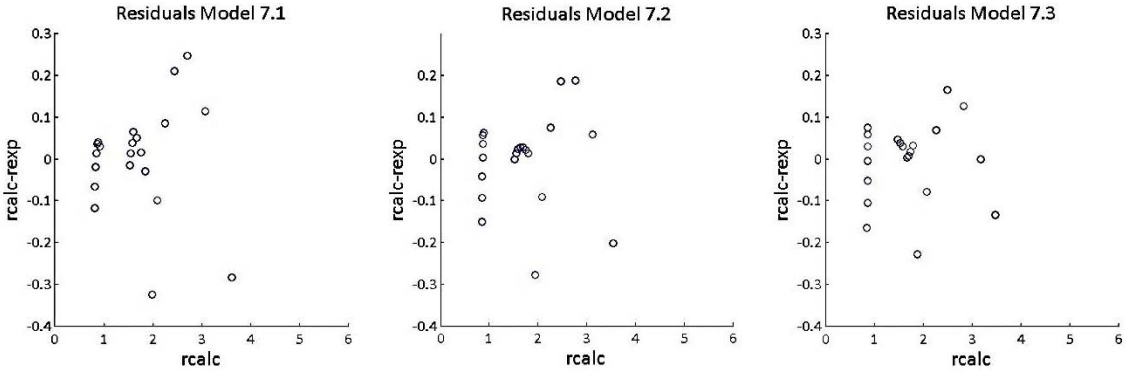

CHAPTER 11

RESUMEN DEL TRABAJO (SPANISH)

Extracto

En esta tesis se ha estudiado la síntesis de éteres lineales simétricos de entre 10 y 16 carbonos a partir de la deshidratación de alcoholes primarios sobre catalizadores ácidos. Siguiendo la línea de investigación empezada con trabajos previos sobre la deshidratación de 1-pentanol y 1-hexanol a di-n-pentil éter (DNPE) y di-n-hexil éter (DNHE) respectivamente, este trabajo continua con la serie de éteres simétricos donde se realiza un estudio intensivo de la reacción de deshidratación de 1-octanol a di-n-octil éter y se amplían los estudios sobre las síntesis de DNPE y DNHE.

En una primera etapa, se realiza un barrido catalítico con resinas de intercambio iónico ácidas basadas en poliestireno y divinilbenceno (PE-DVB) donde se evalúan conversión de alcohol, selectividad y rendimiento en éter lineal así como las velocidades iniciales para determinar qué características son más influyentes para llevar a cabo la reacción principal (deshidratación de alcohol a éter lineal) y las que favorecen las reacciones secundarias.

De la misma manera, las síntesis de DNPE, DNHE y DNOE se llevaron a cabo sobre distintas zeolitas, determinándose qué características son necesarias para maximizar la el rendimiento en éter lineal y cómo afectan a la conversión y selectividad.

En el presente trabajo se lleva a cabo también el estudio del equilibrio químico de la reacción de deshidratación de 1-octanol a DNOE sobre la resina termoestable Amberlyst 70, dando así continuidad a los trabajos previos en la determinación de las constantes de equilibrio del DNPE y DNHE. En el estudio de equilibrio se determina la constante de equilibrio así como el carácter térmico de la reacción a la vez que se cotejan los valores de entalpía de formación del DNOE estimados y se propone un nuevo valor para la entropía molar del DNOE.

Por último se realiza un estudio cinético de las síntesis de DNHE y DNOE sobre zeolitas, comparándose con el estudio cinético para la síntesis de DNPE de la bibliografía. Así mismo se lleva a cabo un estudio cinético de la síntesis de DNOE sobre la resina termoestable Amberlyst 70.

En referencia a la síntesis de DNOE sobre Amberlyst 70, se llevan a cabo una serie de estudios preliminares para determinar qué condiciones experimentales (velocidad de agitación, diámetro de partícula de catalizador y masa de catalizador) son necesarias para evitar los efectos de la transferencia de materia externa/interna en la velocidad de reacción observada. Los datos cinéticos se ajustan a modelos cinéticos tipo LHHW-RE y se realiza una selección y discriminación en base a criterios de coherencia fisicoquímica y criterios de ajuste matemático. También se evalúa el efecto de los productos de la reacción (agua y DNOE) así como el disolvente (1,4-dioxano) en la velocidad de reacción y se proponen y evalúan distintos factores para corregir el efecto desactivador del agua en la reacción que se observa.

Respecto a las zeolitas, análogamente a la resina Amberlyst 70, se ajustaron modelos cinéticos LHHW-RE a los datos cinéticos de las síntesis de DNHE y DNOE y se procedió a la selección del modelo cinético con los mismos criterios fisicoquímicos y de ajuste matemático. Así mismo se compararon los modelos cinéticos obtenidos para el DNHE y el DNOE con el modelo para el DNPE de la bibliografía.

1. Introducción

El motor diésel presenta la ventaja de su mayor eficiencia térmica respecto a otros motores de combustión interna. Sin embargo, la combustión del diésel genera contaminantes como las partículas, CO, NOx, SOx e hidrocarburos no quemados que comprometen la calidad del aire las ciudades europeas. Para resolver el problema de las emisiones de los motores diésel existen soluciones que pasan por la modificación del motor, las tecnologías de final de tubo y la reformulación del combustible diésel.

La reformulación del combustible diésel es en general una solución que afecta a todo tipo de motores. Las normativas europeas son cada vez más exigentes en las especificaciones del combustible diésel, estableciendo índices de cetano más altos, densidades más bajas, y limitando el contenido de hidrocarburos poliaromáticos, y compuestos de azufre [1].

Dentro de la variedad de posibles aditivos para reformular el combustible diésel, los compuestos oxigenados y más concretamente los éteres lineales de más de 9 carbonos

constituyen un grupo de compuestos con propiedades excelentes como aditivos. Estos compuestos aumentan el índice de cetano de la mezcla, aumentando la calidad de la combustión además de proporcionar un buen comportamiento de la mezcla en frío y temperaturas de ebullición dentro del rango del diésel [2, 3].

Dentro de los éteres lineales, los éteres simétricos pueden sintetizarse a través de la deshidratación bimolecular de n-alcoholes sobre catalizadores ácidos. De esta manera DNPE, DNHE y DNOE pueden ser sintetizados a partir de 1-pentanol, 1-hexanol y 1-octanol respectivamente [4-10]. La Figura 1 muestra la reacción de deshidratación bimolecular de 1-octanol a DNOE.

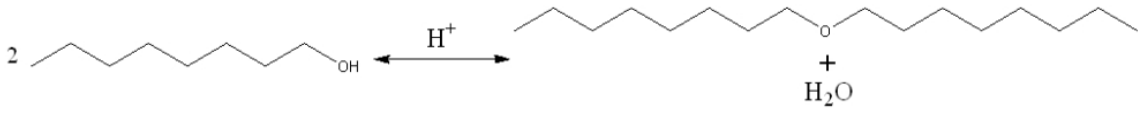

Figura 1. Deshidratación bimolecular de 1-octanol a DNOE

Dentro de los catalizadores ácidos, las resinas de intercambio iónico de PE-DVB y las zeolitas han demostrado ser un grupo de catalizadores muy interesante ya que al ser sólidos su separación de la mezcla de reacción es mucho más fácil que en la catálisis tradicional con ácido sulfúrico [11].

Las resinas de intercambio iónico de PE-DVB ácidas se producen industrialmente mediante la copolimerización de estireno y divinilbenceno en solución acuosa. La polimerización llevada a cabo en un reactor tanque agitado se inicia con peróxido benzoico, y el resultado son pequeñas esferas de catalizador de un copolímero formado por una matriz de PE-DVB (Figura 2).

Figura 2. Esferas de una resina de PE-DVB

En la síntesis de las resinas de PE-DVB puede incluirse un agente porógeno que genera una matriz de PE-DVB macroreticular con porosidad permanente. Sin embargo las resinas tipo gel se sintetizan en ausencia de agente porógeno generando una estructura ausente de porosidad en estado seco pero porosa cuando la matriz de PE-DVB se hincha por el efecto de un solvente polar.

Las resinas macroreticulares contienen porcentajes de DVB altos (8-20% o incluso más). Su estructura es más resistente físicamente pero su matriz polimérica es más rígida, lo que les confiere menos capacidad de hinchamiento que las resinas tipo gel, con porcentajes de DVB más bajos (2-8%). Las resinas de PE-DVB se tratan con ácidos para generar los centros ácidos en su estructura, como por ejemplo la sulfonación con ácido sulfúrico, que genera una estructura polimérica con grupos sulfónicos anclados a los anillos bencénicos de la matriz de PE-DVB.

Las zeolitas son aluminosilicatos de metales del grupo I y II de la tabla periódica. Están formadas por tetraedros de SiO_4^{4-} o AlO_4^{5-} organizados de tal manera que generan estructuras con microporos de tamaño uniforme. Es posible controlar su composición, tamaño de poro y topología, generando un sinfín de estructuras. Se pueden sintetizar hidrotermalmente mediante una fuente de Si, un agente mineralizante y un agente director de estructura. La funcionalización ácida de las zeolitas se lleva a cabo mediante sustitución isomórfica, sustituyendo tetraedros de SiO_4^{4-} por tetraedros de AlO_4^{5-} y así generando cargas negativas que son compensadas con cationes orgánicos como el amonio.

Para que la deshidratación de alcoholes a éteres lineales se lleve a cabo en catalizadores sólidos, los reactivos deben poder acceder desde el medio de reacción a los centros ácidos del catalizador y los productos deben poder salir de los centros ácidos del catalizador y llegar al medio de reacción.

Los pasos de un proceso catalizado por un sólido consisten en (Figura 3):

A. Difusión de los reactivos desde la fase fluida a la película externa del catalizador (transferencia de materia externa).

B. Difusión de los reactivos a través de los poros del catalizador (transferencia de materia interna).

C. Adsorción de reactivos en el/los centro/s activo/s.

D. Reacción química en el/los centro/s activo/s.

E. Desorción de los productos en el/los centro/s activo/s.

F. Difusión de los productos a través de los poros del catalizador (transferencia de materia interna).

G. Difusión de los productos desde la película externa del catalizador hasta la fase fluida (transferencia de materia externa).

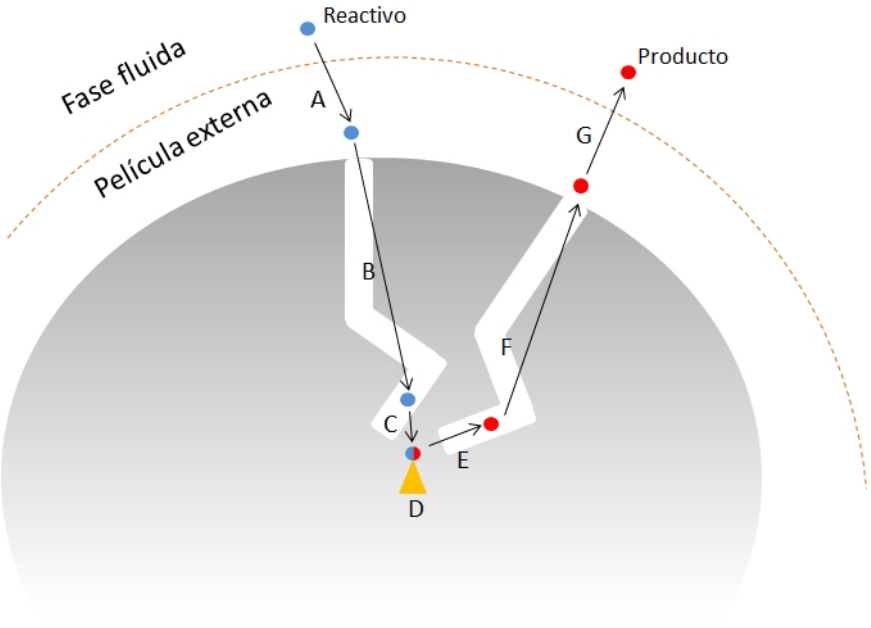

Figura 3. Representación de los pasos en el proceso catalítico

Para representar los procesos de adsorción de las moléculas en los centros activos se utilizan isotermas, que relacionan la cantidad de adsorbato adsorbido en el catalizador y la concentración de adsorbato en la fase fluida. Para expresar la velocidad de reacción en la superficie activa de los catalizadores se utilizan ecuaciones basadas

en los mecanismos Langmuir-Hinselwood-Hougen-Watson (LHHW) y Rideal-Eley (RE). En dichos mecanismos se parten de tres hipótesis: 1) la superficie del catalizador tiene un número fijo de centros activos, 2) todos los centros activos son idénticos y 3) la reactividad de los centros activos sólo depende de la temperatura y no de la naturaleza o la cantidad de otros compuestos presentes en la superficie durante la reacción. El procedimiento para obtener la ecuación cinética a partir de los mecanismos LHHW-RE se basa en asumir que una de las etapas es la limitante y ajustar los datos experimentales a dichas ecuaciones [12].

2. Objetivos

Los objetivos de este trabajo son 1) demostrar que la deshidratación de 1-octanol a DNOE es posible sobre resinas de PE-DVB y zeolitas, 2) llevar a cabo un barrido catalítico con resinas de PE-DVB para evaluar la influencia de sus características morfológicas en la síntesis de DNOE y compararlo con las síntesis de DNHE y DNPE, 3) llevar a cabo un barrido catalítico con zeolitas y evaluar la influencia de sus parámetros texturales en las síntesis de DNOE, DNHE y DNPE, 4) Evaluar el equilibrio termodinámico de la reacción de deshidratación de 1-octanol a DNOE y sus reacciones secundarias más importantes, 5) llevar a cabo un estudio cinético de la reacción de deshidratación de 1-octanol a DNOE sobre la resina termoestable Amberlyst 70 y compararlo con los estudios cinéticos sobre DNPE y DNHE de la bibliografía, 6) llevar a cabo un estudio cinético de la síntesis de DNOE y DNHE sobre zeolitas y compararlo con el estudio cinético de la síntesis de DNPE de la bibliografía.

3. Experimental

En este trabajo se utilizaron 15 resinas de PE-DVB con diferente grado de sulfonación, estructura, porcentaje en DVB y estabilidad térmica así como el copolímero de Teflon ® Nafion NR50. También se utilizaron 6 zeolitas de diferente estructura, número de centros ácidos, y características texturales y el material mesoporoso H-MCM-79. Los reactivos utilizados fueron 1-pentanol, 1-hexanol, y 1-octanol para las síntesis de DNPE, DNHE y DNOE respectivamente y se utilizaron DNPE, DNHE, DNOE, pentenos, hexenos, octenos y agua para análisis.

La instalación utilizada para llevar a cabo las reacciones de deshidratación consiste en un reactor tanque agitado discontinuo de 100 cm^3 que opera entre 413-473 K y una presión de 2.5 MPa para mantener la fase líquida. La toma de muestras se realiza mediante un sistema de muestreo conectado des del reactor a una válvula de muestreo que inyecta 0.2 mm^3 de líquido en un cromatógrafo de gases (HP 190915-001) equipado con un detector de conductividad térmica (TCD). El catalizador es inyectado al reactor mediante un inyector catalítico. Los detalles de la instalación se muestran en la Figura 4.

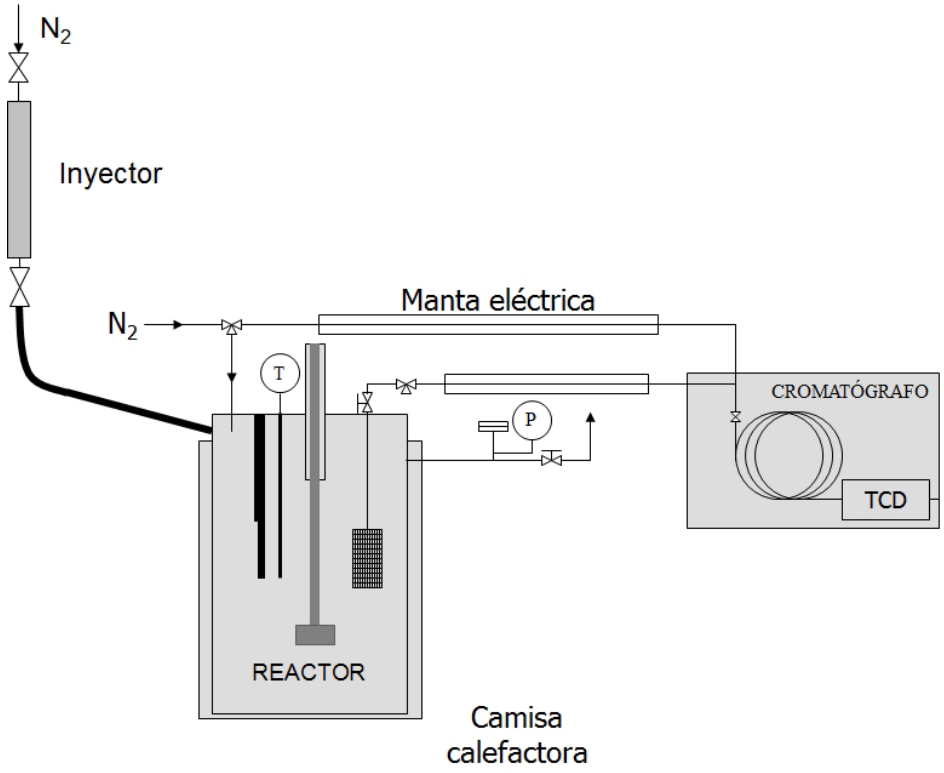

Figura 4. Esquema de la instalación

El procedimiento experimental utilizado para los experimentos con resinas consistió primeramente en el secado de éstas a 383 K a presión atmosférica durante 1 h y después a 373 K y 10 mbar durante 15 h. Para las zeolitas se realizó primeramente su activación a 773 K y después se mantuvieron a 373 K y 10 mbar durante 15 h.

Después del tratamiento de los catalizadores se procede a cargar el reactor con 70 cm^3 de líquido. Una vez la mezcla se presuriza y calienta hasta la temperatura de trabajo (413-473 K) el catalizador se inyecta desde el inyector de catalizador hasta el reactor por diferencia de presión. En el momento de la inyección de catalizador se

empieza a contar el tiempo y se van tomando muestras del medio de reacción cada hora hasta el fin del experimento (6-7 h para todos los experimentos excepto para los experimentos de equilibrio químico).

4. Resultados y discusión

Del estudio sobre la **deshidratación de 1-octanol** sobre **resinas** de intercambio iónico ácidas se concluyó que además de la reacción principal de eterificación de 1-octanol a DNOE, otras reacciones secundarias también tenían lugar. Las reacciones secundarias observadas fueron la deshidratación intramolecular de 1-octanol a 1-octeno, la isomerización de 1-octeno a 2,3 y 4-octeno y la reacción entre 1-octanol y octenos para producir éteres ramificados de 16 carbonos. En la Figura 5 se muestra el esquema de reacción para la deshidratación de 1-octanol.

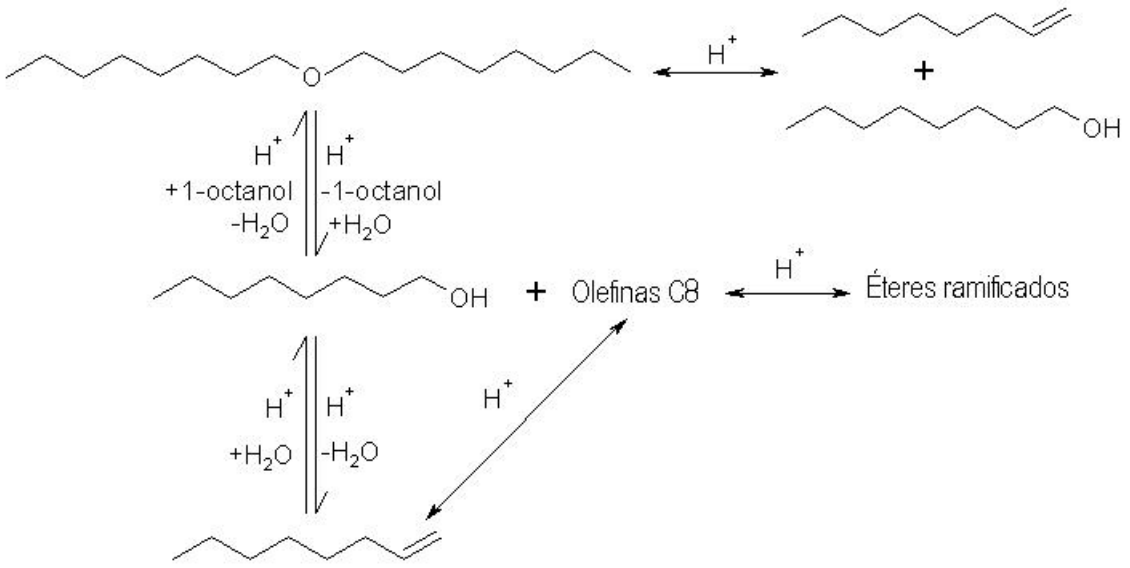

Figura 5. Esquema de reacción para la deshidratación de 1-octanol

Se realizó un análisis de la influencia de las propiedades de las resinas en la reacción de deshidratación de 1-octanol a DNOE. Así mismo, este análisis se extendió a las deshidrataciones de 1-pentanol y 1-hexanol a DNPE y DNHE respectivamente, con esquemas de reacción análogos al mostrado en la Figura 5.

La Figura 6 muestra la conversión de alcohol unificada para los tres sistemas ($X_{ROH} \cdot n^0_{ROH}/W$) en varias resinas. Se vio que la conversión de alcohol fue mayor en

resinas de elevada capacidad ácida como las resinas sobresulfonadas (A-16, A-36 y CT 224). Se observó también una gradación de la conversión de alcohol (1-pentanol, 1-hexanol y 1-octanol) con la longitud de éste en las resinas de estructura más rígida (resinas macroreticulares con porcentajes medios y altos de DVB) poniendo de manifiesto la mayor restricción que los alcoholes sufren para acceder a los centros activos de estas resinas. Sin embargo, las resinas tipo gel y macroreticulares con bajos porcentajes en DVB muestran menos diferencias entre la conversión de los tres alcoholes. La estructura más elástica y la gran capacidad de hinchamiento de las resinas con bajo porcentaje en DVB permitieron a los alcoholes un acceso similar a los centros ácidos sin importar la longitud del alcohol.

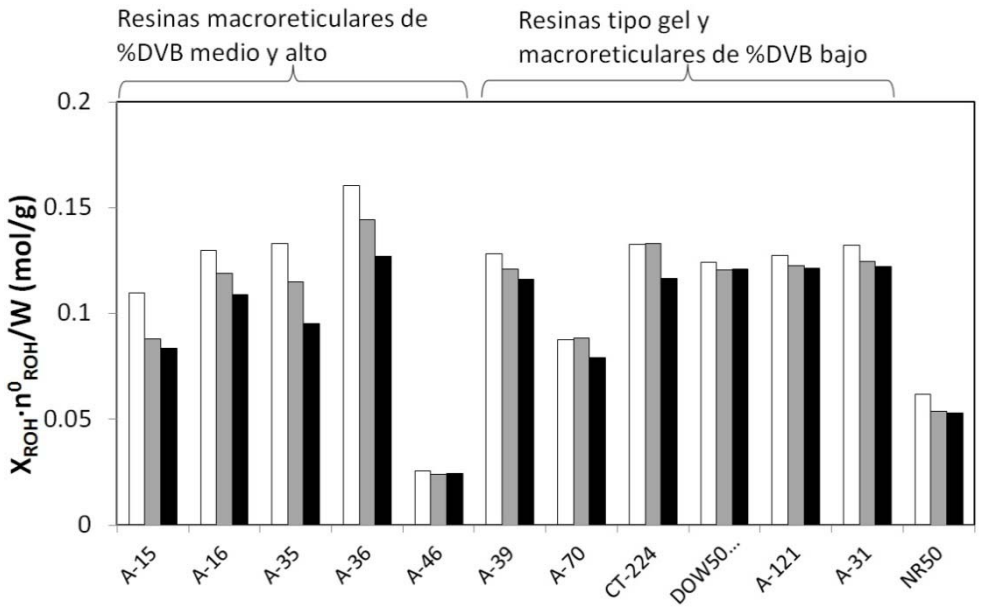

Figura 6. Comparación de la conversión de 1-pentanol (barras blancas), 1-hexanol (barras grises) y 1-octanol (barras negras) en las resinas empleadas, Conversión a t = 6 h, W = 1 g, T = 423 K, P = 2.0 MPa, 70 cm^3 de alcohol

En cuanto a la selectividad se observó que el volumen específico de polímero hinchado (V_{sp}) caracterizado mediante la técnica de ISEC (*Inverse Steric Exclusion Chromatograpy*) [13] es un parámetro de las resinas de PE-DVB clave para correlacionar la selectividad hacia éter lineal. El espacio disponible generado en la fase gel de las resinas tipo gel se ve traducido en valores de V_{sp} grandes (2-3 cm^3/g comparados con las resinas macroreticulares (0.5-1.5 cm^3/g). La Figura 7 muestra claramente como para las resinas tipo gel la selectividad hacia éter lineal es alta para DNPE, DNHE y DNOE. Sin embargo observando las selectividad hacia éter lineal de las

resinas macroreticulares se puede observar que a medida que el parámetro V_{sp} disminuye la selectividad hacia éter lineal también lo hace, siendo mayor este descenso a medida que la longitud del éter aumenta ($S_{OcOH}^{DNOE} < S_{HeOH}^{DNHE} < S_{PeOH}^{DNPE}$).

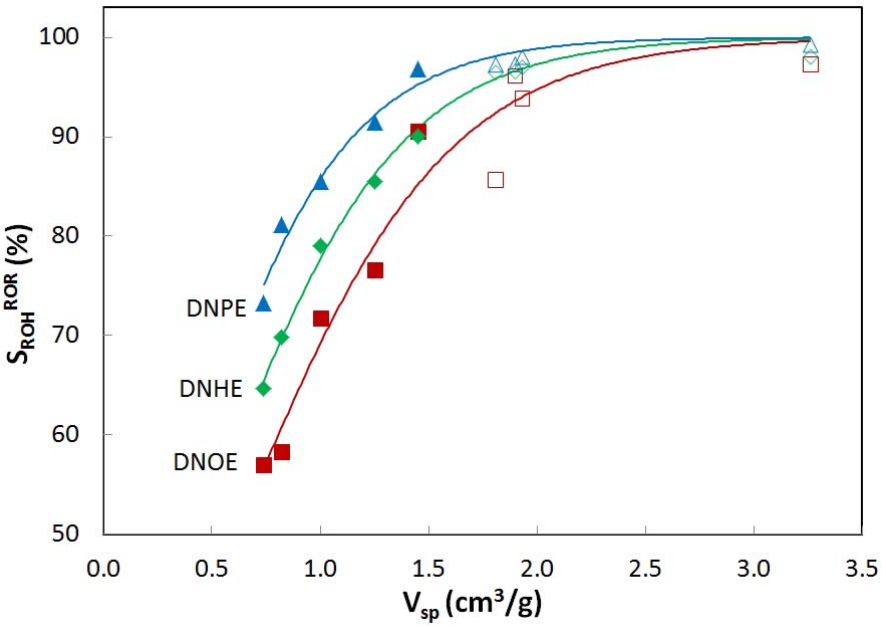

Figura 7. Influencia del parámetro V_{sp} en la selectividad hacia éter lineal (S_{ROH}^{ROR}). S_{OcOH}^{DNOE} de resinas tipo gel (cuadrado vacío) y macroreticulares (cuadrado lleno). S_{HeOH}^{DNHE} de resinas tipo gel (rombo vacío) y macroreticulares (rombo lleno). S_{PeOH}^{DNPE} de resinas tipo gel (triángulo vacío) y macroreticulares (triángulo lleno). t = 6 h, W = 1 g, T = 423 K, P = 2 MPa, 70 cm^3 de alcohol

El análisis de las velocidades iniciales de formación de éter lineal y de consumo de alcohol sobre las resina Amberlyst 46 -sulfonada únicamente a nivel superficial- permitió evaluar la efectividad o rendimiento de los centros ácidos de las resinas. Suponiendo una accesibilidad total de los centros ácidos de la resina Amberlyst 46 se concluyó que para las resinas macroreticulares con porcentajes medios y altos de DVB la fracción de centros ácidos implicada en la síntesis de éter lineal disminuye con la longitud del éter DNPE > DNHE > DNOE (56-79% para el DNPE, 44-67% para el DNHE y 29-52% para el DNOE).

Sobre las **zeolitas** se observó que la conversión de alcohol estaba fuertemente relacionada con la superficie mesoporosa (S_{BJH}) de la zeolita y el número de centros ácidos de ésta ($[H^+]$ obteniéndose una superficie de respuesta (ecuación 1) relacionando el número de moles de alcohol consumidos al cabo de 6 horas (N_{ROH}) con

la superficie mesoporosa (S_{BJH}), la superficie microporosa (S_{micro}) y el número de centros ácidos [H^+].

$$N_{ROH} = a \cdot \left(S_{BJH}{}^2 \cdot [H^+]\right) + b \cdot \left(S_{micro}{}^2 \cdot [H^+]\right) \quad (1)$$

Se observó $N_{PeOH} > N_{HeOH} > N_{OcOH}$ (1-pentanol, 1-hexanol y 1-octanol). A pesar de que la gran parte de conversión de alcohol es atribuible a la superficie mesoporosa (94-98%) la contribución de la estructura microporosa fue mayor para el 1-octanol (6%) que para el 1-pentanol (2%). Este hecho coincide con la mayor selectividad hacia olefinas observada en la deshidratación de 1-octanol, menos impedidas estéricamente en los microporos de las zeolitas que el DNOE.

En general la selectividad a éter lineal siguió la siguiente tendencia: $S_{PeOH}^{DNPE} > S_{HeOH}^{DNHE} > S_{OcOH}^{DNOE}$ lo que pone una vez más de manifiesto el mayor impedimento estérico de las moléculas más voluminosas. Se observó que la selectividad hacia éter lineal disminuía con la temperatura. La deshidratación de alcohol a olefinas se vio promocionada a temperaturas elevadas y en zeolitas de baja superficie mesoporosa y estructura microporosa de microporos estrechos. La selectividad hacia éteres ramificados mostró un comportamiento complejo concluyéndose que la reacción entre olefinas y alcoholes para dar éteres ramificados tiene lugar en la estructura microporosa de las zeolitas.

El rendimiento en éter lineal expresado como el producto de conversión de alcohol y selectividad hacia éter lineal fue mayor en las zeolitas de grandes poros y áreas en el rango de los mesoporos. En la Figura 8 se muestra el rendimiento en éter observado sobre las zeolitas H-BEA-25, H-FAU-6, H-FAU-30, H-MFI-28, H-MOR-20 y H-FER-20.

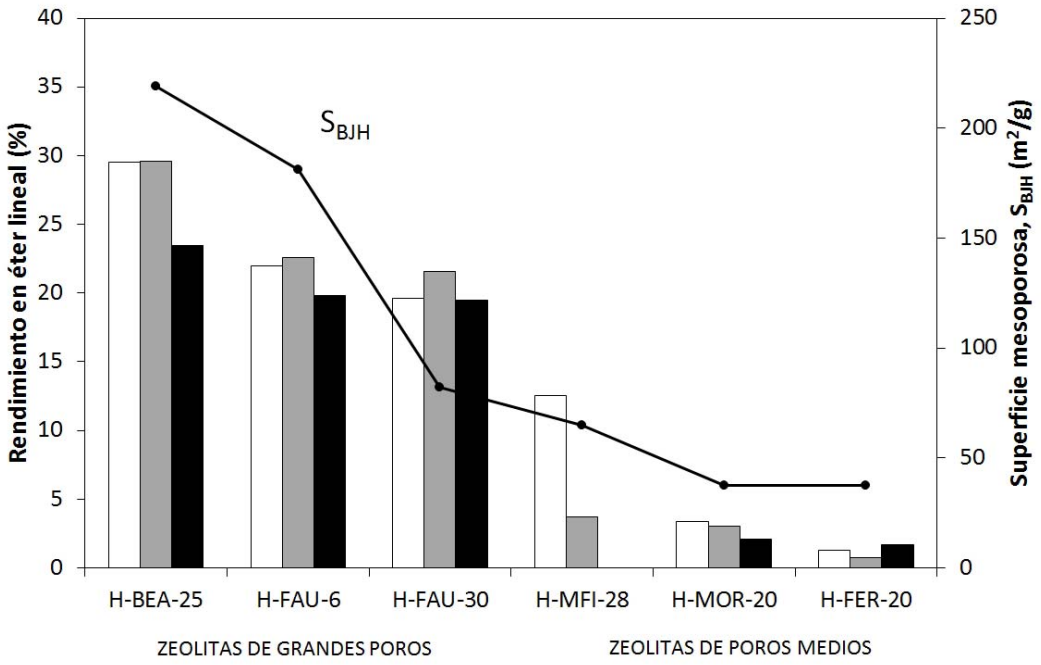

Figura 8. Rendimiento en DNPE (barras blancas), DNHE (barras grises) y DNOE (barras negras) y superficie mesoporosa, S_{BJH} (puntos). Condiciones: W = 1g, T =453 K, P = 2.0 MPa, 70 cm^3 alcohol, t = 6 h)

En el **estudio de equilibrio** de la reacción de deshidratación de 1-octanol a DNOE se determinaron las constantes de equilibrio en el rango de temperaturas 413-453 K sobre la resina termoestable Amberlyst 70. También se determinaron las constantes de equilibrio de las reacciones secundarias más importantes.

El procedimiento experimental para este tipo de experimentos consistió en introducir en el reactor una mezcla de reacción próxima al equilibrio junto con 4 gramos de Amberlyst 70, calentar la mezcla hasta la temperatura de trabajo y dejar evolucionar la mezcla de reacción hasta alcanzar el equilibrio. Para preparar las mezclas de composición cercana al equilibrio se utilizó el disolvente 1,4-dioxano, que permitió trabajar con mezclas de agua-1-octanol-DNOE y octenos sin problemas de miscibilidad entre los componentes [REF 43, 99]. La toma de muestras se realizaba a diario hasta observar que el valor de la constante de equilibrio experimental calculada con la ecuación 2 no variaba significativamente en el tiempo (50-75 h).

$$K = \prod_{j=1}^{S} (a_j)_e^{\nu_j} = \prod_{j=1}^{S} (\gamma_{x,j} \cdot x_j)_e^{\nu_j} = \prod_{j=1}^{S} (\gamma_{x,j})_e^{\nu_j} \prod_{j=1}^{S} (x_j)_e^{\nu_j} = K_\gamma \cdot K_x \qquad (2)$$

Las actividades de los compuestos (a_j), se calcularon mediante las fracciones molares de los compuestos, (x_j) y los coeficientes de actividad de cada compuesto (γ_j), se estimaron mediante el método UNIFAC [14].

Los valores de las constantes de equilibrio entre 413-453 K se ajustaron a la ecuación 3. Se hizo el ajuste para la deshidratación de 1-octanol a DNOE, la deshidratación intramolecular de 1-octanol a 1-octeno y la isomerización de 1-octeno a 2-octeno.

$$\ln K = \left(\frac{-\Delta_r G^0\ (l)}{RT}\right) = \left(\frac{-\Delta_r H^0\ (l)}{RT} + \frac{\Delta_r S^0\ (l)}{R}\right) \qquad (3)$$

La Figura 9 muestra el ajuste de la ecuación 3 a los datos experimentales de lnK (eje y) y 1/T (eje x). Se puede apreciar que del valor de la pendiente de estos ajustes se extrae el valor de la entalpía de la reacción y de la ordenada en el origen el valor de entropía de la reacción, tabuladas en la Tabla 1.

Tabla 1. Energía de Gibbs ($\Delta_r G$), entalpía ($\Delta_r H$) y entropía ($\Delta_r S$) de la reacción de la deshidratación de 1-octanol a DNOE (I), deshidratación intramolecular de 1-octanol a 1-octeno (II) e isomerización de 1-octeno a 2-octeno (III) a 298.15 K

	I	II	III
$\Delta_r H$ (l) ($kJ \cdot mol^{-1}$)	-13.5±1.7	35.4±15.8	-13.5±1.5
$\Delta_r S$ (l) ($J \cdot mol^{-1} \cdot K^{-1}$)	14.0±4.0	75.3±36.6	-4.2±3.6
$\Delta_r G$ (l) ($kJ \cdot mol^{-1}$)	-17.7±2.1	13.0±19.2	-12.3±1.9

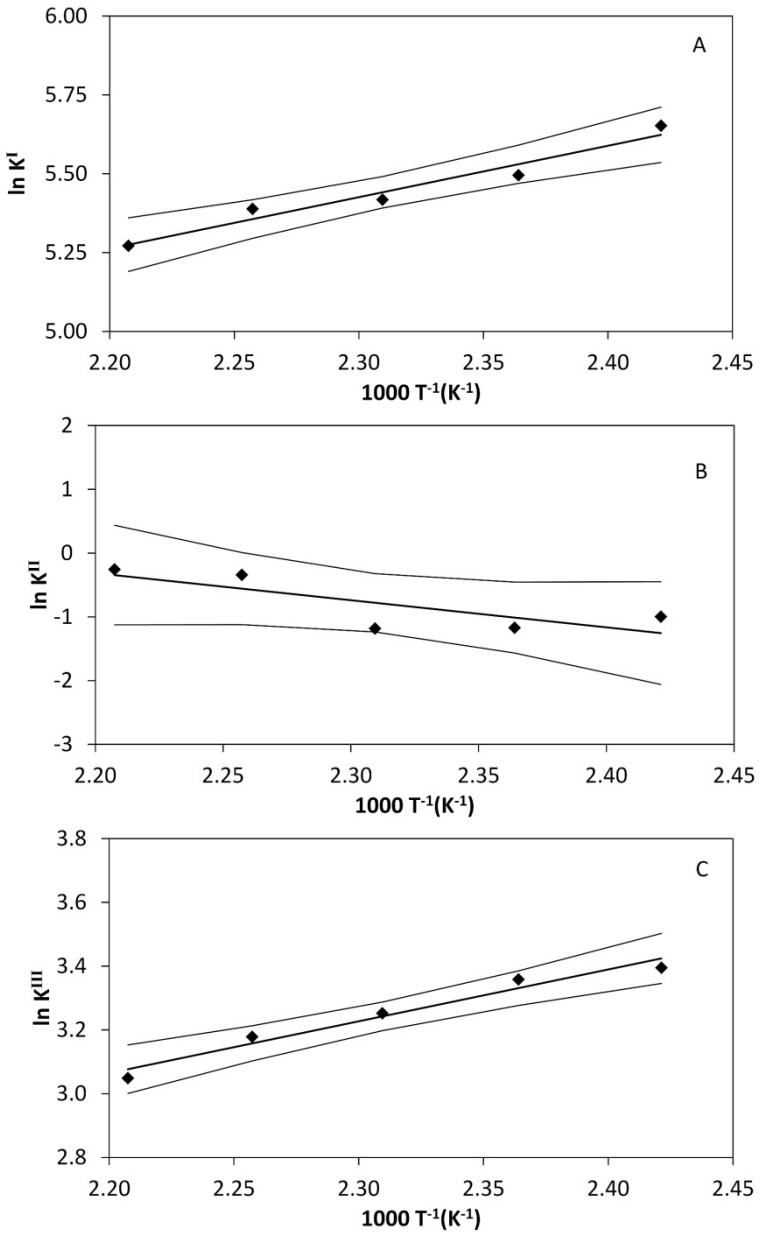

Figura 9. Valores experimentales medios de lnK (rombo) vs. 1/T. Ajuste matemático lineal (línea central) e intervalos de confianza de los valores estimados para el 95% de confianza. (A) deshidratación de 1-octanol a DNOE, (B) deshidratación intramolecular de 1-octanol, (C) isomerización de 1-octeno a 2-octeno

La obtención de las entalpías y entropías de reacción derivadas de los ajustes de la Figura 9 para la deshidratación de 1-octanol a DNOE permitió cotejar datos termodinámicos estimados para el DNOE. El valor experimental obtenido de entalpía de reacción permitió corroborar la bondad del método Benson para estimar la entalpia de formación del DNOE. Sin embargo se observó que la estimación de la entropía molar del DNOE mediante el método de estimación de Benson modificado por

Verevkin [15] no coincidía con el valor deducido mediante la entropía de reacción, proponiéndose de esta manera el valor de 658 ±4 $J \cdot mol^{-1} \cdot K^{-1}$.

Comparando los datos termodinámicos para la reacción de deshidratación de 1-octanol a DNOE con los datos para las síntesis de DNHE y DNPE se observa que a medida que el éter lineal es más grande la entalpía y energías de Gibbs de reacción son más negativas.

Para la realización del **estudio cinético** de la reacción de deshidratación de 1-octanol a DNOE sobre la resina termoestable **Amberlyst 70** se procede inicialmente con un estudio preliminar para determinar qué condiciones del reactor (velocidad de agitación, masa de catalizador y diámetro de partícula) son necesarias para asegurar que la transferencia de materia externa e interna no influyen en la velocidad de reacción. De este estudio inicial se concluyó que operando con masas de Amberlyst 70 comercial entre 1 y 2 g y agitando a una velocidad de 500 rpm no existe influencia de las transferencias de materia externa e interna en la velocidad de reacción.

En una primera fase del estudio cinético se procedió a medir la velocidad de reacción empleando únicamente **1-octanol** como reactivo. 42 modelos cinéticos basadas en los mecanismos LHHW-RE se ajustaron a los datos de velocidades de reacción experimentales. Se analizaron los ajustes, descartando inicialmente los modelos cuyas constantes de adsorción implicaban entalpías y/o entropías de adsorción positivas así como aquellos modelos con energías de activación negativas. Una vez seleccionados los modelos con coherencia fisicoquímica se procedió a evaluar y seleccionar el modelo que más se ajustaba a los datos experimentales por criterios matemáticos de ajuste, como la suma mínima de residuos al cuadrado (RSSQ), una distribución aleatoria de los residuos y el valor mínimo de la raíz de la suma de cuadrados de los errores relativos de los parámetros (RSSQRE).

Del resultado de esta discriminación de modelos, 6 tipos de modelos son los que mejor explicaron los datos cinéticos referentes al 1-octanol como reactivo (ecuaciones 4 y 5):

$$r' = \frac{A \cdot \left[a_{OcOH}^2 - \frac{a_{DNOE} \cdot a_{H2O}}{K}\right]}{(a_{OcOH} + B \cdot a_{H2O})^n} \quad (4)$$

$$r' = \frac{A \cdot \left[a_{OcOH}^2 - \frac{a_{DNOE} \cdot a_{H2O}}{K}\right]}{(a_{OcOH} + B \cdot a_{DNOE})^n} \quad (5)$$

Teniendo en cuenta que n es el número de centros implicados en la reacción (siendo n= 1,2 o 3 en este trabajo), las ecuaciones 4 y 5 agrupan 6 modelos cinéticos. La constante A agrupa la constante cinética y la constante de equilibrio de adsorción del 1-octanol dependiendo del tipo de mecanismo del que se trate (LHHW o RE). La constante B agrupa constantes de equilibrio de adsorción. Para la expresión 4 B = $K_{a,H2O}/K_{a,OcOH}$ y para la expresión 5 B = $K_{a,\ DNOE}/K_{a,OcOH}$.

Los 6 modelos agrupados en las ecuaciones 4 y 5 suponen que la fracción de centros activos libre en el catalizador es menospreciable y la reacción en superficie es la etapa limitante. Entre los modelos derivados de las ecuaciones 4 y 5, los modelos de la ecuación 4 se ajustan mejor y sus parámetros poseen menos incertidumbre (Tabla 2).

Tabla 2. RSSQ y RSSQRE para los modelos cinéticos derivados de las ecuaciones 4 y 5

		RSSQ	RSSQRE
Ecuación 4	n = 1	250	2.58
	n =2	257	1.62
	n = 3	269	0.929
Ecuación 5	n = 1	261	151
	n = 2	278	11.3
	n = 3	300	4.17

De los modelos cinéticos derivados de la ecuación 4 se extraen energías de activación aparente de 120 $kJ \cdot mol^{-1}$ sin embargo la diferencia entre n = 1, 2 y 3 no es obvia por lo que se amplió el rango de datos experimental.

En una segunda etapa del estudio cinético se evaluó la influencia de los **productos** de la reacción (DNOE y agua) así como el **disolvente** utilizado (1,4-dioxano) en la velocidad de la reacción. Para dicho estudio se añadieron DNOE, agua y 1,4-dioxano en cantidades conocidas a diferentes temperaturas y se midieron las velocidades de reacción. Se observó que ni el DNOE ni el 1,4-dioxano afectaban significativamente a la velocidad de reacción, no siendo así para el agua, que produjo un potente efecto desactivador de la reacción. Estos experimentos no sólo permitieron poner de

manifiesto el efecto desactivador del agua sino que también permitió ampliar el rango de datos cinéticos.

Los 42 modelos cinéticos basados en mecanismos LHHW-RE volvieron a ajustarse a los todos los datos experimentales (1-octanol puro y mezclas 1-octanol/agua/DNOE/1,4-dioxano) y se procedió a discriminar los modelos cinéticos de la misma manera (criterios de coherencia fisicoquímica y criterios matemáticos de ajuste) concluyéndose que el modelo que mejor se ajustaba a los datos era el modelo derivado de la ecuación 4 con n = 1 (modelo 9.1), resultando en una energía de activación de 114±7 kJ·mol^{-1}.

Para cuantificar el efecto desactivador del agua en la velocidad de reacción se incorporaron factores correctores de la constante de reacción. Dichos factores correctores se basan en cuantificar la fracción de centros activos bloqueados por el agua mediante isotermas de adsorción. De esta manera la expresión de la constante cinética queda modificada según la ecuación 6:

$$\widehat{k'} = k_0 \cdot f(a_{H2O}) = k_0 \cdot (1 - \theta_{H2O}) \qquad (6)$$

donde k_0 es la constante cinética real y $\widehat{k'}$ la constante aparente. θ_{H2O} representa la fracción de centros activos bloqueados por las moléculas de agua.

Entre las isotermas utilizadas se encuentran modificaciones de la isoterma de Langmuir y la isoterma de Freundlich [16-19] así como una ecuación propuesta en este trabajo.

Los factores de corrección se incorporan a los modelos cinéticos basados en los mecanismos LHHW-RE que no contemplan el agua en su término de adsorción. La discriminación de modelos reveló que sólo la isoterma Freundlich, una modificación de la isoterma de Langmuir y la ecuación propuesta en este trabajo aplicadas al modelo 1.1 (ecuación 7) mejoraron el ajuste del modelo 9.1 en términos de suma mínima de residuos al cuadrado (RSSQ).

$$r' = \frac{A \cdot \left[a_{OcOH}^2 - \frac{a_{DNOE} \cdot a_{H2O}}{K}\right]}{(a_{OcOH})} \quad (7)$$

Se optó por seleccionar el modelo 1.1 (ecuación 7) modificado por la isoterma Freundlich, por ser el modelo con una suma de residuos al cuadrado mínima (RSSQ) y una energía de activación (110 ± 5 kJ·mol^{-1}) en el rango de energías de activación obtenidas en las primeras etapas del estudio (120 kJ·mol^{-1}, 114 ± 7 kJ·mol^{-1}). La ecuación 8 muestra expresión del modelo 1.1 corregido con la isoterma de Freundlich:

$$r' = \frac{A \cdot \left[a_{OcOH}^2 - \frac{a_{DNOE} \cdot a_{H2O}}{K}\right]}{(a_{OcOH})} \cdot \left[1 - K_{H2O} a_{H2O}^{T/K_\propto}\right] \quad (8)$$

El modelo cinético seleccionado plantea un escenario donde una molécula de 1-octanol adsorbida reacciona con otra molécula de 1-octanol de la fase líquida en un mecanismo **Rideal-Eley (RE)** donde el agua desactiva el catalizador siguiendo una isoterma tipo Freundlich.

El estudio cinético sobre las **zeolitas** se realizó en los sistemas de reacción del DNHE y DNOE y las ecuaciones cinéticas obtenidas se compararon con la ecuación cinética para la síntesis de DNPE de la bibliografía. 42 modelos cinéticos basados en los mecanismos LHHW-Re se ajustaron a los datos cinéticos para la síntesis de DNHE sobre las zeolitas H-FAU-6, H-FAU-30, H-BEA-25 y H-MFI-28. Discriminando los modelos de la misma manera que para la resina Amberlyst 70, los modelos derivados de las ecuaciones 9 y 10 fueron los modelos con coherencia fisicoquímica que mejor se ajustaron en términos de suma de residuos al cuadrado (RSSQ) y mínimo error paramétrico.

$$r' = \frac{A \cdot \left[a_{ROH}^2 - \frac{a_{ROR} \cdot a_{H2O}}{K}\right]}{\left(a_{ROH} + \frac{K_{a,ROR}}{K_{a,ROH}} \cdot a_{ROR}\right)^n} \quad (9)$$

$$r' = \frac{A \cdot \left[a_{ROH}^2 - \frac{a_{ROR} \cdot a_{H2O}}{K}\right]}{\left(a_{ROH} + \frac{K_{a,H2O}}{K_{a,ROH}} \cdot a_{H2O}\right)^n} \quad (10)$$

En las ecuaciones 9 y 10, ROR representa el éter lineal (DNOE, DNHE o DNPE) y ROH el alcohol (1-octano, 1-hexanol y 1-pentanol).

Para las zeolitas H-FAU-6, H-FAU-30 y H-MFI-28 la ecuación 9 obtuvo mejor ajuste (menor RSSQ), sin embargo sobre la zeolita H-BEA-25 fue la ecuación 10 la que se ajustó mejor a los datos cinéticos obtenidos en esta zeolita.

Para la síntesis de DNOE, se ajustaron los datos cinéticos sobre la zeolita H-FAU-30 a los mismos 42 modelos cinéticos concluyéndose que los modelos descritos por la ecuación 10 predecían mejor los datos cinéticos.

Tanto para la síntesis de DNOE como de DNHE se obtuvieron valores de energía de activación aparente comprendidos entre 100 y 120 $kJ \cdot mol^{-1}$ sobre todas las zeolitas probadas.

Se comprobó que los modelos cinéticos para la síntesis de DNPE sobre H-BEA-25 de la bibliografía [20] coincidían con los modelos cinéticos obtenidos en este trabajo.

5. Conclusiones

Los éteres lineales simétricos DNOE, DNHE y DNPE pueden obtenerse a partir de la deshidratación bimolecular de 1-octanol, 1-hexanol y 1-pentanol respectivamente sobre zeolitas y resinas de PE-DVB de intercambio iónico.

Las resinas de PE-DVB de intercambio iónico con bajos porcentajes de agente reticulante (DVB) obtuvieron selectividades a éter lineal y conversiones de alcohol altas, maximizando el rendimiento en éter lineal.

La superficie mesoporosa de las zeolitas en combinación con el número de centros ácidos resultó ser clave para la obtención de DNOE, DNHE y DNPE. Sobre zeolitas de baja superficie mesoporosa se favorecieron las reacciones secundarias con menos requisitos espaciales como la deshidratación intramolecular a olefinas.

Del estudio de equilibrio de la reacción de deshidratación de 1-octanol a DNOE se concluye que la reacción de síntesis de DNOE es una reacción exotérmica ($\Delta_r H$ = -13.6 ± 1.7 $kJ \cdot mol^{-1}$ a 298.15 K) permitiendo cotejar datos termodinámicos estimados para el

DNOE y proponer el valor de 658 ±4 $J \cdot mol^{-1} \cdot K^{-1}$ para la entropía molar de DNOE a 298.15 K.

En el estudio cinético de la síntesis de DNOE sobre la resina termoestable Amberlyst 70 se propone un modelo cinético que asume la reacción química como etapa limitante y la fracción de centros activos libre menospreciable. El modelo muestra un escenario donde una molécula de 1-octanol adsorbida reacciona con otra molécula de 1-octanol adsorbida en un mecanismo Rideal-Eley y el agua desactiva el catalizador siguiendo una isoterma tipo Freundlich.

Sobre zeolitas, los modelos cinéticos propuestos para predecir la síntesis de DNOE y DNHE coinciden con los modelos de la bibliografía para la síntesis del DNPE, con energías de activación comprendidas entre 100-120 $kJ \cdot mol^{-1}$.

6. Bibliografía

[1] H.G Pöttering, P. Necas, "Directive 2009/30/EC of the European parliament and of the Council of 23 April 2009 amending Directive 98/70/EC as regards the specification of petrol, diesel and gas-oil introducing a mechanism to monitor and reduce greenhouse gas emissions and amending Council Directive 1999/32/EC as regards the specification of fuel used by inland waterway vessels and repealing Directive 93/12/EC," *Off. J. Eur. Union*, vol. 140, 88-112, 2009.

[2] G.C. Pecci, M.G. Clerici, F. Giavazzi, F. Ancillotti, M. Marchionna, R. Patrini, "Oxygenated Diesel Fuels. Part 1 – Structure and properties correlation," ISAF, 1993.

[3] G. A. Olah, —Cleaner burning and cetane enhancing diesel fuel supplements, U.S. Patent US 5520710, 1996.

[4] J. Tejero, F. Cunill. M. Iborra, J.F. Izquierdo, C. Fité, "Dehydration of 1-pentanol to di-*n*-pentyl ether over ion-exchange resin catalysts," *J. Mol. Catal. A: Chem.,* vol. 182-183, 541-554, 2002.

[5] J. Tejero, C. Fité, M. Iborra, J.F. Izquierdo, F. Cunill, R. Bringué, "Liquid-phase dehydrocondensation of 1-pentanol to di-n-pentyl ether (DNPE) over medium and large pore acidic zeolites," *Microporous Mesoporous. Mater.,* vol. 117, pp. 650-660, 2009.

[6] R. Bringué, M. Iborra, J. Tejero, J.F. Izquierdo, F. Cunill, V.J. Cruz, "Thermally stable ion-exchange resins as catalysts for the liquid-phase dehydration of 1-pentanol to di-*n*-pentyl ether (DNPE)," *J. Catal.,* vol. 244, pp. 33-42, 2006.

[7] R. Bringué, J. Tejero, M. Iborra, J.F. Izquierdo, C. Fité, F. Cunill, "Experimental Study of the Chemical Equilibria in the Liquid-Phase Dehydration of 1-Pentanol to Di-*n*-pentyl Ether," *Ind. Eng. Chem. Res*., vol. 46, pp. 6865-6872, 2007.

[8] R. Bringué, J. Tejero, M. Iborra, J.F. Izquierdo, C. Fité, F. Cunill, "Water effect on the kinetics of 1-pentanol dehydration to di-n-pentyl ether (DNPE) on amberlyst 70," *Top. Catal.*, vol. 45, pp. 1-4, 2007.

[9] R. Bringué, J. Tejero, M. Iborra, J.F. Izquierdo, C. Fité, F. Cunill, "Supported Nafion catalyst for 1-pentanol dehydration reaction in liquid phase," *Chem. Eng. J*., vol. 145, pp. 135-141, 2008.

[10] E. Medina, R. Bringué, J. Tejero, M. Iborra, C. Fité, "Conversion of 1-hexanol to di-n-hexyl ether on acidic catalysts," *App. Catal. A: Gen.,* vol. 374, pp. 41-47, 2010.

[11] A. Corma A, H. García, "Crossing the borders between homogeneous and heterogeneous catalysis: developing recoverable and reusable catalytic systems," *Top. Catal.*, vol. 48, pp. 8-31, 2008.

[12] J.F. Izquierdo, F. Cunill, J. Tejero, M. Iborra, C. Fité. *Cinética de las Reacciones Químicas*. Edicions Universitat de Barcelona, 2004.

[13] K. Jerabek, "Cross-evaluation of strategie, size-exclusion chromatography. (Inverse steric exclusion chromatography as a tool for morphology characterization)," ACS Symp., ser. 635, pp. 211-224, 1996.

[14] R. Witting, J. Lohmann, "Vapor-Liquid Equilibria by UNIFAC Group Contribution. 6. Revision and Extension,"*Ind. Eng. Chem. Res*., vol. 42, pp. 183-188, 2003.

[15] S.P. Verevkin, "Improved Benson Increments for the Estimation of Standard Enthalpies of Formation and Enthalpies of Vaporization of Alkyl Ethers, Acetals, Ketals, and Ortho Esters," *J. Chem. Eng. Data*, vol. 47, pp. 1071-1097, 2002.

[16] E. du Toit, R. Schwarzer, W. Nicol. Acetone condensation on a cation exchange resin catalyst: the pseudo equilibrium phenomenon *Chem. Eng. Sci*., vol. 59, pp. 5545-5550, 2004.

[17] U. Limbeck, C. Altwicker, U. Kunz, U. Hoffmann. "Rate expression for THFsynthesis on acidic ion exchange resin," *Chem. Eng. Sci*., vol. 56, pp. 2171-2178, 2001.

[18] B. Yang, M. Maeda, S. Goto. Kinetics of liquid phase synthesis of *tert*-amyl methyl ether from *tert*-amyl alcohol and methanol catalyzed by ion exchange resin," *J. Chem. Kinet.*, vol. 30, pp. 137-143, 1997.

[19] B. Yang, S. Yang, R. Yao. "Synthesis of ethyl *tert*-butyl ether from *tert*-butyl alcohol and ethanol on strong acid cation-exchange resins," *React. Funct. Polym*., vol. 44, pp. 167-175, 2000.

[20] R. Bringué, "*Thermally stable ion-exchange resins as catalysts for the liquid-phase dehydration of 1-pentanol to di-n-pentyl ether*". Phd Thesis. University of Barcelona, 2007.

Funding statement

This work has been economically supported by the State Education, Universities, Research & Development Office of Spain (Projects CTQ2007-60691/PPQ and CTQ2010-16047).

Acknowledgements

I would like to thank my supervisors, Javier Tejero and Montse Iborra for the guidance during my research period. They introduced me in the world of research, encouraged me in difficult moments and made this work possible. I would like to thank also Fidel Cunill, I really appreciate the opportunity he offered me when I joined the Group of Applied Kinetics and Catalysis. I am also grateful to my co-authors Carles, and Eliana for all the help they offered me during this work.

Further thanks to Dr Brown and Ahmed for the help during my short stay in the University of Huddersfield.

I cannot forget Jordi Guilera, we shared a lot of moments and work in our thesis. I would like to specially thank Roger Marta and Mari Ángeles, their help was priceless and discussing with them about work and life was always a pleasure. I would like to mention my lab mates, Jordi Hug, Rodrigo, Madelin, Xavi and Rafa, we shared a lot of quotidian moments and discussions that made the daily research very gratifying. I would like to mention Eduard as well, as a student he contributed to this work and I want to thank him for his implication in the lab and for the nice conversations we had.

To all my workmates in the Chemical Engineering Department, we have shared a lot of moments at lunch time and quickly we became a small family…

Por último me gustaría agradecer a mi familia por apoyarme al decidir hacer un doctorado, especialmente a mi hermano Jose, que siempre me ha animado en mis proyectos. Una mención muy especial a Daniel, por los consejos más allá de los números y fórmulas.

“Si buscas resultados distintos, no hagas siempre lo mismo”
A. Einstein